UNIVERSITÀ
DEGLI STUDI
DI BRESCIA

DOTTORATO DI RICERCA IN

Genetica Molecolare, Biotecnologie e Medicina Sperimentale

Settore Scientifico Disciplinare
Area 06/Scienze mediche; MED/03 Genetica Medica

XXXIII CICLO

Definition of a new combined immune disease in humans through patients' and murine models' studies: F-BAR domain only protein 1 (*FCHO1*) deficiency.

DOTTORANDA
Dott.ssa Enrica Calzoni

Firma Enrica Calzoni

f.to digitalmente ex art.24 D.Lgs. 82/05

RELATORI
Chiar.mo Prof. Luigi Daniele Notarangelo

Firma Luigi Daniele Notarangelo

f.to digitalmente ex art.24 D.Lgs. 82/05

Chiar.ma Prof.ssa Silvia Clara Giliani

Firma Silvia Clara Giliani

f.to digitalmente ex art.24 D.Lgs. 82/05

Definition of a new combined immune disease in humans through patients' and murine models' studies: F-BAR domain only protein 1 *(FCHO1)* deficiency.

1. Index ..... *- 1 -*

2. Abstract (Ita/Eng) ..... *- 5 -*

3. Introduction and literature review ..... *- 9 -*

3.1. Endocytosis ..... **- 9 -**

3.1.1. Clathrin-mediated endocytosis (CME) ..... - 9 -

3.1.2. Clathrin-independent endocytosis ..... - 13 -

3.2. F-BAR-containing Fer/Cip4 homology domain-only proteins 1 and 2 (FCHO1/2) ..... **- 15 -**

3.3 Physiological functions of CME and its role in the immune system ..... **- 18 -**

3.3.1 Iron metabolism and T-cell activation ..... - 18 -

3.3.2 Cell cycle ..... - 19 -

3.3.3 Cytokine receptors ..... - 20 -

3.3.4 T cell (TCR) receptor ..... - 22 -

3.3.5 B cell (BCR) receptor ..... - 24 -

3.3.6 Other receptors ..... - 24 -

3.3.7 Natural Killer cells ..... - 26 -

3.4. Defects of CME ..... **- 27 -**

3.4.1. Murine knock-out studies ..... - 27 -

3.4.2. Human diseases of CME ..... - 28 -

3.5. Human inborn errors of immunity (IEI) due to deficiency of surface receptors ..... **- 29 -**

3.5.1 Severe Combined Immune Deficiencies (SCID) ..... - 29 -

3.5.2. Combined Immunodeficiencies (CID) generally less profound than SCID ..... - 33 -

3.5.3. Defects of B cells ..... - 35 -

3.5.4. Defects of NK cells ..... - 37 -

3.6. Next Generation Sequencing (NGS) for diagnosis of new gene defects in IEI ..... **- 39 -**

3.7. Hot research tools ..... **- 43 -**

3.7.1. CRISPR/Cas9 technology ..... - 43 -

3.7.2. Induced Pluripotent Stem Cells ..... - 45 -

3.7.3. Artificial Thymic Organoids (ATOs) ..... - 48 -

4. Research topic, significance and impact ..... *- 50 -*

5. Material and Methods ..... *- 51 -*

5.1. Human studies ..... **- 51 -**

5.1.1. Patients ..... - 51 -

5.1.2. WES, targeted sequencing and Sanger sequencing of human samples ..... - 51 -

5.1.3. *In silico* studies and quantitative real-time PCR ..... - 52 -

5.1.4. *In vitro* mutagenesis, transfection, and Western blotting ..... - 53 -

5.1.5. Analysis of RNA splicing ..... - 54 -

5.1.6. *In vitro* T cell activation and proliferation ..... - 55 -

5.1.7. *In vitro* cell-cycle analysis ..... - 55 -

5.1.8. T cell repertoire analysis ..... - 56 -

5.1.9. TCR internalization ..... - 56 -

5.1.10. Transferrin internalization assay ..... - 56 -
5.1.11. Generation of induced pluripotent stem cell (iPSCs) ..... - 57 -
5.1.12. Generation of Artificial Thymic Organoids (ATOs) from iPSCs ..... - 58 -

5.2. Murine studies ..... - 61 -
5.2.1. *In silico* prediction studies ..... - 61 -
5.2.2. Design and screening of *Fcho1* single guide RNAs (sgRNAs) and donor-template DNA ..... - 61 -
5.2.3. Generation of CRISPR/Cas9 *Fcho1*-mutant mice and genotyping ..... - 62 -
5.2.4. Analysis of RNA splicing ..... - 63 -
5.2.5. Mouse Immune Phenotyping ..... - 63 -
5.2.6. *In vitro* T cell activation and proliferation ..... - 64 -
5.2.7. *In vitro* internalization of T cell receptor (TCR) ..... - 65 -
5.2.8. B cell *in vitro* proliferation ..... - 65 -
5.2.9. Statistical analysis ..... - 66 -

6. RESULTS ..... - 67 -

6.1. Clinical characterization and immunological phenotype of the patients. ..... - 67 -

6.2. Studies on patients' variants ..... - 73 -
6.2.1. WES and targeted sequencing ..... - 73 -
6.2.2. Sanger sequencing ..... - 76 -
6.2.3. Effects of *FCHO1* variants ..... - 77 -

6.3. Expression studies on FCHO1 mutated protein and wild type gene ..... - 82 -
6.3.1. Western blotting ..... - 82 -
6.3.2. RNA splicing analysis ..... - 83 -
6.3.3. *In silico* studies and quantitative PCR analysis in physiological conditions ..... - 85 -

6.4. *In vitro* functional studies ..... - 89 -
6.4.1.T cell activation and proliferation ..... - 89 -
6.4.2.T cell cycle and apoptosis assay ..... - 91 -
6.4.3. T cell repertoire ..... - 92 -
6.4.4.T cell Transferrin internalization ..... - 94 -
6.4.4. Internalization of T cell Receptor (TCR) ..... - 96 -

6.5. Induced Pluripotent Stem Cells (iPSCs) ..... - 98 -

6.6. Generation of *Fcho1*-mutant mice ..... - 100 -

6.7. On-going experiments (human and murine) ..... - 108 -
6.7.1. Artificial Thymic Organoids (ATOs) ..... - 108 -
6.7.2. Analysis of murine RNA splicing ..... - 110 -
6.7.3. Mouse Immune Phenotyping ..... - 113 -
6.7.4. TCR and CD3 receptor internalization studies ..... - 117 -
6.7.5. T cell *in vitro* activation and proliferation ..... - 119 -
6.7.6. B-cell *in vitro* proliferation ..... - 120 -

7. Future Perspectives ..... - 122 -

7.1. Studies on *in vitro* differentiation of iPSCs into naïve T-cells ..... - 122 -

7.2. Murine studies ..... - 122 -

8. Discussion ..... *- 124 -*

9. Collaborations and publications ..... *- 129 -*

9.1. Collaborations ..... **- 129 -**

9.2. Publications and presentations ..... **- 130 -**

10. Bibliography ..... *- 133 -*

10. Acknowledgments e Ringraziamenti ..... *- 145 -*

11. Appendix ..... *- 146 -*

2. Abstract (Ita/Eng)

L'endocitosi mediata da clatrina (CME) è la via principale di endocitosi usata dalle cellule eucariotiche per internalizzare proteine di superficie (cargo) e molecole extracellulari, attività che consente lo svolgimento di una ampia gamma di processi biologici, tra cui il signalling intra-cellulare, l'internalizzazione di nutrienti e fattori di crescita, e la differenziazione e maturazione cellulare. Le molecole F-BAR domain only proteins 1 and 2 (FCHO1/FCHO2) intervengono durante il primo step della formazione dell'invaginazione di membrana rivestita da clatrina (pit). Questo studio presenta il primo caso di severa immunodeficienza dovuta a difetti genetici riguardanti la CME. Attraverso l'applicazione di tecniche di Whole Exome Sequencing e analisi di un pannello di geni correlati a immunodeficienze congenite (Primary Immunodeficiency Disease, PID), sono state identificate cinque diverse varianti bialleliche nel gene *FCHO1* con perdita di funzione (loss of function, LOF) in cinque pazienti caratterizzati da profonda linfopenia di tipo T e severe e ricorrenti infezioni batteriche, micobatteriche, virali e fungine. Solo un paziente è al momento in vita a 3.5 anni da trapianto allogenico di cellule staminali ematopoietiche con chimerismo completo del donatore. Studi eseguiti per valutare gli esiti molecolari delle varianti geniche riscontrate in *FCHO1* hanno rivelato la presenza di una proteina tronca nel caso dei pazienti 2 e 3, di nessuna proteina nel paziente 4. Il paziente 1 e 5 erano portatori di varianti in omozigosi in un sito di splicing con risultante skipping esonico nel cDNA (P1) o mRNA decay (P5). Analisi *in silico* di espressione molecolare e qPCR hanno rivelato una diversa espressione cellulare o tissutale dei geni *FCHO1* e *FCHO2*. In particolare, il primo è espresso prevalentemente in tessuti linfoidi e nelle cellule del sistema immunitario. Esperimenti *in vitro* di stimolazione e attivazione delle cellule T provenienti dal paziente 2 hanno rivelato una marcata riduzione della proliferazione, normale internalizzazione del recettore delle cellule T (T-cell receptor, TCR) e difettiva internalizzazione del recettore della transferrina, notoriamente dipendente da clatrina. Non è stata notata alcuna anomalia nel TCRβ (TCRB) repertoire. Questi studi dimostrano che la malattia da deficit di *FCHO1* è una nuova forma di immunodeficienza combinata con difettiva proliferazione e aumentata morte indotta da attivazione delle cellule T e difettiva internalizzazione mediata da clatrina.

Per comprendere a fondo le funzioni del gene *FCHO1* e studiare ulteriormente l'impatto di mutazioni patogeniche in mammiferi, in questo studio sono state sviluppate e utilizzate due

piattaforme con l'intento di modellare la malattia *in vitro* e *in vivo*. La tecnologia "Artificial Thymic Organoid" (ATO) consente di analizzare *in vitro* gli stadi di maturazione di cellule T naïve da cellule staminali pluripotenti indotte (induced pluripotent stem cells, iPSCs). Studi su iPSCs derivate da fibroblasti del paziente 1 e da cellule staminali ematopoietiche CD34+ del paziente con l'uso di questa piattaforma sono in corso e contribuiranno a svelare l'origine del difetto cellulare.

In letteratura non è riportato alcun studio su modelli murini con difetto in *Fcho1*. In questo studio, grazie all'uso della tecnologia di editing genico CRISP-Cas9, sono stati generate tre modelli murini *Fcho1* knock-in. Analisi preliminary sul fenotipo immunologico, attivazione. *In* vitro di cellule T e B e internalizzazione del recettore TCRαβ/CD3 suggeriscono presenza di un fenotipo lieve di tipo B nei topi mutanti.

Clathrin-mediated endocytosis (CME) is the major endocytic pathway by which eukaryotic cells internalize surface cargo proteins and extracellular molecules, thereby allowing for a broad range of biological processes, including, but not limited to, cell signaling, uptake of nutrients and growth factors, and cell fate and differentiation. The F-BAR domain only proteins 1 and 2 (FCHO1/FCHO2) are involved in the first stage of clathrin coat pit formation, also called nucleation. This study presents the first known cases of a severe immunodeficiency due to a genetic defect affecting CME. By using Whole Exome Sequencing and genomic analysis of a targeted PID gene panel, biallelic loss-of-function *FCHO1* variants were identified in five patients with profound T cell lymphopenia manifesting as recurrent and severe infections of bacterial, mycobacterial, viral and fungal origin. Only one patient is currently alive with full donor chimerism at 3.5 years after allogeneic hematopoietic stem cell transplantation. Studies aimed at assessing the molecular consequences of the *FCHO1* variants showed expression of truncated products in patient 2 and 3, whereas no protein was detected in patient 4. Patient 1 and patient 5 carried a homozygous splice-site variant, leading to skipping of exon 6 in the cDNA (patient 1) or mRNA decay (patient 5). *In silico* expression and qPCR analysis demonstrated differential expression of the *FCHO1* and *FCHO2* genes, with the former being predominantly expressed in lymphoid tissues and immune system cells, strongly associating the role of *FCHO1* variants with the pathogenesis of the disease. Analysis of T cell *in vitro* activation in patient 2 revealed markedly reduced T cell proliferation, normal TCR internalization in response to CD3 cross-linking and abolished transferrin internalization in activated T cells. No abnormalities of TCRβ (TCRB) repertoire were observed. These studies demonstrated that *FCHO1* deficiency is a novel form of combined immunodeficiency with impaired T-cell proliferation, increased activation-induced T-cell death, and defective CME.

To better understand the functions of the *FCHO1* gene and further study the impact of its pathogenic mutations in mammalian organisms, two disease-modeling platforms were set up in this study and are currently used for further investigations. The Artificial Thymic Organoid (ATO) technology allows *in vitro* studies of T cell maturation from induced pluripotent stem cells (iPSCs). This technology will help unraveling the origin of the T-cell defect in naïve T-cells differentiated from *FCHO1*-deficient iPSCs derived from Patient 1's fibroblasts and from Patient 2's CD34+ Hematopoietic Stem Cells.

No *Fcho1*-genetically modified mouse has ever been reported in literature. In this study, taking advantage of the CRISP-Cas9 technology, three *Fcho1* knock-in mutant mice were generated. Preliminary analysis on immunological phenotype, T-cell and B-cell *in vitro* activation and TCRαβ/CD3 receptor internalization suggested the presence of a mild B-cell phenotype in *Fcho1* mutant mice.

3. Introduction and literature review

3.1. Endocytosis

3.1.1. Clathrin-mediated endocytosis (CME)

Clathrin-mediated endocytosis (CME) is the major endocytic pathway by which eukaryotic cells internalize surface cargo proteins and extracellular molecules, thereby enabling a broad range of biological processes, including cell signaling, nutrients- and growth factors- uptake, and cell fate and differentiation. The first identification and observation of clathrin-coated vesicles (CCV) dates back to year 1964 in studies on protein uptake in oocytes of mosquito *Aedes Aegypti*. The deposition of protein yolk was observed to trigger invagination of the oocyte membrane and the formation of "pits", which maturated into bristle-coated vesicles containing the yolk protein (1). The actual definition of clathrin as a lattice-like coating protein was established in a later study performed on vesicles obtained from brain, adrenal medulla and a lymphoma cell line. A protein with molecular weight of 180 kDa, arranged in a hexagons and pentagons network, was described as the major component coating vesicles of different sizes involved in the internalization of extracellular material, not associated with secretory operations, and called clathrin (2). Since then, many studies have uncovered the biological functions of clathrin and CME and its involvement in physiological and pathological processes including, but not limited to, cellular signaling, development, immunity, infections and genetic disorders. However, many questions on clathrin biology, evolution and regulation, remain still unanswered. Clathrin-coated vesicles are small (60-120 nm) and transport into the cytoplasm cargo molecules such as transferrin, immunoglobulins, low-density lipoproteins, hormones, among many others (3). The endocytosis of extracellular material occurs constitutively (transferrin and LDL) or upon stimulation by binding of a ligand (EGFR, receptor Tyr-kinases). Coated vesicles also generate from intracellular membranous compartment, but the term clathrin-mediated endocytosis refers exclusively to the extracellular intake of molecules from the plasma membrane. After internalization, the cargo is sorted into endosomes and either recycled back into surface, further processed to more mature endosomes or degraded inside lysosomes. In this way, CME regulates the intake of extracellular molecules and

also the expression of surface receptors and proteins, the turnover of membrane components, the activation of signaling pathways and the composition and recycling of synaptic vesicles. Some viruses (Rhinovirus, Vesicular Stomatitis Virus), bacteria (Listeria monocytogenes, Candida albicans) and toxins (Botulin toxin B, Cholera toxin) take advantage of CME to penetrate into their target cells. Since the first description of CME, more than 50 years ago, over 50 proteins have been identified as part of the CME machinery. The whole process is formally divided in five stages: nucleation, cargo selection, coat assembly, scission and uncoating (Figure 3.1) (4). The entire cycle lasts less than 1 minute.

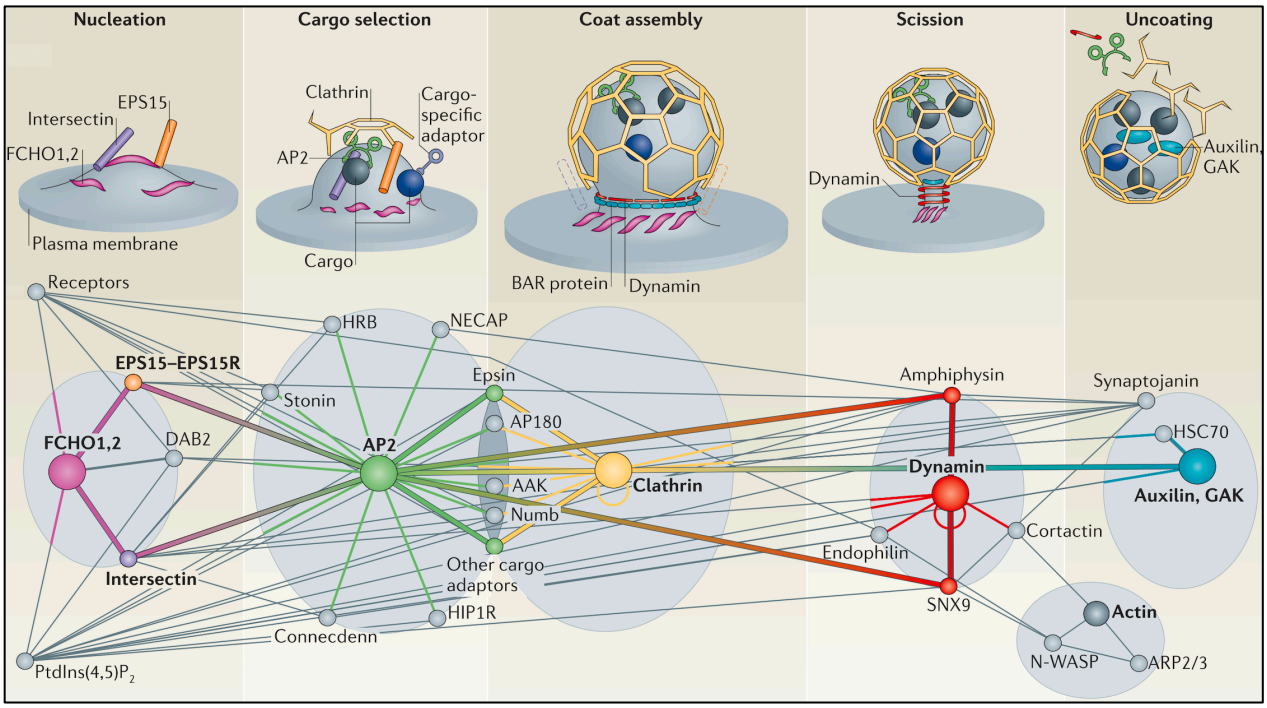

Figure 3.1. The clathrin-coated vesicle cycle. Stages of clathrin-coated vesicle formation and internalization (nucleation, cargo selection, coat assembly, scission and uncoating) with the main proteins involved. FCHO1/2 (pink), AP2 (green), Clathrin (yellow), Dynamin (red) and Auxilin, GAK (turquoise) are the principal hubs of CME (From McMahon and Boucrot, Nat. Rev. Mol. Cell. Biol., 2011) (4).

Nucleation, also called initiation, is the first step in the organization of the clathrin-coated vesicle, and a key moment of regulation of the endocytic events. It triggers an invagination at the plasma membrane (called clathrin coated pit, CCP) and it is reported to initiate either randomly at no preferred sites or not-randomly at defined positions (hotspots). In the first case, nascent CCPs are not stabilized by the arrival of the nucleation and adaptor protein machinery, do not mature further and eventually collapse (called abortive events) (5). On the contrary, hotspots corresponding to real endocytic sites have endocytosis-promoting properties. CCP maturation and development is sustained by the CME adaptor machinery (6). Whether cargo molecules constitute an essential component for the nucleation or are only passive passengers, is still an open question. It is known that, for a successful coated-vesicles maturation, early adaptor proteins are recruited by self-associating and binding to the Phosphatidylinositol 4,5-biphosphate ($PI(4,5)P_2$) of the cell membrane, inducing and stabilizing the membrane curvature (7). $PI(4,5)P_2$ regulation and turnover is required for initiation, stabilization, growth and maturation of the CCP. Bulk levels regulate CCP assembly, but $PI(4,5)P_2$ turnover by 5'-dephosphorylation plays a role in many stages of the formation of the vesicle. In support of this notion, several phosphatases, like the SH2-domain-containing inositol 5'-phosphatase, SHIP2, and the synaptojanin (Sjn) 1, are part of the CME machinery (8). The nucleation proteins comprise the adaptors FCH domain only (FCHO) proteins, the SGFR pathway substrate 15 (EPS15) and the intersectins (9). During cargo selection, the nucleation module recruits the adaptor protein 2 (AP2), which is the most abundant component of CCV after clathrin (10). Different adaptor proteins have been found in different cells (AP1, AP2, AP3, AP4), AP2 is specifically involved in CCV formation at the plasma membrane (11), acting as a "bridge" that links clathrin to the cargo, the $PI(4,5)P_2$ and the adaptor proteins. In different cell types, different adaptors and accessory proteins are part of the CME machinery. Nucleation and adaptor proteins always bind to the adaptor AP2, which is therefore considered the major hub of interactions during CCV maturation. If AP2 is depleted, nucleation still take place, but clathrin is not recruited and a CCV does not form (12). AP2 proteins keep sampling the inner side of the membrane and bind weakly to $PI(4,5)P_2$, rapidly dissociating form it. If AP2 encounters a nucleation protein complex ($PI(4,5)P_2$/FCHO/EPS15/Intersectin), it binds one clathrin triskelion and recruits more AP2/clathrin triskelia, which then stably associate with $PI(4,5)P_2$, and, in turn, start building the clathrin hexagons and the CCV (Figure 3.2) (13).

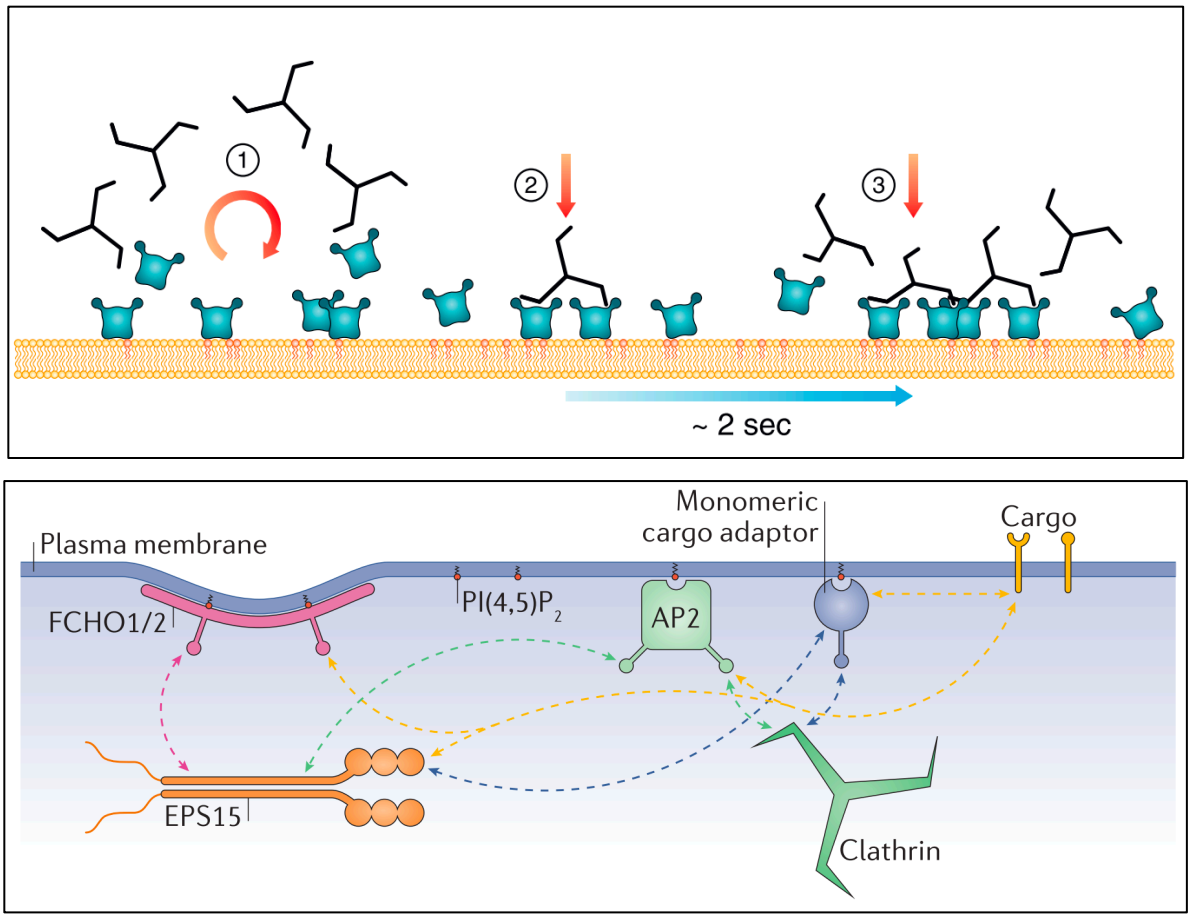

Figure 3.2. Recruitment of Clathrin during the First Five Seconds of Coated Pit Formation. Upper panel, schematic representation of the early events during initiation of coated pit formation. (1) AP2 weakly binds $PI(4,5)P_2$, (2) First initial stably association of two AP2 and one triskelia at plasma membrane, (3) Incorporation of more AP2/clathrin triskelia blocks and initial CCP formation. (From E. Cocucci et al., Cell., 2012) (13). Lower panel, pioneer module that initiates membrane budding. (From M. Kaksonen et al., Nat. Rev., 2018) (3).

After cargo selection, the coat assembly takes place. AP2 and accessory proteins recruit clathrin triskelia that polymerize into hexagonal structures, thus stabilizing the membrane curvature and simultaneously displacing certain nucleation and accessory proteins, like EPS15 and epsin, that in fact are not found in the budded CCV (14). During scission, the enzyme dynamin, recruited by BAR domain containing proteins amphiphysin, endophilin and sorting nexin 9, polymerizes around the neck of the CCP, favoring GTP hydrolysis and membrane fission (15). During the last step of the CME cycle (uncoating), dynamin facilitates the disassembly of the clathrin triskelia by

the ATPase heat shock cognate 70 (HSC70) and its cofactor auxilin (cyclin G-associated kinase (GAK) in non-neuronal tissues. The CCV can thus detach and travel to its target endosome the protein of the CME machinery are released back into the cytoplasm and become available for another round of CME, and (16).

3.1.2. Clathrin-independent endocytosis

Intake of extracellular material inside cells occurs also through mechanisms other than CME, that are dependent on molecules (caveolin) or completely independent (clathrin- and caveolin-independent internalization), whose all specific cargos are not fully defined yet (Figure 3.3) (4).

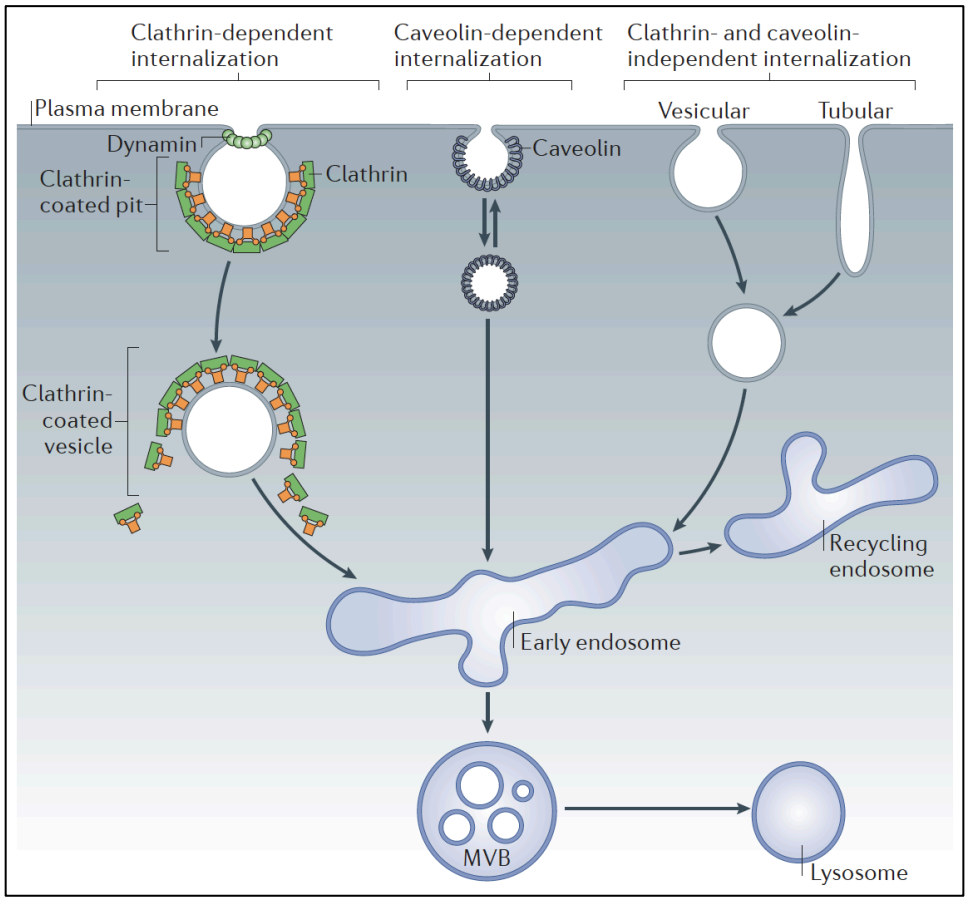

Figure 3.3. Clathrin-dependent and -independent internalization pathways. Most common pathways of cellular endocytosis: clathrin-dependent, caveolin-dependent and clathrin- and

caveolin-independent internalization (From H. T. McMahon and E. Boucrot, Nat. Rev. Mol. Cell. Biol., 2011) (4).

Caveolae are cholesterol- and glycosphingolipids-enriched plasma membrane domains that contain caveolin and are involved in the uptake of toxins and viruses (17), as well as endocytosis of some receptor of immune cells like interleukin-2 receptor β chain (18) and the common gamma-chain receptor (19). Clathrin-mediated endocytosis relies on GTP hydrolysis to produce mechanical energy used by dynamin to constrict the cellular membrane and reach hemi-fission with the support of the BIN/amphiphysin/Rsv (BAR) domain-containing protein amphipysin and endophilin (N-BAR protein) (20, 21). Clathrin-independent endocytosis, however, does not necessarily rely on dynamin, but often takes advantage of BAR proteins to perform the scission of the nascent CCV at plasma membrane level. The N-BAR protein endophilin, specifically the endophilin-A2 (endoA2), has been associated with the uptake of the Shiga and Cholera toxin, defining a new endocytic route of fast endophilin-clathrin-independent-mediated endocytosis (FEME) (22, 23). Several receptors are endocytosed upon binding of their ligand (α_{2a}- and β_1-adrenergic receptors, dopaminergic D3 and D4 receptors, EGF-, HGF-, VEGF- receptors, and IL-2 receptor) following the FEME pathway. Another clathrin-independent pathway of internalization was shown to be dependent on flotillins, proteins that have been identified in purified endosomes and reported to act in cholera toxin B internalization (flotillin-1) (24) and in T-cell activation and in T-cell Receptor (TCR) recycling to the immunological synapse (25). Clathrin- and caveolin-independent internalization also occur when ligands are in high concentrations at the plasma membrane, where they are ubiquitinated and internalized with the aid of Eps15 and epsin, but without clathrin intervention (ubiquitinated epidermal growth factor (EGF) receptor (EGFR) internalization (26, 27).

3.2. F-BAR-containing Fer/Cip4 homology domain-only proteins 1 and 2 (FCHO1/2)

Membranes of eukaryotic cells are in a dynamic flux and continuously changing in shape and composition, through fission and fusion of carriers and molecules to and from the plasma membrane or intracellular organelles (28). Membrane fission is a biological process depending on GTPases of the dynamin family, promoted by the membrane-associated BAR domain proteins (29). The N-terminal Bin/Amphiphysin/Rvs (BAR) domain is highly conserved in eukaryotes and found in many families of protein associated with dynamic changes of the plasma membrane (the F-BAR, the N-BAR and the I-BAR domain family) (30). F-BAR, N-BAR and I-BAR proteins homodimerize to induce a growing curvature of the flat membrane with a radius that is specific for each family. F-BAR domain is associated to a shallow degree of concavity, N-BAR to a more profound degree and I-BAR to a convexity that protrudes outside of the membrane (Figure 3.4) (31).

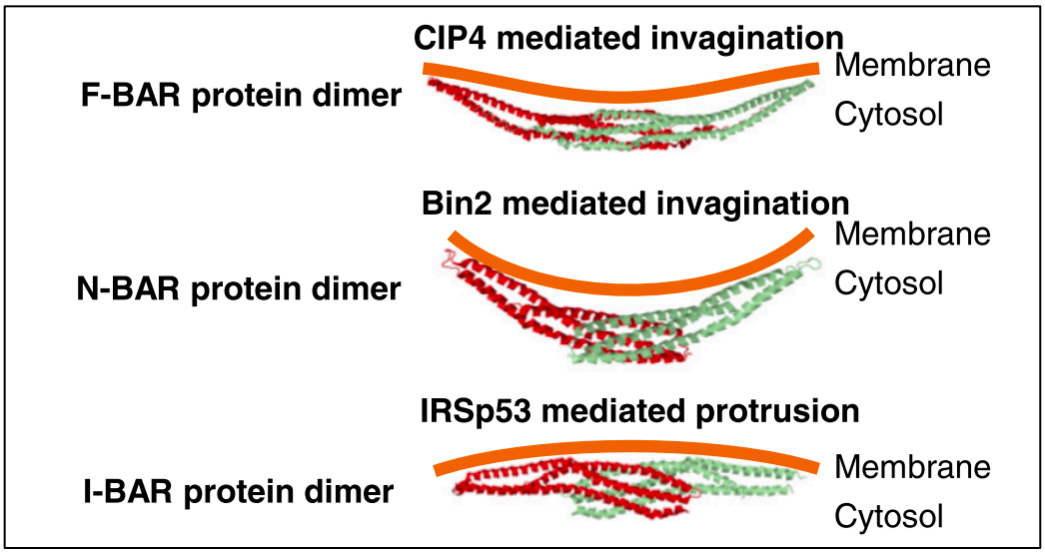

Figure 3.4. Membrane curvature determined by BAR domain proteins. F-BAR, N-BAR, and I-BAR proteins bind to cell membrane and lead to different forms of curvature changes (Adapted from Liu et al., J. of Hem. & Onc., 2015) (31).

Because of their diverse curvature properties, BAR proteins are involved in distinctive biological processes. F-BARs and N-BARs take part in invagination operations of endocytosis and phagocytosis, I-BARs intervene in angiogenesis, and formation of filipodia and lamellipodia. The F-BAR family comprises 9 members (CIP4, FCHO, SrGAP, PACSIN, PSTPIP, FCHSD, FES/FER, NOSTRIN, GAS7 subfamily). At the N-terminus of the protein, the F-BAR domain binds to the $PI(4,5)P_2$ on the inner side of the cellular surface. After binding, F-BAR proteins polymerize and self-organize to induce curvature formation through helical lattices formation (32). At the C-terminal, most of the F-BAR proteins contain one or more Src homology 3 (SH3) domains, which allow interaction with proline-rich proteins (Wiskott-Aldrich syndrome protein (WASP), neural (N)-WASP, and Wasp family verproline-homologous protein (WAVE). After binding, actin-related protein 2/3 (Arp 2/3) and G-actin are recruited, and actin nucleation and polymerization follow (31). The membrane-sculpting F-BAR domain-containing Fer/Cip4 homology domain-only proteins 1 and 2 (FCHO1/2) are the only members of the FCHO subfamily. FCHO proteins cluster at cellular membrane sites before clathrin arrival and dissociate before the CCV detaches from the membrane. FCHOs were initially thought to be fundamental for initiating the budding of the plasma membrane and CME (33). However, it was then demonstrated that they are specifically involved in the process of maturation and stabilization of clathrin-coated pit and growth sustainance of the clathrin coat, but are not essential for coated pit initiation (13). The human *FCHO1* gene is located on Chromosome 19; it is 3204 base-pair long and encompasses 29 total exons including 26 coding exons (Chromosome 19: 17,747,718-17,788,568 forward strand; GRCh38:CM000681.2, ENST00000596536.5) (34). The human FCHO1 protein is 889 amino acid-long and its structure is schematically represented in Figure 3.5. The *FCHO2* gene, located on Chromosome 5, is 4921 base-pair long with 26 total and coding exons encoding for a 810 amino acid-long protein (Chromosome 5: 72,956,041-73,090,522 forward strand; GRCh38:CM000667.2, ENST00000430046.7) (35). The murine *Fcho1* gene (CL57BL6 strain), located on chromosome 8, is 3073 base-pair long, includes 26 exons and encodes for an 873-aminoacid-protein (Chromosome 8: 71,708,387-71,725,716 reverse strand; GRCm38:CM001001.2; ENSMUST00000093444.12) (36), murine *Fcho2* on Chromosome 13, is 5122 base-pair long with 26 total and coding exons for a 809 aminoacidic long protein (Chromosome 13: 98,723,403-98,815,449 reverse strand; GRCm38:CM001006.2; ENSMUST00000040340.15) (37).

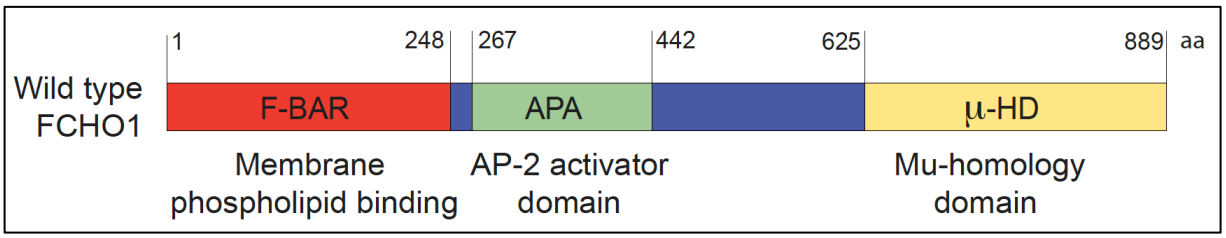

Figure 3.5. FCHO1 protein. Schematic representation of wild type human FCHO1 protein with the three different domains (F-BAR, APA and μ-HD) and the corresponding aminoacidic (aa) positions.

The N-terminal F-BAR domain mediates attachment to phospholipids of the cell membrane, whereas the C-terminal μ-homology (μ-HD) domain interacts with the adaptors epidermal growth factor receptor substrate 15 (EPS15) and intersectin 1, which hetero-oligomerize during linking to the μ-HD. Other fundamental accessory proteins converge on the μ-HD, which was therefore described, along with AP2, as an endocytic hub of CME (38). The linker region of FCHO1 acts as an allosteric activator of the adaptor protein 2 (AP2) complex, enabling recruitment of clathrin to the assembling coat. The AP2 complex is a bridge between the cargo and clathrin and is maintained in a closed conformation at resting state. After binding to FCHO1, AP2 is converted into an open and active conformation, and the FCHO1-AP2-cargo complex stabilizes the nascent coated pit and initiates the clathrin assembly (39, 40). FCHO proteins were first described as proteins part of the CME machinery in 2010 (33). Many open questions on their biology, differential expression and functions still need to be addressed.

3.3 Physiological functions of CME and its role in the immune system

Constitutive or ligand-triggered internalization of many receptors relies on CME. Receptors bind to metabolites, like cholesterol or iron, to growth factors, like epidermal growth factor (EGF), to signaling molecules, like cytokines, or to other molecules, like immunoglobulins, triggering responses of internalization of the complex receptor-molecule and/or activation of downstream signals.

3.3.1 Iron metabolism and T-cell activation

Iron is a metabolite essential to all living organisms, especially vertebrates, and its uptake from the environment and molecular distribution to the eukaryotic cells relies on specific and well-defined mechanisms. Free iron is insoluble in water and plasma, therefore needs to be carried by transport proteins. To this purpose, vertebrates use an 80 kDa protein with two iron-affinity binding sites called transferrin. Circulating iron-free apotransferrin forms holo-transferrin after binding to 2 $Fe^{(3+)}$ ions. The transferrin receptor (TfR, CD71) is a transmembrane glycoprotein which binds to- and allows the uptake of- extracellular transferrin-iron complexes from the outside space into the cellular cytoplasm, and the amount of internalized iron is strictly dependent on this mechanism (41). TfR1 mediates iron uptake in all cells and is highly expressed in rapidly proliferating cells. By contrast, TfR2 is selectively expressed in hepatocytes and erythroid precursors (42). Once formed, the complex holo-transferrin-TfR on the extracellular side of the cellular membrane is internalized by CME. TfR (TfR1/2) is a cargo known to be internalized by CME (43) and, in resting conditions, TfR1 is minimally expressed on the surface immune cells. The importance of iron for adaptive immunity is documented in studies conducted in mice and rats. In animals kept under an iron-deficient diet, thymocytes were the first cell compartment affected by deprivation and showed decreased proliferative response after only one week of iron-deficient diet. Anemia and reduced storage of iron were observed starting from three weeks after the beginning of the diet (44). Splenic lymphocytes were also shown to be affected by iron-deficient anemia and incapable of mounting a proper blastogenic response in vivo (45). The increased expression of CD71, and subsequent iron internalization, is fundamental to initiate and sustain proliferation of quiescent T-cells (46). In humans, mitogen-stimulated T lymphocytes,

induction of transferrin receptor by IL-2 activating signal is important for DNA synthesis and efficient cellular proliferation (47). Naïve CD4+ and CD8+ T cells are physiologically maintained in a quiescent state (G0 phase of the cell cycle), but after T-cell receptor (TCR) interaction with the MHC complex on antigen presenting cells (APCs) and co-receptor-ligand (CD28, ICOS) binding, they become activated, shred CD62L/L-selectin from surface, upregulate CD44 (marker of effector T-cells), Interleukin-2 (IL-2) receptor (IL-2R or CD25/CD122/CD132) and TfR1 (CD71) and undergo clonal expansion. CD25 and CD71 are late markers of T-cell activation. Their expression on T-cell surface begins 24 hours after activation, peaks at 48/72 hours, and starts declining 96 hours after activation. CD69, a membrane-bound type II C-lectin receptor, is a classical early marker of lymphocyte activation. It is rapidly expressed on the cell surface within hours (being detectable after 30-60 minutes) and declines after 4-6 hours (48). Another mechanism of iron-related cellular homeostasis involves iron availability to regulate cellular sensitivity to the IFN-g/STAT1 signaling pathway. Iron uptake triggers a signal leading to IFN-g signaling-chain-internalization and to IFN-g/STAT1 T lymphocytes refractoriness, controlling the clonal expansion of activated T-cells (49). Moreover, iron is important during thymocyte proliferation and maturation, particularly from the CD44- CD25+ CD4- CD8- CD3- double negative 2 phase to the CD4+ CD8+ CD3- double positive phase (50) and in fact, CD71 expression marks immature cycling thymocytes (51). Iron was also described to play a role in the T-helper-driven pathogenesis of some autoimmune/autoinflammatory conditions, like Multiple Sclerosis. Its deposition was found responsible for promoting secretion of pro-inflammatory cytokines by T-helper cells via the RNA-binding protein PCBP1, underlying once again the importance of iron homeostasis and metabolism in the activation and suppression of the immune system (52).

3.3.2 Cell cycle

In eukaryotes, the cell cycle is a series of events that drive generation of two daughter cells from one mother cell and is formally divided in the G_0 phase (quiescence), Interphase (G_1 or first growth phase, S or DNA replication phase, G_2 or growth phase), Mitosis (chromosome separation) and Cytokinesis (separation of cellular component). Mitosis separates the genomic material in an identical manner into the two daughter cells. A fundamental step of mitosis is the generation of the mitotic spindle that drives the equal separation of the sister chromatids (53). Studies on mitosis

have revealed another important role of clathrin, besides endocytosis, which is the stabilization of the spindle apparatus to aid separation of chromatids. No major nucleation or adaptor proteins that are seen in CME are found at the spindle apparatus level. The heavy chain domain of clathrin binds to the microtubule of the spindle via their N-terminal domain (54) with the help of the spindle protein transforming acidic coiled-coil protein 3 (TACC3) and the cytoskeleton-associated protein 5 (CKAP5) (55). Whether CME arrests or persists during mitosis is still an open question. Initially, CME was thought to stop during mitosis and many studies confirmed this hypothesis (56-59). However, most of these experiments were performed by use of compounds like Nocodazole, S-Trityl-L-cysteine, or RO-3306 to block mitosis, or by starving cells in serum-free media, thereby falsely increasing the amount of TfR on cellular surface and erroneously deducting that CME stops during mitosis, or mis-leading to a low estimate of the endocytic rate. More recent studies showed that CME is not arrested during mitosis, but rather continues unperturbed throughout all the phases of cellular division. Recycling of endosomes or internalized receptor is diminished during metaphase and reactivated during anaphase; the downregulation of TfR seen on cellular surface is caused by its retention in endosomes and not by CME arrest. Altogether, these data suggest an important role of CME and iron/TfR not only for the preparation of the cellular division, but also during mitosis (60).

3.3.3 Cytokine receptors

Many of the processes that control function and development of the immune system require cytokines signaling, including growth, maturation and differentiation of hematopoietic cells, mature white blood cells fitness, downregulation of the immune response and return to homeostasis status. Endocytosis plays a fundamental role in cytokines signaling. Endocytic mechanisms regulate plasma membrane receptor signaling through different mechanisms, including internalization of the receptor and termination of the signal, recycling of receptors to cellular surface, endocytic sorting and intracellular storage or sequestration of receptors. In some cases, the mechanisms involved in internalization of cytokine receptors are well defined, but for the most part they are still controversial (61). Cytokine receptors are linked to a broad spectrum of downstream signal pathways, making cytokine biology a very complex topic. The majority of cytokines receptors are internalized through clathrin-independent endocytosis. The Interleukin-1

receptor (IL-1R) superfamily is composed by 4 members: IL-1, IL-18, IL-33 and IL-36 receptors. IL-1R undergoes constitutive and ligand-triggered caveolin-1 or cholesterol-mediated internalization and does not require clathrin intervention (62). On the contrary, during internalization, IL-36R seems to co-localize both with the CME-cargo TfR and with the cholera toxin, which is internalized by clathrin-independent endocytosis, suggesting that this cytokine follows both clathrin dependent- and independent- endocytosis (63). Many receptors of the g-common chain (CD132) family undergo clathrin-independent endocytosis. The common g chain is a subunit of multiple cytokine receptors that can bind IL-2, IL-4, IL-7, IL-9, IL-15 and IL-21(64). Interaction of the cytokine with the specific γ-chain receptor triggers activation of the Janus Kinase (JAK) and Signal Transducer and Activator of Transcription (STAT) pathway, which ultimately turns on nuclear transcription of target genes involved in cellular development and proliferation. The g-common chain internalization is dependent on dynamin and actin polymerization, but is not reported to depend on CME (65). The IL-2 receptor is a heterotrimer composed of IL-2Rα (CD25), IL-2Rβ (CD122), and IL-2Rγ. IL-2 signal is required for T cell proliferation, antigen-induced cell death and boosting of cytolytic activity of NK cells. Interaction of IL-2R with its ligand IL-2 triggers activation of a signal for T-cell proliferation, CME internalization of the complex IL-2R/IL-2 and its degradation in lysosomes. Interestingly, when CME is inhibited and TfR internalization does not occur, IL-2R are still partially able to be endocytosed, suggesting the presence of an alternative mechanism to CME for IL-2R internalization (66). IL-7 plays a fundamental role in T-cell development and IL-7 signaling is downregulated with a negative feedback through IL-7R internalization after ligand binding. Studies on human and mouse IL-7 receptor alpha chain (IL-7Rα) showed that human IL-7 is a pivotal cytokine for differentiation into T-cell lineage, but not for B-cell and NK-cell development. Specifically, IL-7 governs the critical transition of maturating thymocytes from the early double negative stage to the double positive CD4+ CD8β+ stage (67). CME is the only identified mechanism for IL-7R internalization at both steady state and after binding to IL-7, and is thought to be fundamental for a proper IL-7 signal transduction (68). One of the most studied receptors is the Tumor Necrosis Factor Receptor 1 (TNFR1), however, the route of TNFR1 internalization is still not fully defined. TNFR1 is internalized after binding to its ligand, TNF-a, and is not recycled back to the cellular surface (69). It has been demonstrated that TNFR1 colocalizes on the cell surface with caveolin rich domains, but not with clathrin-coated pits (70). Interestingly, inhibition

of caveolin-1 or flotillin-2 does not affect internalization of TNFR1 (71). FAS cell surface death receptor (Tumor necrosis factor receptor superfamily member 6, TNFRSF6, CD95) and its ligand FASL (Tumor necrosis factor ligand superfamily member 6, TNFSF6, CD95L) are involved in regulation of apoptosis, or programmed cell death. Among other functions, they determine the physiological elimination of self-reactive thymocytes and thymocytes that fail to rearrange their T cell receptor, as well as lead to activation-induced T cell death, responsible to bring the immune response back to homeostasis status. Internalization of the death receptor Fas (CD95) is also still debated. Data suggests that clathrin-independent endocytosis is the primary way of CD95 internalization, but there are also reports on clathrin and dynamin intervention during CD95 endocytosis (72).

3.3.4 T cell (TCR) receptor

T cell receptor (TCR) is a complex formed by six different subunits. TCR recognizes short peptides (antigen fragments) bound to Major Histocompatibility Complex (MHC). MHC I molecules are expressed on the surface of all the nucleated cells, and present peptides to CD8+ cytotoxic T-cells. By contrast MHC II molecules are expressed by antigen-presenting cells (APCs) and present peptides to CD4+ T helper cells, thereby inducing T cell activation and immunological responses. The majority of T cells express two TCR subunits, α and β, joined by disulfide bonds and encoded by genes that undergo a process called somatic recombination, where variable (V), diversity (D), joining (J) domains are subject to genetic rearrangements. A minority of T cells express γ and δ subunits that show a different type of antigen specificity. The TCR complex is also composed by genetically related CD3γ, CD3δ and CD3ε subunits that are parts of the same C-type immunoglobulin superfamily. TCR is completed by the CD3ζ subunit which, with its long intracellular tail, is structurally very different from the other TCR and CD3 subunits. The CD3ζ displays three copies of the immunoreceptor tyrosine-based activation motif (ITAM) that auto-phosphorylates upon stimulation of the TCR and couples with the 70-kD zeta-associated protein (ZAP-70), a tyrosine kinase that plays a pivotal role in the initiation of T-cell downstream signaling. A structural model is presented in Figure 3.6 (73).

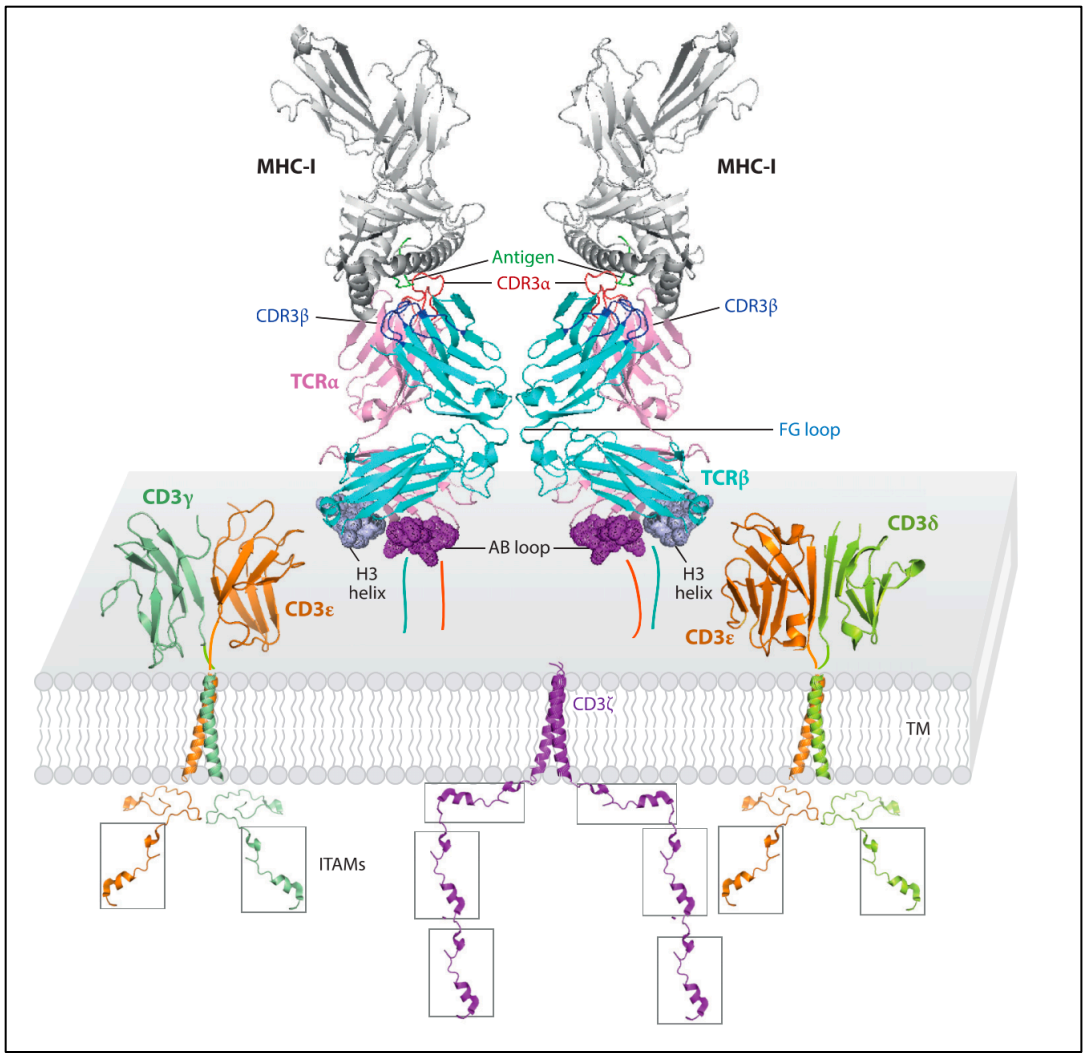

Figure 3.6. Structural model of the TCR-CD3 complex. From A. Alcover et al., Annu. Rev. Immunol., 2018 (73).

Many cell biology processes that participate at T cell maturation and effector functions are dependent on the correct TCR assembly and function. The TCR/CD3 complex is constitutively internalized and recycled back to the surface, and many cycles are rapidly repeated before it is eventually degraded in lysosomes. Engagement of the TCR by MHC on APCs in the immunological synapse also leads to internalization of the TCR/CD3 complex and triggers multiple downstream signals that ultimately determine T cell activation and proliferation (73). TCR/CD3 internalization has anecdotally been attributed to CME, but recent studies showed that activation of TCR/CD3 triggers its internalization through clathrin-independent endocytosis,

orchestrated by flotillins, into a specialized sorting compartment. This mechanism was also demonstrated to control recycling of TCR back to the immunological synapse. Moreover, flotillins were shown to have a fundamental role in the phosphorylation of protein downstream to TCR and CD69/CD25 expression of T cell surface, with a role in T-cell activation (25).

3.3.5 B cell (BCR) receptor

Surface antigen recognition molecules of B cells (B cell receptor, BCR) are composed by 2 heavy chains and 2 light chains joined by disulfide bonds. On mature B cells, BCR is made by one of either IgM or IgD, associated with one Igα/β (CD79A/CD79B) heterodimer containing the immunoreceptor tyrosine-based activation motifs (ITAM), responsible for the intracellular signaling (74). During the recognition process of humoral immunity, membrane immunoglobulins bind surface antigens, associate with the coreceptor CD19 and organize in microclusters, triggering BCR/antigen internalization and activation of downstream signals through the Bruton Tyrosine Kinase (BTK) (phosphorylates Phospholipase C, which hydrolyzes Phosphatidylinositol 4,5-bisphosphate (PIP_2) into inositol triphosphate (IP3) and diacylglycerol (DAG), which is the cytoplasmic key regulator of B cell development activated upon stimulation of the BCR, that ultimately lead to MHC class II antigen presentation to helper T cells (75). CD19 and CD21 are fundamental for activating downstream signals through the recruitment of intracellular adaptors (76). BCR is known to be mainly internalized through CME and its internalization is regulated by the activation of downstream signaling (77). In addition to CME, another BCR endocytic mechanism has been described, which is clathrin-independent and relies on lipid rafts internalization and BCR delivery into the endocytic compartment (78).

3.3.6 Other receptors

Cluster of differentiation antigen 4 (CD4) and 8 (CD8) are T-cell antigen surface receptors that define the T-helper (CD4) and the T-cytotoxic (CD8) subsets. CD4 binds to antigen presented through surface MHC-II of APCs, CD8 binds to antigen presented through the MHC-I of all nucleated cells. CD4 is also one of the co-receptors that the human immunodeficiency virus (HIV), by using of the Nef protein, uses for entering inside its target cells and simultaneously

downregulating its surface expression. Studies on CD4 internalization were extensively performed during *in vitro* infection with HIV, and showed that Nef interacts with the clathrin adaptor protein complexes 2 and 1 (AP2 and AP1), triggering CME internalization and downregulation of CD4. Many *in vitro* studies were also performed using HeLa or Jurkat cells, which underlined the importance of CME for CD4 internalization (79, 80). To carry out their cytotoxic functions, CD8+ T-cells releases granules containing cytotoxic molecules in the immunological synapse. These granules are then recycled by the CD8+ T cells and re-used in multiple rounds of killing through CME mechanisms (81). Studies that analyzed the CD8 receptor internalization concluded that this process is dependent on CME. However, most of them were performed using *in vitro* constructs, transfecting cells that normally do not express CD8 with CD8-plasmids or CD8-LDL-hybrid plasmids (82), or with CD8 tagged with reporter molecules (83). Caution should be used when drawing conclusions from systems that (over)-express a molecule normally not present in the cellular subset used, or from studies done in pathological condition, like HIV infection. How CD4 and CD8 are internalized in T-lymphocytes, is still an open question.

CD5 is a glycoprotein constitutively expressed on T cells and on the B1a subset of B cells, and a key regulator of lymphoid homeostasis in these cellular subsets. CD5 internalization is dependent on CME. In immature T cells, CD5, CD28, CD43 and Fas contribute to the medullary negative selection of thymocytes (84). In mature T cells, CD5 acts as a synergic costimulatory molecule with TCR/CD3 stimulation (85). The effect of CD5 on BCR, however, can be both inhibitory or costimulatory, depending on the ligand that binds the CD5 receptor (86, 87). Overexpression of CD5 is speculated to impact lymphoid homeostasis, disrupting thymic negative selection and increasing generation of autoreactive T cell clones, altering regulation of activation of mature T cell, lacking inhibition of B cell tolerance and co-stimulation in immature and mature B cells, respectively (88).

CTLA-4 is a surface receptor expressed in activated T-cells, which function is that of depressor of the activating signals through competing with CD28 in binding B7-1/2. CTLA-4 plays a fundamental role in preventing excess T-cell stimulation, downregulating of the signal and avoiding autoimmunity phenomena, and is removed from the plasma membrane through a CME pathway (89). In activated T-cells, CTLA-4 is rapidly internalized and recycled back to the cellular surface with many cycles involving clathrin-mediated endocytosis (90). Moreover, recent studies showed that, after binding to B7-1/2, CTLA-4/B7-1/2 internalize as a complex, removing the

costimulatory receptor from the APCs surface and impeding further transmission of the activating signal (91).

3.3.7 Natural Killer cells

Natural Killer (NK) cells are part of the innate immune system, but in many aspects are related to T cells (killing mechanisms shared with CD8+ cytotoxic T cells, secretion of IFN-g, recognition of MHC antigens). They exert their functions of recognition and killing of infected or transformed cells through NK-receptors (NKR) that mediates activating signals (aNKR) or inhibitory signals (iNKR). iNKR, like the human killer cell Ig-like receptors (KIRs), engage with MHC class I (MHC-I) expressed on surface of normal cells and prevent unnecessary killing by NK cells (92, 93). Surface levels of KIRs determine the threshold of NK cells activation and critically controls NK cells activation and NK cell MHC-I-tolerance. CME was identified as the mechanism regulating KIRs surface expression, through AP-2-mediated internalization of nonengaged KIRs and subsequent downregulation of NK-cell inhibition, making NK-cells more prone to activation. When KIRs bind to the MHC-I, on the contrary, CME is reduced, and NK cells activation is prevented (94).

One of the mechanisms used by NK cells and CD8+ cytotoxic T cells to induce apoptosis and kill infected or transformed cells is represented by the release of cytotoxic granules at the immunologic synapse. The granules contain proteases that, upon uptake from the target cell, induce death by apoptosis, which is entirely dependent on perforin (95, 96). Perforin determines a Ca^{2+} influx into the cells by creation of membrane pores in the target cellular membrane, which in turn triggers a healing response involving intracellular endosomes and lysosomes, that fuses to the membrane to carry on reparation processes (97). Perforin also triggers internalization of granzyme B and perforin in large vesicles (gigantosomes) through CME. Absence of internalization shifts death of cells from controlled apoptosis to uncontrolled necrosis, and is thought to be responsible of the lack on inflammation in apoptotic granzyme/perforin targeted cells (68).

3.4. Defects of CME

3.4.1. Murine knock-out studies

CME is a well-regulated process ubiquitously present in many types of cells. It's therefore not surprising that disruption of any of the main components of CME does not allow embryonic physiological development and results in early intra-uterine death. Knock-out of the μ2 subunit of the AP-2 complex in mice leads to arrest of intra-uterine growth and death during early embryonic development (before blastocyst stage) and demonstrated the indispensability of AP-2 and CME for mammals' embryonic development (98). Embryonic arrest of development with Notch signaling disruption is seen in the absence of both epsin 1 and epsin 2, two endocytic adaptors involved in CME. However, single knock-out mice do not present any visible phenotype and have normal viability, growth and fertility. Intercrossing of double epsin 1 and epsin 2 heterozygous generated three-allele mutant mice, but no double epsin 1/2 knock-out mice, confirming embryonic lethality of the latter genotype. Mice born with only one allele of epsin 1 or epsin 2 were affected by increased pre- and peri-natal mortility, growth failure, reduced fertility (99). Knock-out mice for the endocytic adaptor Eps15 do not manifest any defects of embryonic development, mouse growth or fertility, or increased mortality. However, experiments on hematopoietic stem cell transplantation (HSCT) uncovered the role of Eps15 in regulation of marginal zone cell numbers (100). Eps15L is a Eps15 homologous and a redundant accessory protein of CME. Both adaptors are essential during development and double Eps15/Eps15L knock-out mice are embryonically lethal. Because of their function in regulating TfR internalization, lack of Eps15 or Eps15L leads to a phenotype restricted to the erythrocyte-compartment with microcytic hypochromic anemia. Eps15L plays a unique role in the nervous system, that cannot be supplied by Eps15 (101). In mice, Picalm is an adaptor protein that binds to AP2 during the cargo selection phase of CME, and is essential for iron metabolism and hematopoiesis. Deleterious mutations of *Picalm* gene in mice cause severe anemia, low white blood cell count with reduced progenitors, both myeloid and erythroid, in bone marrow, underlying the important role of iron metabolism in the hematopoietic stem cell niche (102).

3.4.2. Human diseases of CME

Most of the genetic defects that disrupt CME-related proteins in human have often syndromic features, and affect the nervous, the immune and/or the muscular system.

In the Lowe oculocerebrorenal syndrome, a rare X-linked recessive disorder, mutations disrupting the polyphosphoinositide 5-phosphatase protein (OCRL1) cause accumulation of the $PI(4,5)P_2$ and alteration of actin cytoskeleton and CME that ultimately lead to a severe phenotype of eye abnormalities (congenital cataracts, impaired vision, glaucoma), reduced muscular tone, mental disability, developmental delay and Fanconi syndrome.

Hermansky–Pudlak syndrome (HPS) is a rare autosomal recessive lysosomal-disease due to mutations in the b1 subunit of the AP-3 (HPS2) with impaired transport of membrane proteins to late endosomes and alteration of maturing melanosomes in melanocytes, platelets storage and granules movement of NK and T Cytotoxic cells, and a phenotype of oculocutaneous albinism, increase risk of bleeding and immunodeficiency (neutropenia) with severe respiratory infections and pulmonary fibrosis (103).

Diseases due to mutations in the protein family of Dynamins are the centronuclear myopathy and the Charcot-Marie-Tooth disease (the dominant, intermediate B form, CMTDIB). Centronuclear myopathy (*DNM2* gene) is inherited in an autosomal dominant pattern and is characterized by myopathy and skeletal muscle atrophy starting in early childhood. Skeletal (scoliosis, high arched palate) and cardiac (cardiomyopathy) defects, along with neural abnormalities are also often present. The dominant, intermediate B form of Charcot-Marie-Tooth disease (autosomal dominant) is a neuropathy of the peripheral nervous system and presents in late childhood/early adulthood with lower limb weakness and atrophy with gait instability, paresthesia, muscle wasting and sometimes, associated neutropenia and cataracts. All of these genetic syndromes present with severe phenotype and are often associated with premature early death (104).

3.5. Human inborn errors of immunity (IEI) due to deficiency of surface receptors

Inborn errors of immunity, previously referred to as primary immunodeficiencies, are diseases of the immune system resulting from mutations that alter the expression of encoded proteins or molecules (105). Since 2013, the International Union of Immunological Societies (IUIS) has been publishing updated classifications of Inborn Errors of Immunity (IEI) describing main clinical and laboratory features with the aim of supporting physicians at the bedside, and laboratories for research and molecular diagnosis. The last update of year 2019, adds 65 new conditions to the previous update, bringing the total number of distinct disorders up to 406, with 430 different identified gene defects, organized in ten tables according to their pathogenesis (106, 107). IEI presents with a broad range of phenotypical manifestations, from increased susceptibility to infections, autoimmunity or autoinflammation to malignancies.

3.5.1 Severe Combined Immune Deficiencies (SCID)

Severe Combined Immunodeficiencies are diseases affecting both cellular and humoral immunity and are defined by CD3+ T-cell lymphopenia (CD3+ T cells < 300/μL). Patients with SCID can present with normal number of defective B cells (SCID T- B+) or reduced B cells (SCID T- B-). NK cells can be present or absent (NK+ or NK-). A summary of known forms of SCID is presented in Figure 3.7 (106).

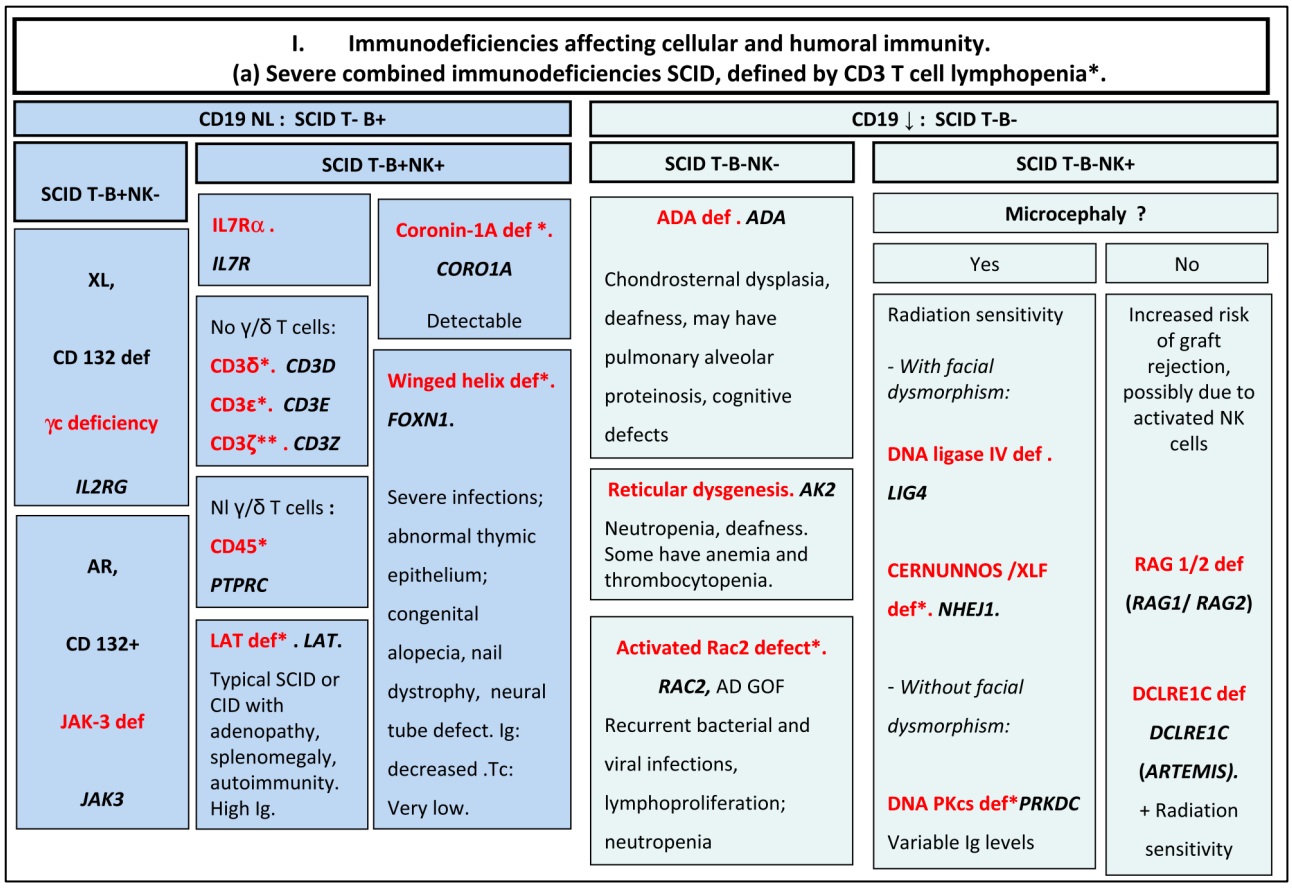

Figure 3.7. Immunodeficiencies affecting cellular and humoral immunity I. Severe combined immunodeficiencies defined by T cell lymphopenia. * T cell lymphopenia in SCID is defined by CD3+ T cells < 300/μL. AD autosomal dominant transmission, ADA adenosine deaminase, AR autosomal recessive transmission, GOF gain-of function mutation, Ig immunoglobulins, NK natural killer, SCID severe combined immunodeficiency, Tc T cells, XL X-linked transmission. (From Bousfiha et al. Journal of Clinical Immunology, 2020) (106).

SCID with normal count of B cells and absent NK cells are the X-linked SCID and JAK-3 deficiency. X-linked SCID, SCIDX1, or γ-chain deficiency is the most common T- B+ NK- form of severe combined immunodeficiency (SCID), publicly known as the "Bubble Boy Disease". The causative gene was first mapped to chromosome X in 1987 (108), further described in 1989 (109), and finally identified in 1993 as *ILR2G* or *CD132* (110). Because the phenotype of X-linked SCID human patients is more severe than that of exclusive IL-2 defects in mice, it was first speculated and then demonstrated that the γ-chain is one shared component of the receptor complex of many

cytokines (IL-2, IL-4, IL-7, IL-9, IL-15, IL-21) (111). X-linked SCID and JAK 3 deficiency present with a indistinguishable clinical and immunological phenotype, characterized by failure of T-cell and NK cell to develop normally, by physiological numbers of dysfunctional B cell with consequentially lack of both cellular and humoral immunity (112). Affected individuals face life-threatening infections in early life, and need to be promptly treated with bone marrow transplantation (113). Being a lethal condition curable through hematopoietic stem cell transplantation made the disease a great candidate for Gene Therapy approach, which has proven to provide full correction of the phenotype and disease through *ex-vivo* infection of CD34+ patients' cells with defective γ-chain Moloney retrovirus-derived vector (114).

SCID with normal count of B and NK cells comprise the autosomal recessive IL-7R alpha chain deficiency, CD3δ, CD3ε and CD3ζ deficiencies, CD45 deficiency, LAT deficiency, Coronin-1A and FOXN1 deficiencies. Defects in the IL-7R alpha chain abrogates T cell development and causes a T- B+ NK+ SCID with markedly reduced T cells, defective proliferation to mitogens but normal or elevated CD20+ B cells, with inability of the immune system to clear the body from viral and protozoal infections, that can be severe and persistent. Patients present with severe failure to thrive, abnormalities of the gastro-intestinal tract, lack of the thymic shadow on chest X-ray, fungal and bacterial infections predominantly of the gastro-intestinal tract and death in infancy, if not promptly treated with HSCT (115).

CD3δ, CD3ε and CD3ζ deficiencies are caused by defects in the *CD3D*, *CD3E* and *CD3Z* genes resulting in disrupted thymocytes-TCR mediated activation and signaling early in thymic development. Patients' immunological phenotype shows low T cells, normal B cells, low immunoglobulins, normal NK and no γδ T cells. Clinical presentation is usually of severe gastrointestinal, respiratory and skin infections in early life with chronic diarrhea and failure to thrive. These diseases can be cured with Hematopoietic Stem Cell Transplantation with full immune reconstitution (116-118).

A major leukocyte cell surface molecule is the leukocyte-common antigen (LCA, CD45), which is an integral membrane protein tyrosine phosphatase expressed in multiple isoforms on all hematopoietic cells, except red cells. Naïve T cells express the CD45RA isoform, which, after activation, shifts to the CD45RO isoform (memory T-cells). CD45 is essential during T and B cell activation and signal transduction, as well as for integrin-mediated adhesion and migration. Homozygous or compound heterozygous mutations in *CD45* gene with signaling defects in

lymphocytes cause a severe T- B+ NK+ SCID. Peripheral T cell numbers are dramatically reduced, and B cell maturation is impaired. Patients present in infancy with hepato-spleno-megaly, lymphadenopathy, lung and respiratory tract infections of both viral and bacterial origin, pancytopenia and failure to thrive. HSCT is required for survival (119, 120).

The group of SCID displaying reduced count of B cells includes ADA deficiency, reticular dysgenesis, activated Rac2 defect, DNA ligase IV deficiency, CERNUNNOS/XLF deficiency, DNA PKcs (PRKDC) deficiency, RAG1/2 deficiency and DCLRE1C deficiency.

3.5.2. Combined Immunodeficiencies (CID) generally less profound than SCID

Combined Immunodeficiencies (CID) generally less profound than SCID are presented in Figure 3.8 of the 2019 IUIS Phenotypical classification (Figure 3.8) (106).

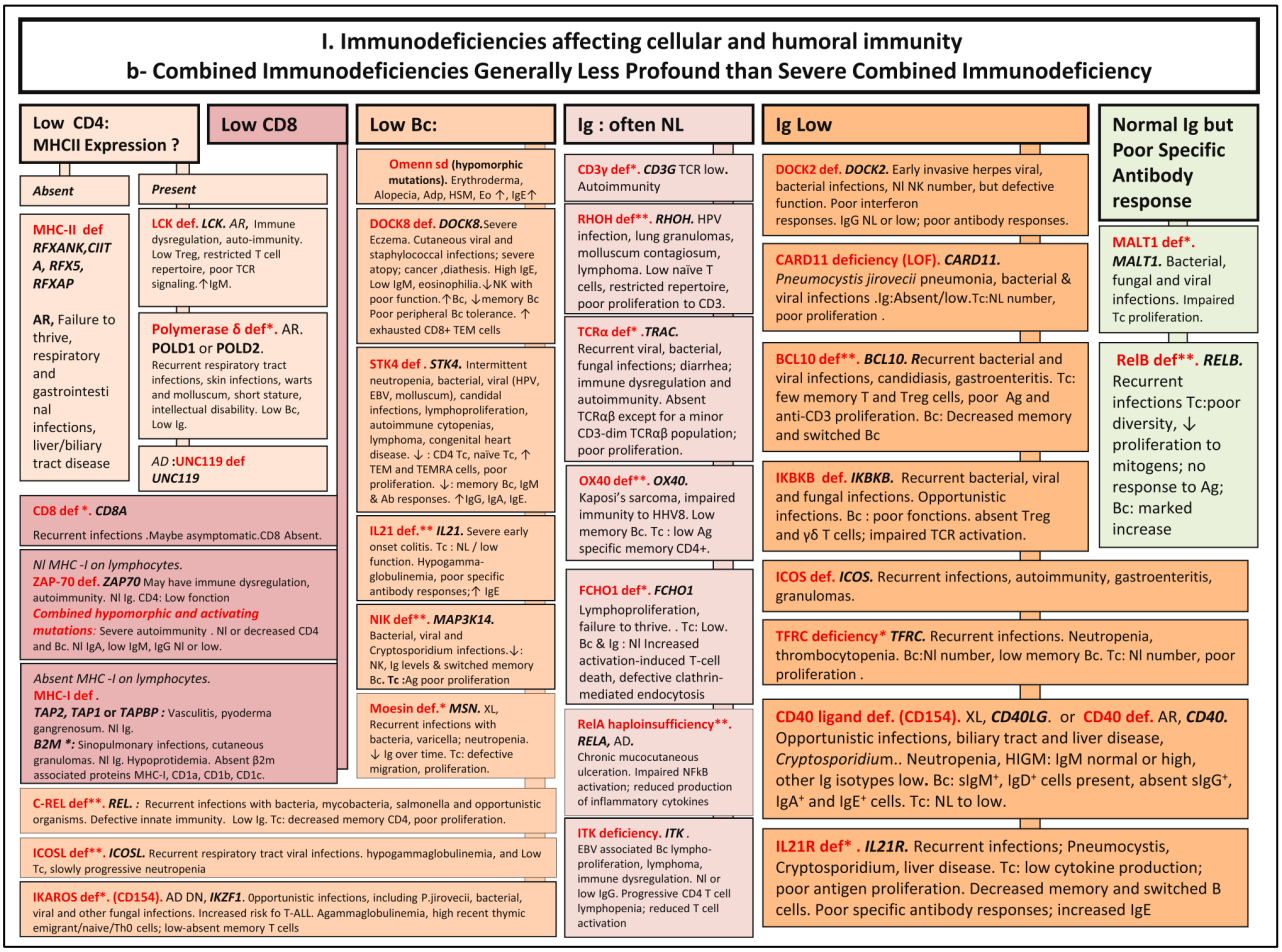

Figure 3.8. Immunodeficiencies affecting cellular and humoral immunity II. Combined Immunodeficiencies (CID) are generally less profound than SCID. AD autosomal dominant transmission, ADA adenosine deaminase, Adp adenopathies, Ag antigen, AR autosomal recessive transmission, β2m bêta-2 microglobulin, Bc B cells, CBC complete blood count, CD cluster of differentiation, CVID common variable immunodeficiency, def deficiency, EBV Epstein-Barr virus, Eo eosinophilia, GOF gain-of-function mutation, HHV8 human herpes virus 8, HIGM hyper IgM syndrome, HPV human papillomavirus, HSM hepatosplenomegaly, Ig immunoglobulins, MHC major histocompatibility complex, Nl normal, NK natural killer, SCID

severe combined immunodeficiency, Tc T cells, TCR T cell receptor, Treg regulatory T cells, XL X-linked transmission. (From Bousfiha et al., Journal of Clinical Immunology, 2020) (106).

IL-21 is part of the group of cytokines that share the γ-chain receptor. The role of IL-21 as primary cytokine for human B cell differentiation in vivo was first described in year 2011 (121). Patients with IL-21R deficiency (inherited as an autosomal recessive trait) present with a clinical phenotype of Combined Immunodeficiency (CID). They tend to display normal numbers of T and B cells, but poor antigen proliferation, decreased memory and switched B cells, impaired antibody production, variable dysfunction of NK cells and defective T cell responses to antigens. Clinically, these patients suffer from severe and recurrent respiratory and gastrointestinal infections, in particular cryptosporidial, often associated with chronic cholangitis and liver disease. Because of the impaired function of immune cells and the severity of the disease, patients require to be early diagnosed and transplanted with HSC (121).

Patients with CD3γ deficiency present with a highly variable clinical severity of immunodeficiency and autoimmunity. T, B cells and Ig number are normal, but TCR expression is decreased (122). Some patients show early onset of severe recurrent infections that can be lethal, while others present with mild symptoms or can be asymptomatic into young adulthood (123). TCRα deficiency (mutation in *TRAC* gene) also presents as CID and is characterized by recurrent infections (respiratory infections, otitis media, candidiasis, diarrhea), failure to thrive, immune dysregulation and autoimmunity (hypereosinophilia, vitiligo and alopecia areata) with T cells that are mostly TCRγδ cells, absent TCR-αβ cells (124).

Clinical presentation with CID, but without features of autoimmunity, is seen in patients with CD8 deficiency (mutation in the *CD8A* gene, coding for the CD8α subunit of the CD8 receptor). Due to the pivotal role of CD8α in cytotoxic T cell precursors survival and development, mutation in the coding gene causes complete peripheral absence of CD8+ T cells (both CD3- and CD3+), normal CD4+ T, B and NK cells. Patient can be asymptomatic or present in early adulthood with history of recurrent bacterial and viral infections (125).

The importance of iron for the adaptive immunity is documented in studies conducted on mice and rats. In humans, it was observed that lymphocytes responses to mitogens are dramatically decreased in both anemic and nonanemic iron-deficient patient and iron deficiency was speculated to be a potential causative factor of immune deficiency (126). The first immunodeficiency caused

by defects of iron metabolism was described many years later and comprised in the group of Combined Immunodeficiencies generally less profound than SCID. Patients with homozygous mutation in the *TFRC* gene (*TFRC* deficiency) develop a Combined Immunodeficiency (CID) with normal numbers, but poorly proliferating T-cells. B-cells are not diminished in absolute count, but memory B-cells number are decreased. Both T-cell and B-cell functions are impaired, with reduced proliferation in response to mitogens (PHA), phorbol-12-myristate-13-acetate (PMA) and ionomycin, and to cross-linking of the TCR with antibody anti-CD3+. Moreover, B-cells cannot proliferate and fail to secrete IgG and IgE in response to stimulation with anti-CD40 and IL-4. No erythrocyte development and function impairment or anemia is observed in these patients because transferrin uptake in erythroid precursors can partially be rescued by STEAP3, a metalloreductase that associates with TfR1. Because of failure to internalize, TfR1 is hyper-expressed on the lymphocyte surface, allowing identification of the disease at birth and facilitating early cure by HSCT (127).

3.5.3. Defects of B cells

Primary B cell immunodeficiency is a heterogeneous group of B cell disorders with reduction or complete absence of serum Immunoglobulins, causing increased risk of encapsulated bacterial infections (S. pneumoniae and H. influenzae in particular, but also Giardia infections). A summary of these defects is presented in Table 3.1.

Disease	Genetic defect	Inheritance	OMIM	Classification according to IUIS 2019	Main clinical and immunological features
Agammaglobulinemia	*BTK*	XL	300300	Predominantly antibody deficiencies	Severe bacterial infections. All Ig isotypes decreased in majority of patients
	IGHM	AR	601495		
	IGLL1		613500		
	CD79A		613501		
	CD79B		612692		
CVID phenotype	Unknown	Variable	107265	Predominantly antibody deficiencies	Most have recurrent infections. Other possible associated features: polyclonal lymphoproliferation, autoimmunity and/or granulomatous disease
Common variable immune deficiency with no gene defect specified			186845		
			112210		
			120650		
CD19 deficiency	*CD19*	AR	186845		
CD81 deficiency	*CD81*	AR	112210		
CD20 deficiency	*CD20*	AR	120650		
CD21 deficiency	*CD21*	AR	604907		
TACI deficiency	*TNFRSF13B*	AR/AD	606269		
BAFF receptor deficiency	*TNFRSF13C*	AR			

Table 3.1. Defects of cellular surface receptors or signaling causing predominantly antibody deficiencies. XL: X-linked; AR: autosomal recessive, AD: autosomal dominant; Ig: immunoglobulins; CVID: common variable immune deficiency; CD: cluster of differentiation; TACI: tumor necrosis factor (TNF) superfamily member transmembrane activator and CAML interactor; BAFF: B cell-activating factor of the TNF family.

The 2019 IUIS Phenotypical classification groups these defects in the family of predominantly antibody deficiencies. Age of onset is very variable (but often in early infancy) and respiratory infections like pneumonia with empyema and bronchitis or bronchiolitis that can turn into chronic lung disease are common, as well as recurrent otitis in children and sinusitis in adults, and severe diarrhea and enteroviral infections. Autoimmune disorders and Nervous System involvement are also present in some cases. Patients are generally healthy between infections' episodes, treatment, which should be started as soon as possible, is gammaglobulin replacement and antibiotics (128). Inheritance varies from the most common autosomal recessive, with homozygous or compound heterozygous mutations (CD19, CD81, CD20, CD21, BAFF-R and some TACI deficiencies, as well as the autosomal recessive form of Agammaglobulinemia) to the X-linked Agammaglobulinemia (Bruton tyrosine kinase (BTK) agammaglobulinemia) and the autosomal dominant form of TACI deficiency.

Because of the absence or markedly decreased number of B cells, Agammaglobulinemia presents with severe reduction of all isotypes of serum immunoglobulins (Ig). X-linked agammaglobulinemia (XLA) is the most common type of agammaglobulinemia and is caused by mutations in the Bruton Tyrosine Kinase (BTK) gene. BTK is the cytoplasmic key regulator of B-cell development activated upon stimulation of B cell receptors (BC), a B cell surface multimeric complex composed by one immunoglobulin (that extends above the cell membrane into the extracellular space) and the CD79 molecule (that extends inside the cytoplasm). Autosomal Recessive Agammaglobulinemia (AGM) comprises 8 genetically distinct diseases involved in humoral immunity. AGM1, AGM2, AGM3 and AGM6 are caused by genetic defects coding for protein that are part of the B cell surface receptor complex. Immunoglobulin heavy chain constant region m (IGHM gene, AGM1) (129) and immunoglobulin lambda-like polypeptide 1 (*IGLL1* gene, AGM2) (130) bind together to form a molecular complex expressed on pre-B cell surface which regulates immunoglobulin gene rearrangements during B-cell differentiation. CD79A

antigen or immunoglobulin-associated alpha (*CD79A* gene, AGM3) (131) and CD79B antigen or immunoglobulin-associated beta (*CD79B* gene, in AGM6) (132) link with disulfide bonds to form the CD79 complex involved in signal transduction. Affected patients present with severe infections (especially of lungs, respiratory tract and gastrointestinal tract) in early life, failure to thrive, diarrhea, and absence of lymph nodes can also occur. Many develop chronic lung disease with bronchiectasis and do not respond to T cell-dependent and independent immunizations. With known family history, early diagnosis allows to perform treatment with gammaglobulin replacing therapy and to prevent infections.

CD19 is a surface protein found in B cells and Follicular Dendritic Cells and is one of the earliest B cell specific antigens to be expressed. CD19 is a type I transmembrane protein, is involved in B cell signaling through modulation of BCR dependent and independent pathway and maintains balance between humoral response and induction of tolerance. Target of Antiproliferative Antibody 1 (TAPA-1 or CD81) is also involved in B cell responses. CD19 and CD81 deficiencies determine decrease of IgG and IgA or IgM (CD19 deficiency), low IgG, normal or low IgA and IgM (CD81 deficiency). Patient with CD81 deficiency can also experience glomerulonephritis that can result in renal failure (133, 134).

CD20 is also a B lymphocyte surface antigen and is involved in development, differentiation and maturation of B cell into plasma cells, as well as CD21 or Complement Receptor type 2 (CR2). CD21 interacts with CD19 and CD81 forming the B cell coreceptor complex, greatly increasing B cells response to antigens. CD20 and CD21 deficiencies, from defects in *CD20* and *CD21* genes, also result in low serum IgG, but display normal or elevated IgM and IgA, and impaired anti-pneumococcal response (CD21 deficiency) (135, 136).

3.5.4. Defects of NK cells

CD16 is a low-affinity receptor expressed on NK cells and phagocytes. In NK cells, CD16 binding to its ligand IgG Fc enables association with the immunoreceptor tyrosine-based activation motif-containing adaptors TCRζ and Fc-εRI-γ promoting phosphorylation and signal transduction, and displays a pivotal role in host defense against viral infections. Patients with altered NK cells function due to CD16 deficiency (encoded by the *FCGR3A* or Immunoglobulin G Fc receptor III-2 gene and inherited as autosomal recessive trait) suffer from severe viral infections, in particularly

recurrent respiratory tract infections and herpes virus infections (Varicella Zoster Virus, Epstein-Barr virus and Human Papilloma Virus). The discovery of the molecular mechanism underlying this specific disease allowed the definition of the role of CD16 in spontaneous NK cell cytotoxicity (137).

3.6. Next Generation Sequencing (NGS) for diagnosis of new gene defects in IEI

From the identification of the first immunological disease in year 1952 (138), up to 406 distinct disorders of immunity have been reported as of today (106). Clinical manifestations range from autoimmunity or autoinflammation, to increased infections susceptibility, allergy and malignancy. IEI are historically considered rare diseases (defined by an incidence below 1:2000 (Europe) (139) and a prevalence below 200.000 patients (USA). However, the advent of Newborn Screening Programs for disorders of the immune system revealed that IEI are more common than what is generally thought (140). This notion was also underlined by recent epidemiologic studies that not only estimated the overall incidence of IEI to 1:1200 people worldwide, but also predicted that only the 30.6% of IEI affects patients under 15 years of age, suggesting that the adult population is the one actually struck the most by IEI (141).

The advances in- and increased accessibility of- Next Generation Sequencing (NGS) techniques from their advent in 2005 have determined exponential progress in the field of monogenic inborn errors of immunity, allowing the discovery of novel disease-causing genes as well as the description of new clinical phenotypes. On one side, they have contributed in defining the actual prevalence and incidence of IEI, in both pediatric and adult populations (141), developing new diagnostic strategies and adding new insights to clinical treatments. On the other side, allowing early identification of diseases that would have sometimes manifested only later in an individual's life (for example, CID-G/AI RAG deficiency (142), they have generated new debates and open questions on optimal treatment modalities, especially if before the onset of symptoms. Studies of the underlying mechanisms causing immune defects have contributed in understanding the diseases' pathophysiology, but also the complexity of the biology of the innate and adaptive immune system (143, 144) and its interaction with microbes (145).

NGS, also called second generation sequencing, deep-sequencing or high-throughput sequencing, is used to sequence entire genomes (Whole Genome Sequencing, WGS) or entire exomes (Whole Exome Sequencing, WES) or gene panels. NGS studies are particularly useful under three specific settings. The first setting comprises a group of patients with autosomal recessive inheritance, of coming from families with reported consanguinity, or from small communities with high probability of inbreed occurrence or regions likely identical by descent. The second group (autosomal or X-linked recessive or dominant) comprises unrelated individuals who share a rare

and very characteristic disease. The third group contains unrelated patients that are not part of the first and second group, but present with a very lethal and possibly unusual disease of early onset (*de novo* mutations). Studies should be performed not only on the proband's DNA (patient), but also on his/her mother and father (trio design), to rule out/in the possibility of a *de novo* mutation (146).

Because of the overall limited costs, WES represents the most common approach used for diagnosis and research. However, it has been gradually replaced with WGS, which allows coverage of non-coding or regulator regions and introns, and is qualitatively superior to WES for the identification of copy number variation (CNVs) and unknown exons (147). The first protocol for WES was described in 2009 (148) and many different approaches for WES and WGS have followed since then. One of the most used protocol for NGS requires shredding of the proband's DNA into short fragments that are fused with adaptors to create a library. After amplification, a step that is not required in all the NGS protocols, and sequencing cycles, the reads are mapped to genomes of reference and differences between these sequences are finally called variants (alleles that resulted being different from the comparison to the reference sequence). A workflow of the technique is presented in Figure 3.9 (From I. Meyts et al., JACI, 2016) (149).

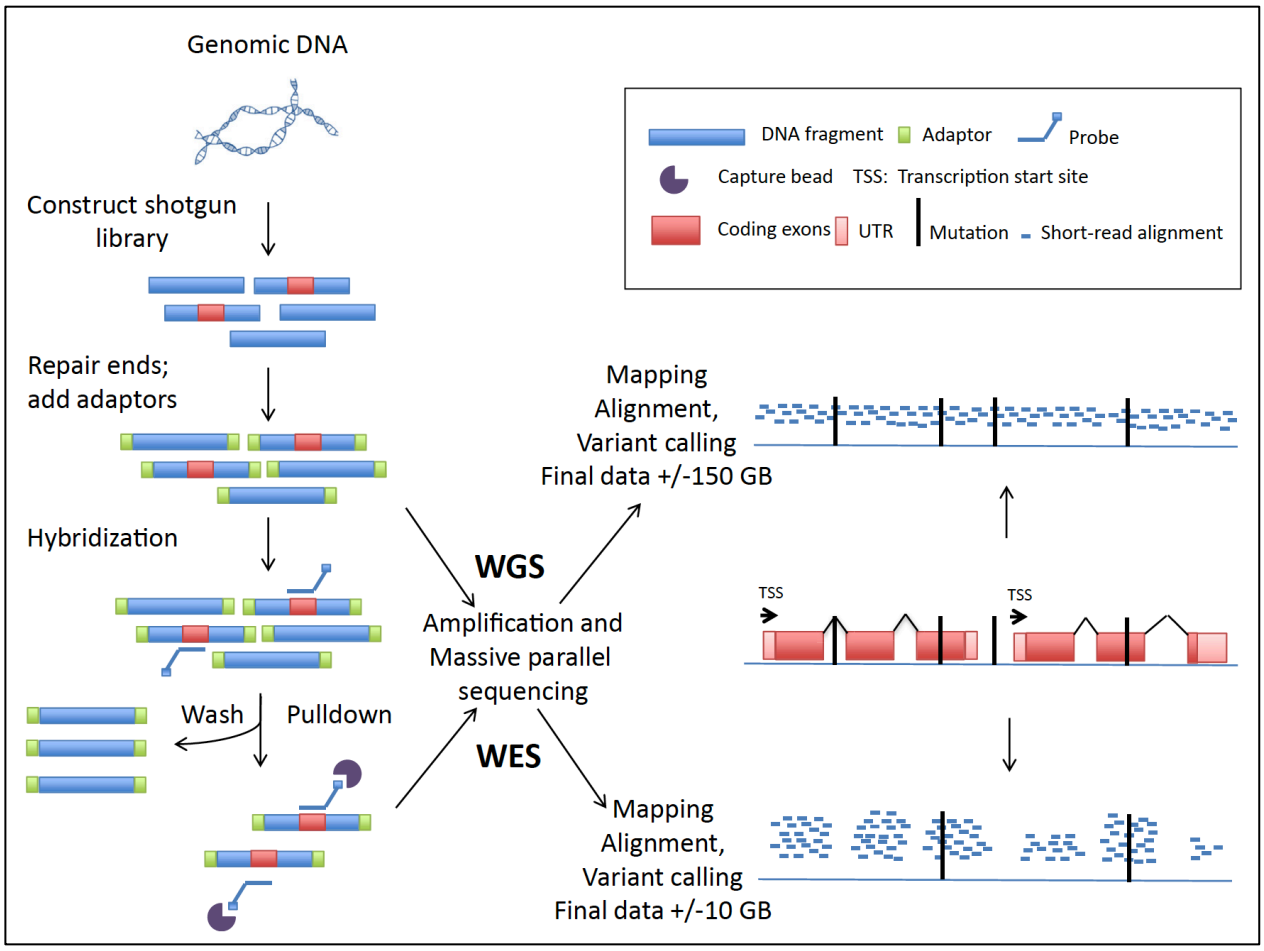

Figure 3.9. Workflow for NGS. Schematic representation of the whole genome and whole exome sequencing workflow. TSS, Transcription start site; UTR, untranslated region. (From I. Meyts et al., JACI, 2011) (149).

The real diagnostic challenge of WES is the selection, among an incredibly vast pool of resulting variants (usually from 20.000 to 50.000), of the few, if not only, candidate variant determining the phenotype. WES files are analyzed upon consideration of variants and gene features. Variant prioritization follows filtering pipelines based on the information on allele frequency (frequency < 1% is considered rare), assessed by using public databases (Exome Aggregation Consortium, among others) on thousands of individuals from various ethnic groups. The potential effect that the variant produces on the wild type phenotype is assessed by deleteriousness prediction scores. Generally, variants that are very likely to be deleterious are the nonsense, splice-site and frameshift mutations.

For missense variants, the most used prediction scores are the Sorting Intolerant from Tolerant (SIFT) and the Polymorphism Phenotyping v2 (PolyPhen2). However, the most reliable is the combined annotation-dependent depletion (CADD) score, which incorporates information from different scores. A CADD score of 15 is usually used as the lower standard cut off for variants' deleteriousness (CADD scores range from 1 to 99). A more accurate estimation is given by the combination of the CADD score with the mutation significance cutoff (MSC) score, which is a good indicator of the cut-off between not disease- and disease-causing variants. The MSC score overcomes the problem of the high false negative rate of the CADD score. In fact, some genes tend to gain variants that are actually disease-causing with low CADD scores (and display lower MSC scores), contrary to other genes that tend to gain variants with high CADD scores that are not disease-causing (and display higher MSC scores).

At the gene level, variant prioritization is based on the relevance for the affected protein in pathways that are related to the phenotype and clinical presentation of the patient. For immunodeficiencies, genes that are involved in the immune responses or related to functions of the immune system, are taken into account. To this purpose, publication of data on gene expression in human cell lines and types, human tissues and organs are fundamental (ExPASy, BioGPS, STRING, BioGRID, Aminoride, MatInspector..).

It is important to understand that NGS is a tool to generate hypothesis (149). Experimental validation of the presumptive causative variant found through NGS study must always follow. Guidelines have been proposed for a correct genotype-phenotype validation workflow, especially when genetic studies are performed on single patients. The following three criteria have been deemed as essential for a variant's validation: the candidate genotype must not be found in healthy individuals; an alteration of expression or protein function must be experimentally demonstrated and must be confirmed through studies on relevant cellular or animal phenotype (150).

3.7. Hot research tools

3.7.1. CRISPR/Cas9 technology

Since the discovery that the genetic information of an individual was enclosed in the double-strand Deoxyribonucleic acid (DNA) of the nucleus, scientists have been contemplating the idea of changing and manipulating an organism's genome. Initial successful approaches witnessed the incorporation of specific genomic sequences of interests into introns by using of encoded "meganucleases" (151), but the first targeting of site-specific nucleases was possible with the development of the Zinc-Finger (ZNF) technology (152). Because of the technical difficulties of the application, ZNF were rapidly overtaken by TAL effector nucleases (TALENs) (153). However, the real advance in genome editing field was reached when clustered regularly interspaced palindromic repeats (CRISPR) found in *Escherichia coli* (154) were associated with proteins containing a nuclease domain (Cas) and showed DNA targeting activity in *Staphylococcus epidermidis* (155).

Soon, it became clear that the new gene editing CRISPR/Cas9 system allowed to target virtually any genomic area of interest with a one nucleotide-precision. Here, a nuclease (Cas9) is guided to a DNA strand by a specific "guide" RNA (CRISPR) and recognizes protospacer adjacent motif (PAM), sequences of 2-6 nucleotides flanking the Cas9-targeted DNA and fundamental for Cas9 binding and activity. The CRISPR/Cas9 system generate DNA breaks that can be repaired by homology-directed repair (HDR), if a donor DNA template is provided, with a precise editing or a gene knock in, or by nonhomologous end-joining (NEHJ) repair, most likely resulting in indels (insertion/deletion) with frameshift of the reading frame and generation of a premature stop codon (Figure 3.10) (156).

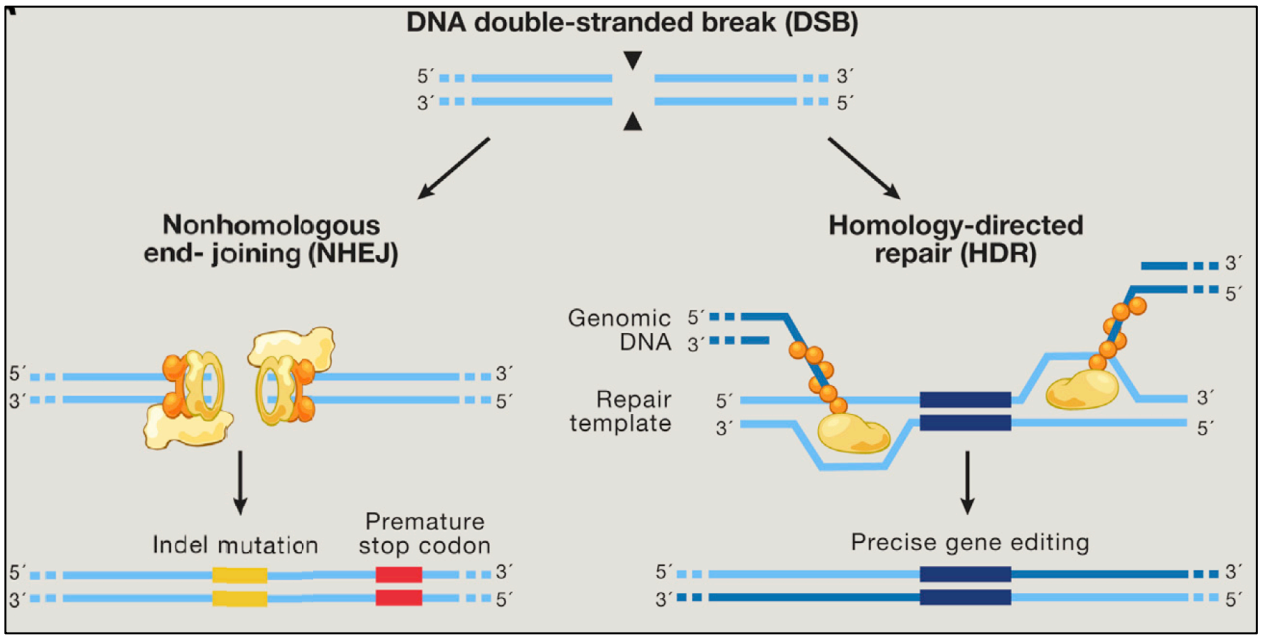

Figure 3.10. DNA Repair Machinery. Genome Editing Technologies Exploit Endogenous DNA Repair Machinery. DNA double-stranded break generated from CRISPR/Cas9 are repaired by NHEJ or HDR. (Adapted from Hsu P. D. et al., Cell, 2014) (156).

Different CRISPR/Cas9 systems are today available, each one with distinguished features. The crRNA/tracrRNA (type II) system introduced an additional amelioration, combining a crRNA (which provides the specific sequence specificity with a 20-nucleotides region complementary to the target DNA) with a tacrRNA (a universal molecule that hybridize to the crRNA and facilitates the guiding) that both finally assemble with a Cas9 forming ribonucleoprotein (RNP) (Figure 3.11) (157).

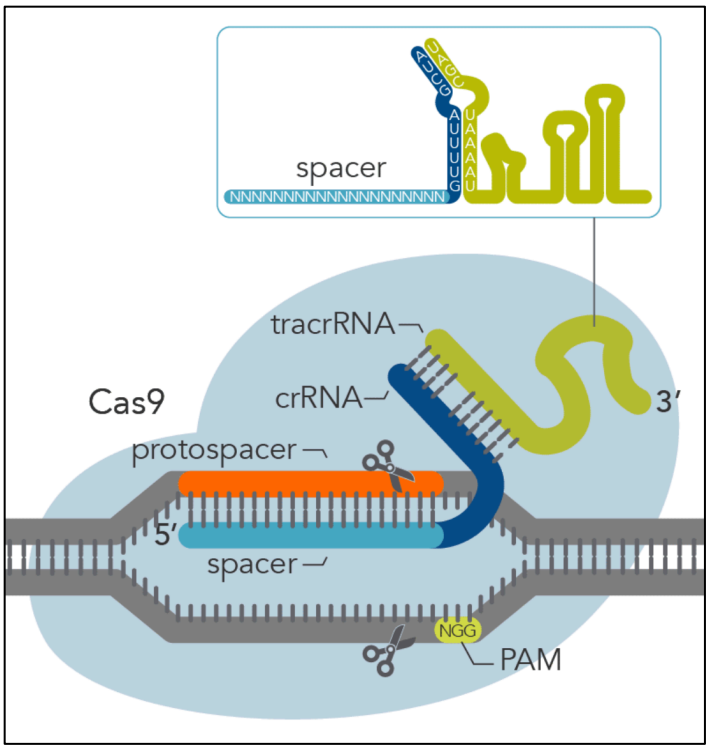

Figure 3.11. Alt-R CRISPR-Cas9 System II. Components of the Alt-R CRISPR-Cas9 System II for directing Cas9 endonuclease to genomic targets. (From Integrated DNA Technologies) (157).

Depending on the target, CRISPR/Cas9 efficiency can reach 80% or even more. The technology can be used to engineered cells and experimentally model a phenotype, to perform systematic analysis of gene expression and functions, thus validating a genotype-phenotype correlation, or to correct mutations responsible of inherited disease and assessing rescue of the phenotype, or to generate animal models (Drosophila, zebrafish, mice, among others).

3.7.2. Induced Pluripotent Stem Cells

The possibility of reprogramming mature cells that can be easily obtained from human subjects (fibroblast, CD34+ cells from PBMCs) into pluripotent stem cells (induced pluripotent stem cells, iPSCs) has revolutionized the field of scientific research, by providing a potentially endlessly

source of patient-derived cells that can be possibly differentiated into any mature cell of the human body (Figure 3.12) (158).

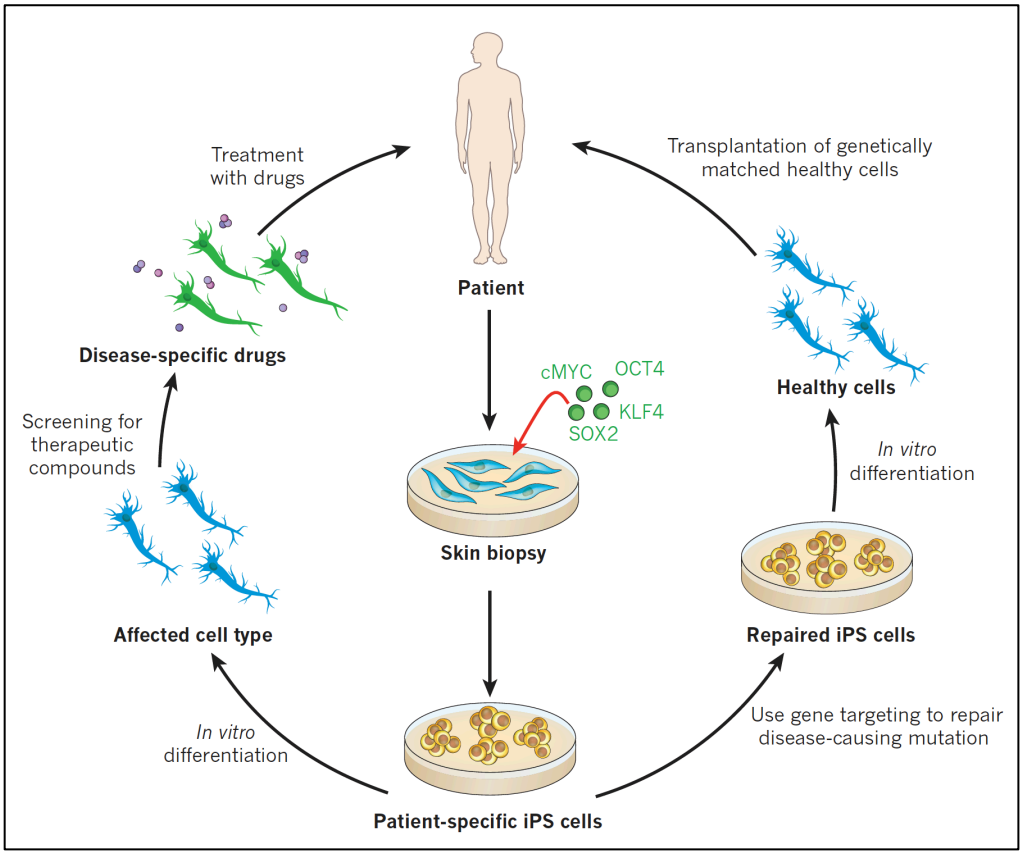

Figure 3.12. Medical applications of iPS cells. When the disease-causing mutation is known, gene targeting could be used to repair the DNA sequence (right). Alternatively, directed differentiation of the patient-iPSCs into the affected subtype, for example neuronal, (left) will allow the patient's disease to be modelled in vitro. (From D. A. Robinton et al., Nature, 2012) (158).

Four factors (the "Yamanaka" factors: Oct3/4, Sox2, c-Myc, and Klf4) were identified as the core transcription factors for generating iPSCs (159). Initially, the Yamanaka factors were introduced into the cells by using of a retroviral integrating vector, that has been later replaced by systems with less chances of disrupting genome integrity, and that are routinely used for iPSCs reprogramming today (Sendai virus, episomes, base-modified mRNA). Like embryonic stem cells

(ESC), iPSCs express genes involved in preservation of stemness, can grow indefinitely (self-renewal) and are able to differentiate into the three germ layers (Ectoderm, Endoderm, Mesoderm). Patient-derived iPSCs are used for a variety of studies, such as drug screening, regenerative medicine, cell replacement therapy as well as serving as disease models.

Because of the lack of- or the difficulties in obtaining- specimens, iPSCs have been broadly applied in the field of neurology and cardiovascular diseases. In the field of immunology, iPSCs have been used for the characterization of the molecular mechanisms underlying new diseases, and they helped gaining new insights on the biology of the innate and adaptive immunity. For example, differentiation of patient-derived iPSCs into lymphoid progenitors and thymic epithelial progenitors underlined the critical role of exostosin-like 3 (EXTL3) in the expansion of hematopoietic progenitor cell (HPC) and thymic epithelial cell differentiation (160). Similarly, in PAX-1 deficiency, iPSCs were *in vitro* differentiated into thymic epithelial progenitor (TEP) to perform gene expression profile studies, unraveling a role for *PAX-1* during thymus development and function (161).

In other studies, iPSCs helped identifying new therapeutic approaches for known diseases. Reticular Dysgenesis (RD) is a rare form of SCID due to mutations in adenylate kinases 2 (AK2) that plays a fundamental role in energy homeostasis. Studies performed on myeloid maturation of AK2-deficient iPSCs not only recapitulated the disease's phenotype, but showed that antioxidant treatment restored iPSCs differentiation into mature granulocytes, suggesting antioxidant therapy as a potential supportive therapy for patients with RD (162). *In vitro* gene correction experiments of Wiskott-Aldrich iPSCs were able to restore the T-cell differentiation, overcoming the stop in the double positive CD8+ CD4+ development stage (163) and gene correction studies on Fanconi-anemia-specific iPSCs showed the possibility of obtain disease-free myeloid and erythroid cells (164). The potential for successful autologous cell therapy was explored with iPSCs studies on X-SCID subjects (165) and on patients with X-linked chronic granulomatous disease (X-CGD) (166), while studies on dendritic cells and macrophages derived *in vitro* from iPSCs broadened the field of application of iPSCs technology to cell therapy (167).

3.7.3. Artificial Thymic Organoids (ATOs)

Because of the scarce availability of thymic samples, studies of human T-cell development have been historically challenging. Discovery that the mouse stromal Notch ligand Delta-like-1 (DLL-1) cell line was able to support T-cell *in vitro* differentiation from pluripotent cells (168) paved the way for the development of the OP9-DL1 assay where functional T-cells are generated from human cord blood- or bone marrow- derived hematopoietic stem cells (HSCs) (169, 170). In this system, hematopoietic stem cells (HSCs) are co-cultured with a monolayer of the stromal line OP9-DL1 expressing Notch ligand to generate CD7+ pro-T cells, that further progress into CD4+ immature single positive cells and into CD4+ CD8+ double positive T cell precursors after 30 days of differentiation. One of the limitations of this assay, however, is the low yield of mature CD8+ or CD4+ T cell expressing TCRαβ/CD3. The idea that a 3-dimensional thymic architecture was as important as the cellular and soluble signals for T cell development, combined with the advances in technologies on reconstructive models for tissue repair, led to the first successful experiments on tissue-engineered thymic organoids as a supportive environment for *in vitro* T cell maturation (171). Unfortunately, this technology was dependent on primary thymic tissue and had a very high variability between experiments. The organoid technology was ameliorated and further developed in a serum-free 3D organoid system (Artificial Thymic Organoid, ATO) which was shown to efficiently support human *in vitro* T cell differentiation from CD34+ (172) and iPSCs (173).

In the iPSCs-ATOs system, T cell *in vitro* maturation follows a multi-step protocol starting from iPSCs that are first differentiated into CD56+ EPCAM- Embryonic Mesodermal Progenitors (hEMPs), subsequently aggregated with MS5-DLL4 cells (murine stromal cells engineered with human Notch-ligand (DLL4) to form an organoid that undergoes hematopoietic induction for two weeks, and finally under T cell differentiation for 5 to 7 weeks (Figure 3.13). To achieve T cell differentiation, iPSCs are stimulated with the human Delta-like 4 (DLL4), a Notch-ligand, and cytokines for T cell induction (SCF, Flt3L and IL-7). In this system, before becoming naïve TCRαβ+/CD3+ CD8+ or CD4+ T cells, hEMPs move through different stages of maturation, from the multipotent CD34+ CD7− CD1a− early thymic progenitors (ETP), to the CD34+ CD7+ CD1a− and CD34+ CD7+ CD1a+ pro-T cells, mimicking development process in the thymus. Both the CD34+-ATO and the iPSCs-ATO technologies allows monitoring of thymic maturation of T cell progenitors and the identification of developmental defects of T cell, if present (174).

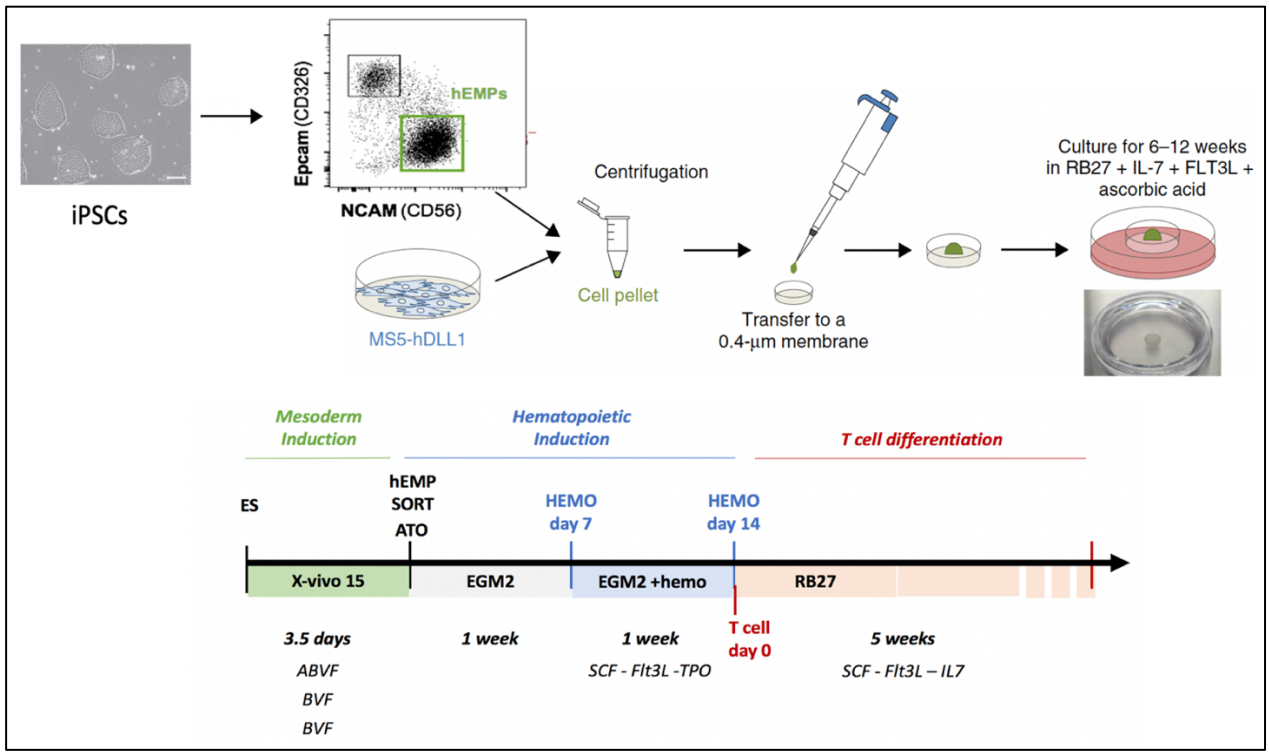

Figure 3.13. Artificial Thymic Organoids experiment layout. Experiment layout for *in vitro* generation of naïve T cells from human iPSCs (Adapted from Montel-Hagen A et al., Cell Stem Cell. 2019) (172).

4. Research topic, significance and impact

Data presented in this study identified the first form of severe immunodeficiency due to defects of clathrin-mediated endocytosis and provided additional evidence in support of the critical role played by iron cellular metabolism in human T cell function and homeostasis. Further experiments on ATOs and murine models are required to uncover the precise molecular mechanisms of the disease.

5. Material and Methods

5.1. Human studies

5.1.1. Patients

All study participants were recruited after obtaining informed consent, and the study was approved by the institutional review board of the referring institutions (National Institutes of Health protocols 06-I-0015 and 16-I-N139).

5.1.2. WES, targeted sequencing and Sanger sequencing of human samples

For patient 1 and patient 2, genomic DNA samples were extracted from PBMCs (using Ficoll-Hypaque gradient centrifugation) by using the DNeasy Blood & Tissue Kit (69506; Qiagen). After quality control, whole-exome sequencing (WES) for family 1 was performed with the VCRome 2.1 capture kit from NimbleGen and sequenced as paired-end 75-bp reads with the Illumina HiSeq 2500 Platform (Illumina). For family 2, WES was performed with the Agilent Human V5 (51MB) Kit (Agilent Technologies) coupled with paired-end 125-bp reads by using HiSeq 2500. All DNA samples were sequenced so that more than 85% of the bases were covered at 203 or greater. All sequenced DNA reads were mapped to the hg19 human genome reference by using the Burrows-Wheeler Aligner with default parameters. Single nucleotide variant and indel calling were performed by using the Genome Analysis Toolkit (version 3.4; the Broad Institute, http://www.broadinstitute.org/gatk/). For patient 3, genomic DNA was enriched with the HaloPlex Target Enrichment System (Agilent Technologies), and targeted sequencing of 500 primary immune deficiency genes and data analysis were performed, as previously described (175). For patients 4 and 5, genomic DNA was isolated from whole blood by using the Gentera Puregene Cell Kit (Qiagen). Exome capture was performed by using the Agilent SureSelect V5, 51MB (Agilent Technologies). The Illumina HiSeq-2500 (Illumina) was used to perform paired-end sequencing, generating 100 base reads. The average coverage of the exome for patient 4 and patient 5 was 97x and 86x, respectively. Sequence processing and mapping to the human reference

genome assembly GRCh37 was performed with the Burrows-Wheeler Aligner, SAMtools, and Picard Tools. Variants were called by using the Genome Analysis Toolkit. For all filtered variants, CADD PHRED scores, CADD_MSC, and pLi algorithms were used to assess the in silico predicted pathogenicity. *FCHO1* mutations were verified on genomic DNA by means of Sanger sequencing in patients and in family members. Primer pairs are shown in Table 5.1.

Patient	**Primer**	**Sequence (5' – 3')**
Patient 1	Ex.6.1 Forward	CCTAACCTCAGGTGATCCGT
	Ex.6.2 Forward	CCTAACCTCAGGTGATCCGT
	Ex.6.1 Reverse	CCATAATCGAGGTGGATGAC
Patient 2	Ex.24 Forward	AGGCACCAGTGAAACCAAGA
	Ex.24 Reverse	CCCAGGAAGCAGAGAGGGAA
Patient 3	Ex.19 Forward	GGATGAGGCTTGGGAAAAAT
	Ex.19 Reverse	CCTCATTGGCCTAACTCTGC
Patient 4	Ex.6.3 Forward	CCACTGCTAAGGTGTTTGAG
	Ex.6.2 Reverse	TTAACATCTCTCTTCTCACACAG
	Ex.6.4 Forward	TCCATCTTTACCTCATTCTCCT
	Ex.6.3 Reverse	ATCCAAATAGCCCCATAATCG
Patient 5	Ex.4.1 Forward	GCTATGAACTCTTATACATGCCTAAA
	Ex.4.1 Reverse	AATGAATGAATAAAAACAACTCTGTC
	Ex.4.2 Forward	AAACTTGCCTCTCTCTTCAGA
	Ex.4.2 Reverse	TGACTCTTCCCACTTTAACTTC

Table 5.1. Primers sequences. Sequences of Primers used for Sanger confirmation of FCHO1 mutations in the 5 patients and respective family members.

5.1.3. *In silico* studies and quantitative real-time PCR

In silico analysis on expression of *FCHO1/FCHO2* were preformed using online free platforms: Bioproject (https://www.ncbi.nlm.nih.gov/bioproject/280600) and BioGPS (http://biogps.org). For quantitative real-time PCR, normal donor PBMCs were stained and underwent fluorescence-activated cell sorting for surface expression of CD3 (eFluor450 mouse anti-human CD3, clone OKT3, catalog #48003742, Fisher Scientific), CD4 (allophycocyanin [APC]–Cy7 mouse anti-human CD4 antibody, clone SK3, catalog #341095, BD Biosciences), CD8 (PE mouse -antihuman CD8 antibody, clone RPA-T8, catalog #301008), CD19 (peridinin chlorophyll-protein complex/Cy5.5 mouse anti-human CD19 antibody, catalog #302230, clone HIBI19; BioLegend),

and CD56 (fluorescein isothiocyanate [FITC] mouse anti-human CD56 antibody, clone NCAM16.2, catalog #340723, BD Biosciences), respectively, by using FACS Aria. Sorted cells were pelleted (8000 g x 5 minutes) and total RNA was extracted from cells by using the RNeasy Micro Kit (Qiagen), according to the manufacturer's instructions. For each sample, cDNA was generated from RNA in a total volume of 20 μL by using the qScript cDNA Synthesis Kit (Quantabio). Real-time PCR was performed with TaqMan Fast Advanced Master Mix (Applied Biosystems) and TaqMan probes for human ACTB (Hs99999903_m1), FCHO1 (Hs00322606_m1), and FCHO2 (Hs01564786_m1), all from Thermo Fisher Scientific. Experiments were run on a 7500 Real Time PCR System (Applied Biosystems) with 7500 Real Time PCR software (version 2.3; Life Technologies). Data were analyzed by using the 22DCt method after normalization to the *ACTB* gene as an endogenous control and by using water as a negative control.

5.1.4. *In vitro* mutagenesis, transfection, and Western blotting

Targeted mutagenesis for mutations in P2 (c.2023dupG, p.V675Gfs*33) and P3 (c.1304_1305del, p.F436Wfs*7) was performed by using the Phusion Site-Directed Mutagenesis Kit (Thermo Fisher), according to the manufacturer's instructions. Wild-type (WT) cDNA of the human *FCHO1* gene from a pDONR-223 vector (Arizona State University) was introduced in an N-terminal tagged pCMV-HA-N vector (Addgene), and the mutagenic primers FCHO1.P2 and FCHO1.P3 (Table 5.2), which were designed by using the Phusion Site Directed Mutagenesis Kit (Thermo Fisher) instructions, were used.

Mutation	**Primer**	**Sequence (5' – 3')**
Patient 2	FCHO1.P2 Forward amplification	CCACCACCACCTGGTCCTCAGCTTCCG
	FCHO1.P2 Reverse amplification	GGTCCCGCTGAACACACGCACGATG
Patient 3	FCHO1.P3 Forward amplification	GTTCTTGGACACCTGCTCCTCTGACTGC
	FCHO1.P3 Reverse amplification	CTTTGGGCCGCCCCTGGAGTCAGCCTTTG
Patient 4	FCHO1.P4 Forward amplification	CAGCAACGGGACCCCCCATGGGGAC
	FCHO1.P4 Reverse amplification	GTCCCCATGGGGGGTCCCGTTGCTG

Table 5.2. Mutagenesis Primers. Sequences of primers used for *in vitro* mutagenesis.

Successful mutagenesis was confirmed my means of plasmid DNA sequencing at Macrogen (Macrogen). One day before transfection, 293T cells were seeded (at 500,000 cells per well in a 6-well plate) in complete Dulbecco modified Eagle medium (DMEM/High Glucose from HyClone, 10% FBS from Gemini Bio-Products, 1% MEM Non-Essential Amino Acid from Corning, and 1% L-glutamine from HyClone). Transfections were carried out with the Lipofectamine 3000 Transfection Kit (Invitrogen), according to the manufacturer's protocol. Cells were transfected with 600 ng of FCHO1 WT, FCHO1.P2, or FCHO1.P3 plasmid DNA. After 24 hours, cells were harvested and used in immunoblotting. 293T transfected cells (10 Million) were lysed with RIPA-NTG buffer (30 mmol/L Tris-Cl, 150 mmol/L NaCl, 1% NP-40, 1% Triton X-100, 10% glycerol, and protease inhibitor) with protease inhibitor cocktail (Halt Protease Inhibitor Single-Use Cocktail 1003; Thermo Scientific) for 30 minutes on ice. Lysates were denaturated by using Bolt LDS Sample Buffer 43 and Bolt Reducing Agent 103 (Life Technologies) at 708C for 15 minutes, loaded on 4-12% Bis-Tris Gel, and separated by using SDS-PAGE. Proteins were transferred to nitrocellulose membrane by using the iBlot 2 System (Invitrogen). Blots were probed overnight with 1:2000 dilutions of rat Anti-HA High Affinity mAb (11867423001; Roche), and 1:2000 dilution of rabbit anti-β-actin mAb (4967S; Cell Signaling) as a loading control. Bands were revealed by using SuperSignal West Femto kit (Fisher Scientific). For the mutation c.189dupC (P4), HEK293T cells were transfected with N-terminal FLAG-tagged FCHO1 WT (Genecopoeia) or FCHO1.P4 plasmid DNA. The latter was generated by using the QuikChange II XL Site-Directed Mutagenesis Kit (Agilent Technologies) with FCHO1.P4 primers (Table 5.2). One day after transfection by using the TransIT-LT1 Transfection Reagent (Mirus Bio), cells were lysed in RIPA buffer (Millipore), 50 mmol/L EDTA (Thermo Scientific), and protease inhibitors (Thermo Scientific). Electrophoresis of lysates was performed on 4-12% precast polyacrylamide gels (Invitrogen), followed by immunoblotting with the following antibodies as indicated in figure legends: anti-FLAG (F3165, Sigma-Aldrich) and anti-β-actin (Sigma-Aldrich).

5.1.5. Analysis of RNA splicing

RNA extracted from PBMCs derived from one healthy donor and from the father and mother of patient 1 was retrotranscribed with random primers and the ImProm-II Reverse Transcription System (Promega), according to the manufacturer's instructions. RT-PCR for FCHO1 transcript

was performed by using primers (Forward, 5'-TCTCCACAGAGACCATCAGG-3'; reverse, 5'-GATGCTGGACTCAGCCCTG-3') with an annealing temperature of 64°C and sequenced by Sanger sequencing.

5.1.6. *In vitro* T cell activation and proliferation

For analysis of human T cell activation, PBMCs from patient 2 and 2 healthy control subjects were cultured in 200 mL of serum-supplemented RPMI (SH30027.01; GE Healthcare Life Sciences) in round-bottom 96-well plates with 1 mg/mL anti-CD3 (OKT3, catalog #14-0037-82; eBioscience) and 1 mg/mL Protein A (catalog #P6031; Sigma-Aldrich) for 24 and 48 hours. Cells were collected at 24 and 48 hours, washed with serum supplemented PBS, and stained with Live/Dead (L34959; Invitrogen) staining and fluorochrome-conjugated CD3-PE/Cy7 (317334; BioLegend), TCRαβ-FITC (555547; BD PharMingen), CD71-APC (17-0719-42; Invitrogen), CD69-BV510 (310936; BioLegend), and CD25-eFluor780 (47-0259-42; Invitrogen) for 15 minutes at 4°C (dark). On washing with serum supplemented PBS, expression of CD69, CD25, and CD71 by CD3+ cells was analyzed by using flow cytometry (LSRFortessa; BD) and FlowJo software (version 10.5.2; TreeStar). For analysis of human T cell proliferation, PBMCs were incubated with the CellTrace violet Cell Proliferation Kit (1 mmol/L; Invitrogen). After 20 minutes, 10 volumes of RPMI/10% FBS were added, and the cells were washed twice with RPMI/10% FBS. A total of 1 x 10^5 cells was seeded into 96-well plates and stimulated with Dynabeads CD3/CD28 (bead/cell ratio of 1:1; Invitrogen) for 4 days. Cells were then stained with fluorochrome-conjugated CD4 and CD8 antibodies (BD Biosciences) for 30 minutes at 4°C (dark) and washed twice with PBS twice, and CellTrace Violet expression was analyzed by using flow cytometry (Becton Dickinson FACSCanto II) and FlowJo software (version 10.5.2; TreeStar).

5.1.7. *In vitro* cell-cycle analysis

Total PBMCs were stimulated with Dynabeads Human T-Activator CD3/CD28 (Thermo Fisher) for 3 days. Cells were washed with PBS, fixed in 66% EtOH for 3 hours at 48°C, and then washed twice in PBS and stained with Propidium Iodide (50 mg/mL) for 30 minutes at 37°C in the presence of RNase A (100 mg/mL), followed by analysis with flow cytometry.

5.1.8. T cell repertoire analysis

DNA was extracted from whole PBMC. Multiplex Polymerase chain reaction (PCR) on V and J gene, was used to amplify the rearranged CDR3β7. PCR products were sequenced using the Illumina HiSeq platform (Illumina). High-throughput sequencing of T cell receptor β (TRB) was performed by Adaptive Biotechnologies (Adaptive Biotechnologies).

5.1.9. TCR internalization

PBMCs from patient 2 and 1 healthy control subject were either left unstimulated or stimulated with 0.5 mg/mL anti-CD3 (OKT3, catalog #14-0037-82; eBioscience) plus 0.5 mg/mL anti-CD28 (catalog #302914; BioLegend) in 500 mL of serum-supplemented RPMI at 37°C for 2, 15, and 30 minutes. At each time point, cells were collected, washed with serum supplemented PBS, and stained with Live/Dead (L34959; Invitrogen) staining and fluorochrome-conjugated CD3-eFluor450 (48-0037-42; eBioscience) and TCRαβ-APC (17-9986-42; eBioscience) for 15 minutes at 4°C (dark). Cells were washed with serum-supplemented PBS, acquired, and analyzed by using flow cytometry (LSRFortessa; BD) and FlowJo software (version 10.5.2; TreeStar).

5.1.10. Transferrin internalization assay

PBMCs from patient 2 and 2 healthy control subjects were cultured in 200 mL of serum-supplemented RPMI (SH30027.01; GE Healthcare Life Sciences) in round-bottom 96-well plates with 1 μg/mL anti-CD3 (OKT3, catalog #14-0037-82; eBioscience) and 1 μg /mL Protein A (catalog #P6031; Sigma-Aldrich) at 37°C for 48 and 72 hours. At each time point, cells were collected and washed with PBS at 300 rcf units for 5 minutes and resuspended in 250 mL of RPMI serum-free media with 25 mmol/L HEPES (H3375-100G; Sigma) and 0.5% of BSA (15260-037; Life Technologies). Cells were starved for 30 minutes at 37°C, washed once with PBS, resuspended in serum-free RPMI with biotinylated transferrin (T23363; Invitrogen) and 0.5% BSA, and pulsed for 30 minutes at 48°C. Medium were then changed to serum-supplemented RPMI, and temperature was shifted to 37°C for 0, 10, and 30 minutes to stimulate biotinylated

transferrin trafficking. Internalization was stopped by incubating cells on ice and washing with cold PBS, followed by staining and flow cytometry. For the different time point of transferrin internalization, the percentage of surface transferrin expression was calculated as follows: [Median fluorescence intensity (MFI) of surface transferrin at time x / MFI of surface transferrin at time 0 minute] x 100. Cells were then stained with Live/Dead (L34959; Invitrogen) staining and fluorochrome-conjugated CD3-PE/Cy7 (317334; BioLegend), TCRab-FITC (555547; BD PharMingen), and streptavidin-PE (554061; BD Biosciences) antibodies for 15 minutes at 4°C (dark) and then washed with serum-supplemented PBS twice analyzed by using flow cytometry (LSRFortessa; BD) and FlowJo software (version 10.5.2; TreeStar).

5.1.11. Generation of induced pluripotent stem cell (iPSCs)

Primary skin fibroblasts from patient 1, PBMCs from patient 2, and a healthy control (BJ fibroblast line, ATCC) were reprogrammed to iPSCs by infection with the non-integrating CytoTune-iPS 2.0 Sendai Reprogramming kit (Thermo Fisher Scientific, A16517) following manifacturer's instructions. Primary fibroblasts were plated in 6 well dishes 2 days prior transduction in complete Dulbecco modified Eagle medium (DMEM/High Glucose from HyClone, 10% FBS from Gemini Bio-Products, 1% MEM Non-Essential Amino Acid from Corning, and 1% L-glutamine from HyClone). At 60-80% confluency, cells were transduced using the CytoTune™ 2.0 Sendai reprogramming vectors at the appropriate MOI and incubated overnight. Medium was fully changed after 24 hours of infection; cells were then allowed to grow for 6 days with medium change every other day. On day 7, cells were replated in different concentrations (5.000 to 30.000 cells/well) in 6 well plates coated with 1% Gelatin and Mouse Embryonic Fibroblast (MEFs) feeder cells. Medium was changed to iPSCs medium (Essential 8™ Medium, catalog #A1517001, TermoFisher Scientific) on day 8 and cells were cultured until colonies formed. PBMCs from patient 2 were plated in 24 well plate in serum-supplemented RPMI (SH30027.01; GE Healthcare Life Sciences) medium 4 days prior transduction, then transduced using the CytoTune™ 2.0 Sendai reprogramming vectors at the appropriate MOI and incubated overnight. Medium was replaced with fresh medium after 24 hours of infection, cells were collected and plated in 6 well plates coated with 1% Gelatin and mouse embryonic fibroblast (MEFs) feeder cells. Medium was switched to complete StemPro-34 (catalog #1063901, TermoFisher Scientific) without cytokines

and changed every other day. On day 7, half medium was replaced with complete iPSCs medium (Essential 8™ Medium, catalog #A1517001, TermoFisher Scientific) and on day 8, entirely replaced with iPSCs medium. Cells were cultured until colonies formed. Reprogrammed cells were karyotyped to ensure genomic integrity, tested for genetic identity (Sanger sequencing) and expression of stemness genes with quantitative PCR (*OCT4*, *NANOG*, *SOX2*, *KLF4*, from Integrated DNA Technologies) summarized in Table 5.3. Data were analyzed by using the 22DCt method after normalization to the *ACTB* gene as an endogenous control and by using water as a negative control.

Gene	**Primer**	**Sequence (5' – 3')**
ACTB	Forward amplification	TGAAGTGTGACGTGGACATC
	Reverse amplification	GGAGGAGCAATGATCTTGAT
OCT4	Forward sequencing	CCTCACTTCACTGCACTGTA
	Reverse sequencing	CAGGTTTTCTTTCCCTAGCT
NANOG	Forward amplification	TGAACCTCAGCTACAAACAG
	Reverse amplification	TGGTGGTAGGAAGAGTAAAG
SOX2	Forward sequencing	CCCAGCAGACTTCACATGT
	Reverse sequencing	CCTCCCATTTCCCTCGTTTT
KLF4	Forward amplification	GATGAACTGACCAGGCACTA
	Reverse amplification	GTGGGTCATATCCACTGTCT

Table 5.3. Primers Sequences. Sequence of primers used for analysis of stemness in iPSCs.

5.1.12. Generation of Artificial Thymic Organoids (ATOs) from iPSCs

Artificial Thymic Organoids (ATOs) were generated by aggregating a DLL4-expressing stromal cell line (MS5-hDLL4) with iPSCs cells differentiated into human Embryonic Mesodermal Progenitors (hEMPs) as previously described (173). Induced Pluripotent Stem Cells (iPSCs) were cultured in Matrigel-coated 6-well plates (catalog #356234, Corning) in NutriStem hPSC XF Medium (catalog #05-100-1A, Biological-Industries). At 50-60 % confluency, iPSCs were treated with TrypLE Express Enzyme (catalog #12604013, ThermoFisher) for 5 minutes at 20°C, washed with PBS and counted. 3 x 10^6 cells per well were plated on Matrigel coated 6 well-plates in 3 mL X-VIVO 15 medium (Lonza catalog #04-418Q, Lonza) with addition of 10 ng/ml of rhActivin A (catalog #338-AC-010, R&D Systems), rhBMP4 (catalog #314-BP-010, R&D Systems),

rhVEGF (catalog #298-VS-005, R&D Systems), rhFGF (catalog #233-FB-025, R&D Systems), and 10 mM of ROCK inhibitor Y-27632 dihydrochloride (catalog #1254, Tocris). Cells were cultured in X-VIVO 15 with 10 ng/ml of rhBMP4, rhVEGF, and rhFGF for 3.5 days with daily medium change. At day 3.5, cells were washed 3 times with PBS and incubated with TrypLE Express Enzyme for 5 minutes at 20°C, washed with PBS and stained with antibodies anti-CD56 FITC (clone MEM-188, catalog #304604, Biolegend) and anti-CD326 (Epcam) AF488 (clone MH99, catalog #53832642, ThermoFisher). Events were acquired on a CANTO II cell analyzer (BD Biosciences) and analyzed using FlowJo software version 10.5.2 (Tree Star, Ashland, OR). 10.000 CD56+ CD326- hEMPs were aggregated in 6 µl of hematopoietic induction medium (EGM2 complete, catalog #CC-4176; 10 uM ROCK inhibitor Y-27632 dihydrochloride, catalog #1254, Tocris; 10 uM TGF-βRI inhibitor SB-431542, catalog #1614, Tocris) with 500.000 MS5-hDLL4 (cultured in Dulbecco modified Eagle medium (DMEM/High Glucose (HyClone), 10% FBS (Gemini Bio-Products), 1% MEM Non-Essential Amino Acid (Corning) and 1% L-glutamine (HyClone) and harvested by trypsinization with Trypsin-EDTA (catalog #5-52F00H, BioConcept) to generate one ATO. Two ATOs were plated on a 0.4 mm Millicell transwell insert (catalog #PICM0RG50, EMD Millipore) in 6-well plates with 1 mL hematopoietic induction medium per well. During the first week of culture, hematopoietic induction medium was completely changed every other day. During the second week of culture, hematopoietic induction medium with addition of 5 ng/ml hematopoietic cytokines rhTPO (catalog #300-18, Peprotech), rhFLT3L (catalog #300-19, Peprotech), and 50 ng/ml of rhSCF (catalog #300-07, Peprotech) was changed every other day. At the beginning of the third week, or the first week of T-cell induction, medium was changed to T-cell induction medium (RPMI, 4% B27 supplement (ThermoFisher Scientific), 30 mM L-ascorbic acid 2-phosphate sesquimagnesium salt hydrate (Sigma-Aldrich) reconstituted in PBS, 1% penicillin/streptomycin (Gemini Bio-Products), 1% Glutamax (ThermoFisher Scientific), with 10 ng/ml rhSCF, 5 ng/ml rhFLT3L, and 5 ng/ml rhIL-7 (catalog #200-07, Peprotech) and completely changed every 3 or 4 days. After 5 to 7 weeks of T cells differentiation, ATOs were collected by adding PBS to each well and dissociated by pipetting with 1 mL pipette. Cells were filtered through 70 µm strainers, pelleted, resuspended in PBS with 2% fetal bovine serum, counted, and stained with antibodies summarized in Table 5.4.

Antibody	Clone	Catalog #	Source
CD1a APC	HI149	300110	Biolegend
CD3a PECy7	SK7	341111	BD Biosciences
CD4 APC	-	555349	BD Biosciences
CD5 PECy7	UCHT2	300622	eBioscience
CD7 APCCy7	M-T701	564020	BD Biosciences
CD8a APCCy7	SK1	557834	BD Biosciences
CD8b PB	RPA-T8	558207	BD Biosciences
CD34 PE	-	345802	Becton Dickinson
CD45 PerCPCy5.5	HI30	564106	BD Bioscience
CD56 FITC	MEM-188	304604	Biolegend
TCRβ PE	-	555548	BD Biosciences
DAPI	-	D9542-10MG	Sigma Aldrich

Table 5.4. List of Antibodies and dyes used for human FACS staining. APC, Allophycocyanin; FITC, fluorescein isothiocyanate; PerCP, peridinin chlorophyll protein; DAPI: 4′,6-diamidino-2-phenylindole.

Events were acquired on a BD Canto II cell analyzer (BD Biosciences) and analyzed using FlowJo software version 10.5.2 (Tree Star).

5.2. Murine studies

5.2.1. *In silico* prediction studies

In silico analysis on murine *Fcho1* gene were preformed using online free platforms and softwares: Aminode (http://www.aminode.org/?gene=FCHO1); Ensembl (http://www.ensembl.org/Homo_sapiens/Gene/Summary?db=core;g=ENSG00000130000;r=19:17747718-17788568; http://www.ensembl.org/Mus_musculus/Gene/Summary?db=core;g=ENSMUSG00000070000;r=8:71708387-71725716), BLAST (https://blast.ncbi.nlm.nih.gov/Blast.cgi), Expasy (https://www.expasy.org/) and MacVector (version 17.0.10).

5.2.2. Design and screening of *Fcho1* single guide RNAs (sgRNAs) and donor-template DNA

A series of single guide RNAs (sgRNAs) were designed on Benchling on-line platform (176) to specifically target the region around c.120-1 of *Fcho1*. Seven sgRNAs (Table 5.5) were evaluated for the optimal distance to the target site (3 to 8 base-pairs), the possibility to easily remove the PAM sequence in the sg-RNA-specific DNA donor template and the on-target and off-target scores (On Target Scores 35.2 to 70.2, and Off Target Scores 28.4 to 42.9) as previously reported (177, 178).

Name	**Targeted gDNA Strand (- or +)**	**Sequence**
sgRNA#1	-	CGAGTATGTCTCCTCGATGT
sgRNA#2	+	CTGACCCAGGGCCAACATCG
sgRNA#3	-	TGTCTCCTCGATGTTGGCCC
sgRNA#4	-	GTCTCCTCGATGTTGGCCCT
sgRNA#5	+	TTTGCCCCTTCTCTGACCCA
sgRNA#6	-	TGTTGGCCCTGGGTCAGAGA
sgRNA#7	+	CTTTGCCCCTTCTCTGACCC

Table 5.5. SgRNA Sequences. Sequence of sgRNA analyzed. - : negative, + : positive

NCBI blast was used to search the genome for sequence similarity. 3 sgRNAs (sgRNA#2, sgRNA#5 and sgRNA#7, provided by Synthego) were selected for further *in vitro* screening with the Guide-it™ sgRNA Screening Kit (catalog # 632639, Takara). According to manufacturer's instructions, 725 base-pair long genomic DNA was amplified by PCR (Forward Primer: GATTCTGAGTGCTAGCATCAGAAGTG, Reverse Primer: CAATGTCTACACATGTGTTC GAGTAGAC), cut products were run on Agarose 2% gel. The donor-template DNA for homology-mediated repair (HDR) was designed based on sgRNA#7 intrinsic characteristics. The DNA sequence is the following, highlighted in red the G>C 120-1 mutation: GAGACATACTCGAAGGCCATGGCCAAACTCTCCAAGCTAGCCAGCAACGGGACCCC CATGGGGTAAGTGCAGCTGGATGGGTGAGGGACACTCAAGAATGCCTTTCTCAGGG TACTGTAATCTGCTCTTTGCCCCTTCTCTGACCCACGGCCAACATCGAGGAGACATA CTCGAAGGCCATGGCCAAACTCTCCAAGCTAGCCAGCAACGGGACCCCCATGGGGT AAGTGCAGCTGGATGGGTGAGGGACACTCAAG.

The desired mutation in the donor template prevented simultaneously additional cutting after incorporation into the targeted mouse genome.

5.2.3. Generation of CRISPR/Cas9 *Fcho1*-mutant mice and genotyping

108 murine zygotes were microinjected with- and 120 murine zygotes were electroporated with 1 µg/µl of sgRNA#7 (Synthego), 1 µg/µl of DNA donor template (Integrated DNA Technologies) and 250 ng/µl Cas9 (Integrated DNA Technologies). Zygotes were then implanted into recipient foster mothers and pups were born two and a half weeks later (F0). At 21 days of age, tails from pups (31 in total) were collected, gDNA was extracted and analyzed by PCR and Sanger sequencing for the presence of the splicing mutation in the *Fcho1* gene (genomic region spanning 7902 – 8628, 726 bp long). For this purpose, genomic DNA was isolated from tail of 3- to 4-week-old newborn *Fcho1* mutated pups by using the DNeasy Blood & Tissue Kit (69506; Qiagen) and was analyzed by PCR and Sanger sequencing for the presence of mutations in the *Fcho1* gene. PCR was performed using Phusion Hot start II (Lifetechnologies Cat# F-549L) in a 20 µL reaction following the manufacturer's instruction. A genomic region of 836 base-pair was amplified using the following primers: Forward primer: 5′-GATTCTGAGTGCTAGCATCAGA

AGTG -3′, Reverse primer: 5′- GTTACAGATGTGTACACAAGCTCATCT - 3′, provided by Integrated DNA Technoligies, annealing temperature 62°C. F0 mice were bred with w/t B6 mice to get heterozygous F1 mice, which were in turn bred to obtain homozygous F2 mice. Experiments were performed on mice from F2 or later generations. Animal work was performed in pathogen-free conditions, in accordance with the US Public Health Service Policy on Human Care and Use of Laboratory Animals, with protocols approved by the National Institute of Allergy and Infectious Diseases Animal Care and Use Committee (Protocol LCIM 16E). All mice described were on a C57BL/6 background.

5.2.4. Analysis of RNA splicing

RNA extracted from whole splenocytes derived from *Fcho1* mutant mice and *w/t* mice was retrotranscribed with random primers and the ImProm-II Reverse Transcription System (Promega), according to the manufacturer's instructions. RT-PCR for *Fcho1* transcript of 421 base pairs was performed by using primers (Forward, 5'-CTTTGAGGTCCTCTACCATTG-3'; Reverse, 5'-GAGAGAACACCAGCCAGAA -3') with an annealing temperature of 60°C and sequenced by meaning of Sanger sequencing.

5.2.5. Mouse Immune Phenotyping

Blood from *Fcho1*-mutant and *w/t* mice of 6 – 7 weeks old was drawn in EDTA and Complete Blood cell Count (CBC) was performed. Red Blood Cell lysis was performed 3 times using 10X RBC Lysis Buffer (Multi-species) (catalog # 00-4300-54, ThermoFisher) diluted 1:10 in sterile distilled water, white blood cells were then resuspended in FACS buffer and stained with Antibodies listed in Table 5.6. *Fcho1*-mutant and *w/t* mice were sacrificed at 8 to 12 weeks of age. Single-cell suspensions were obtained from thymys and spleen and stained with antibodies listed in Table 5.6. Samples were acquired by using flow cytometry (LSRFortessa; BD) and analyzed with FlowJo software (version 10.5.2; TreeStar).

Antibody	Clone	Catalog #	Source
B220 V500	RA3-6B2	561226	BD Bioscience
B220 PeCy7	RA36B2	552772	BD Bioscience
CD3ε AF700	500A2	557984	BD Pharmingen
CD4 PerCPCy5.5	RM/4-5	553052	BD Bioscience
CD4 Pacific Blue	GK1.5	100428	BioLegend
CD8 PE	SK1	344706	BioLegend
CD8 PerCPCy5.5	SK1	344710	BioLegend
CD11β BV650	M1/70	563402	BD Bioscience
CD19 APCCy7	6D5	115530	BioLegend
CD19 PB	1D3	11019382	eBioscience
CD21 PB	7E9	123413	BioLegend
CD24 PE	M1/69	553262	BD Bioscience
CD25 PE	PC61	102008	BioLegend
CD44 APCCy7	IM7	560568	BD Bioscience
CD45 PECy7	30-F11	25045182	ThermoFisher
CD45 PerCPCy5.5	104	552950	BD Bioscience
GR1 BV605	RB6-8C5	108440	BioLegend
NK1.1 APC	PK136	17594182	ThermoFisher
TCRβ PECy5	H57-597	553173	BD Bioscience
DAPI	-	D1306	ThermoFisher
Live/Dead Aqua530	-	L34957	ThermoFisher
Live/Dead PO	-	L34959	Invitrogen

Table 5.6. List of Antibodies and dyes used for murine FACS staining. APC, Allophycocyanin; FITC, fluorescein isothiocyanate; PerCP, peridinin chlorophyll protein; DAPI: 4′,6-diamidino-2-phenylindole.

5.2.6. *In vitro* T cell activation and proliferation

For analysis of T cell activation, 5 x 10^5 whole splenocytes from *Fcho1*-mutant and *w/t* mice were cultured in 200 μL of serum-supplemented RPMI (SH30027.01; GE Healthcare Life Sciences) in round-bottom 96-well plates with 1 μg/mL anti-CD3 (clone 145-2C11, catalog #BE0001-1, BioXCell) plus 1 μg/mL anti-CD28 (clone 37.51, catalog #BE0015-1, BioXCell) at 37°C for 24, 48 and 72 hours. Cells were collected, washed with serum supplemented PBS, and stained with Live/Dead staining and fluorochrome-conjugated CD3, CD4, CD8, CD25, CD44, CD62L, CD69, CD71 (Table 4.5) for 15 minutes at 4°C (dark). Expression of activation markers was analyzed by using flow cytometry (LSRFortessa; BD) and FlowJo software (version 10.5.2; TreeStar). For

analysis of T-cell proliferation, whole splenocytes from *Fcho1*-mutant and *w/t* mice were incubated with the CellTrace violet Cell Proliferation Kit (1 mmol/L; Invitrogen). After 20 minutes, 10 volumes of RPMI/10% FBS were added, and the cells were washed three times with RPMI/10% FBS. A total of 5 x 10^5 cells was seeded into 96-well plates and stimulated with 1 μg/mL anti-CD3 plus 1 μg/mL anti-CD28 for 72 hours. Cells were then stained with fluorochrome-conjugated CD4 and CD8 antibodies (Table 4.5) for 30 minutes at 4°C (dark) and washed twice with PBS twice, and CellTrace Violet expression was analyzed by using flow cytometry (Becton Dickinson FACSCanto II) and FlowJo software (version 10.5.2; TreeStar).

5.2.7. *In vitro* internalization of T cell receptor (TCR)

5 x 10^5 whole splenocytes from *Fcho1*-mutant and *w/t* mice were either left unstimulated or stimulated with 1 μg/mL anti-CD3 plus 1 μg/mL anti-CD28 and Brefeldin A (1000x solution, catalog #420601, BioLegend) in 200 μL of serum-supplemented RPMI at 37°C for 5 and 15 minutes. At each time point, cells were collected, washed with serum supplemented PBS, and stained with Live/Dead staining and fluorochrome-conjugated CD3, CD4, CD8, CD45, TCRαβ (Table 4.5) for 15 minutes at 4°C (dark). Cells were washed with serum-supplemented PBS, acquired, and analyzed by using flow cytometry (LSRFortessa; BD) and FlowJo software (version 10.5.2; TreeStar).

5.2.8. B cell *in vitro* proliferation

For analysis of B cell activation, untouched resting B cells were isolated by whole splenocytes from *Fcho1*-mutant and *w/t* mice by using of the CD43 (Ly-48) MicroBeads, mouse kit (catalog # 130-049-801, Miltenyi Biotec), incubated with the CellTrace violet Cell Proliferation Kit (1 mmol/L; Invitrogen), washed three times and plated at 2.5 x 10^5 cells in 200 μL of serum-supplemented RPMI (SH30027.01; GE Healthcare Life Sciences) in round-bottom 96-well plates with 1 μg/ml LPS from Escherichia coli (catalog #ALX-581-013-L001, Enzo Life Sciences), 5 μg/ml F(ab')2 goat anti-mouse IgM (catalog #AB_2338469, Jackson ImmunoResearch), 10 μg/ml rat anti-mouse CD40 (catalog #553788, BD Bioscience) at 37°C for 48 and 72 hours. Cells were

collected, washed with serum supplemented PBS, and stained with Live/Dead staining and fluorochrome-conjugated CD45+, CD19+, B220+ (Table 4.5) for 15 minutes at 4°C (dark), washed twice with PBS twice, and CellTrace Violet expression was analyzed by using flow cytometry (Becton Dickinson FACSCanto II) and FlowJo software (version 10.5.2; TreeStar).

5.2.9. Statistical analysis

Results are indicated as medians plus or minus SDs. 2-tailed Mann-Whitney test for comparing 2 groups or multiple t test (alpha 0.05, not corrected for multiple comparison) were used for statistical significance assessment. Statistically significant P values in the figures: *P < .05; **P < .005; ***P < .0005; ****P < .0001.

6. RESULTS

6.1. Clinical characterization and immunological phenotype of the patients.

In this study, 5 patients (P1-P5) from unrelated families of Italian (P1), Turkish (P2, P3, and P5) and Algerian (P4) origin (Figure 6.1) with biallelic *FCHO1* mutations and combined immunodeficiency, manifesting as recurrent and severe infections of bacterial, mycobacterial, viral, and fungal origin and profound T cell lymphopenia (Table 6.1) are reported. Three patients (P3, P4, P5) died in childhood, P1 died 14.8 years after successful allogeneic hematopoietic stem cell transplantation (HSCT), whereas P2 is alive with full donor chimerism 3.5 years after allogeneic HSCT and has cleared pre-transplantation infections.

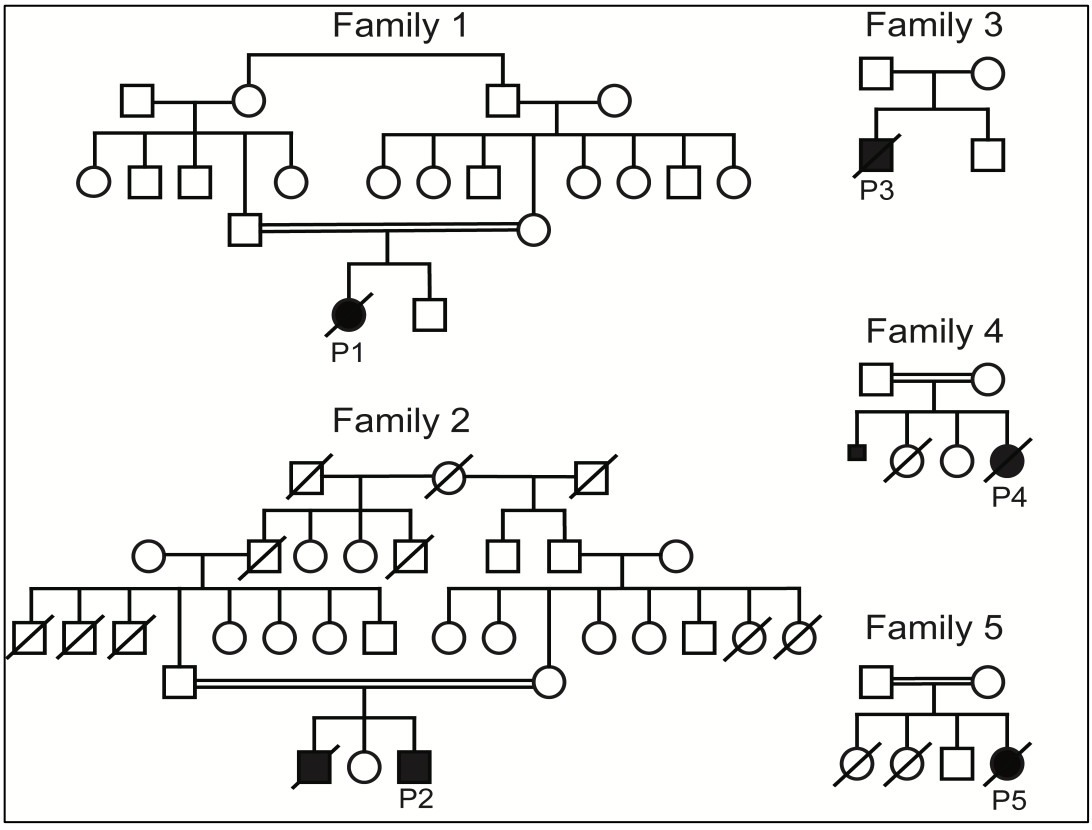

Figure 6.1. Pedigrees of patients. Patients (P1-P5, from family 1-5) with *FCHO1* mutations.

Patient 1 (P1), of Italian origin, was born to first-cousin parents (Figure 6.1, Family 1) and manifested recurrent respiratory (pneumonias and bronchiolitis) and gastrointestinal tract infections since the first months of life. At the age of 3 years, she was admitted for severe *Pneumocystis jirovecii* pneumonia, diarrhea, and growth failure (weight, 12.9 kg, less than the third percentile; length, 97 cm, less than the third percentile). Laboratory examinations at admission revealed profound lymphopenia (Table 6.1), with absolute lymphocyte count (ALC) of 700 cells/μL and CD3+ T cell count of 6 cells/μL, with 2 cells/μL CD4+ and 2 cells/μL CD8+ cells. Neutrophil count at the time was normal for age (7940 cells/μL) and no abnormalities of B-cell phenotype (absolute count and antibodies production), or NK cells were observed.

Clinical features	P1	P2	P3	P4	P5
Demographic					
Origin	Italian	Turkish	Turkish	Algerian	Turkish
Age at evaluation	3 y	18 mo	8 y	2.5 y	6 y
Infections					
Respiratory tract	Pneumonias, PJP, bronchiolitis	Pneumonias, bronchiolitis	Pneumonias	Pneumonias	Pneumonias
Gastrointestinal tract	Chronic diarrhea	Chronic diarrhea	—	Colitis	—
Others	Disseminated *Mycobacterium genavense* infection	—	Varicella, EBV viremia	Skin abscess, dermatophytosis	EBV viremia, fungal pneumonia
Growth failure	+	+	—	—	+
Lymphoproliferation					
Splenomegaly	+	—	+	+	—
Lymphadenopathy	+	—	+	+	—
Malignancies	—	—	EBV-negative DLBCL	—	—
Outcome	Deceased 14.8 y after HSCT	Alive and well 3.5 y after HSCT	Deceased	Deceased	Deceased
Laboratory data					
ALC (cells/μL)	**700**	**1000**	**542**	**1159**	**1200**
ANC (cells/μL)	7940	3100	5650	4575	3570
$CD3^+$ (cells/μL)	**6**	**360**	**184**	**823**	**792**
$CD4^+$ (cells/μL)	**2**	**245**	**27**	**100**	**95**
$CD8^+$ (cells/μL)	**2**	**82**	**108**	**206**	**308**
$CD19^+$ (cells/μL)	459	180	**65**	220	120
$CD16/CD56^+$ (cells/μL)	192	320	103	116	120
IgG (mg/dL)	470 (on IVIG)	460	2230	833	909
IgA (mg/dL)	24	26	109	**9**	112
IgM (mg/dL)	45	**30**	173	**29**	428

Table 6.1. Clinical and laboratory features of *FCHO1*-mutated patients. ALC, Absolute lymphocyte count; ANC, absolute neutrophil count; DLBCL, diffuse large B-cell lymphoma; GI, gastrointestinal; IVIG, intravenous immunoglobulins; PJP, *Pneumocystis jirovecii* pneumonia. Abnormal values for age are shown in boldface.

An abdominal computed tomographic (CT) scan showed splenomegaly and diffuse mesenteric lymphadenopathy. Lymph node biopsy specimen grew *Mycobacterium genavense*. At the age of 3 years and 7 months, the patient received a matched unrelated donor hematopoietic cell transplantation with myeloablative conditioning. The clinical course after transplantation was complicated by chronic graft-versus-host disease (GVHD), autoimmune hemolytic anemia and portal hypertension, that led to the implantation of a transjugular intrahepatic portosystemic shunt. Her mycobacterial disease resolved, but because of the intestinal chronic GVHD and the formation of adherences, she remained with low weight (35.9 kg) and height (128 cm). She continued to experience episodes of steroid-resistant hemolytic intermittent anemia that required therapy with anti-CD20 monoclonal antibody (Rituximab). Because of recurrent episodes of intestinal hemorrhages and sub-occlusions, she underwent intestinal resection surgery that was complicated by hypotension, hemorrhage and desaturation, and led to the patient's death in the following days, 14.8 years after HSCT.

Patient 2 (P2), a boy born to consanguineous parents of Turkish origin (Figure 6.1, Family 2), had recurrent respiratory tract infections and growth failure (weight, 7.8 kg, less than the third percentile) since 6 months of age. Laboratory investigations revealed T cell lymphopenia (ALC of 1000 cells/μL and CD3+ T cell count of 360 cells/μL, with 245 cells/μL CD4+ and 82 cells/μL CD8+ cells), decreased serum IgM levels (30 mg/dL) with normal levels of IgG (460 mg/dL) and IgA (26 mg/dL) for age, but poor antibody responses (Table 6.1). No thymic shadow was visible at chest radiography, and a chest CT scan demonstrated diffuse bronchiectasis (Figure 6.2, A and C). He was initially treated with intravenous immunoglobulin and antimicrobial prophylaxis and received a matched unrelated donor hematopoietic cell transplantation with myeloablative conditioning at the age of 2.5 years. The post-transplantation course was complicated by engraftment syndrome, which was successfully treated with steroids, and grade II acute graft-versus-host disease (GVHD). He is currently alive and well, with full donor chimerism at 6 years of age. His older brother was admitted at 1 year of age with a history of recurrent pneumonias, diarrhea, candidiasis, and growth failure (weight 5 kg, less than the third percentile) since the age of 7 months. Laboratory tests revealed T and B cell lymphopenia, hypogammaglobulinemia, and impaired antibody responses, for which he was treated with intravenous immunoglobulin. At the age of 6 years, he had severe pneumonia, *Candida species*–related sepsis, and vesicular lesions on

his back. Despite extensive antibacterial and antifungal therapy, he developed multiorgan failure and died.

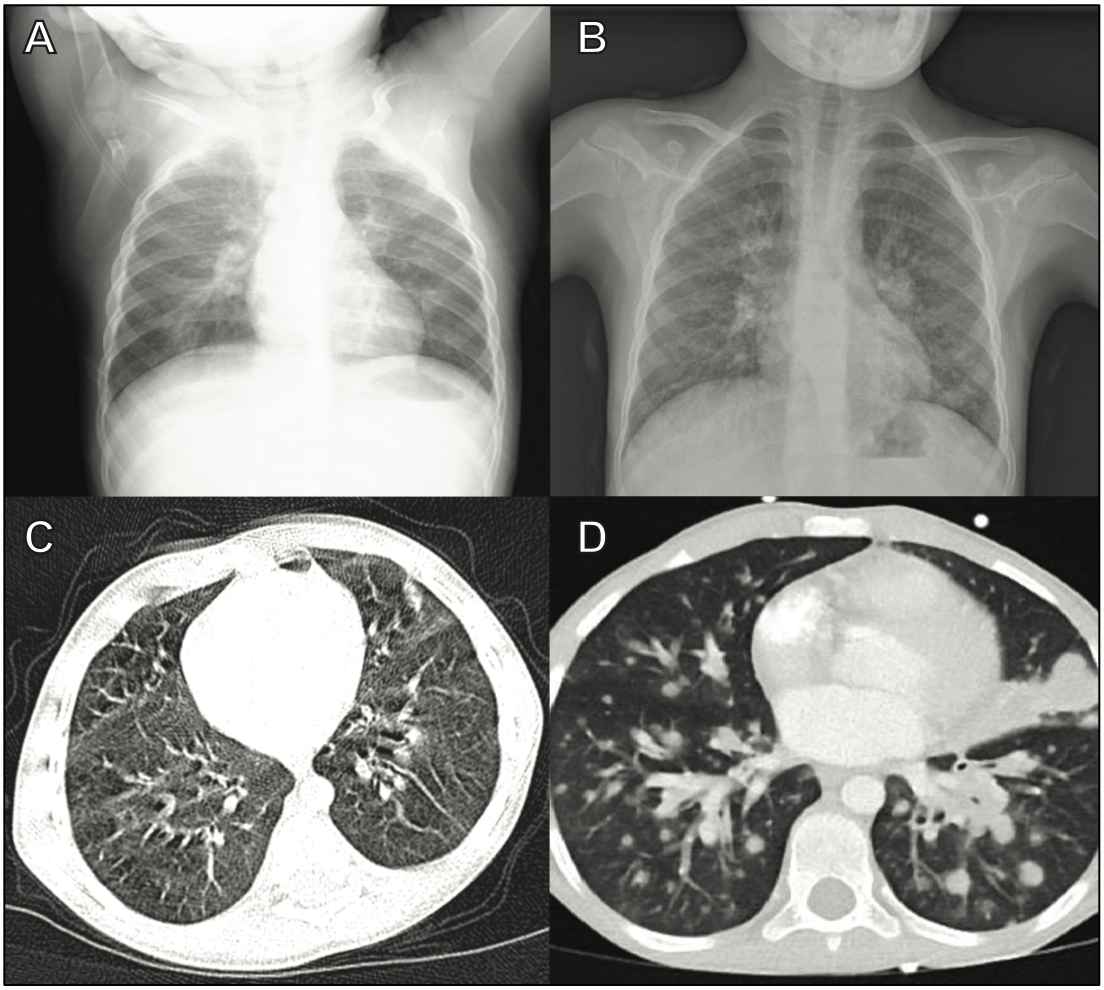

Figure 6.2. Chest radiography. Anteroposterior chest radiography showing lack of thymic shadow in P2 (A) and P3 (B) and non-contrast chest CT scan showing bronchiectasis in P2 (C) and multiple parenchymal nodules in P3 (D).

Patient 3 (P3), a male child born to apparently nonconsanguineous parents from the same small village in Turkey, was admitted at the age of 8 years because of fever and dyspnea (Figure 6.1, Family 3). At admission, laboratory work-up revealed T-cell and B-cell lymphopenia (ALC of 542 cells/μL and CD3+ T cell count of 184 cells/μL, with 27 cells/μL CD4+ and 108 cells/μL CD8+ cells, 65 cells/μL CD19+ B cells) (Table 6.1), no thymic shadow was visible at chest radiography,

parenchymal pulmonary nodules were observed at chest CT scan (Figure 6.2, B and D). Ultrasound studies revealed diffuse lymphadenopathy, and high levels of EBV viremia (178,000 copies/mL) were found. During follow-up, both lymphopenia and neutropenia were observed; a bone marrow biopsy specimen was consistent with hemophagocytic lympho-histiocytosis. Because of persistent lymphadenopathy, a lymph node biopsy was performed which revealed a diffuse EBV-negative large B cell lymphoma. His clinical course was complicated by respiratory failure, leading to death.

Patient 4 (P4) (Figure 6.1, Family 4), a female child born to consanguineous parents of Algerian origin, had an older sister with a history of disseminated BCG, chronic diarrhea, and recurrent pneumonias who died from a severe pneumonia resulting in acute respiratory failure. P4 herself had recurrent pneumonias, chronic diarrhea, skin abscesses, and refractory dermatophytosis at 4 months of age. By 2.5 years of life, she experienced neuromotor regression, with an inability to stand or sit, ataxia, hypermetria, and tremors. Immunologic evaluation at 2.5 years of life was notable for CD4+ and CD8+ T cell lymphopenia (ALC of 1159 cells/μL and CD3+ T cell count of 823 cells/μL, with 100 cells/μL CD4+ and 206 cells/μL CD8+ cells), reduced IgM (29 mg/dL) and IgA (9 mg/dL) levels, reduced B-cell numbers, and nearly absent memory B cells (Table 6.1). She continued to experience severe recurrent pneumonias and died at 4 years of age of respiratory failure.

Patient 5 (P5) (Figure 6.1, Family 5), a female child born to first-cousin parents of Turkish origin, was admitted at 6 years of age with fever, dyspnea, oral thrush, new-onset ataxia and seizures. She had no history of prior recurrent infections. Chest and abdominal CT revealed bilateral areas of consolidation and nodular opacities, as well as hepatic lesions that were identified as granulomas on histologic analysis. Cultures of bronchoalveolar lavage fluid were positive for *Klebsiella pneumoniae*. Brain magnetic resonance imaging revealed multiple 1.5-cm nodules in the right cerebellar hemisphere. Laboratory testing at that time was notable for T cell lymphopenia (ALC of 1200 cells/μL and CD3+ T cell count of 792 cells/μL, with 95 cells/μL CD4+ and 308 cells/μL CD8+ cells), increased IgM levels (428 mg/dL) (Table 6.1), and EBV viremia (38,000 copies/mL). During hospitalization, she had worsening respiratory failure accompanied by increasing size of cerebellar lesions despite treatment with meropenem, vancomycin, metronidazole, acyclovir, and amphotericin B. Histologic analysis of the brain lesions revealed angio-centric and angio-destructive lymphoid infiltrate admixed with histiocytes, with atypical CD20+ lymphoid cells

positive for EBV and CD30, which is consistent with a diagnosis of lymphomatoid granulomatosis. She was treated with Rituximab and prednisone, but died of respiratory failure.

With no apparent clear definitive clinical diagnosis, the five patients were considered affected by Severe Combined Immunodeficiency of unknown genetic origin with profound T-cell lymphopenia manifesting as recurrent and severe infections.

6.2. Studies on patients' variants

6.2.1. WES and targeted sequencing

To define the genetic origin of the disease, whole-exome sequencing (WES) (P1, P2, P4, and P5) and targeted sequencing of a large panel of primary immune deficiency–related genes (P3) on genomic DNA extracted from patients' samples were independently performed. Variants were annotated by using the Ensembl Variant Effect Predictor (VEP) or by using the Genome Analysis Toolkit (GATK) and filtered by using a software for exploring forms of human genetic variation (Genome MINIng, GEMINI (179) based on the autosomal recessive model of inheritance. Filtering strategy that was applied to the WES results is reported in Figure 6.3.

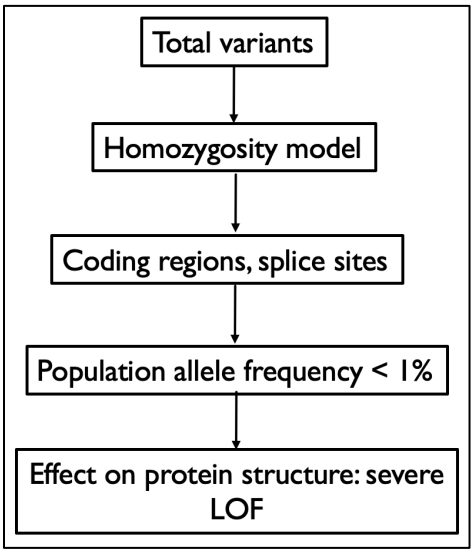

Figure 6.3. Filtering strategy. Strategy used for analysis of WES. LOF: loss of function.

Variants were initially prioritized by the homozygosity model, based on the autosomal recessive mode of inheritance. The choice of which model to apply was driven by the familiar history and clinical presentation of the disease (consanguinity in the family and/or provenience from a small community or regions likely identical by descent with high probability of inbreed occurrence, healthy parents, disease not found in every generations of the family, no gender differences in humans affected, high severity of the clinical presentation). Variants were then filtered for coding

regions and splice sites, then for minor allele frequency of less than 0.01 (rare variants), as reported in the ExAC browser. Finally, variants were prioritized by the severity of the effect on the protein structure (severe loss of function) and the involvement in functions of the immune system of the genes affected. Blacklisted nonpathogenic common variants (nonpathogenic, cohort-specific common variants that cannot be removed from the analysis) were filtered out (180). For patient 3, targeted sequencing of 365 primary immune deficiency related genes and data analysis were performed on genomic enriched DNA (Haloplex enrichment technology, PID Panel) with a percentage of gene coverage of 97.3%, as previously described (175). For all filtered variants, Combined Annotation Dependent Depletion scores (CADD PHRED and CADD_MSC) and probability of loss of function intolerance (pLi) algorithms were used to assess the pathogenicity. Variant conservation and functional prediction, gene expression pattern, and available known biological knowledge were used to prioritize the candidate variants to identify the disease causal variant from rare family private variants. Role in the immune system was also taken into account. The final variants considered (14 for P1, 13 for P2, 26 for P4, 29 for P5 and 6 for P3) with type, transcript, protein effect, are shown in Table 6.2.

Rare homozygous exonic and splice-site genetic variants identified in P1, P2, P4, and P5 by using whole-exome sequencing

	Gene	Type of variant	Transcript variant	Protein effect of the variant	EXAC MAF	gnomAD MAF	CADD PHRED score	CADD_MSC	pLi
P1	*FCHO1*	splice_acceptor_variant	NM_001161357.1:c.120-1G>C	NP_001093646:p.Asp4Val	—	—	26.3	5.744	1
	HOOK2	missense_variant	NM_001100176:c.11A>T	NP_006480:p.Pro256Ala	1.3E-04	1.1E-04	28.1	5.751	0
	NOVA1	missense_variant	NM_006489:c.766C>G	NP_001242941:p.Asp9Gly	8.2E-06	4.1E-06	24.3	3.313	0.98
	MYH10	missense_variant	NM_001256012:c.26A>G	NP_002552:p.Ala268Val	3.3E-05	2.2E-05	25.0	5.355	1
	P2RX5	missense_variant	NM_002561:c.803C>T	NP_056308:p.Arg662Gln	1.5E-04	1.6E-04	23.9	3.313	0
	KANK2	missense_variant	NM_015493:c.1985G>A		3.8E-04	4.0E-04	16.8	3.313	0.98
	SH3GLB2	splice_region_variant	NM_001287046:c.739-5C>T	NP_056093:p.Pro828Ser	4.8E-05	3.3E-05	13.0	5.263	0.37
	SASH1	missense_variant	NM_015278:c.2482C>T	NP_849188:p.Glu1324Gly	1.2E-03	1.2E-03	17.8	3.313	0
	RP1L1	missense_variant	NM_178857:c.3971A>G	NP_039228:p.Glu52Gln	—	—	0.0	0.009	0
	OR10H1	missense_variant	NM_013940:c.154G>C	NP_055861:p.Arg20His	8.7E-03	8.6E-03	9.5	3.313	0.64
	SETX	missense_variant	NM_015046:c.59G>A	NP_001156787:p.Ala130_Ala132del	9.1E-03	9.3E-03	0.2	0.006	0.2
	FBXL17	inframe_deletion	NM_001163315:c.388_396delGCT	NP_001078920:p.Ser93_His94ins	2.1E-03	8.2E-04	12.0	5.778	0.98
	LNP1	inframe_insertion	GCCGCC	SerAspArgLeuProArgArgHisSerHis	—	—	4.2	3.313	0
	NOP9	inframe_insertion	NM_001085451:c.260_261insGGAA TTCCGATGCCGATCGTCTGACC GTCTTCCTAGAAGGCATTCTCA TGAGGACCA NM_001286367:c.504_509dupGGAGGA	GluAspGlnGluPheArgCysArgSer NP_001273296:p.Glu168_Glu169dup	—	—	10.8	3.313	0
P2	*FCHO1*	frameshift_variant	NM_001161357.1:c.2023dupG	NP_001154829.1:p.Val675Glyfs*13	—	—	34.0	5.744	1
	ZNF730	frameshift_variant	NM_001277403:c.906dupT	NP_001264332:p.Lys303*	3.9E-03	3.6E-03	23.3	3.313	0
	MEGF9	missense_variant	NM_001080497:c.502A>G	NP_001073966:p.Thr168Ala	2.0E-03	1.9E-03	16.1	3.313	0.92
	AKAP8	missense_variant	NM_005858:c.676G>A	NP_005849:p.Glu226Lys	3.0E-03	2.5E-03	24.4	3.313	0.98
	KIAA0947	missense_variant	NM_015325:c.4610C>G	NP_056140:p.Ser1537Cys	—	—	23.2	3.313	1
	SV2C	splice_region_variant	NM_001297716:c.1137+3G>T		6.6E-05	6.1E-05	22.0	3.313	0
	GALR3	missense_variant	NM_003614:c.935G>T	NP_003605:p.Arg312Leu	8.0E-04	1.4E-03	15.8	5.745	0.02
	FAM105B	missense_variant	NM_138348:c.345G>T	NP_612357:p.Gln115His	6.5E-03	6.6E-03	15.7	3.313	0.97
	AP3B1	missense_variant	NM_003664:c.2995G>A	NP_003655:p.Val999Met	3.8E-03	4.1E-03	14.0	0.879	1
	TRIO	missense_variant	NM_007118:c.7292A>C	NP_009049:p.Asp2431Ala	—	—	16.8	3.313	1
	MAP1S	missense_variant	NM_001308363:c.1831C>T	NP_001295292:p.Arg611Cys	4.2E-04	2.0E-04	13.4	3.313	0.64
	CSDC2	splice_region_variant	NM_014460:c.300-6C>T		2.8E-03	2.8E-03	5.0	5.764	0.08
	PCNT	missense_variant	NM_006031:c.5771C>T	NP_006022:p.Ala1924Val	7.4E-03	6.0E-03	0.5	0.001	0

P4	*FCHO1*	frameshift_variant	NM_001161357.1:c.184_185insC	NP_001154829.1:p.Met64Hisfs*104	8.2E-06	—	28.9	5.744	1
	AIM1L	disruptive_inframe_deletion		NP_001034864.2:p.Asp539_	7.1E-05	—	2.4	5.798	0
	KIAA0040	missense_variant	NM_001039775.3:c.1593_1643delC	Pro555del	—	—	14.8	10.903	0
	THADA	missense_variant	GTGAAGGGCCCCGGTGCTCCTG	NP_055471.2:p.Asn65Lys	4.4E-05	3.0E-05	10.3	3.313	0
	CAND2	splice_acceptor_variant	ATGCCTCATTTCCCACCTGGAA	NP_071348.3:p.His1663Gln	—	—	32.0	3.313	0
	MUC4	missense_variant	AGAGGT		—	1.6E-03	7.6	3.313	0
	ZNF718	missense_variant	NM_014656.2:c.195C>A	NP_060876.5:p.Ala1198Thr	2.2E-03	2.4E-03	3.3		NA
	DGKQ	missense_variant	NM_022065.4:c.4989C>G	NP_001034216.2:p.Asn317=	9.5E-04	1.7E-03	19.3	3.313	0
	DGKQ	splice_region_variant	NM_001162499.1:c.492-1G>A	NP_001338.2:p.Arg240His	—	—	9.9	3.313	0
	GRK4	frameshift_variant	NM_018406.6:c.3592G>A		4.9E-04	5.2E-04	31.0	3.313	0
	HTT	splice_region_variant	NM_001039127.5:c.951T>C	NP_892027.2:p.Arg222Lysfs	8.2E-04	7.9E-04	8.6	3.313	1
	ADH1B	missense_variant	NM_001347.3:c.719G>A		8.2E-05	8.9E-05	24.5	3.313	0.19
	MTTP	missense_variant	NM_001347.3:c.272-3C>T	NP_000659.2:p.Arg313Cys	2.3E-04	3.5E-04	15.5	0.002	0.01
	TXNDC5	missense_variant	NM_182982.2:c.655_656insA	NP_001287714.1:p.Pro913Leu	—	3.3E-04	12.3	3.313	0
	KLHL31	missense_variant	NM_002111.8:c.529-3C>T	NP_110437.2:p.Arg37Gln	2.0E-03	2.3E-03	26.1	3.313	0.02
	ZP3	splice_region_variant	NM_000668.5:c.937C>T	NP_001003760.2:p.Val111Met	6.9E-04	7.5E-04	0.6	3.313	0
	FBXW8	missense_variant	NM_001300785.1:c.2738C>T		—	0.0E+00	23.9	3.313	0
	DZIP1	missense_variant	NM_030810.4:c.110G>A	NP_699179.2:p.His294Asp	3.1E-04	3.4E-04	24.4	3.313	0
	GOLGA6L2	missense_variant	NM_001003760.4:c.331G>A	NP_945319.1:p.Pro657Leu	9.6E-05	—	11.4	3.313	0
	DENND4A	missense_variant	NM_001110354.1:c.536-4T>A	NP_001291317.1:p.Ala806Pro	—	—	16.3	3.313	0
	ZFPM1	disruptive_inframe_deletion	NM_153348.2:c.880C>G	NP_001307764.1:p.Ser1315Gly	1.4E-03	1.2E-03	10.2	3.313	0.03
	WRAP53	missense_variant	NM_198968.3:c.1970C>T	NP_722520.2:p.Leu446_Ala447del	4.1E-04	3.5E-04	7.7	23.7	0.62
	USP22	missense_variant	NM_001304388.1:c.2416G>C	NP_060551.2:p.Val63Met	1.7E-05	8.1E-06	24.7	5.562	0.98
	ECSIT	missense_variant	NM_001320835.1:c.3943A>G	NP_056091.1:p.Leu205Met	—	4.1E-06	0.1	3.313	0.02
	RFX1	missense_variant	NM_153813.2:c.1334_	NP_057665.2:p.Ser49Ile	2.5E-05	4.5E-05	26.1	3.313	1
	NOTCH3	missense_variant	1339delCTCTGG	NP_002909.4:p.Gln280Arg	1.6E-04	2.3E-04	28.7	12.19	0.21
			NM_018081.2:c.187G>A	NP_000426.2:p.Val2021Met					
			NM_015276.1:c.613C>A						
			NM_016581.4:c.146G>T						
			NM_002918.4:c.839A>G						
			NM_000435.2:c.6061G>A						

P5	*FCHO1*	splice_donor_variant	NM_001161357.1:c.27+1G>A		—	—	33.0	5.744	1
	PTCD3	missense_variant	NM_017952.5:c.1028G>A	NP_060422.4:p.Arg343Gln	3.3E-05	4.5E-05	26.2	3.313	0
	NIFK	frameshift_variant	NM_032390.4:c.683_684delTG	NP_115766.3:p.Val228Glyfs	—	—	24.3	3.313	0
	ARPP21	missense_variant	NM_001267619.1:c.1871C>T	NP_001254548.1:p.Ser624Leu	—	—	23.4	3.313	0
	XIRP1	missense_variant	NM_194293.2:c.4991G>A	NP_919269.2:p.Arg1664Gln	2.9E-04	3.9E-04	16.7	3.313	0
	TOPAZ1	missense_variant	NM_001145030.1:c.4783A>G	NP_001138502.1:p.Ile1595Val	2.8E-03	1.7E-03	22.6	3.313	0.99
	DNAH1	missense_variant	NM_015512.4:c.888G>C	NP_056327.4:p.Gln296His	6.5E-04	6.6E-04	8.9	22.1	0
	PRKCD	missense_variant	NM_006254.3:c.1928G>A	NP_006245.2:p.Arg643His	9.9E-05	1.1E-04	23.8	26.5	1
	CFAP44	missense_variant	NM_001164496.1:c.5396G>A	NP_001157968.1:p.Arg1799Gln	—	2.8E-05	23.4		0
	ZNF595	splice_acceptor_variant	NM_182524.3:c.634+2C>T		—	—	0.4	4.487	0
	MAST4	missense_variant	NM_001164664.1:c.6014C>G	NP_001158136.1:p.Thr2005Ser	1.5E-04	1.7E-04	6.9	3.313	0.01
	C5orf63	missense_variant	NM_001164479.1:c.37A>G	NP_001157951.1:p.Arg13Gly	4.3E-05	5.0E-05	22.9		0
	AP5Z1	missense_variant	NM_014855.2:c.1162G>A	NP_055670.1:p.Val388Ile	5.8E-05	5.7E-05	10.6	23.8	0
	RADIL	missense_variant	NM_018059.4:c.1142T>C	NP_060529.4:p.Leu381Pro	—	—	16.4	3.313	0
	SKAP2	missense_variant	NM_003930.4:c.583C>A	NP_003921.2:p.Arg195Ser	—	—	31.0	8.906	0.91
	GARS	missense_variant	NM_002047.3:c.269A>G	NP_002038.2:p.Asp90Gly	8.3E-06	4.1E-06	24.7	22.9	0.79
	CDK13	missense_variant	NM_003718.4:c.4247C>A	NP_003709.3:p.Pro1416His	9.1E-05	5.7E-05	26.6	3.313	0.75
	MAMDC4	splice_region_variant	NM_206920.2:c.796+7C>T		—	—	10.9	3.313	0
	ANAPC2	missense_variant	NM_013366.3:c.522G>C	NP_037498.1:p.Gln174His	8.2E-06	—	20.7	3.313	0.99
	KMT2D	missense_variant	NM_003482.3:c.8669C>G	NP_003473.3:p.Pro2890Arg	—	1.2E-05	25.0	0.001	1
	RGS11	missense_variant	NM_183337.2:c.647G>A	NP_899180.1:p.Arg216His	2.8E-05	3.8E-05	0.5	3.313	0
	TMEM8A	missense_variant	NM_021259.2:c.1139C>T	NP_067082.2:p.Ser380Leu	3.7E-04	3.5E-04	14.6	3.313	0
	FTSJ3	missense_variant	NM_017647.3:c.485G>A	NP_060117.3:p.Arg162His	8.2E-06	8.1E-06	27.3	3.313	0.48
	GNA13	missense_variant	NM_006572.5:c.445A>G	NP_006563.2:p.Ile149Val	2.5E-04	2.6E-04	23.7	5.785	0.53
	AXIN2	missense_variant	NM_004655.3:c.986G>A	NP_004646.3:p.Ser329Asn	1.6E-05	1.6E-05	23.1	21.7	0.12
	RNF213	splice_region_variant	NM_001256071.2:c.11972+8C>T		3.2E-03	3.6E-03	3.1	3.313	0
	MYO1F	missense_variant	NM_012335.3:c.943G>A	NP_036467.2:p.Gly315Arg	1.7E-04	1.7E-04	16.2	3.313	0.16
	F2RL3	missense_variant	NM_003950.3:c.554G>A	NP_003941.2:p.Arg185His	—	9.4E-06	24.1	3.313	0
	PCNT	missense_variant	NM_006031.5:c.7252G>A	NP_006022.3:p.Gly2418Ser	2.5E-05	3.3E-05	12.8	0.001	0

Variants identified on targeting sequencing of >500 immune-related genes

P3	Homozygous variants								
	FCHO1	frameshift_variant	NM_001161357.1:c.1305_1306del	NP_001154829.1:p.Phe436Trpfs*9	—	—	33.0	4.74	1
	Heterozygous variants								
	C1QB	splice_acceptor_variant	NM_000491:c188-1G>T		—	—	32.0	19.64	0.16
	CCDC40	missense_variant	NM_001243342.1:c.2891A>G	NP_000482.3:p.His964Arg	—	8.9E-02	4.3	0	0
	EMR2	missense_variant	NM_013447.4:c.185C>T	NP_038475.2:p.Met62Thr	1.5E-04	3.2E-05	1.2	2.31	0
	IL17F	missense_variant	NM_052872.3:c.230G>A	NP_443104.1:Arg77His	5.8E-05	4.5E-05	26.2	2.31	0.04
	PARN	missense_variant	NM_002582.4:c.1785T>G	NP_002573.1: Asp595Glu	2.3E-04	2.1E-04	5.7	2.31	0
	TNFAIP3	missense_variant	NM_006290.3:c.1189T>C	NP_001257436.1:Ser397Pro	—	—	28.3	2.31	1

Table 6.2. Results of WES and targeted sequencing of primary-immune deficiency-related genes. Rare homozygous exonic and splice-site genetic variants identified in P1, P2, P4 and P5 and variants identified on targeting sequencing of >500 immune-related genes. MAF, Minor allele frequency; NA, not applicable.

Among these variants, in each patient, functional filtering and annotation identified 5 different *FCHO1* mutations as the most likely causative of the disease (candidate variant). The mutation found in patient 1 was a substitution of a guanine with cytosine in position c.120-1, acceptor splice site of intron 5 (P1, c.120-1G>C). In patient 2, 3 and 4, frameshift mutations disrupting the reading frame of FCHO1 protein were identified. Specifically, patient 2 carried a duplication of the nucleotide guanine in position c.2023, causing translation of glycine instead of valine in position p.675 (c.2023dupG, p.Val675Glyfs*13). Patient 3 carried a deletion of one nucleotide in position c.1305_1306, with translation of tryptophan instead of phenylalanine in position p.436 (c.1305_1306del, p.Phe436Trpfs*9) and patient 4 carried a duplication of a cytosine in position c.189, causing translation of a histidine instead of methionine in position p.64 (c.189dupC, pMet64Hisfs*104). The mutation found in patient 5 was a donor splice site mutation of a guanine substituted by adenine in position c.27 (c.27+1G>A).

6.2.2. Sanger sequencing

To validate the results from the WES and the targeted sequencing, *FCHO1* mutations were confirmed and verified on genomic DNA by means of Sanger sequencing in controls, patients and in available healthy family members (Father and Mother) (Figure 6.4).

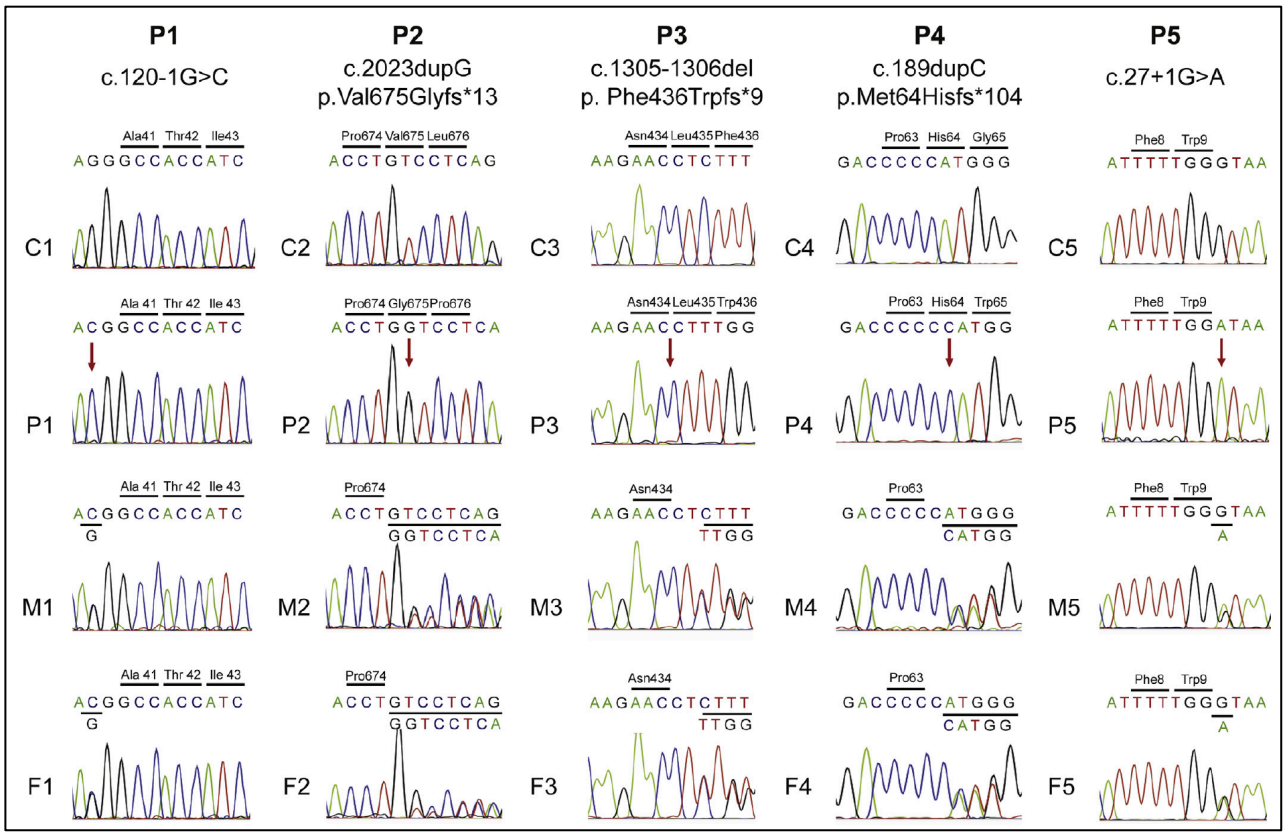

Figure 6.4. Sanger Sequencing Chromatograms. Chromatograms of *FCHO1* genomic DNA sequences in healthy control subjects (C1-C5), patients (P1-P5), and heterozygous carriers (mother, M1-M5; father, F1-F5) for each family. Red arrows indicate localization of homozygous mutations in the patients.

In all the 5 patients, Sanger sequencing confirmed the presence of the suspected pathogenic variants in both alleles of the *FCHO1* gene (homozygous state), and in one allele only (heterozygous state) in the respective parents, attesting the carrier status of the latter. Healthy control subjects demonstrated a homozygous state for the wild type *FCHO1*.

6.2.3. Effects of *FCHO1* variants

The human *FCHO1* gene is located on chromosome 19, is 3214 base-pair long, comprises 29 exons and encodes for an 891-aminoacid-protein (transcript ID ENST00000594202.5, isoform FCHO1-002). The FCHO1 protein is composed of three domains, the N-terminal F-BAR domain, which

binds to phosphatidylinositol 4,5-biphosphate on the inner side of the cell membrane, the C-terminal μ-homology domain, which mediates interaction with the epidermal growth factor receptor substrate 15 and cargo molecules, and a linker region APA (allosteric activator of the adaptor protein 2 complex). Figure 6.5 schematically represents wild type FCHO1 protein and the predicted effects of patients' mutations on its structure.

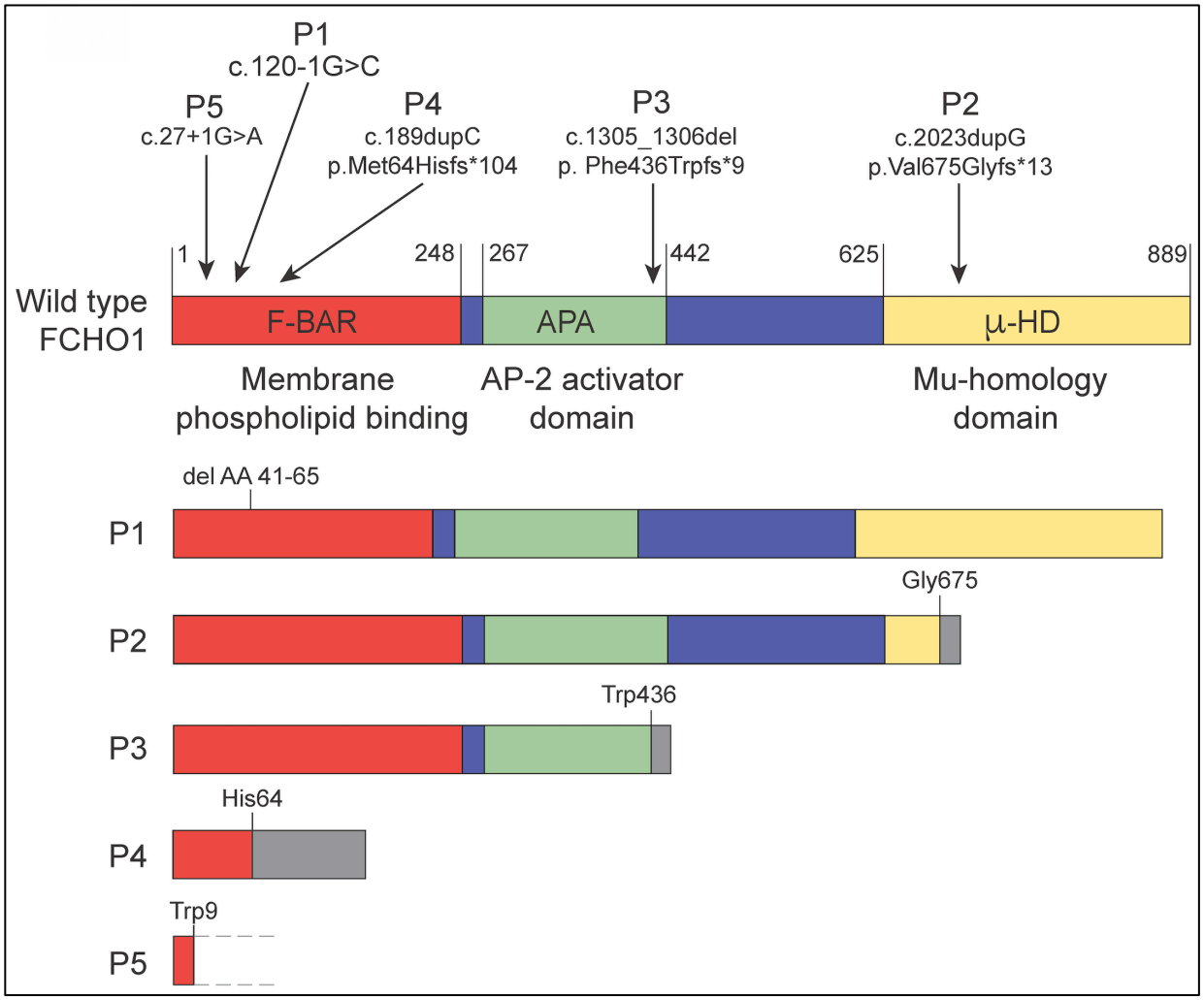

Figure 6.5. Schematic representation of FCHO1 protein and the predicted effects of mutations on its structure. Black arrows indicate the position of the mutation as respective of the wild type protein. Gray boxes represent spurious amino acid sequences downstream of frameshift mutations. Dashed lines in P5 indicate undefined effects of the splice-site mutation

downstream of Trp9. P1 – P5, patient 1 to 5. AP-2, Adaptor protein 2; μHD, μ-homology domain.

Patient 1 and patient 5 carried two different homozygous splice-site mutation (P1, c.120-1G>C and P5, c.27+1G>A, respectively). The splice-site mutation of P1 at acceptor splice site of intron 5 was predicted to result in complete exon 6 skipping, whereas the mutation of P5 was predicted to disrupt the intron 2 donor splice site and the correct FCHO1 amino acid sequence after tryptophan in position p.9 due to mRNA decay (Figure 6.5). Patient 2, 3 and 4 carried homozygous frameshift mutations (P2, c.2023dupG, p.Val675Glyfs*13; P3, c.1305_1306del, p.Phe436Trpfs*9; P4, c.189dupC, pMet64Hisfs*104, respectively) (Figure 6.5). These frameshift mutations were predicted to disrupt the in-frame reading of the protein and caused premature termination in aminoacidic position p.168 (P4), p. 445 (P3) and p.688 (P2).

Three mutations (patient 1, 4 and 5) fell in the first half of the F-BAR protein domain, one mutation (patient 3) close to the C-terminus of the AP-2 binding domain and one mutation (patient 2) in the first half of the μ-homology domain. All these positions are highly conserved through different species, including human, sus, canis, mus, felis and bovis, as schematically represented in Figure 6.6, suggesting that, throughout evolution, they remained crucial for the proper function of the protein.

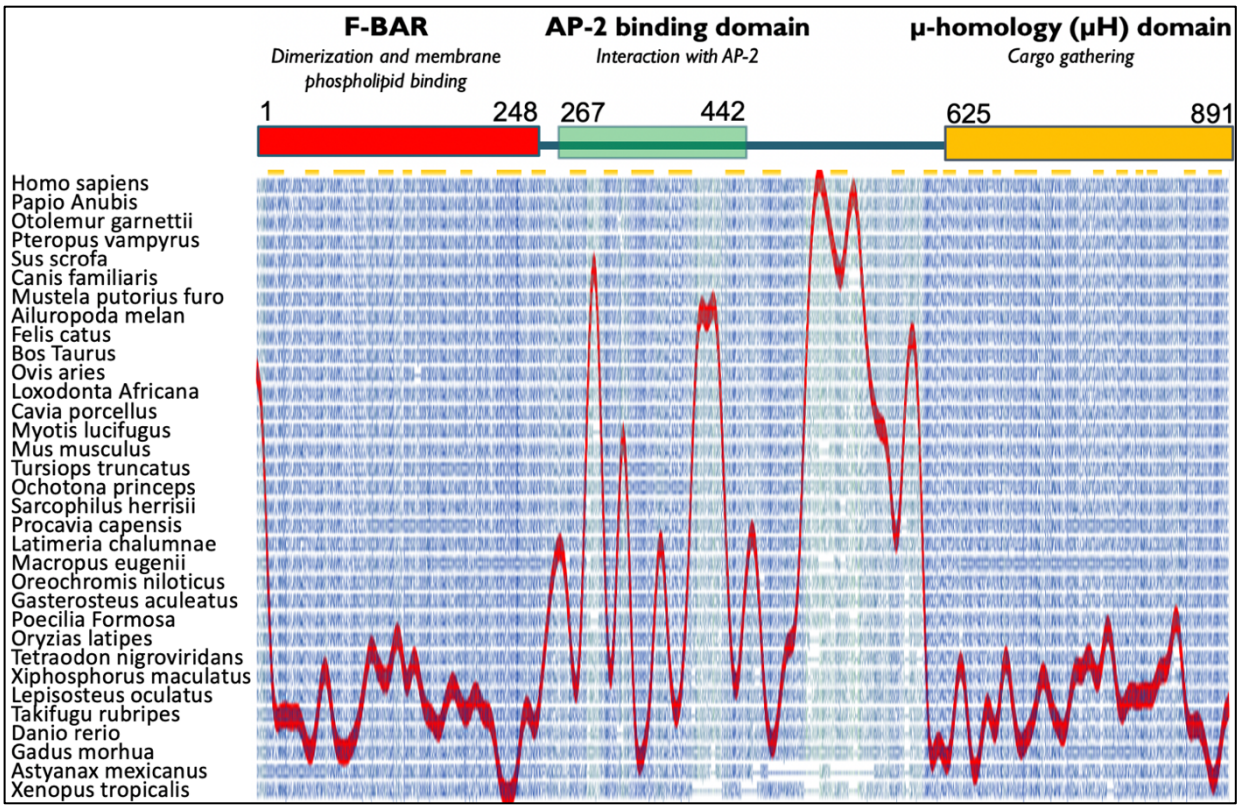

Figure 6.6. Evolutionary conservation of FCHO1. On top, schematic representation of the FCHO1 human protein. Local maxima indicate protein regions with relatively low evolutionarily constrains, while local minima indicate Evolutionarily Constrained Regions (ECRs).

Frameshifts variants of patient 2, 3 and 4 were predicted to disrupt the in-frame reading and cause premature termination of the protein, with a partial or complete absence of the μ-homology domain. Lack of this domain, which is pivotal in mediating interactions with CME adaptor proteins, is reasonably leading to a drastic loss of function of the FCHO1 protein. Moreover, the deleteriousness of the insertions or deletions variants and the single nucleotide variants was assessed by using of the scaled CADD score (CADD-Phred). A CADD score of 15 is usually used as standard cut off for a variant's deleteriousness (181). Some genes tend to gain variants that are actually disease-causing with low CADD scores (and display low MSC), contrary to other genes that tend to gain variants with high CADD scores that are not disease-causing (and display higher MSC). For the c.120-1G>C (P1), c.2023dupG (P2), c.1305_1306del (P3), c.189dupC (P4) and c.27+1G>A (P5) variants, CADD-Phred scores were 26.3, 34, 28.9, 33 and 33, respectively,

significantly higher than the MSC score which, for the *FCHO1* gene, is 5.744. Finally, the pLI (Loss of Function Intolerance Score) for *FCHO1* is 1, as reported in ExAC. Genes with a pLI score above 0.9 are considered to be highly intolerant to loss of function mutations, therefore suggesting that the *FCHO1* is a gene particularly intolerant to loss of function mutations. These data altogether strongly support the role of the identified *FCHO1* variants in the pathogenesis of the disease.

6.3. Expression studies on FCHO1 mutated protein and wild type gene

6.3.1. Western blotting

Patients P2, P3, and P4 carried homozygous frameshift mutations predicted to cause disruption of the protein translation with premature termination in the aminoacidic position p.688 (P2), p. 445 (P3) and p.168 (P4) (Figure 6.5). To investigate the actual consequences of the *FCHO1* variants at a protein level, and because of the lack of commercial antibodies suitable for western blotting, 293T cells were transfected with lipofectamine with HA- (11 kDA) or FLAG- (11 kDa) tagged FCHO1 constructs, or with no construct (mock). The constructs contained cDNA of the HA- or FLAG- tag, followed wild type *FCHO1* cDNA or mutagenized with the patient's mutations for P2, P3 and P4. Cells were let grow in culture the appropriate time to allow protein expression. Western blotting analysis was performed on protein lysates from transfected 293T cells with antibody against HA- and FLAG-tag (Figure 6.7).

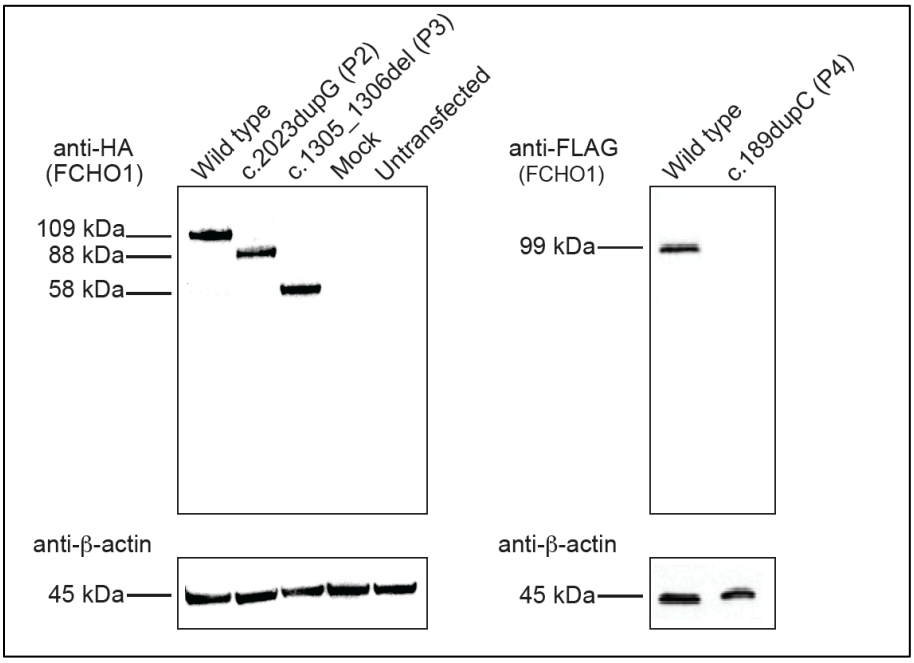

Figure 6.7. Western Blotting. Western blot of protein lysates from 293T cell lines transfected with plasmids encoding HA-tagged (P2 and P3) or FLAG-tagged (P4) WT or mutant FCHO1 cDNA.

Wild type FCHO1 protein is 891 aminoacid long, with a molecular weight of 98 kDa. Mutations found in patient 2 (c.2023dupG, p.Val675Glyfs*13), patient 3 (P3, c.1305_1306del, p.Phe436Trpfs*9) and patient 4 (P4, c.189dupC, pMet64Hisfs*104) were thought to generate truncated proteins of 688 (77 kDa), 445 (47 kDa) and 168 (19 kDa) aminoacid long, respectively. Cells transfected with *wild type* HA-cDNA-FCHO1 showed expression of a product of 109 kDa (HA 11 kDa + *w/*t FCHO1 98 kDa), whereas cells transfected with P2 or P3 HA-cDNA-FCHO1 showed expression of truncated products of 88 and 58 kDa, corresponding to the predicted molecular weight for FCHO1 of P2 (77 kDa) and P3 (47 kDa), plus 11 kDa of the HA-tag. No protein was detected in P4, most likely because of mRNA decay, while a 99 kDa protein was detected in cells transfected with *wild type* FLAG-cDNA-FCHO1 (FLAG 11 kDa + *w/*t FCHO1 98 kDa). No protein expression was found in mock and un-transfected 293T cells and β-Actin (45 kDa) served as a protein-loading control and was equally detected in all samples. These findings confirmed that the *FCHO1* variants affect the protein architecture determining its premature truncation or absence of translation.

6.3.2. RNA splicing analysis

P1 was homozygous for a splice-site mutation (c.120-1G>C) at the acceptor splice site of intron 5, which was predicted to result in exon 6 skipping. Because no pre-HSCT specimens were available, RT-PCR analysis was performed in PBMCs obtained from her parents, who are both heterozygous for the mutation, and from one healthy donor (control), to test the consequences of the mutation on the FCHO1 mRNA (Figure 6.8).

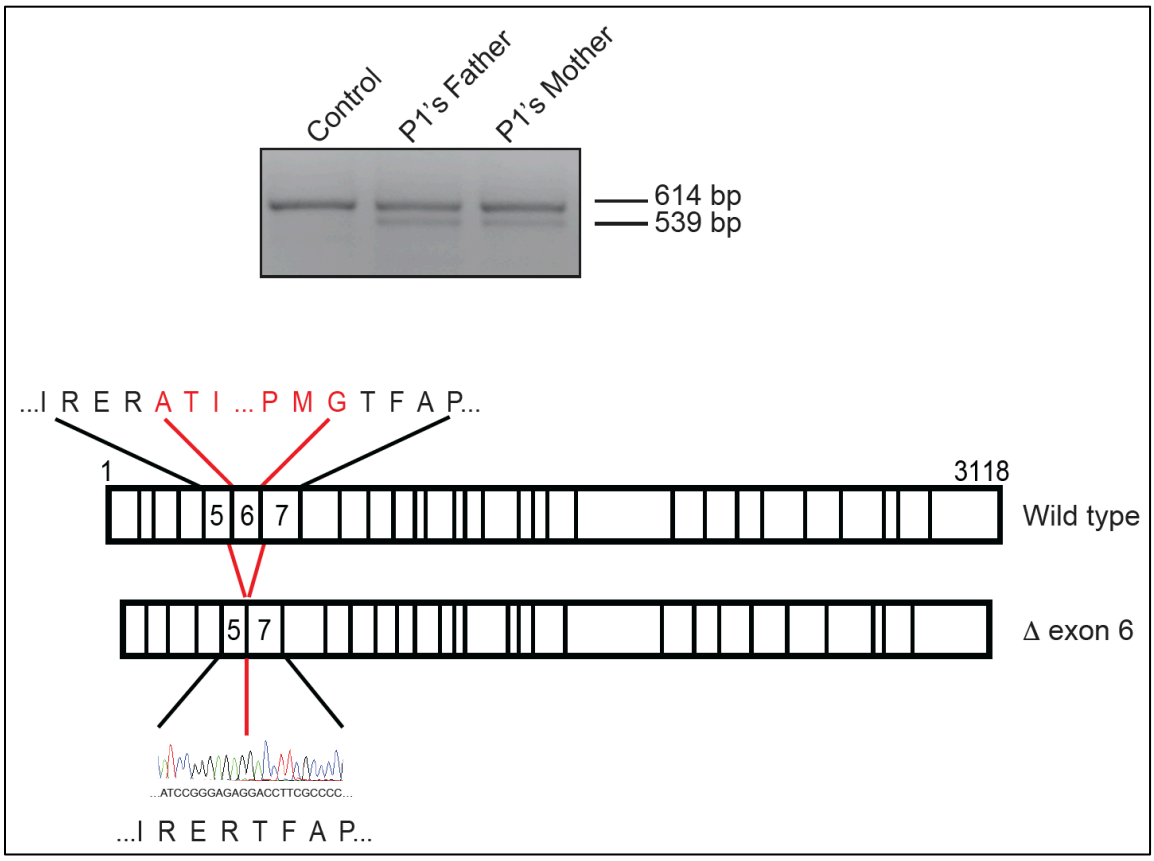

Figure 6.8. RT-PCR. Upper panel, RT-PCR amplification of partial (exons 4-9) FCHO1 transcript in PBMCs from a healthy control subject and from P1's father and mother. Lower panel, schematic representation of effects at the transcript level, as predicted on cloning and sequencing of the 614-bp (top) and 539-bp (bottom) products, respectively.

Amplification of cDNA with primers spanning a 614 base pair long region between exons 4 and 9, identified 2 bands in cDNA obtained from P1's parents, one of 614 base pair long, the other 539 base pair long. Only one band (614 bp) was identified in cDNA extracted from PBMC from healthy donor. Cloning and sequencing of the bands established that the lower (539 bp) corresponds to a product lacking exon 6, confirming that the splice-site mutation (c.120-1G>C) of P1 caused an in-frame, internally truncated FCHO1 protein lacking 24 amino acids (41 to 65) within the F-BAR domain (Figure 5.4). P5 was homozygous for the c.2711G>A mutation, which was predicted to disrupt the intron 2 donor splice site and the correct FCHO1 amino acid sequence after Trp9, most

likely for mRNA decay phenomenon (Figure 6.5). Unfortunately, no samples were available to test the consequences of this mutation at the cDNA level.

6.3.3. *In silico* studies and quantitative PCR analysis in physiological conditions

The F-BAR protein superfamily comprises two members, the membrane-sculpting F-BAR domain-containing Fer/Cip4 homology domain-only proteins 1 and 2 (*FCHO1*/*FCHO2*). Whether *FCHO1* and *FCHO2* are functionally redundant or have distinct functions is unclear. To better understand the roles of *FCHO1* and *FCHO2* in human biology, *in silico s*tudies on on-line databases were performed to assess their differential RNA expression in human tissues (Figure 6.9).

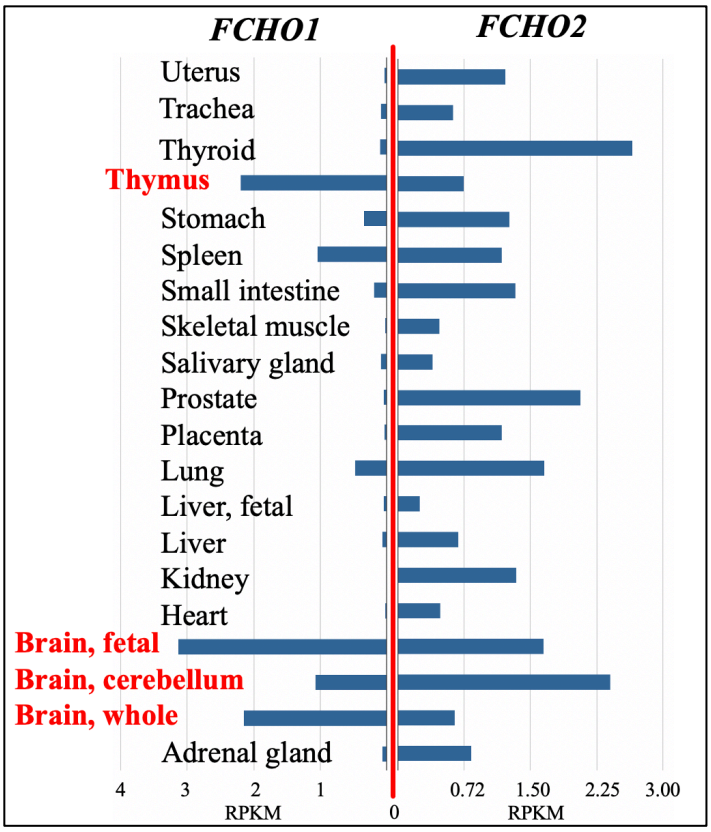

Figure 6.9. FCHO1/FCHO2 RNA expression in human tissues. Expression of RNA in different human tissue as reported by http://biogps.org/#goto=welcome. In red are highlighted

cells with a predominant expression of FCHO1 RNA. RPKM: normalized unit of transcript expression.

FCHO1 showed elevated expression restricted to the thymus and brain (fetal and whole brain) tissues, whereas *FCHO2* seemed to be broadly expressed, including organs like the thyroid, gastrointestinal apparatus (stomach, small intestine, liver), skeletal muscle, prostate, placenta and lungs, among others. Interestingly, the two genes appeared to be almost equally expressed in the spleen. No data on expression in the Bone Marrow (primary lymphoid organ for B-cells production) were reported in literature. *In silico* analysis of RNA expression in human cells was also performed (Figure 6.10).

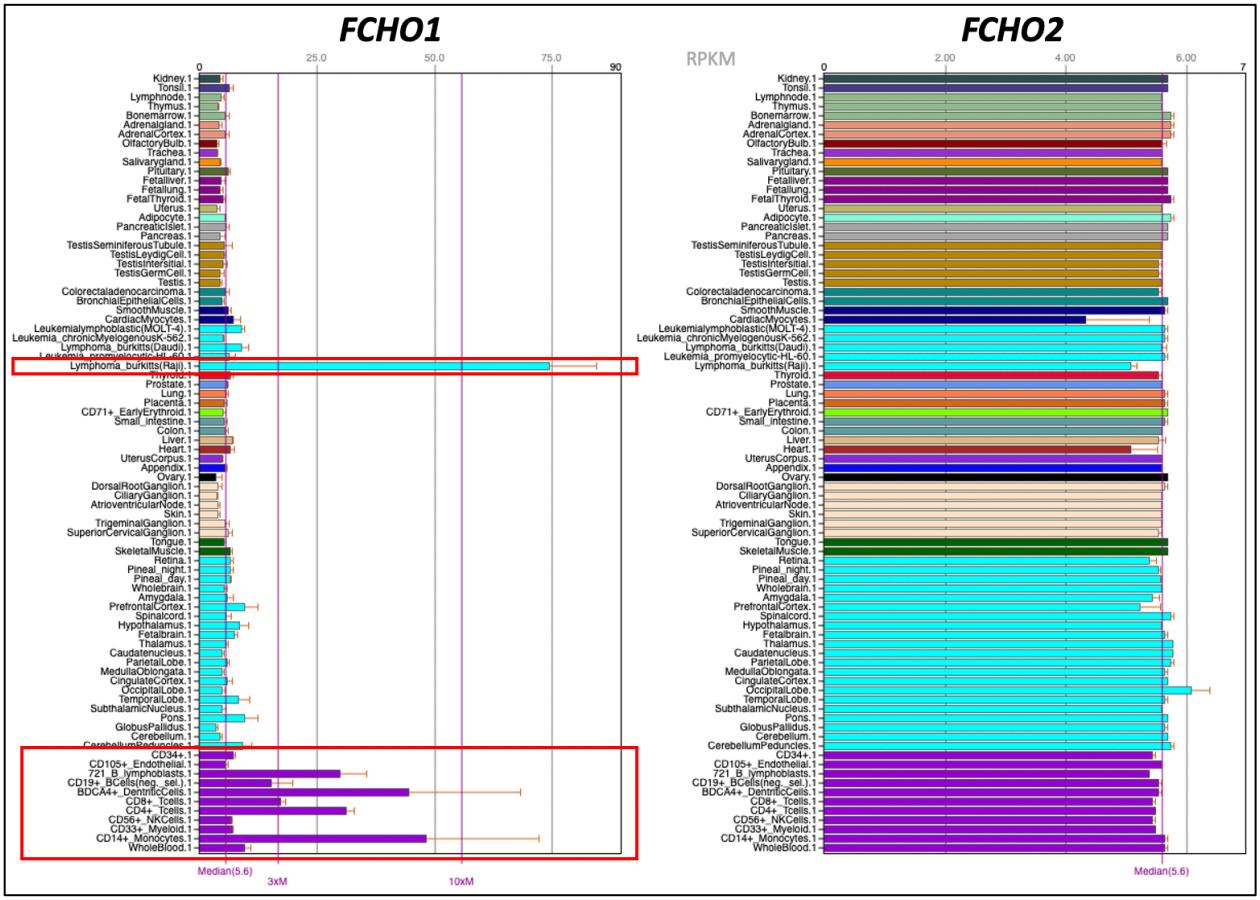

Figure 6.10. FCHO1/FCHO2 RNA expression in human cells. Expression of RNA in different human cells as reported by https://www.ncbi.nlm.nih.gov/bioproject/280600.

Highlighted in red are cells with a predominant expression of *FCHO1* RNA. RPKM: normalized unit of transcript expression.

FCHO1 showed a pattern of expression mostly restricted to cells of the immune system, in particular CD19+ B cells, CD8+ and CD4+ T cells, dendritic cells and CD14+ monocytes, lymphoma Burkitt (Raji) cell lines and lymphoblasts with 25 to 75 normalized unit of transcript expression (RPKM), way above the median of expression (5.6 RPKM).

To assess differential expression of *FCHO1* and *FCHO2* genes in selected cellular populations, sorted CD4+ and CD8+ T cells, CD19+ B cells, CD56+ natural killer cells isolated from healthy human subjects, as well as fibroblasts, and the K562 erythroleukemic cell lines were used to perform quantitative PCR analysis (Figure 6.11).

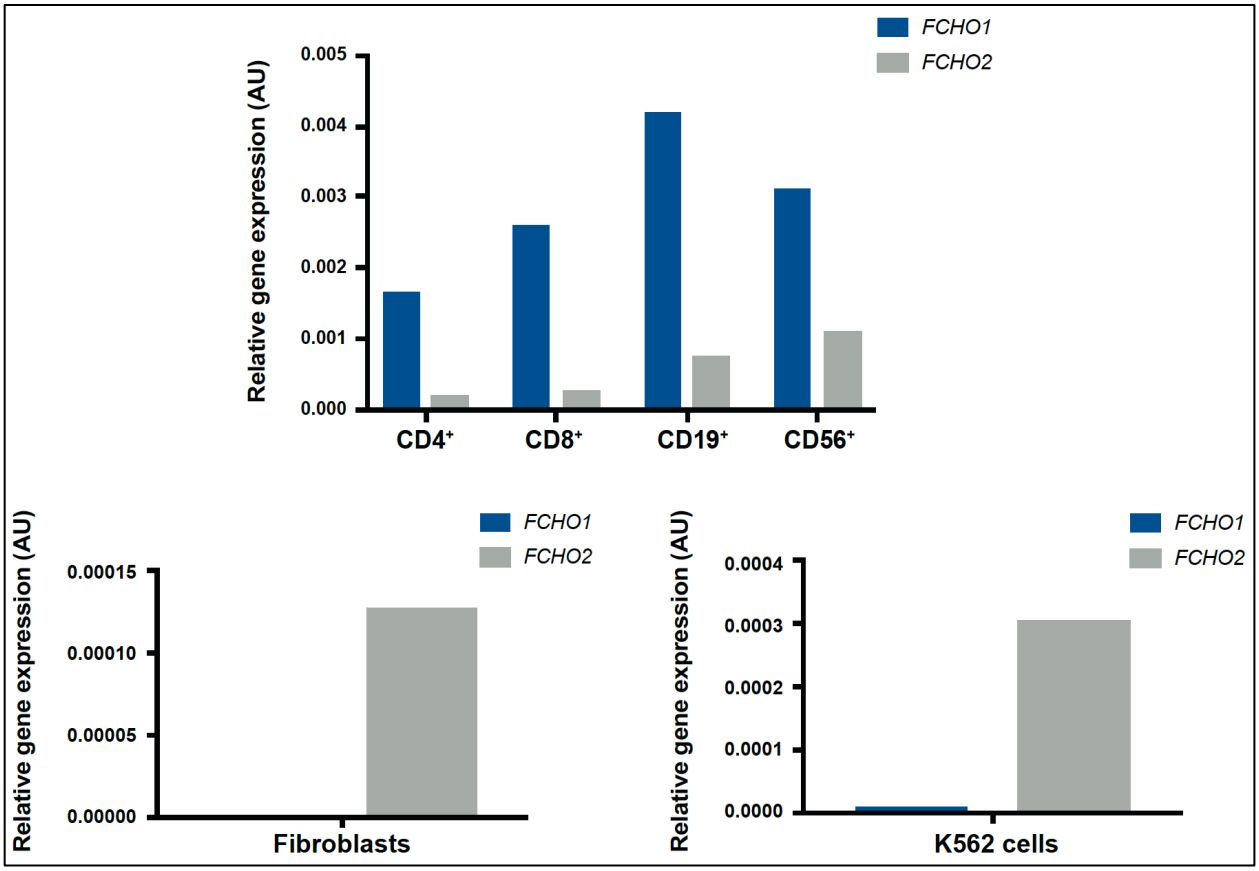

Figure 6.11. Quantitative PCR analysis. Relative expression of FCHO1 and FCHO2 transcripts in healthy donors' lymphoid subpopulations (CD4+, CD8+, CD19+, and CD56+ cells), fibroblasts, and K562 cells.

Relative gene expression of *FCHO1* versus *FCHO2*, normalized to *β-actin* reference gene expression levels within the same sample to determine Δ cycle threshold (CT) values, showed that *FCHO1* was predominantly expressed in lymphoid cells (CD4+ and CD8+ T cells, CD19+ B cells and CD56+ NK cells), from 2 to 4 times more for *FCHO1* as compared to *FCHO2,* whereas *FCHO2* appeared to be more abundantly expressed in fibroblasts and K562 cells (3 to 10 folds). Altogether, these data suggest that, while *FCHO2* is broadly expressed, *FCHO1* is specifically restricted to the immune system, supporting the role of the identified variants in the pathogenesis of the patients' clinical presentation of SCID.

6.4. *In vitro* functional studies

6.4.1.T cell activation and proliferation

To clarify the mechanisms underlying the T cell lymphopenia observed in the patients, *in vitro* T cell activation and proliferation in PBMCs from healthy subjects and P2, the only patient from whom pre-HSCT PBMCs were available, were analyzed. T cells from P2 and 2 healthy controls were stimulated *in vitro* for 24 and 48 hours with soluble anti-CD3 plus Protein A and to induce the expression of surface activation markers. In activated T cell, CD69 is one of the first molecule appearing on the cellular surface (becoming visible around 12 hours after stimulation and reaching a peak at 36 hours after stimulation), followed by CD25 and CD75 (starting at 24 hours with peaks at 48 hours after stimulation). Compared to two healthy controls, P2's PBMCs displayed normal expression of early and late T-cell activation markers (CD69, CD25, and CD71), with a kinetic comparable to healthy controls (Figure 6.12).

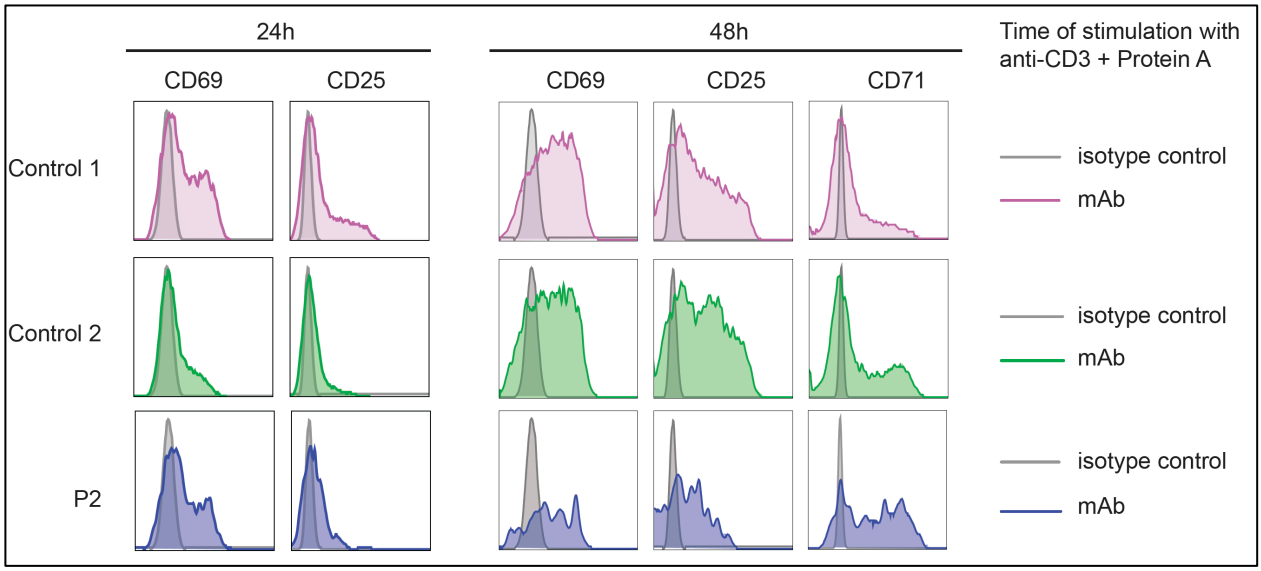

Figure 6.12. Activation markers expression. Surface expression of CD69, CD25, and CD71 after 24 and 48 hours of stimulation with anti-CD3 plus Protein A in T cells from 2 healthy control subjects (pink and green) and Patient 2 (P2, violet). Staining with isotype control is shown in gray.

When stimulated, T cells undergo several rounds of cell division in order to mount a proper response. To this purpose, P2's and one control's PBMCs were left unstimulated or activated *in vitro* through Dynabeads CD3/CD28 stimulation and stained with Cell Trace Violet (CTV), a nuclear dye used to track proliferation cycles. Compared to T cells from a healthy donor, P2's T cells showed reduced proliferation upon activation through CD3/CD28 for both CD4+ and CD8+ T cells (Figure 6.13). In particular, T cells from P2 were able to enter only 3 to 4 rounds of cell division, whereas T cells from control subjects entered 6 to 7 rounds of proliferation.

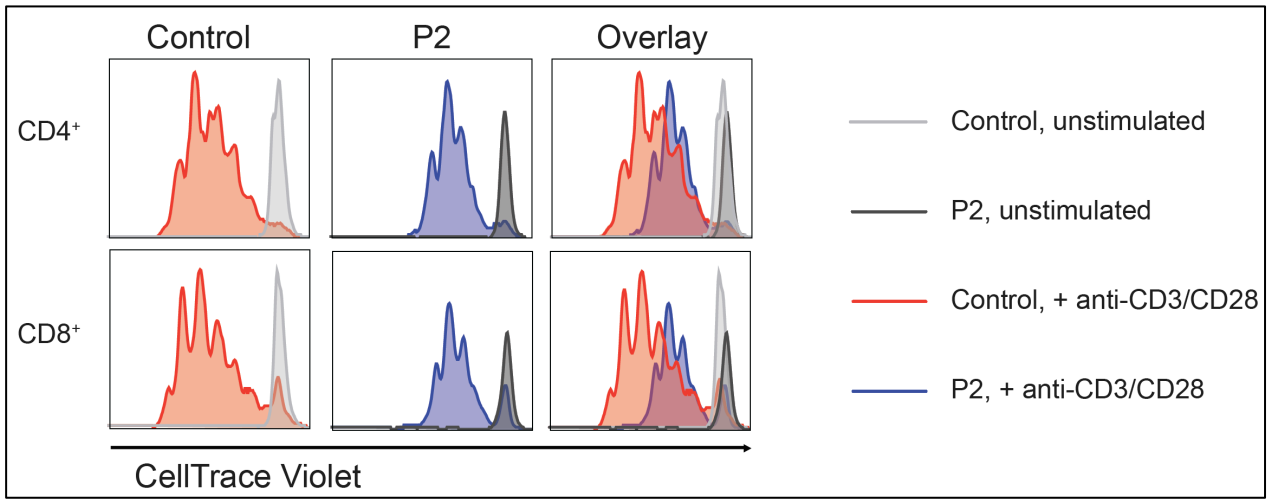

Figure 6.13. T cell *in vitro* proliferation. Dilution of Cell Trace Violet staining in Dynabeads CD3/CD28-stimulated CD4+ (top) and CD8+ (bottom) T cells from a healthy control subject (left panels) and patient 2 (P2, middle), with overlay shown in right panels.

These results showed that *FCHO1* deficiency does not prevent the activation of T cells, but strongly impairs their proliferation.

6.4.2.T cell cycle and apoptosis assay

Prior studies demonstrated that clathrin-mediated endocytosis is important for a successful mitosis (M) (59, 60). After 72 hours of activation through soluble CD3/CD28, PBMCs from P2 and from two healthy controls were stained with propidium iodide (PI), which by staining the DNA marks cells in the G0/G1, S, and G2/M phases of the cell cycle, as well as hypodiploid (Hypod.) cells.

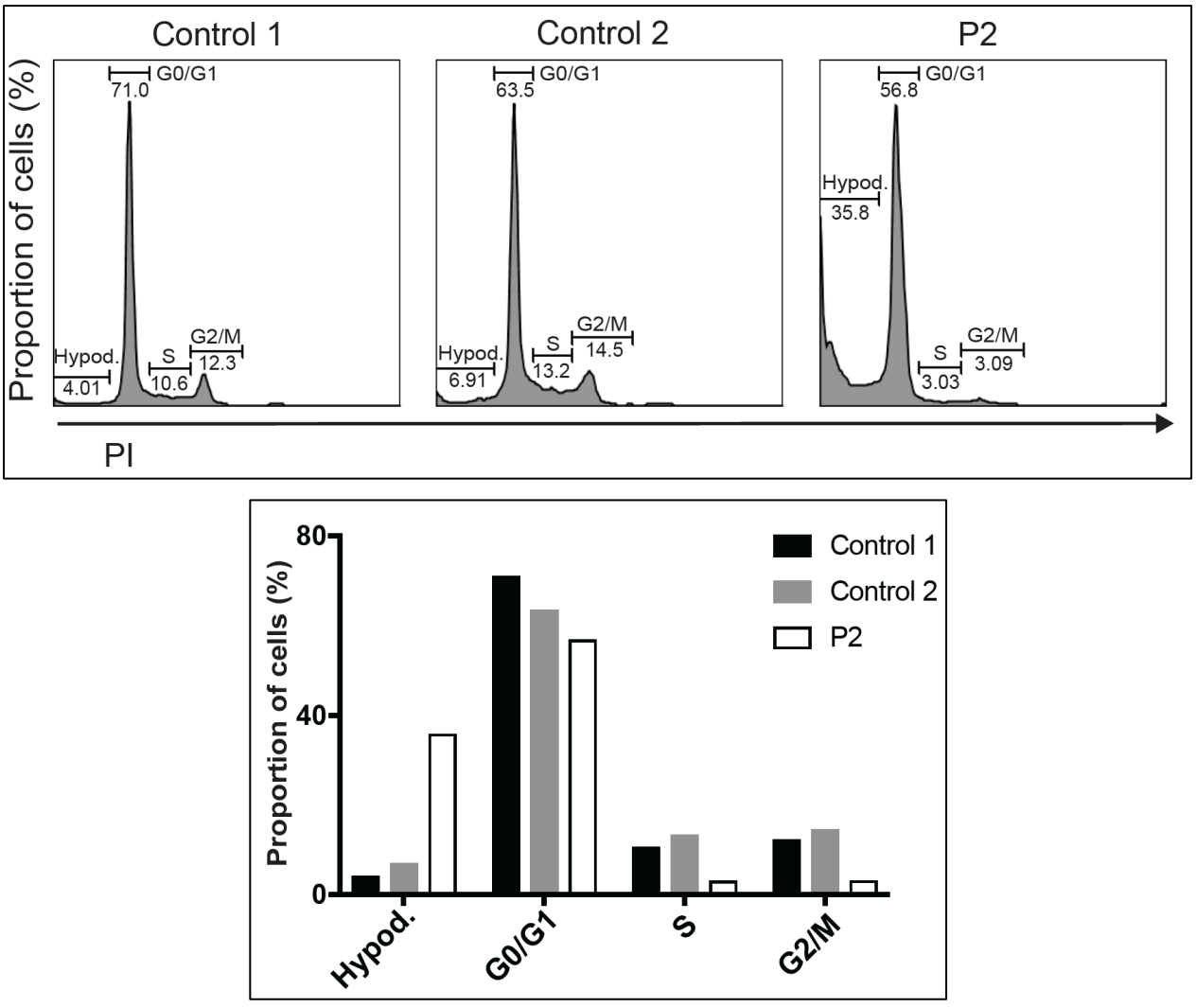

Figure 6.14. T cell cycle. Upper panel, Fluorescence-activated cell sorting (FACS)–based cell-cycle analysis on CD3/CD28 T-cell in P2 and 2 healthy controls. Lower panel, proportion of cells within the cell cycle in two controls and P2. Hypod., hypodiploid. Bottom, Proportion of PBMCs that were hypodiploid or in various phases of the cell cycle.

P2's T cells showed a high percentage of hypodiploid cells, a marker of cell death, and reduced percentages of cells in the S and G2/M phases of the cell cycle (Hypod.: 35.8%, G0/G1: 56.8%, S: 3.03%, G2/M: 3.09%), compared to two healthy control subjects (Hypod.: 4.01% and 6.91%, G0/G1: 71.0% and 63.5%, S: 10.6% and 13/2%, G2/M: 12.3% and 14.5%) (Figure 6.14), strongly suggesting that activated *FCHO1* deficient PBMCs are unable to successfully complete the S phase of the cell cycle and prevented to move to the G2/M phase and rapidly dying.

6.4.3. T cell repertoire

High throughput sequencing of the TCR (TCRβ (TCRB) repertoire) is a powerful tool to analyze the T cell ability to successfully rearrange VDJ genes and produce a vast array of functional TCRs (182). T cell repertoire performed on whole PBMC from P2 and one healthy control revealed no significant bias for productive VDJ rearrangements nor differences in TRB V and J gene usage. No abnormalities of T-cell diversity, composition, and clonal abundance in circulating T cells from P2 were observed (Figure 6.15).

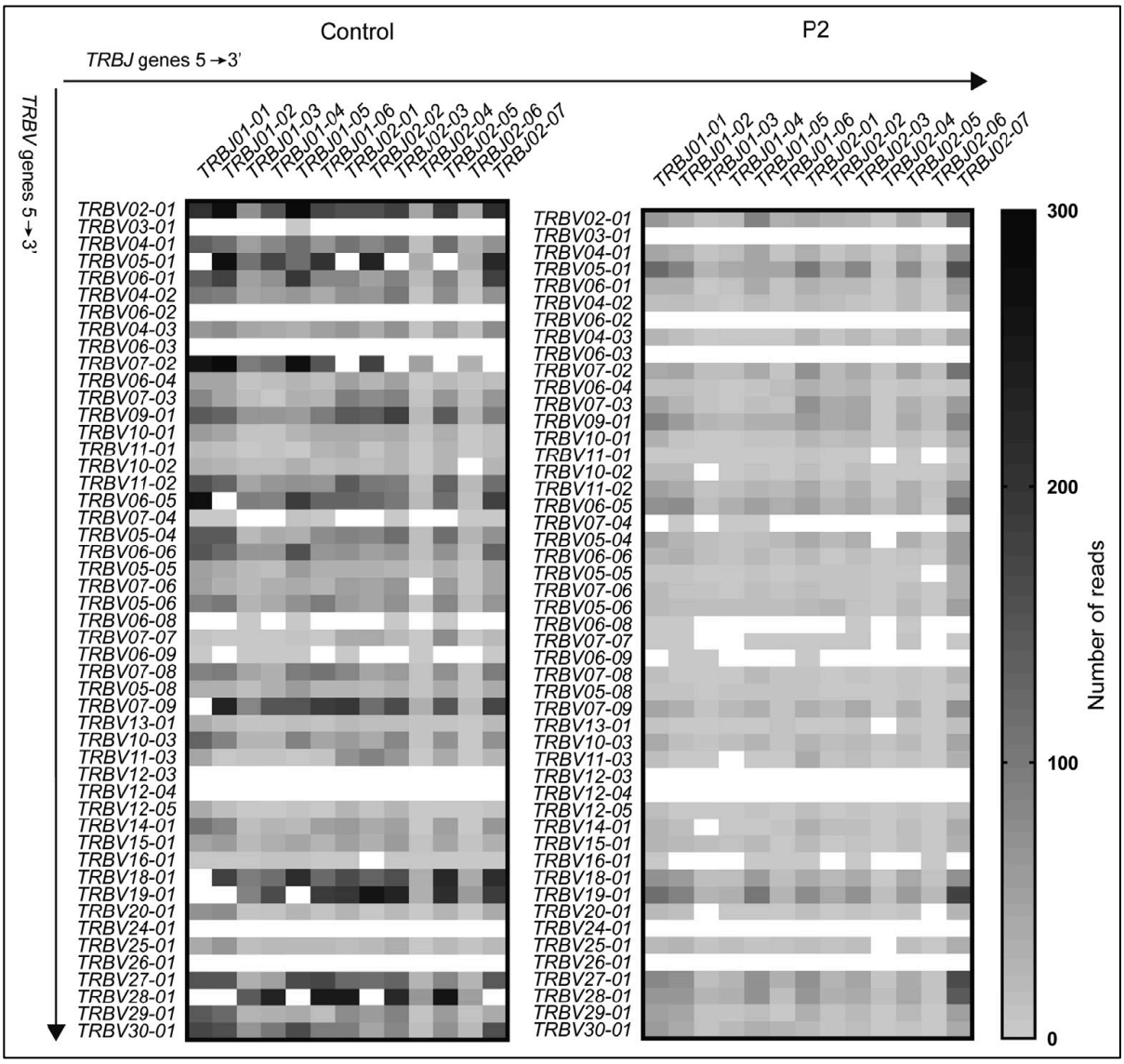

Figure 6.15. TCRβ (TRB) repertoire. TCRβ (TRB) repertoire of peripheral blood T cells from a healthy control subject and P2. Shown is a heat map of TRBV-TRBJ gene productive rearrangements among total sequences obtained

Overall, these results strongly suggest that defective T cell proliferation and increased activation-induced cell death, rather than impaired thymic output, are major contributors to the T cell lymphopenia observed in patients with *FCHO1* deficiency.

6.4.4.T cell Transferrin internalization

Transferrin internalization in cells relies mainly on clathrin-dependent endocytosis. Transferrin-receptor expression (CD71) on the surfaces of PBMCs is minimal in resting state but increases at 48 and 72 hours after T cell receptor (TCR) activation. Once TfR (CD71) is expressed on cellular surface, extracellular transferrin carrying two molecules of iron is able to bind to its receptor, CD71, on cell surface. After the binding, the complex is internalized through clathrin-coated endosomes which will then be released upon acidification and deliver iron inside the cell cytoplasm. The CD71 is recycled back to the cell surface and iron-depleted transferrin is released outside the cell membrane. To investigate whether *FCHO1* mutations affect clathrin-mediated endocytosis, PBMCs from P2 and 2 control subjects were stimulated *in vitro* with soluble anti-CD3 and Protein A for 48 and 72 hours.

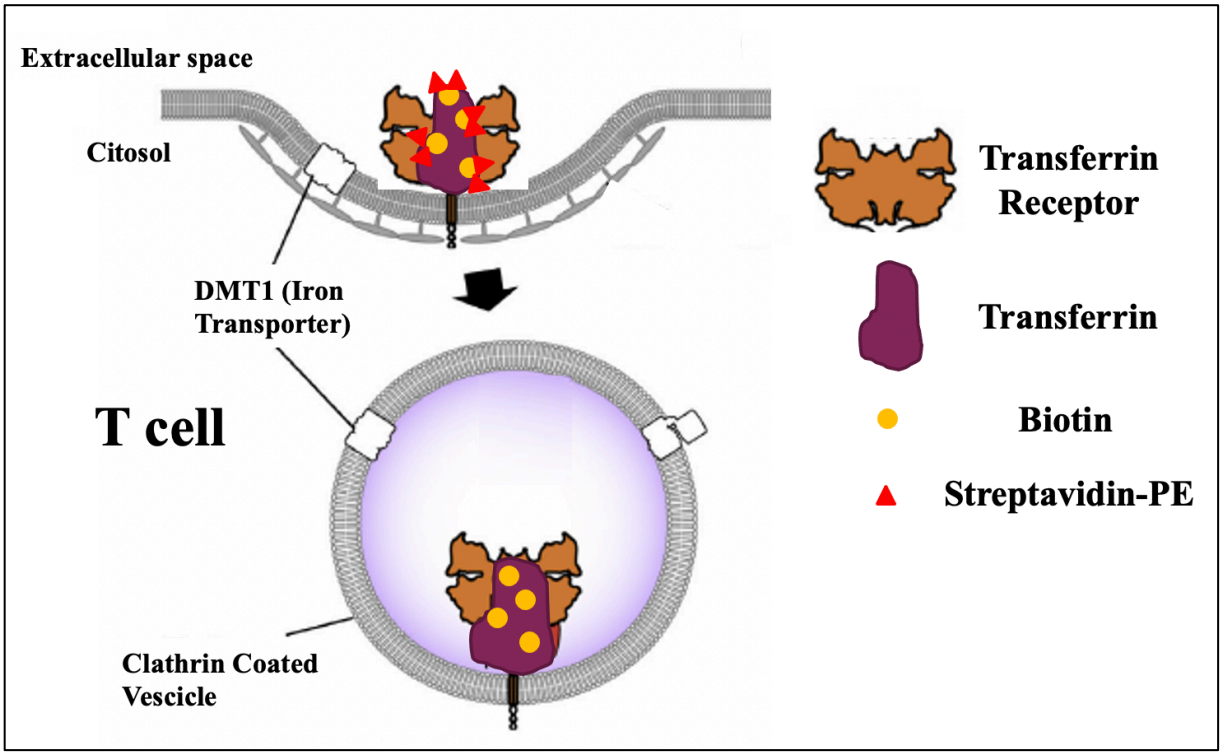

Figure 6.16. Schematic representation of transferrin internalization assay. Biotinylated transferrin in the extracellular matrix bound to the transferrin receptor is stained with Streptavidin-PE. Internalized transferrin-transferrin receptor does not bind to Streptavidin-PE.

A pulse-chase experiment was then performed by addition of biotinylated transferrin (Figure 6.16), followed by streptavidin–phycoerythrin (PE) staining, to measure the amount of biotinylated transferrin remaining on the cell surface after 10 and 30 minutes of internalization stimulation. Transferrin internalization was readily observed in control T cells, at both 48 hours and 72 hours after stimulation with anti-CD3 and Protein A. However, at both time points (10 minutes and 30 minutes) of transferrin internalization challenge, this was minimally detectable in P2 T cells (Figure 6.17). These data confirm impaired CME internalization of transferrin in activated *FCHO1* mutated T cell, underlining the importance of *FCHO1* in iron metabolism and T cell proliferation.

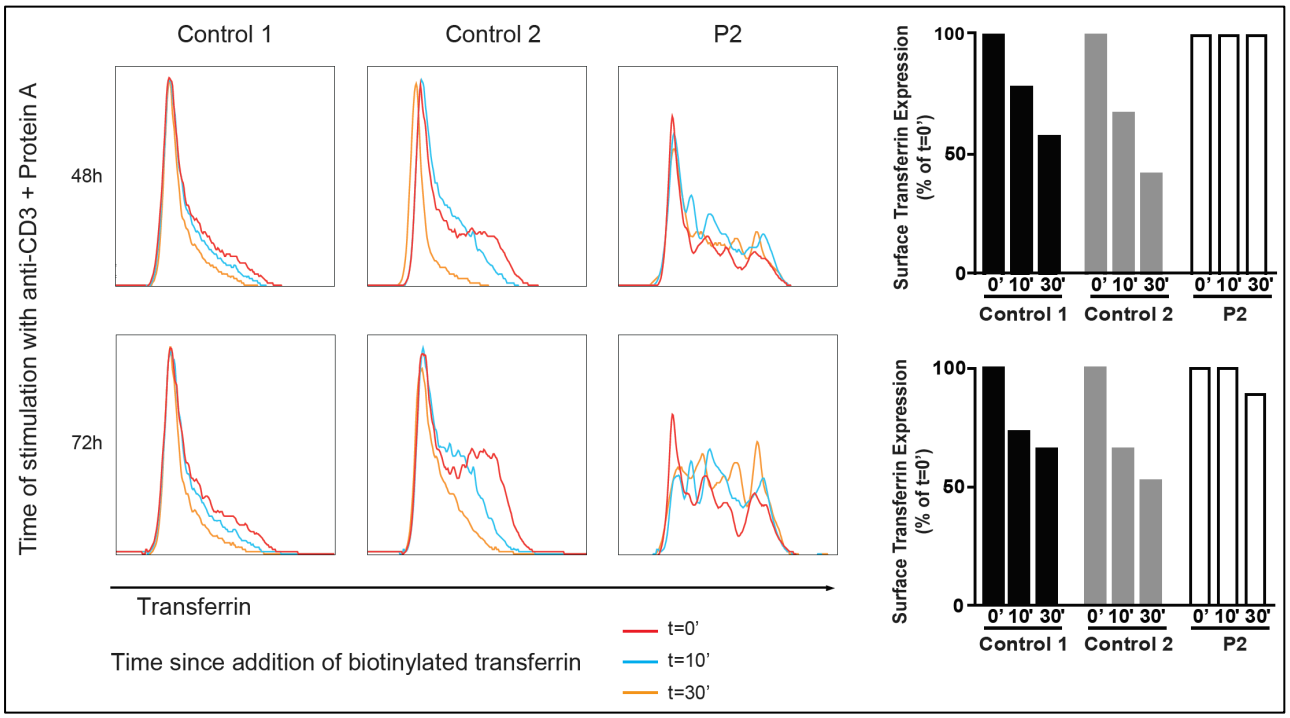

Figure 6.17. Transferrin internalization assay. Left panel, FACS analysis of the kinetics (t=0, 10 and 30 minutes) of transferrin internalization in T cells from 2 healthy control subjects and P2 on stimulation with anti-CD3 plus Protein A for 48 hours (top) and 72 hours (bottom). Right panel, graphic representation of biotinylated transferrin present on the cell surface at time point t= 10- and 30-minutes relative to t=0 minutes.

6.4.4. Internalization of T cell Receptor (TCR)

In literature, TCRαβ internalization is reported as possibly dependent on clathrin-endocytosis (73). However, recent studies showed that TCRαβ triggering leads to its rapid uptake through a clathrin-independent pathway. Immediately after internalization, TCR is incorporated into a mobile and long-lived endocytic network demarked by the membrane-organizing proteins flotillins (25). In this study, to assess if TCRαβ internalization was compromised by defects of clathrin-internalization, PBMCs from a healthy control and from P2 were analyzed (Figure 6.18).

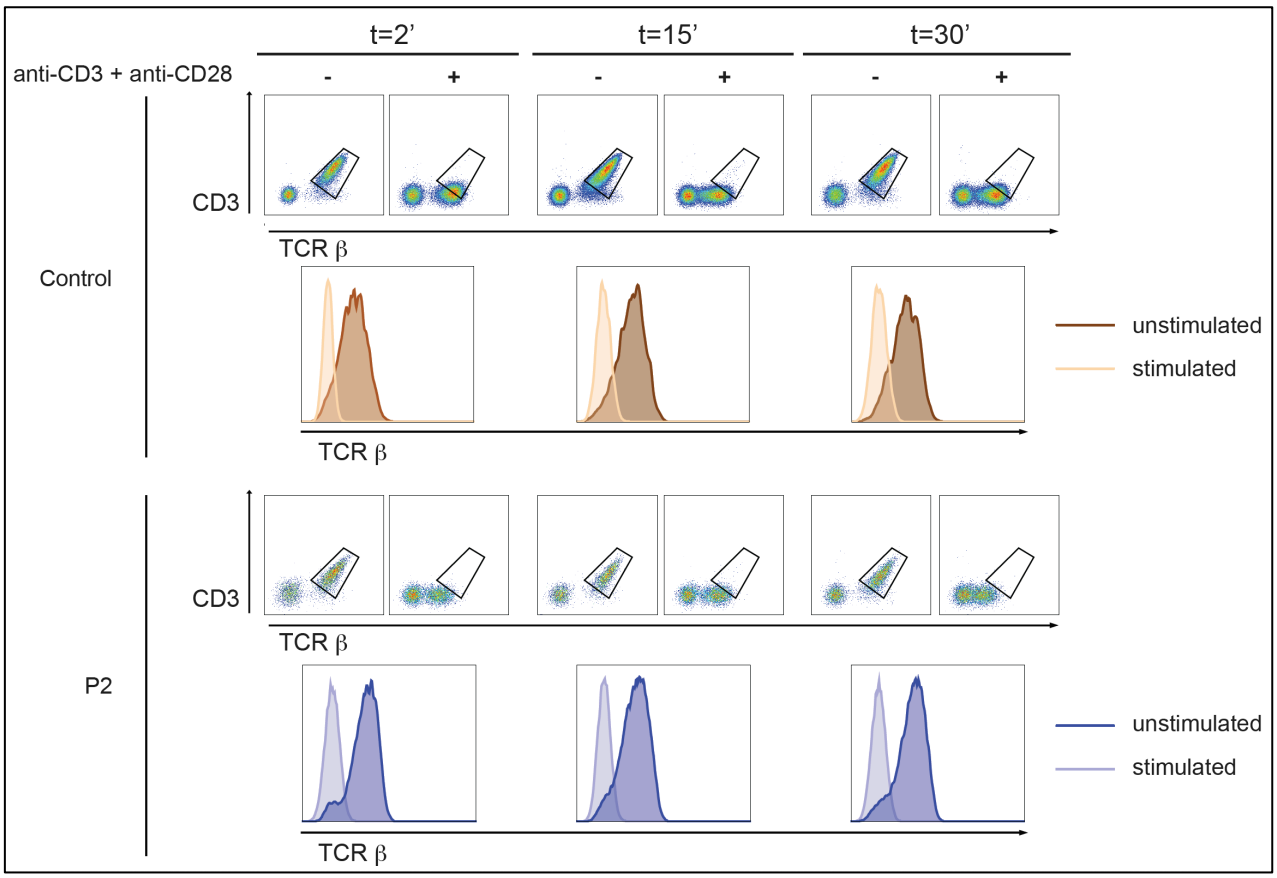

Figure 6.18. TCRαβ/CD3 internalization assay. Flow cytometric analysis of the kinetics of TCRβ surface expression in unstimulated and anti-CD3/CD28–stimulated PBMCs from a healthy control subject (top) and P2 (bottom). CD3+ TCRαβ+ gated on live cells, singlets, whole cells, CD45+ cells.

Cells were stimulated with soluble anti-CD3 and anti-CD28 for 2, 15 and 30 minutes, then surface TCRαβ and CD3 expression was analyzed at flow cytometry. In both control and P2's PBMCs, TCRαβ/CD3 were expressed on cellular surface at time point 0 and their internalization was preserved at all time points, suggesting that internalization of TCR/CD3 is preserved in *FCHO1* mutated T cell, likely because not dependent on CME.

6.5. Induced Pluripotent Stem Cells (iPSCs)

To test *in vitro* T cell differentiation from hematopoietic precursors taking advantage of the Artificial Thymic Organoids (ATO) technology, induced pluripotent stem cells (iPSCs) from patient 1 and 2 were generated. Skin fibroblasts from Patient 1 and CD34+ cells from peripheral blood from Patient 2 were reprogrammed into induced Pluripotent Stem Cells (iPSCs) by using of the non-integrating Sendai virus. After colony picking, iPSCs clones were tested for stemness gene-expression (*OCT4*, *NANOG*, *SOX2*, *KLF4*) by Real Time Quantitative PCR (Figure 6.19, upper panel).

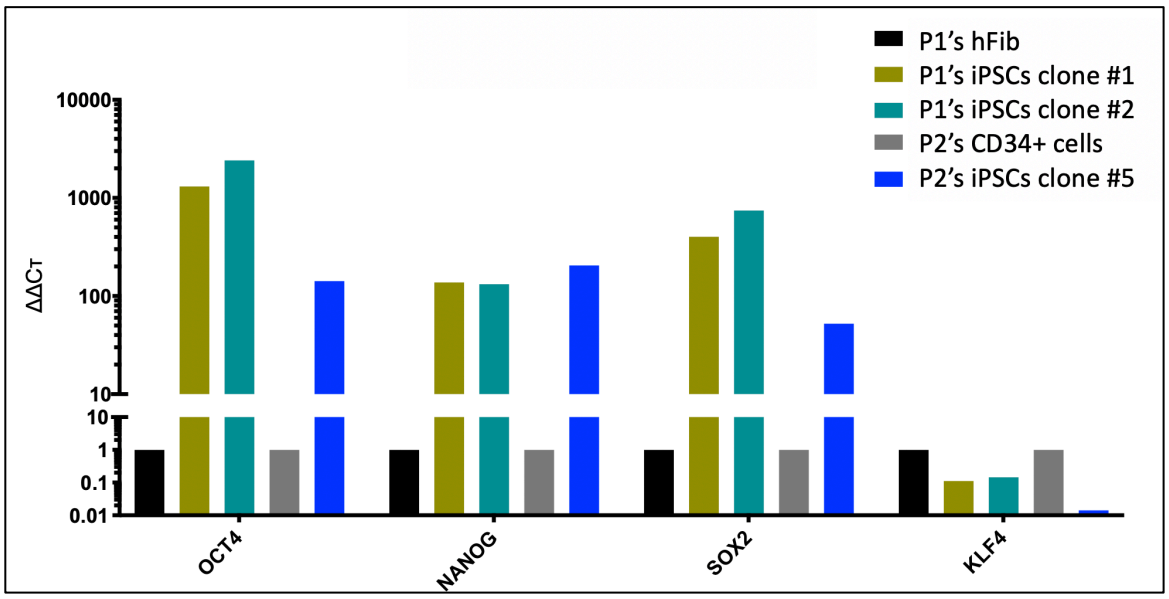

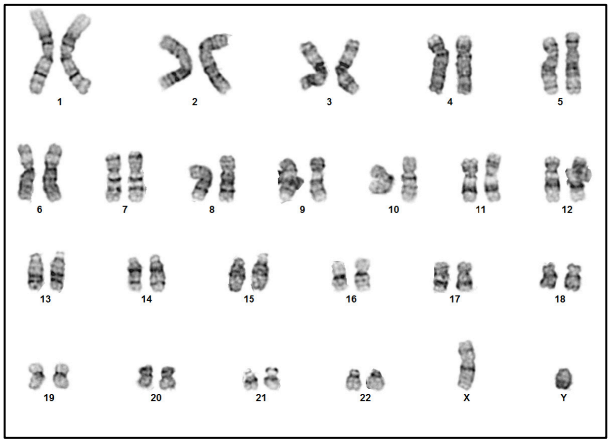

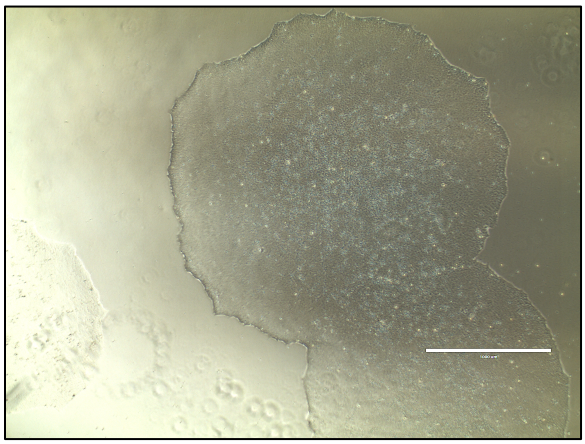

Figure 6.19. Real-time PCR and Karyotype of iPSCs. Upper panel, gene expression on Real-time PCR for stemness genes of two iPSCs clones from Patient 1 (P1's iPSCs clone #1, clone#2, in green) compared to the parent Fibroblast line (P1's hFib, in black) and one clone from Patient 2 (P2's iPSCs clone#5, in blue) compared to the parent CD34+ cell line (P2's CD34, in gray). Lower panel, left, karyotype analysis on P2's iPSCs, clone #5. Lower panel, right, picture of a iPSCs colony (P2) on Matrigel coating.

Gene expression of iPSCs was compared to the expression in the respective parental line (fibroblast or CD34+). All clones displayed increased expression of stemness genes, compared to the parental line (*OCT4*, *NANOG*, *SOX2*). Kruppel-like factor 4 (*KLF4),* together with other three endogenous Yamanaka pluripotency factors, triggers the reprogramming of differentiated cells into iPSCs and specifically, it suppresses the expression of differentiating genes in the early steps, while introducing expression of pluripotency- and stemness- genes in the late steps of reprogramming. When iPSCs are successfully reprogrammed, *KLF4* expression lowers, as shown in Figure 6.19 (upper panel). Data were normalized to the ACTB gene as an endogenous control. iPSCs were also analyzed for karyotype, which was shown to be a normal XY karyotype (Figure 6.19, lower panel, left), genetic identity of the mutation described, as respective of the parental line and presented with iPSCs characteristic morphology (Figure 6.19, lower panel, right), confirming the successful generation of iPSCs clones.

6.6. Generation of *Fcho1*-mutant mice

To investigate the functions of the *FCHO1* gene and further study the impact of its pathogenic mutations in a mammalian organism, a knock-in mouse model taking advantage of the CRISPR-Cas9 technology was generated. No *Fcho1*-genetically modified mouse has ever been reported in literature. *In silico* analysis of the evolutionary conservation of FCHO1 showed a highly conserved profile among species (including Homo sapiens and Mus musculus), particularly in the F-BAR and μ-homology domains region (Figure 6.6). This murine model study was designed with the meaning of introducing the splice site mutation (c.120-1 G>G) of the first identified *FCHO1* patient (P1) in a knock-in mouse. The human mutation fell in the highly conserved F-BAR domain that is pivotal for protein function. Subsequent exon skipping showed to cause impaired FCHO1 dimerization and protein binding to the phospholipids of the inner side of the cellular membrane and disruption of FCHO1 activity, resulting in a very severe phenotype of human immune deficiency. The murine *Fcho1* gene (CL57BL6 strain), located on chromosome 8, is 3073 base-pair long, includes 26 exons and encodes for an 873aa-long protein (transcript ID ENSMUST00000093444.12, isoform Fcho1-201). *In silico* protein alignment studies demonstrated 85% pairwise identity of the murine protein compared to the human one, with 795 identical shared sites (Figure 6.20).

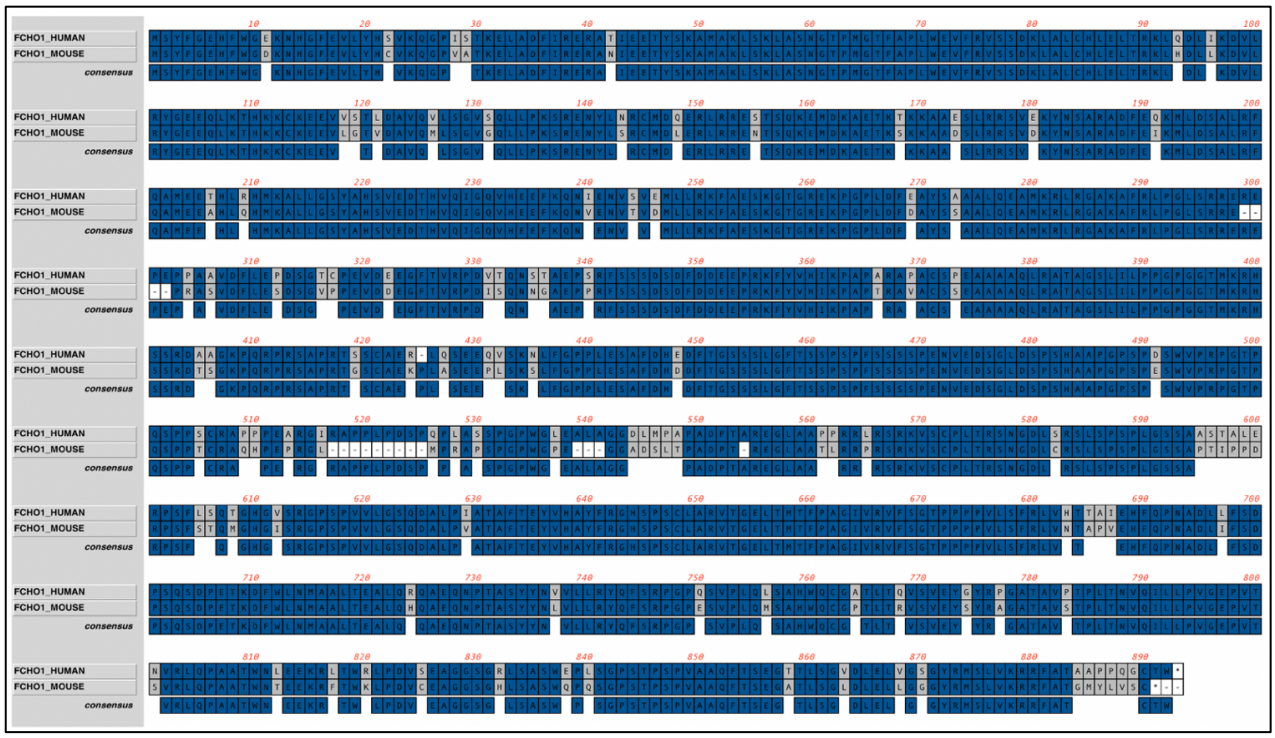

Figure 6.20. Human versus murine protein alignment. Alignment of human FCHO1 (upper raw) and murine Fcho1 (middle raw). Bottom raw: identical amino acids (consensus).

The human splice site mutation G>C in position c.120-1 is located at the acceptor splice site of intron 5. In the mouse, the equivalent position c.120-1 is found at the acceptor splice site of intron 2 (Figure 6.21).

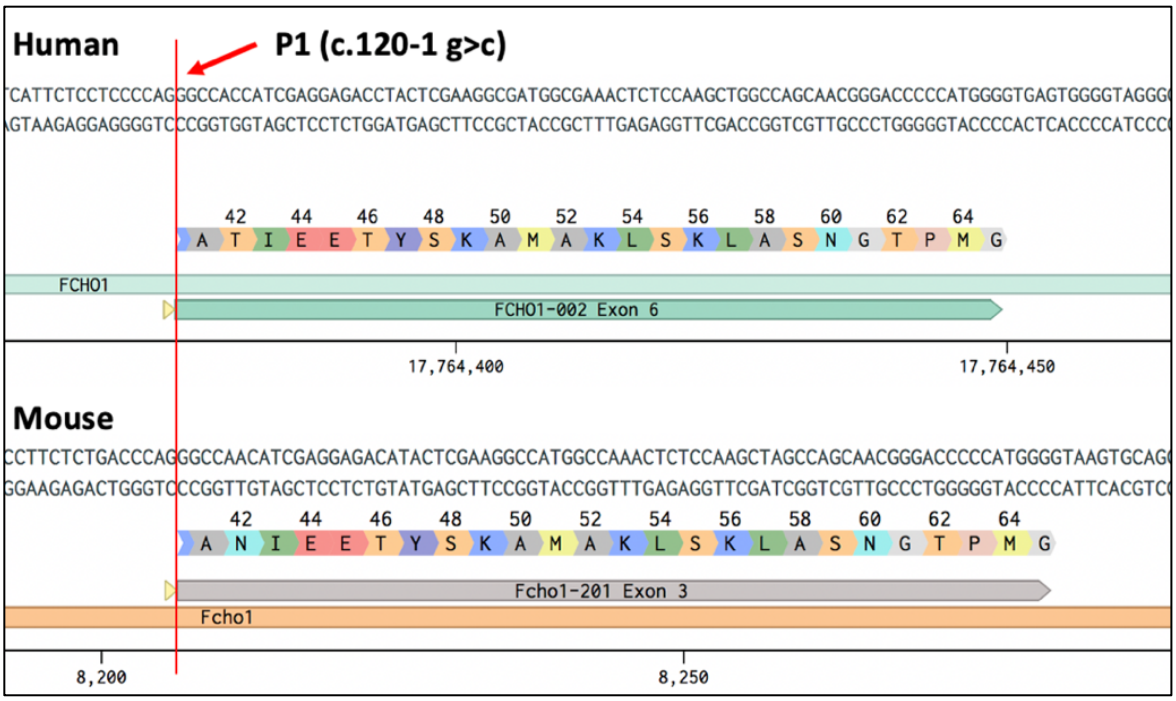

Figure 6.21. Alignment of human and murine genes. Alignment of *FCHO1* human (upper panel) and *Fcho1* mouse (lower panel) genomic DNA in proximity of the c.120-1 G>C mutation (red bar). Yellow arrow before exon 6 in human and exon 3 in mouse marks the splice site.

CRISPR-Cas9 technology allows generation of knock-in mice through introduction of a desired mutation in the genomic DNA (Figure 6.22). First, the Cas9 nuclease is directed to a specific DNA site by a guide RNA (gRNA). Once the DNA site is recognized, the nuclease cuts the DNA strands. If a homologous DNA template is provided, the strands are subsequently repaired by homology-mediated repair (HDR).

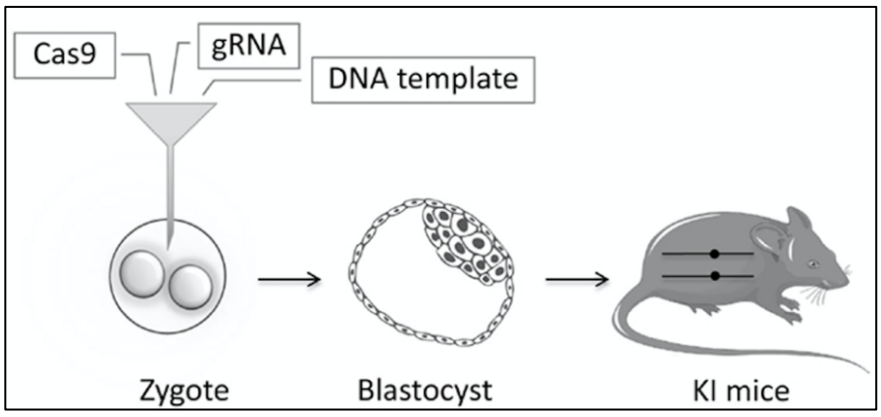

Figure 6.22. Generation of a k/i mouse. Experiment layout for the generation of a k/i mouse model with CRISPR-Cas9 technology.

To target the region around c.120-1 of *Fcho1*, a series of single-guide RNAs (sgRNAs) were designed and analyzed for their on-target and off-target scores (Figure 6.23). The off-target score indicates the inverse probability of Cas9 off-target binding, whereas the on-target score represents the cleavage efficiency of Cas9. A higher score means that the sgRNA sequence has less chances to bind to other DNA sequences in the rest of the genome and more chances to bind to the target sequence. The two scores guided the selection of optimal protospacer sequences.

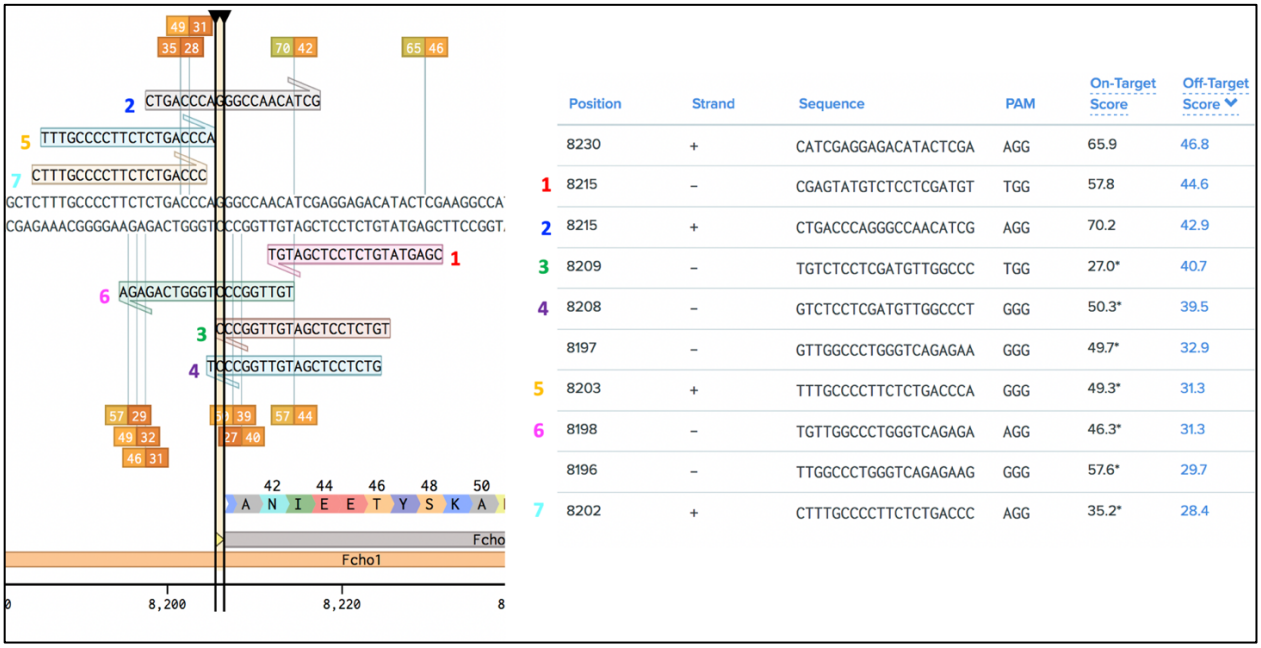

	Position	Strand	Sequence	PAM	On-Target Score	Off-Target Score
	8230	+	CATCGAGGAGACATACTCGA	AGG	65.9	46.8
1	8215	–	CGAGTATGTCTCCTCGATGT	TGG	57.8	44.6
2	8215	+	CTGACCCAGGGCCAACATCG	AGG	70.2	42.9
3	8209	–	TGTCTCCTCGATGTTGGCCC	TGG	27.0*	40.7
4	8208	–	GTCTCCTCGATGTTGGCCCT	GGG	50.3*	39.5
	8197	–	GTTGGCCCTGGGTCAGAGAA	GGG	49.7*	32.9
5	8203	+	TTTGCCCCTTCTCTGACCCA	GGG	49.3*	31.3
6	8198	–	TGTTGGCCCTGGGTCAGAGA	AGG	46.3*	31.3
	8196	–	TTGGCCCTGGGTCAGAGAAG	GGG	57.6*	29.7
7	8202	+	CTTTGCCCCTTCTCTGACCC	AGG	35.2*	28.4

Figure 6.23. SgRNAs design and analysis. 1 to 7 indicates the sgRNAs considered. On the left: location of sgRNAs on the murine *Fcho1* genomic DNA. On the right: Table summarizing genomic location, target strand (+ positive, - negative), nucleotides sequence, Protospacer Adjacent Motif (PAM) sequence and On-Target/Off-Target scores of respective sgRNAs.

Of the 7 sgRNAs initially considered, 3 sgRNAs were selected (sgRNA#2, sgRNA#5 and sgRNA#7) for further screening because of their optimal distance to the target site (3 to 8 base

pairs), the possibility to easily remove the PAM sequence in the sg-RNA-specific DNA donor template and their satisfactory on- and off- target scores (on-target scores 35.2 to 70.2, and off-target scores 28.4 to 42.9). Moreover, for each sgRNAs, the specific off-target genes recognized by the sgRNA were also evaluated. SgRNA#7 showed the best profile for targeting genes that are not involved in murine embryonic development and can therefore impact mice generation (Figure 6.24).

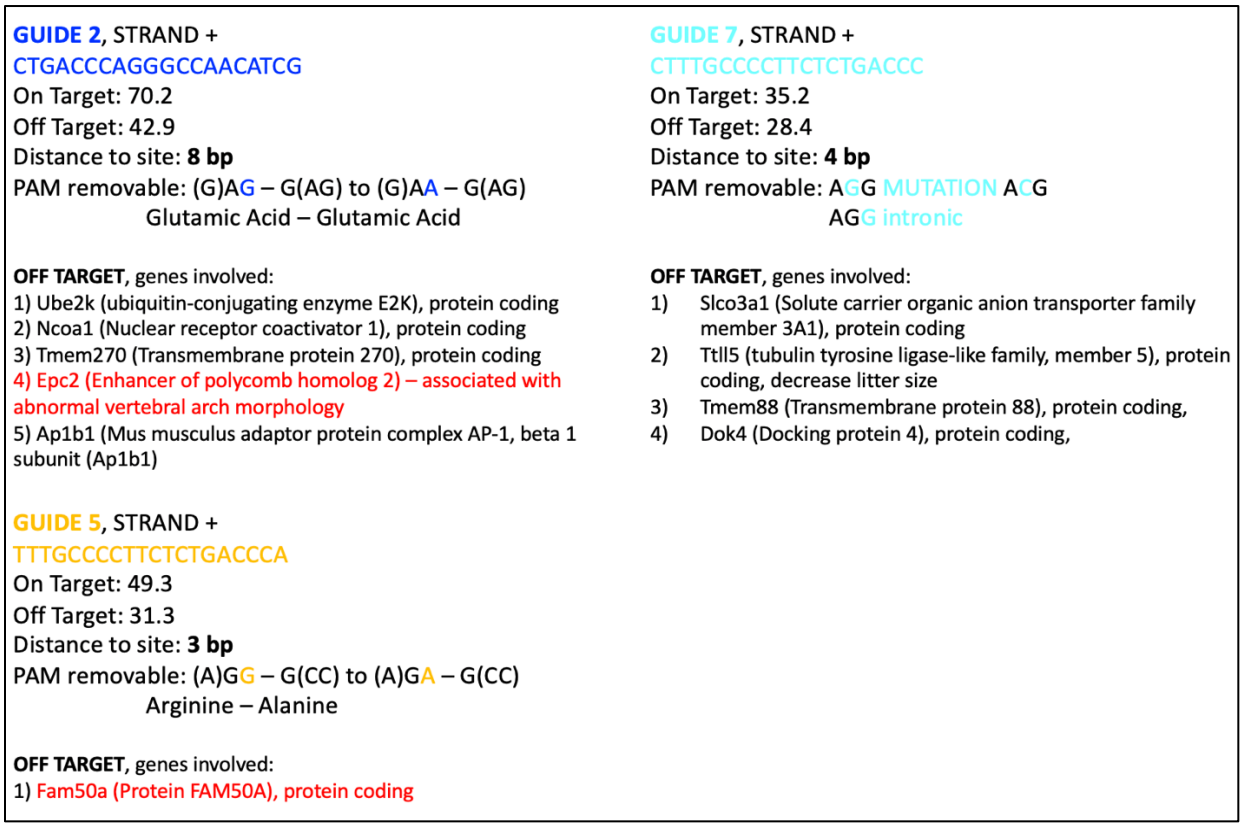

Figure 6.24. SgRNAs profile analysis. Analysis of sgRNA#2 (blue), sgRNA#5 (orange) and sgRNA#7 (turquoise). Red highlights genes that take part in embryonic development.

SgRNA#2, sgRNA#5 and sgRNA#7 were then *in vitro*-screened for the ability to perform a sgRNA driven-Cas9 cut on a genomic DNA. A 725 base-pair long genomic DNA spanning the CRISPR/Cas9 cut site and therefore, the splice site, was amplified by PCR and subsequently incubated with the three sgRNAs respectively. Complete cut of the PCR product was obtained with the sgRNA#7 and only two products were observed (one of 400 base pair, the other of 325

base pair long), while sgRNA#2 and sgRNA#5 displayed a residual PCR un-cleaved product on agarose gel (Figure 6.25).

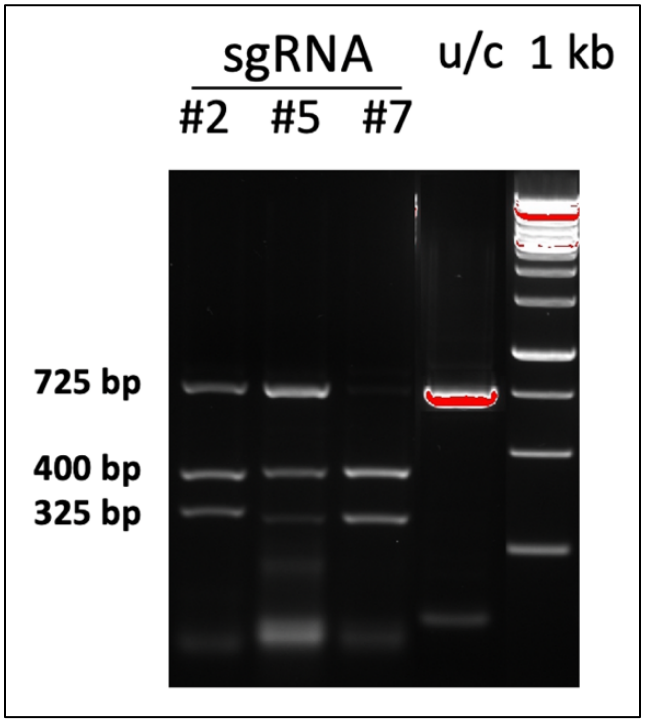

Figure 6.25. SgRNA *in vitro* screening. bp: base-pair; u/c: un-cleaved, 1 kb: 1 kb ladder.

As a result of *in silico* and *in vitro* studies, sgRNA#7 was selected for the generation of the knock-in mouse model. The donor-template DNA for homology-mediated repair (HDR) was designed based on sgRNA#7 intrinsic characteristics. The HDR DNA template resulted in an asymmetric, 163 nucleotides-long single DNA strand with a 54-nucleotide-long short arm and 109-nucleotide-long long arm. Introduction of the 120-1 G>C mutation, at the same time, conveniently disrupted the PAM sequence. This site is fundamental for sgRNA recognition of target DNA and subsequent Cas9 recruitment, disruption impedes the Cas9 from cutting the integrated HDR-donor DNA template, therefore preventing further dsDNA breaks in cells that have already integrated the template donor DNA in their genome. Murine zygotes were microinjected or electroporated with sgRNA#7, the DNA donor template and the Cas9. The zygotes were then implanted into recipient foster mothers. A total of 38 pups were born, 20 from microinjected zygotes (19 alive and 1 dead), 18 from electroporated zygotes (12 alive and 6 dead). After genotyping, 9 possible founders were

selected which were bred with wild-type mice. Sanger sequencing of gDNA of the heterozygous pups showed the presence of intronic small indels (insertion or deletion of one or two nucleotides (Founder B07, G07, E07, F07), a 61-nucleotides long intronic/exonic deletion (Founder G07), a deletion of 6 (intronic) + 11 (exonic) nucleotides (Founder A07) and a point G>C mutation in position c.120-1 (Founder B07, F07) (Figure 6.26). The rest of the founder mice did not carry any interesting mutation.

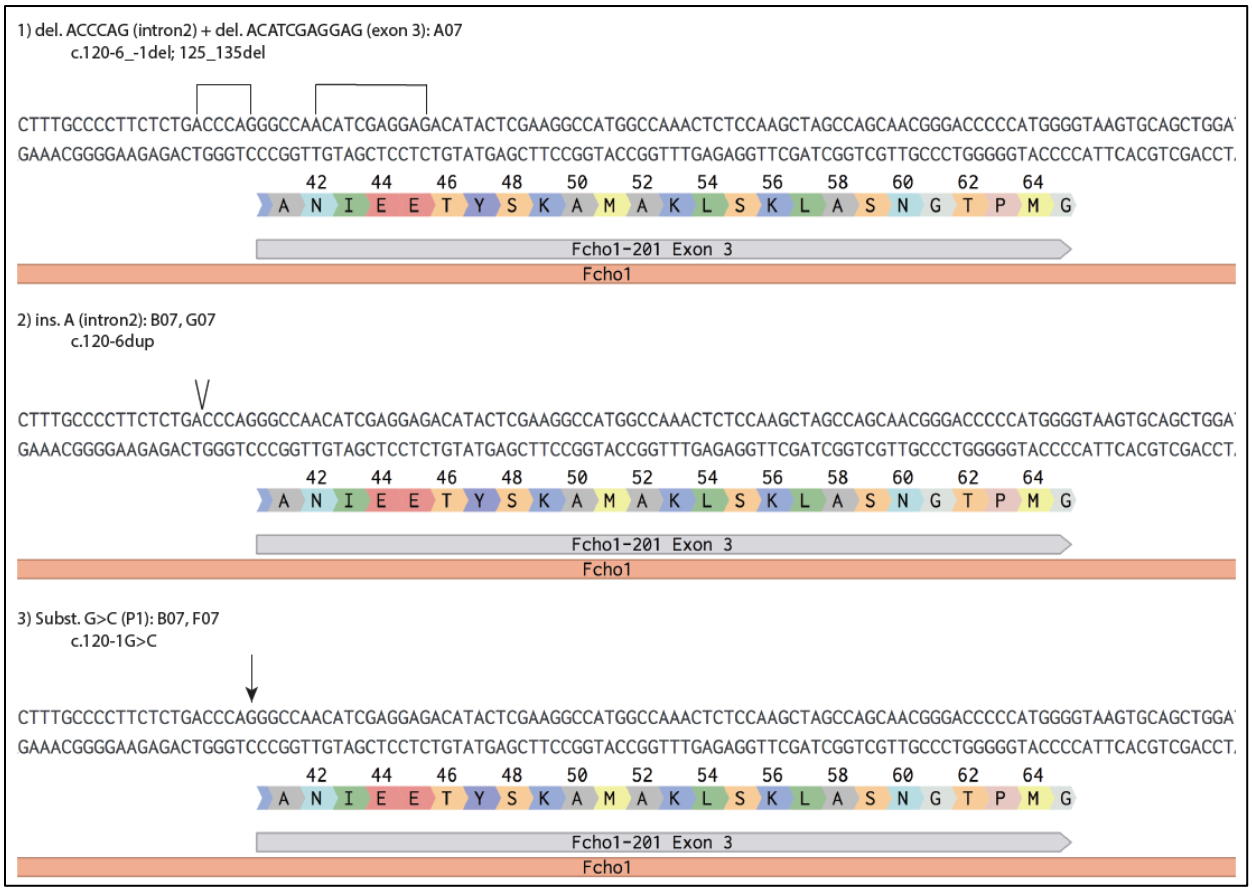

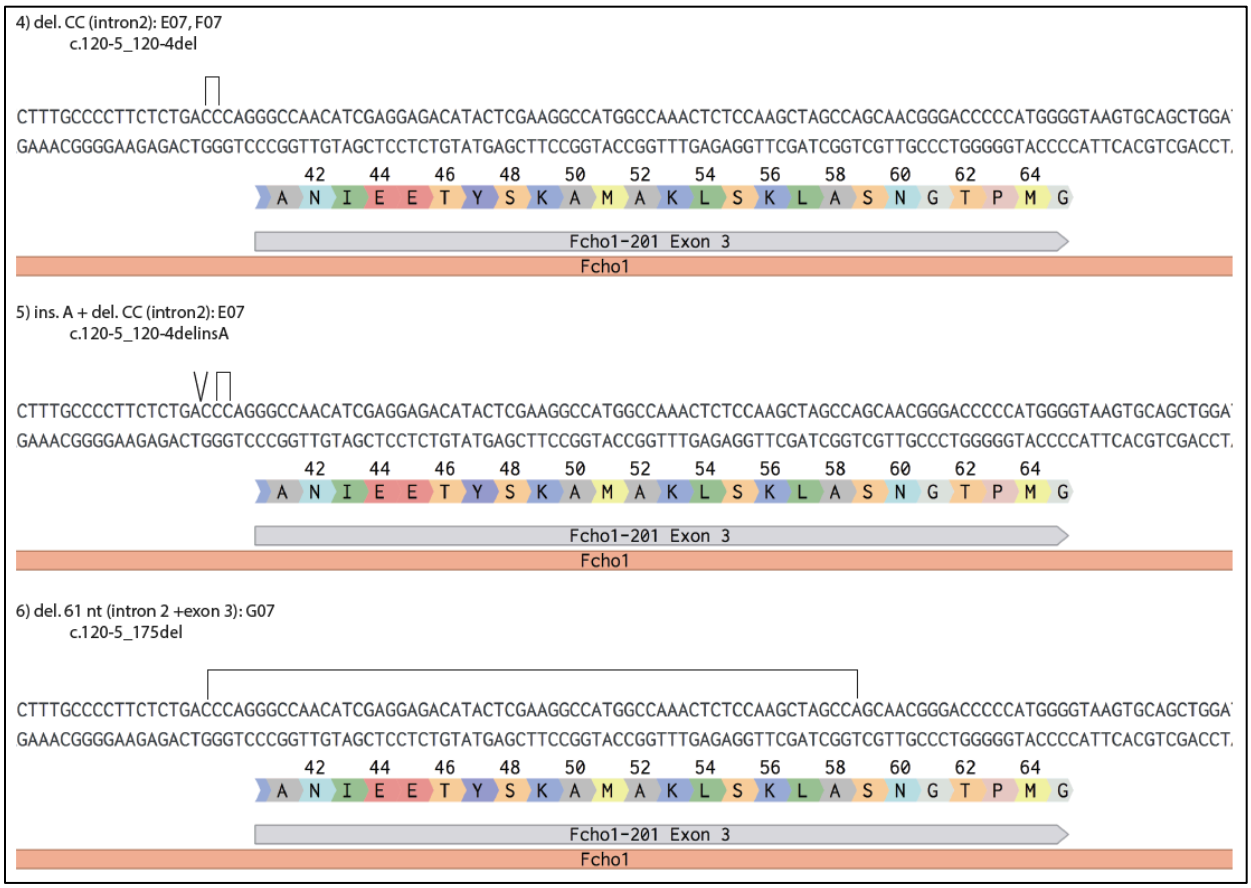

Figure 6.26. Genomic DNA of founder mice. Schematic representation of the genomic DNA mutations of the founder mice (A07, B07, E07, F07, G07).

Further analysis in this study focused on three *Fcho1* mutant mice: the c.120-1 G>C mutant (*Fcho*$^{g>c}$), the mutant with two intronic/exonic *in cis* deletions (*Fcho1*$^{del\_del}$) and the mutant with a 61 nucleotide-long deletion (*Fcho*$^{61nt\_del}$). *Fcho1* mutant mice were born at the expected Mendelian ratio and were healthy and fertile, with no obvious apparent phenotype. Mice experiments were performed on mice from F2 or later generations.

6.7. On-going experiments (human and murine)

6.7.1. Artificial Thymic Organoids (ATOs)

To uncover the functions of *FCHO1* gene in human T cell development, experiments of *in vitro* T-cell maturation from patient-derived induced pluripotent stem cells (iPSCs) taking advantage of the Artificial Thymic Organoid (ATO) technology were performed. Following the ATO protocol, a first round of experiments was successfully performed on iPSCs from a healthy donor. IPSCs were initially differentiated for 3.5 days into CD56+ Epcam- Embryonic Mesodermal Progenitors (hEMPs) (Figure 6.27), which were then aggregated with MS5-DLL4 into ATOs.

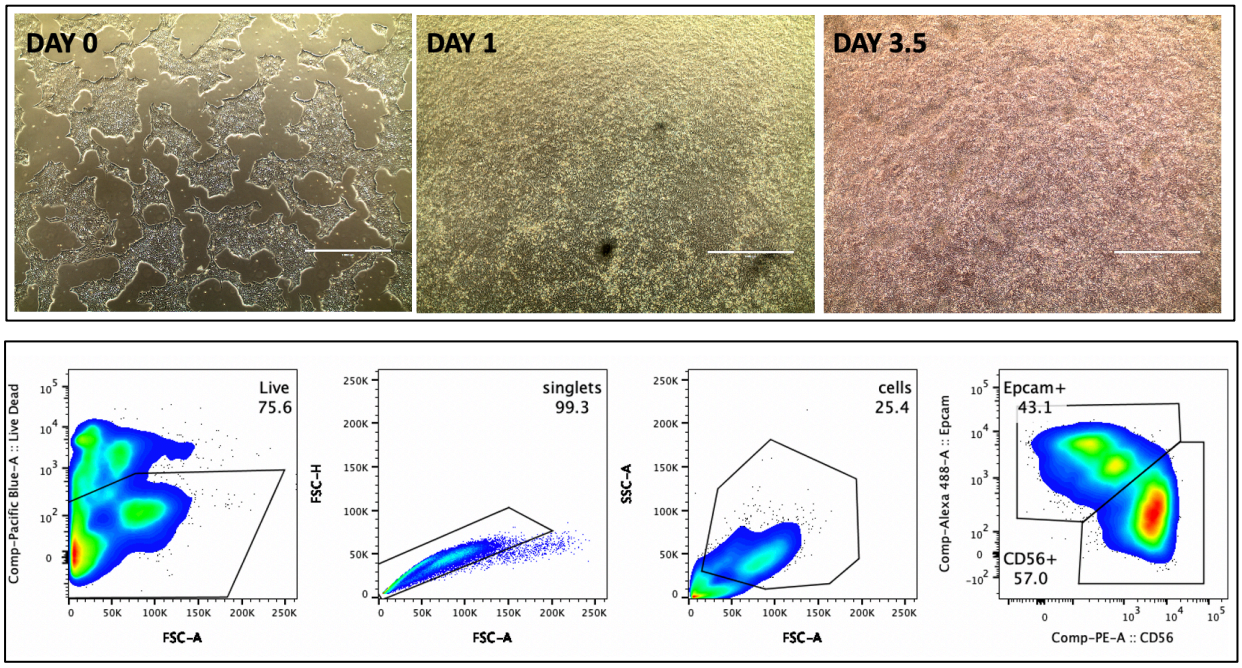

Figure 6.27. CD56+ EPCAM- Embryonic Mesodermal Progenitors (hEMPs) *in vitro* differentiation. Upper panel, differentiation of healthy-donor human iPSCs (day 0, left) into Embryonic Mesodermal Progenitors (hEMP, day 1 and day 3.5, middle and right). Lower panel, FACS staining (Live cells, singlets, whole cells, Epcam+ vs CD56+) of hEMP at day 3.5.

ATOs were then differentiated *in vitro* for 2 weeks into hematopoietic cells, followed by 6 weeks of T cell induction with generation of naïve T cells expressing T cell lineage markers (CD5, CD7

and CD1α) and mature markers (CD4, CD8β, TCRαβ and CD3) (Figure 6.28), demonstrating the successful *in vitro* maturation of iPSCs into naïve T cell.

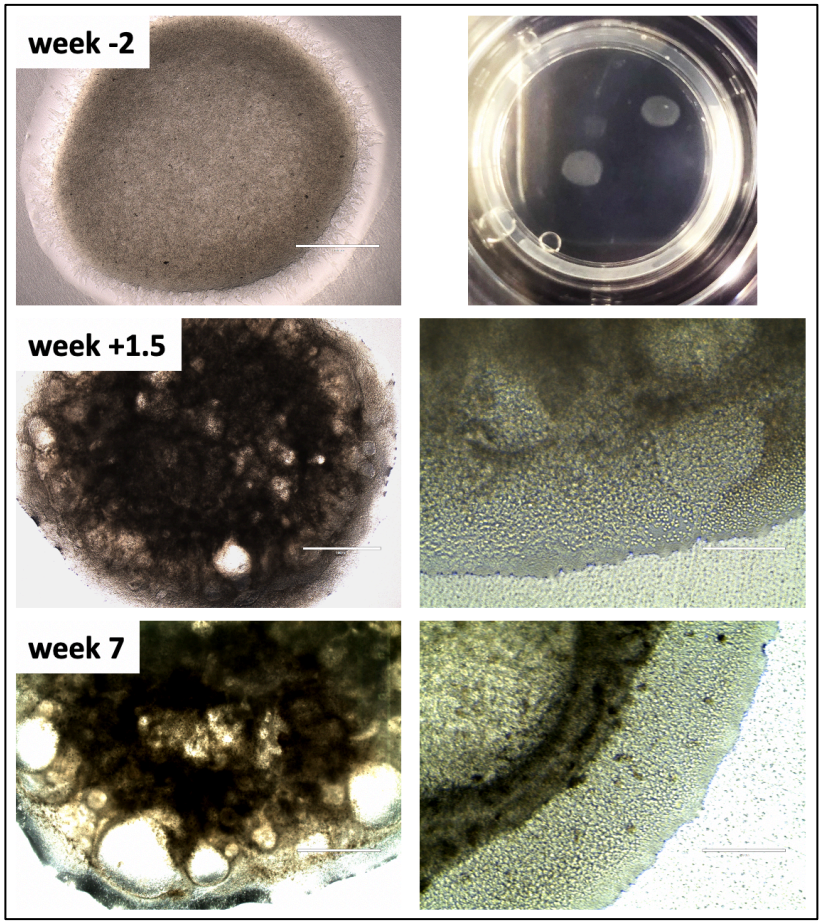

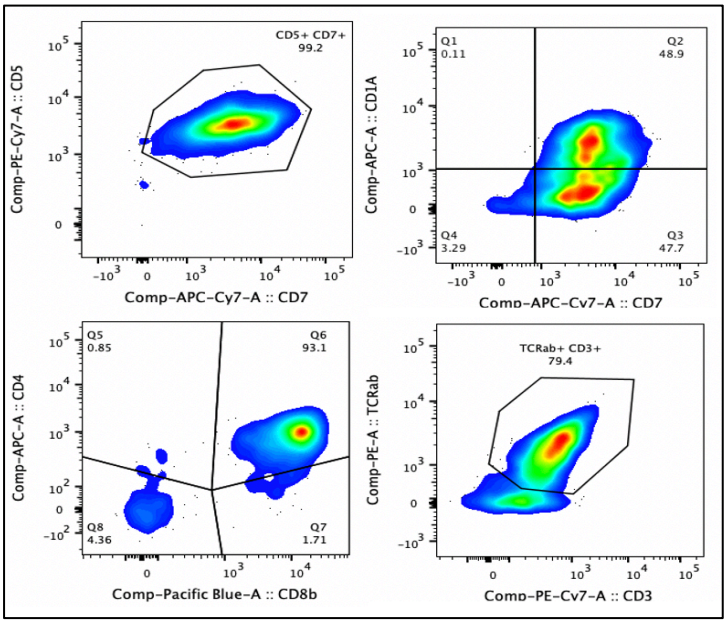

Figure 6.28. Pictures of ATOs and FACS plots of iPSCs differentiated into T cells. Upper panel, ATOs at different stages of T cell maturation (week -2, week +1.5 and week 7). Lower panel, FACS staining of naïve T cells (CD5+, CD7+, CD1α+, CD4+, CD8β+, TCRαβ+, CD3+) differentiated from healthy donor human iPSCs, gated on live CD34- CD45+ CD56- cells.

6.7.2. Analysis of murine RNA splicing

Patient 1 was homozygous for a splice-site mutation at the acceptor site of intron 5, predicted to result in exon 6 skipping. In the mouse, the corresponding mutation was predicted to result in exon 3 skipping. Therefore, RT-PCR analysis of whole splenocytes from two *Fcho1* mutant mice was performed. Amplification with primers in exon 2 and 5 (392 bp-long amplicon) identified 2 bands in both mice: one was below 300 bp and brighter for the *Fcho1*$^{del\_del}$ mutant mouse, the other, around 400 bp and brighter for the *Fcho1*$^{g>c}$ mutant mouse (Figure 6.29). Data on RT-PCR of the *Fcho*$^{61nt\_del}$ mutant mouse are not available (these experiments are ongoing).

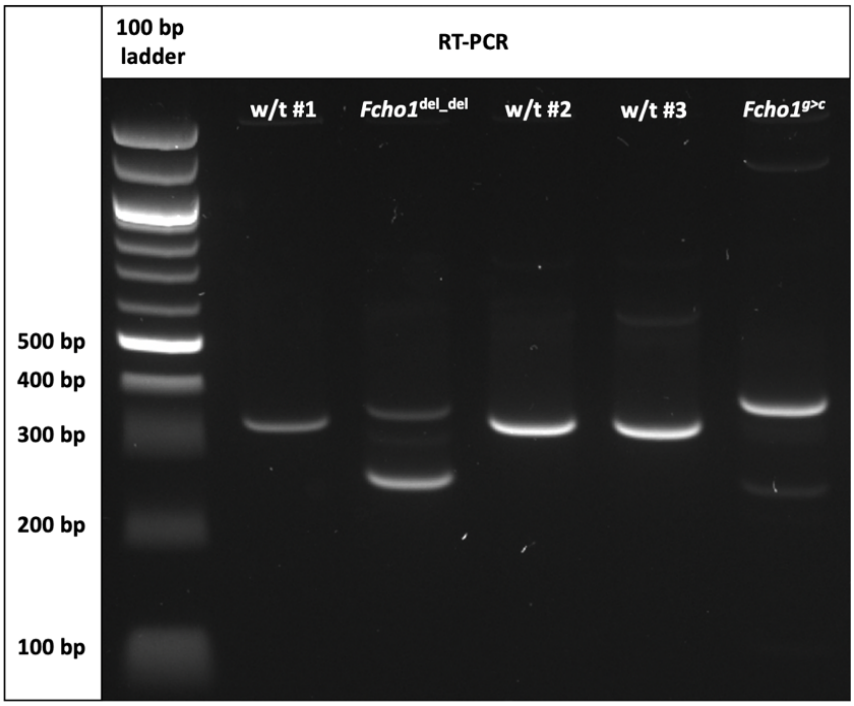

Figure 6.29. RT-PCR run on Agarose gel. RT-PCR on three *wild-type* mice (w/t #1, w/t #2, w/t #3) and two *Fcho1* mutant mice (*Fcho1*$^{g>c}$ and *Fcho1*$^{del\_del}$).

Bands were cut from agarose gel and PCR product was extracted. Sanger sequencing confirmed that the lower band corresponded to a product lacking exon 3 (composed of 75 nucleotides), with an in-frame, internally truncated FCHO1 cDNA, as previously seen in Patient 1's cDNA. The upper band corresponded to a product lacking exon 3 but inserting 38 intronic nucleotides (*Fcho1*$^{g>c}$) or 32 nucleotides (*Fcho1*$^{del\_del}$) of intron 2, upstream of the splice site (Figure 6.30).

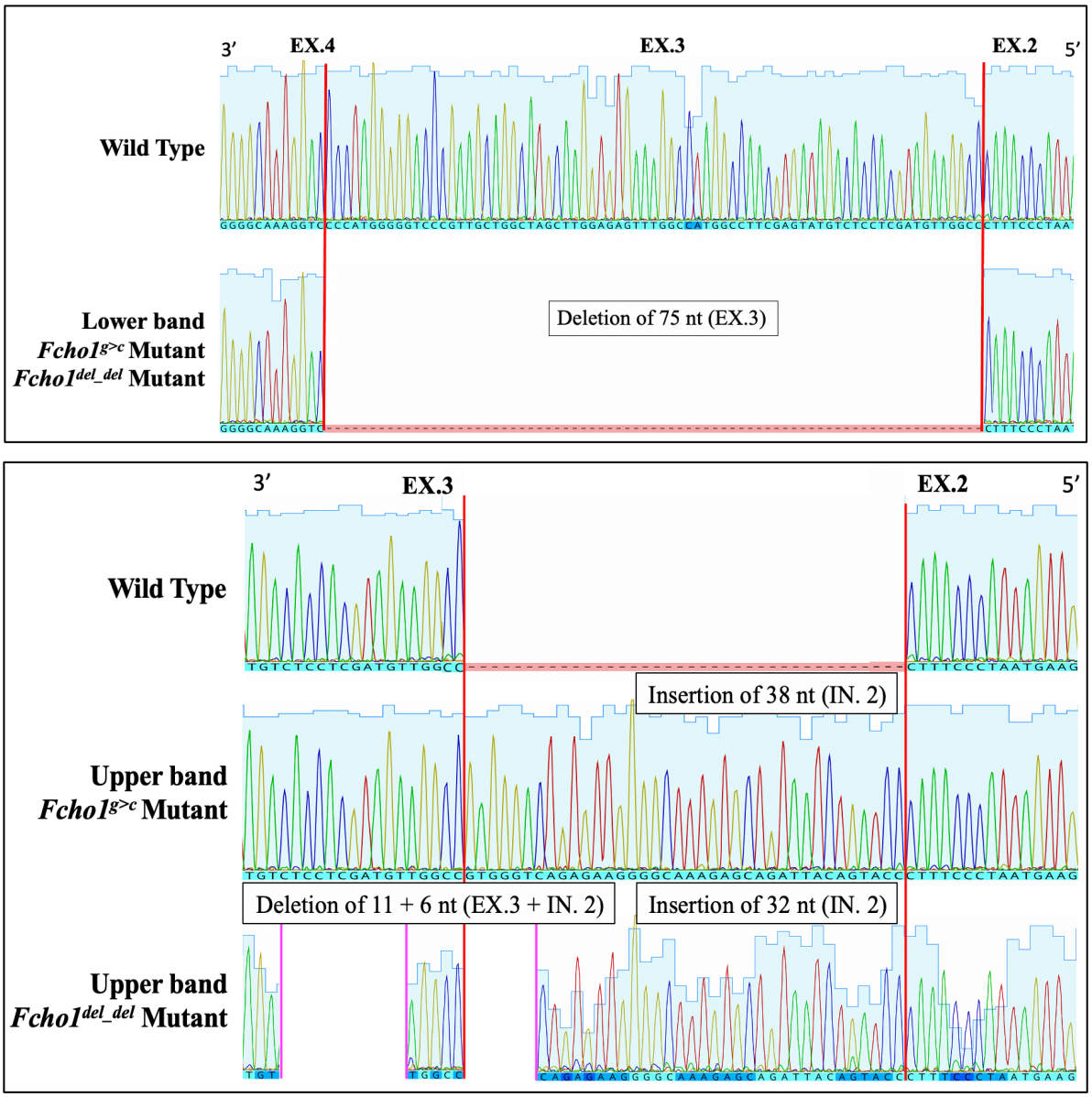

Figure 6.30. Sanger sequencing of RT-PCR. Sanger sequencing performed with reverse primer of RT-PCR of band extracted from Agarose gel from wild type mice and *Fcho1*$^{g>c}$ and *Fcho1*$^{del\_del}$ mutant mice (Upper panel, lower band; Lower panel, upper band). EX., Exon; IN., Intron; nt, nucleotides.

In silico prediction analysis (ExPasy software) of protein products generated from cDNA of two upper bands suggested three possible scenarios of protein translation in the *Fcho1*$^{g>c}$ and *Fcho1*$^{del\_del}$ mutant mice. In the *Fcho1*$^{g>c}$ mutant mouse, the intronic insertion of 38 nucleotides, generated from the defect in splicing, would determine production of an internally truncated protein (Frame 1, Figure 6.31, upper panel) or completely disrupted proteins due to frameshifts and multiple stop codons (Frame 2 and Frame 3, Figure 6.31, upper panel). In the *Fcho1*$^{del\_del}$ mutant mouse, the intronic insertion of 32 nucleotides and intronic/exonic deletion of 11 and 6 nucleotides would determine production of completely disrupted proteins due to frameshifts and multiple stop codons (Frame 1 and Frame 2, Figure 6.31, lower panel), or of a truncated protein lacking the first 50 amino acids (Frame 3, Figure 6.31, lower panel). Unfortunately, there are no commercially available antibodies to detect FCHO1 at protein expression level in mice.

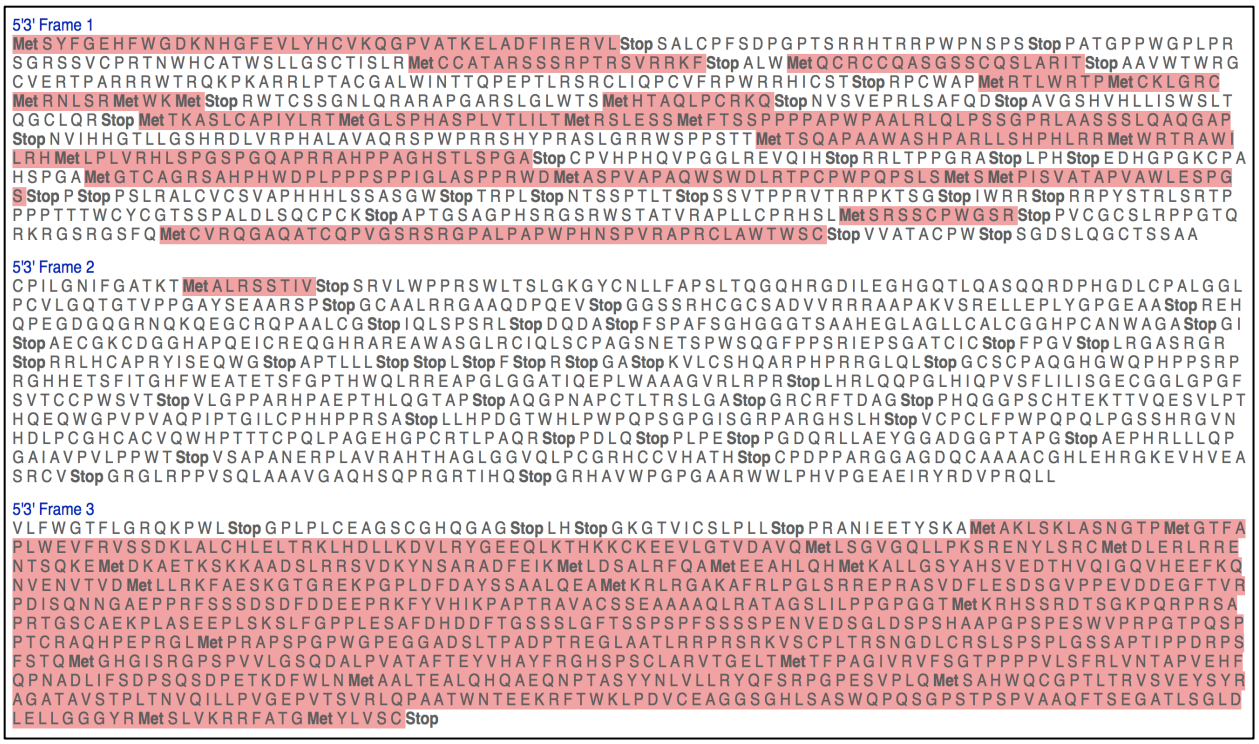

Figure 6.31. *In silico* analysis (ExPasy) of protein products. *In silico* prediction studies on protein translation from the cDNA RT-PCR extracted from upper bands. Upper panel, upper band of *Fcho1*$^{g>c}$ mutant mouse; Lower panel, upper band of *Fcho1*$^{del\_del}$ mutant mouse. Open reading frames are highlighted in red.

Altogether, these data show that *Fcho1* mutations of two mutant mice, the *Fcho1*$^{g>c}$ and the *Fcho1*$^{del\_del}$, cause defects of exon 3 splicing that only partially recapitulate the splice site defect found in the c.120-1 G>C mutation (P1).

6.7.3. Mouse Immune Phenotyping

In order to uncover any disease-related phenotype in *Fcho1* mutant mice, preliminary studies on the immune-phenotype were performed. Flow-cytometry and Complete Blood Count (CBC) on peripheral blood performed on young homozygous *Fcho1*$^{g>c}$ and *Fcho1*$^{del\_del}$ mutants (6.5 to 7.5 weeks old) showed no statistically significant differences as compared to wild-type (w/t) in absolute count of red blood cells (RBC), platelets and hemoglobin (Hb) (Figure 6.32, upper panel).

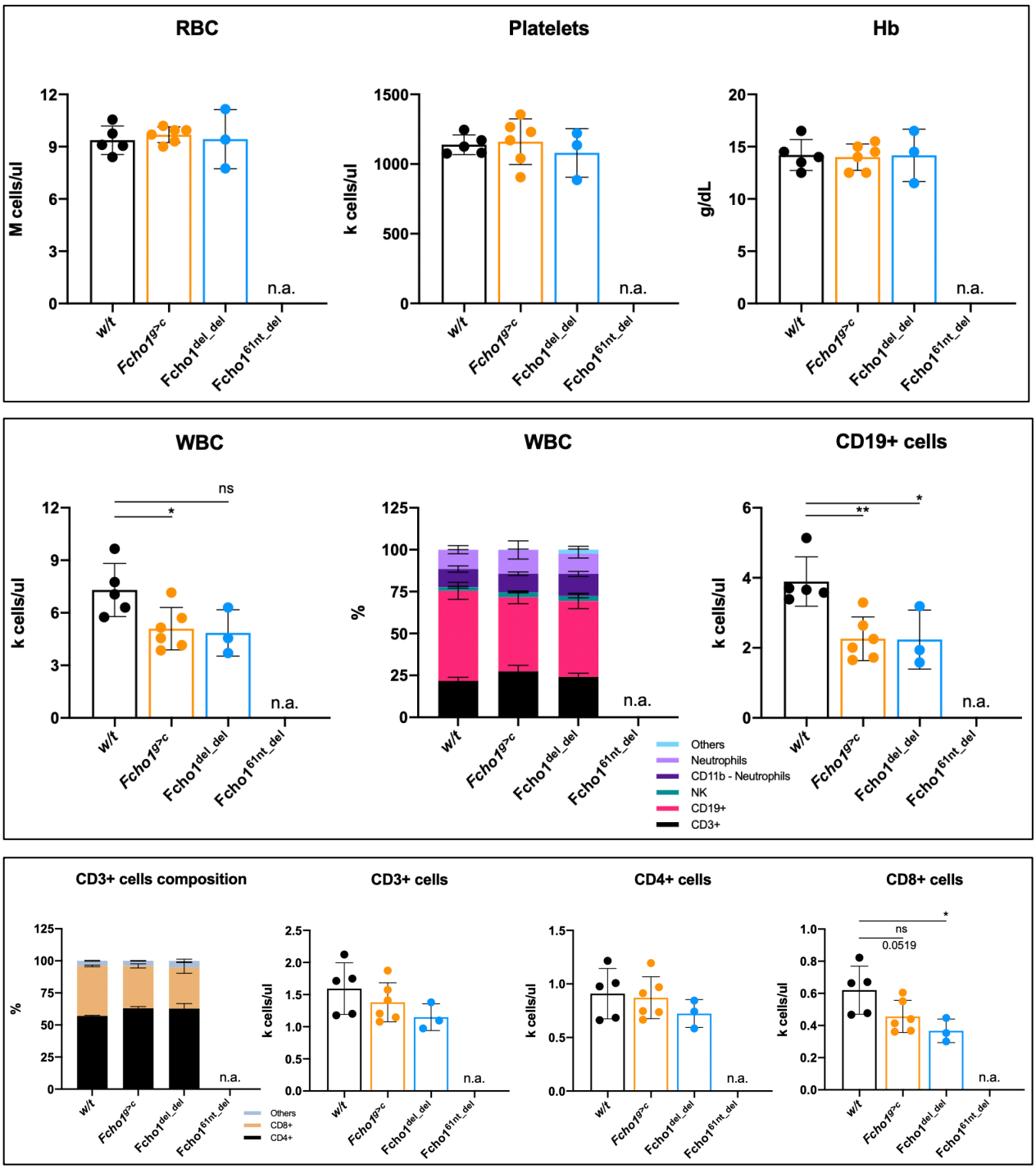

Figure 6.32. Flow-cytometry analysis of Peripheral Blood. Upper panel, absolute count of Red Blood Cells (RBC) (left), Platelets (middle), Hemoglobin (Hb) (right). Middle panel, absolute count of White Blood Cells (WBC) (left), distribution of WBC (middle) absolute count

of B lymphocytes (CD19+ cells) (right), gated on live, singlets, whole cells, CD45+ cells. T cells, CD3+; B cells, CD19+, NK cells, NK1.1+, Granulocytes without Neutrophils, CD11b+ Gr1-, Neutrophils, CD11b+ Gr1+. Lower panel, distribution of CD3+ T cells (left); absolute count of CD3+ T cells (middle left); CD4+ T helper cells (middle right); CD8+ T Cytotoxic cells (right), gated on live, singlets, whole cells, CD45+ cells. W*ild-type* (*w/t*), *Fcho1*$^{g>c}$ homozygous and *Fcho1*$^{del\_del}$ homozygous mouse mutant. Experiments on *Fcho*$^{61nt\_del}$ homozygous mouse are on going. n.a., data not available; ns, not statistically significant; M, million; k, thousand. *: p value < 0.05; **: p value < 0.01.

Analysis on white blood cells (WBC) absolute number showed a statistically significant reduction in total WBC in the *Fcho1*$^{g>c}$ mutant, as compared to wild type. No statistically significant reduction in WBC absolute count in the *Fcho1*$^{del\_del}$ mutant was found, but the number of mice analyzed in the mutant group was small (4 mice). The WBC reduction was predominantly of CD19+ cell origin, as assessed by WBC composition analysis (Figure 6.32, middle panel). In the T-cell compartment, a reduction in absolute numbers of CD8+ Cytotoxic T cells in both *Fcho1*$^{g>c}$ and *Fcho1*$^{del\_del}$ mutant mice was observed (Figure 6.32, lower panel). No alteration of CD4+ T cells, NK cells and granulocytes was noted. Data on peripheral blood of the *Fcho*$^{61nt\_del}$ mouse are not available (these experiments are ongoing). To further investigate the immunological phenotype of *Fcho1* mutant mice, preliminary studies by flow-cytometry of thymus and spleen on adult mice (8 to 12 weeks old) were performed. No abnormalities in cellular absolute count or composition during positive and negative thymic selection of thymocytes were observed in *Fcho1* mutant mice as compared to wild type. (Figure 6.33, upper panel). However, all 3 mutant mice showed reduction in absolute number of total splenocytes, with a predominant B lymphocyte (B220+ CD19+ cells) phenotype. In all three mutants it was observed a slight reduction of follicular mature B cells (CD24^{lo}, CD21^{lo}). An increase in marginal zone (CD24^{hi}, CD21^{hi}) and precursor (transitional 2, T2) cells (CD24^{hi}, CD21^{int}) B cells was present in the *Fcho1*$^{g>c}$ mouse, and a small increase in transitional 1 (T1, CD24^{hi}, CD21^{lo}) B cells in the *Fcho1*^{del_del} and the *Fcho*$^{61nt\_del}$ mouse was observed (Figure 6.33, lower panel). These preliminary results point out to an apparent exclusive B cell phenotype in the *Fcho1* mutated mouse.

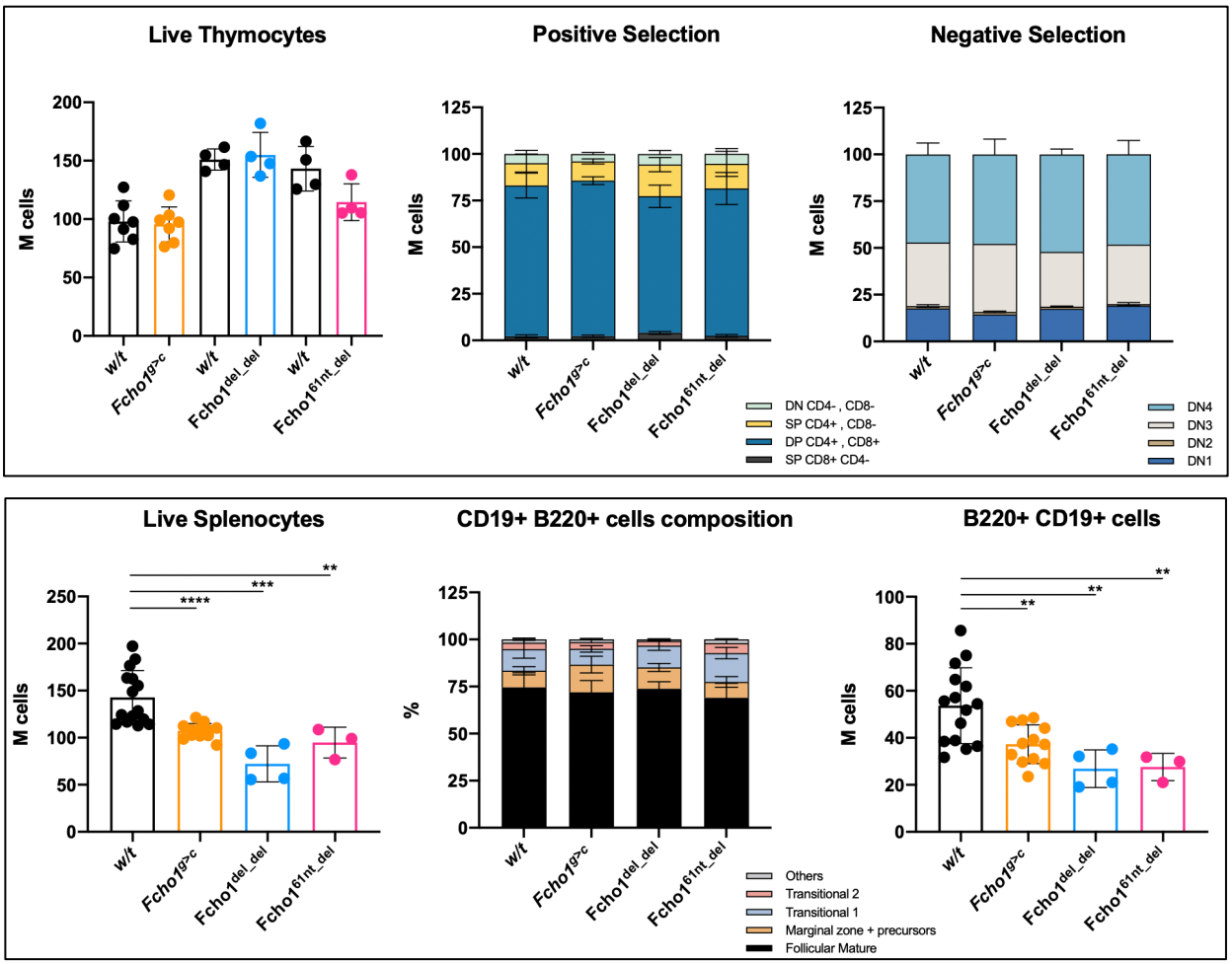

Figure 6.33. Flow-cytometry analysis of thymus and spleen. Upper panel, absolute number of live thymocytes (left, each mutant mice has a w*ild*-type mouse of reference), distribution of cells (gated on live cells, singlets, whole cells, CD45+ cells) under positive selection (double negative, DN CD4- CD8-, single positive CD4+, SP CD4+ CD8-, double positive, DP CD4+ CD8+, single positive CD8+, SP CD8+ CD4-) (middle), and under negative selection (double negative stage 1, DN1 CD44- CD25-, stage 2, DN2 CD44+ CD25-, stage 3, DN3 CD44+ CD25+, stage 4, DN4 CD44- CD25+) (right). Lower panel, absolute number of live splenocytes (left) and absolute number (right) of B lymphocytes (B220+ CD19+ cells, gated on live cells, singlets, whole cells, CD45+ cells), composition (middle) of B lymphocytes (B220+ CD19+ cells, gated on live cells, singlets, whole cells, CD45+ cells, CD19+ B220+ cells). w/t: w*ild*-type mouse; *Fcho1*$^{g>c}$: *Fcho1*$^{g>c}$ mouse mutant; *Fcho1*$^{del\_del}$: *Fcho1*$^{del\_del}$ mouse mutant; *Fcho1*$^{61\ nt\_del}$: *Fcho1*$^{61nt\_del}$

mouse mutant. *: p value < 0.05; **: p value < 0.01; ***: p value <0.001; ****: p value <0.0001. M: million.

6.7.4. TCR and CD3 receptor internalization studies

Patient 1 showed a striking T cell defect with impaired internalization of transferrin receptor (CD71), but no impairment of T cell receptor (TCR) or CD3 receptor internalization, nor of surface expression of activation markers. Experiments on transferrin internalization in mice are under way. Experiments on TCR and CD3 internalization in T helper CD4+ cells and cytotoxic CD8+ T cells from whole splenocytes from the *Fcho1*$^{g>c}$ and the *Fcho1*$^{61nt\_del}$ mutant mice were performed. At two different time points (5 and 15 minutes) after anti-CD3 and anti-CD28 *in vitro* stimulation, it was not noted any major impairment in TCR and CD3 receptor internalization (Figure 6.34). These processes are preserved in *Fcho1* mutated mice, recapitulating our previous findings in the *FCHO1* patients. Data on the *Fcho1*$^{del\_del}$ mutant are not available (on-going experiment).

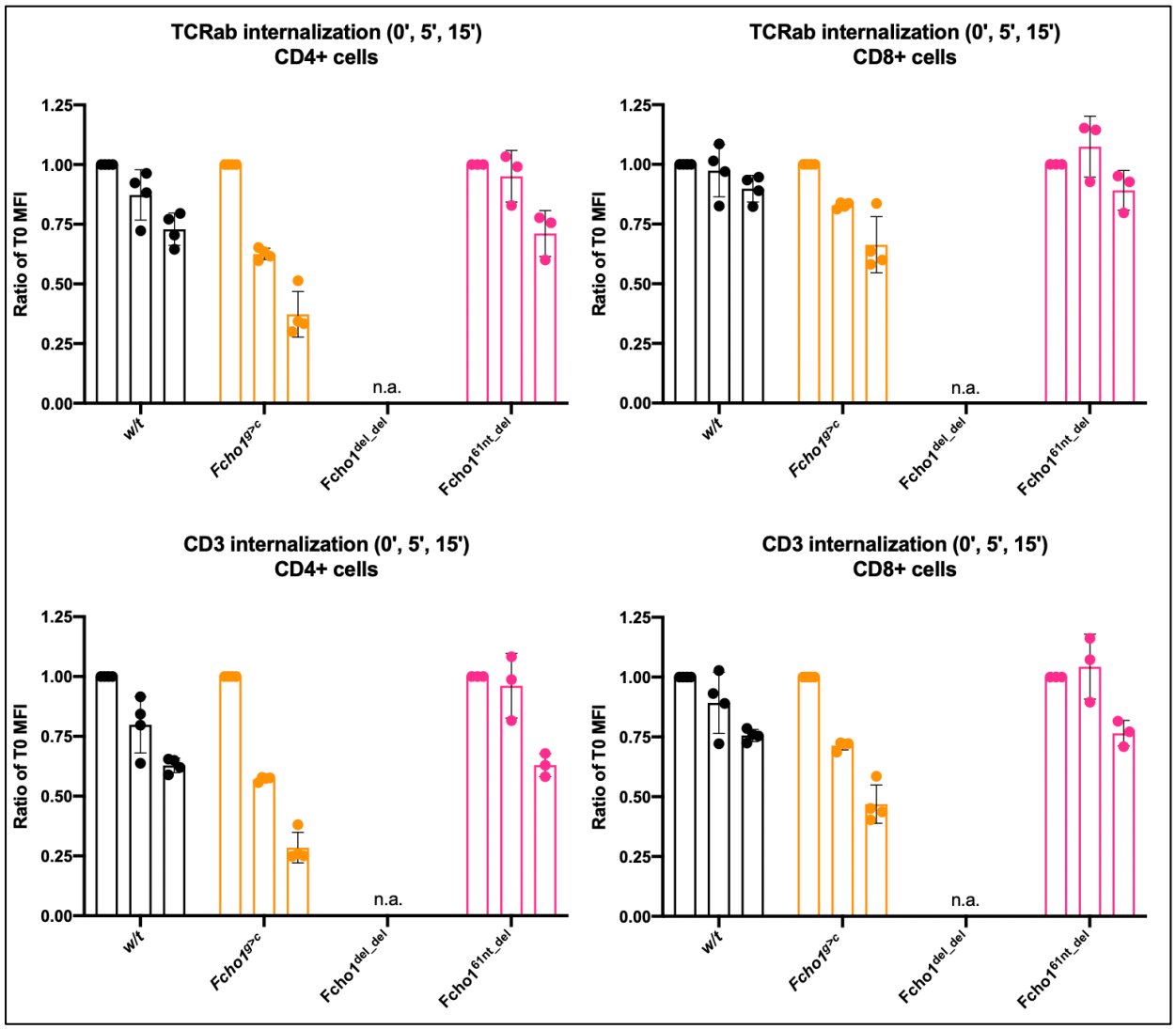

Figure 6.34. Internalization of TCR and CD3 receptor. Upper panel, internalization of T cell receptor (TCR) in CD4+ T cell on the left and CD8+ T cell on the right. Lower panel, CD3+ receptor internalization in CD4+ T cell on the left and CD8+ T cell on the right. Time points 0, 5 and 15 minutes (0', 5', 15') after anti-CD3 and anti-CD28 stimulation. CD4+ and CD8+ cells are gated on live cells, singlets, whole cells, CD45+ cells. w/t: wild type mouse; *Fcho1*$^{g>c}$: *Fcho1*$^{g>c}$ mutant mouse; *Fcho1*$^{del\_del}$: *Fcho1*$^{del\_del}$ mutant mouse; *Fcho1*$^{61\ nt\_del}$: *Fcho1*$^{61nt\_del}$ mutant mouse. MFI, mean fluorescence intensity; n.a., not available.

6.7.5. T cell *in vitro* activation and proliferation

Preliminary *in vitro* studies on proliferation and expression of activation markers on T cells from splenocytes from the *Fcho1*$^{g>c}$ mutant mouse were performed. CD4+ and CD8+ T cell from whole splenocytes obtained from the *Fcho1*$^{g>c}$ mutant mouse activated *in vitro* with 72 hours of anti-CD3 + anti-CD28 stimulation. Cells of the *Fcho1*$^{g>c}$ mutant mouse were able to express activation markers (CD69, CD71, CD44 and CD25) with a kinetic comparable to the wild type (Figure 6.35) and to proliferate (4 rounds of proliferation), similarly to w/t cells and (Figure 6.36), and did not show any activation or proliferation impairment.

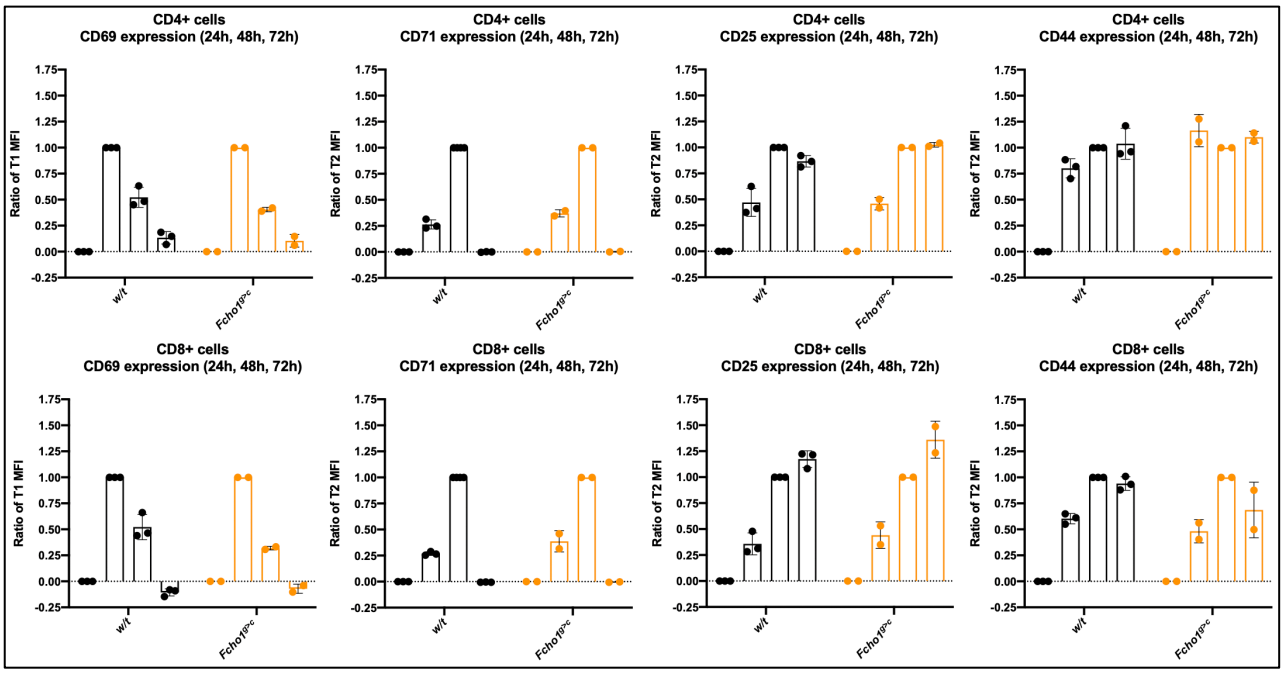

Figure 6.35. Surface expression of markers of T cell activation. Surface FACS staining of T cell activation markers (CD69, CD71, CD25 and CD44) in CD4+ cells (upper panel) and CD8+ cells (lower panel) at time point 1 (T1, 24h), time point 2 (T2, 48h) and time point 3 (T3, 72h) of CD3/CD28 *in vitro* stimulation. CD4+ and CD8+ cells are gated on live cells, singlets, whole cells, CD45+ cells. w/t: wild type mouse; *Fcho1*$^{g>c}$: *Fcho1*$^{g>c}$ mutant mouse. MFI, mean fluorescence intensity.

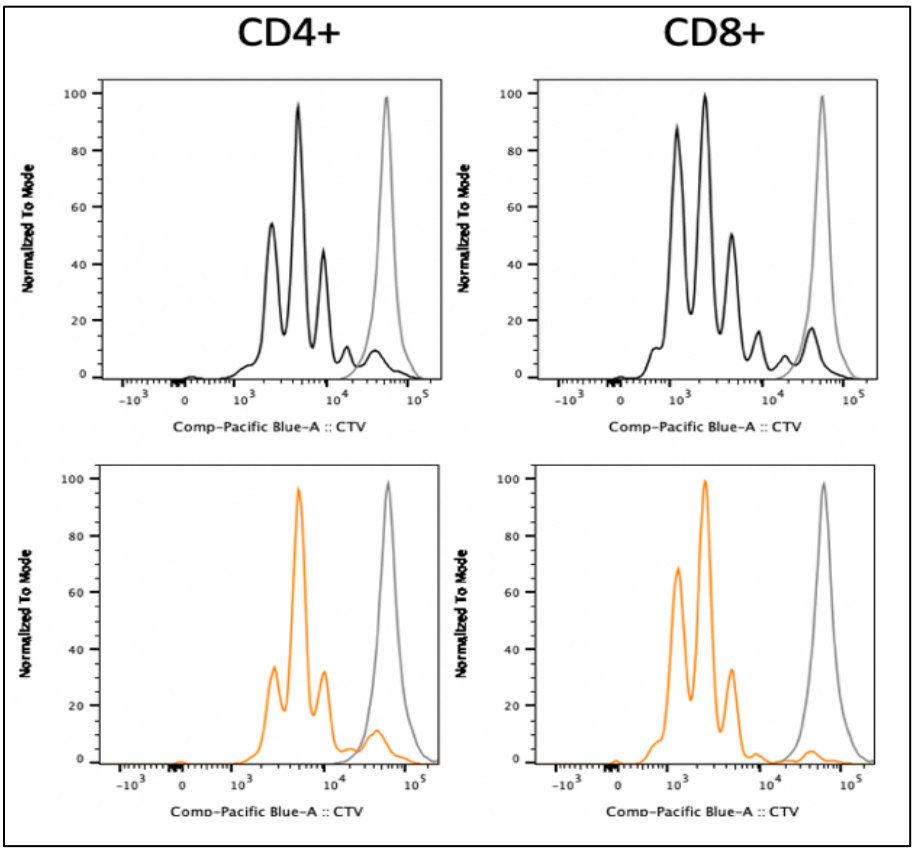

Figure 6.36. T cell proliferation. Dilution of Cell Trace Violet (CTV) staining as a readout of 72 hours CD3/CD28-induced proliferation of CD4+ (left) and CD8+ (right) T cells from whole splenocytes of a wild type (upper panel, black) and the *Fcho1*$^{g>c}$ mutant mouse (lower panel, orange). In gray, staining before CD3/CD28 stimulation (time point 0). CD4+ and CD8+ cells are gated on live cells, singlets, whole cells, CD45+ cells.

6.7.6. B-cell *in vitro* proliferation

Suspecting a phenotype skewed to the B cell compartment and to assess the ability of *Fcho1* mutated mouse B cells to properly proliferate *in vitro*, CD19+ B-cells purified from whole splenocytes of w/t and *Fcho1*$^{61\ nt\_del}$ mutant mice were stained with Cell Trace Violet (CTV) and activated *in vitro* through LPS/IgM/CD40 stimulation for 72 and 96 hours. No abnormalities in activation, survival, death rate, or proliferation cycles were observed in B-cells from *Fcho1*$^{61nt\_del}$ mutant mouse as compared to wild type (Figure 6.37). However, these preliminary results will

need further investigation, as a mix of potent activators was used. It will be important to test separate stimuli at different doses to identify any possible impairments in B cell response.

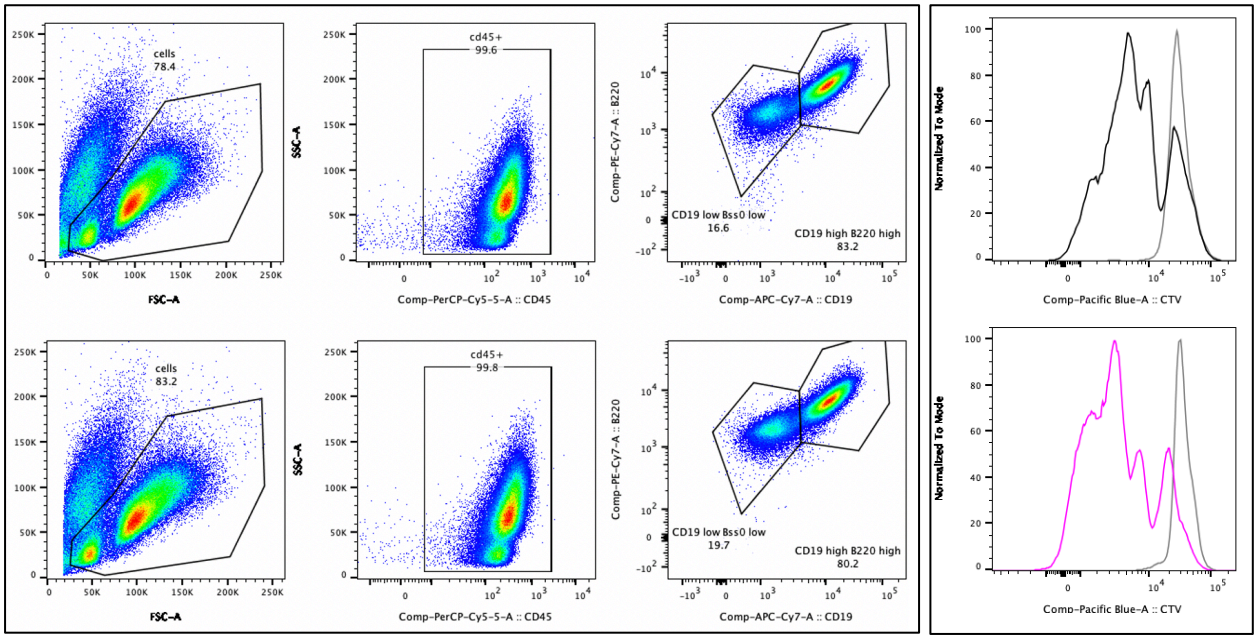

Figure 6.37. B-cell *in vitro* proliferation. FACS staining (gates are in sequence, and (whole) cells are gated on singlets) (left panel) and dilution of Cell Trace Violet staining (on CD45+ cells) (right panel) in 72 hours LPS/Cpg/IgM/CD40-stimulated CD19+ B220+ B cells from *wild-type* mouse (upper raw, black) and *Fcho1*$^{6\ nt\_del}$ mutant mouse (lower raw, pink).

7. Future Perspectives

7.1. Studies on *in vitro* differentiation of iPSCs into naïve T-cells

The Artificial Thymic Organoid (ATO) technology has shown to be a reliable and reproducible tool for *in vitro* differentiation and maturation of induced pluripotent stem cells (iPSCs) into naïve CD3+ TCRαβ T-cells (173). In this study, iPSCs were successfully generated from patient 1's fibroblasts and patient 2' CD34+ HSCs, respectively. Moreover, the ATO protocols was tested on heathy donor iPSCs and proven to be able to generate naïve T cells. Taking advantage of the ATO system, generation of naïve *FHCO1* deficient TCR/CD3 T cells will provide new insights on the effects of *FCHO1* mutations on the maturation of T cell from staminal precursors, and the identification of any block during T cell development.

The platform will also allow generation and collection of naïve *FCHO1* deficient T-cells, that can be used for further *in vitro* studies, including receptor internalization and surface recycling (TfR, TCR, IL7R, IL2R, among others), cell-death (Annexin V, Caspase staining), confocal microscopy aimed at CME identification, and TCR repertoire, among others. Application of the CRISPR/Cas9 technology to *FCHO1* deficient patient-derived iPSCs to generate a *FCHO1* k/i iPSCs line should be considered to assess the rescue of the phenotype.

7.2. Murine studies

There is no antibody for the detection of Fcho1 at the protein level currently available on the market. Few data are published on FCHO1/FCHO2 expression in both humans and mice. Further studies on expression (mRNA and protein) in both wild type and *Fcho1* mutant mice, at different stages of embryonal, fetal and adult development, need to be performed in order to uncover the differential expression of the two genes and better define the tissue or cellular restriction of one gene compared to the other. In *Fcho1* mutant mice, deeper analysis of the cDNA splicing defects (including cloning of the splicing products) should be addressed. Studies on the three *Fcho1* mutant mice need to be completed with a deep characterization of the immunological phenotype, predominantly focusing on CD19+ B cells, including analysis of the bone marrow, lymph nodes

and peritoneal compartments. Further analysis will include *in vitro* T-cell and B-cell activation, T-cell and B-cell repertoire, immunohistochemistry and *in vivo* challenges with TLP-KLK and *Pneumocystis carinii* infection, to assess the ability of the *Fcho1* mutant mice to respond to immune system perturbations and stressor events. Finally, competitive bone marrow transplantation studies might help in understanding if rescue of the phenotype with HSCT is possible.

8. Discussion

Inborn errors of immunity (IEI) are diseases of the immune system resulting from mutations that alter the expression of encoded proteins or molecules (105), which clinical presentation ranges from mild, if existing, symptoms to extremely serious diseases presenting early in life. The updated total number of IEI is 406, with 430 different identified gene defects (106, 107). Severe Combined Immune Deficiency (SCID) is one of the most severe form of IEI, it is considered a life-threatening emergency and it can be, in some cases, cured through hematopoietic stem cell transplantation (HSCT) (183) or gene therapy (114, 184, 185). The molecular definition of IEI is important not only for the correct clinical assessment of patients and to offer the earliest and best available treatment (especially if SCID), but is also can provide new insights, as well as exploration of new targeted therapeutic approaches (186, 187), in the field of the immune disorders and the immune system. The development and subsequent affirmation of Next Generation Sequencing (NGS) technologies and the astounding advances of the most recent years in the area of laboratory tools and techniques (including, but not limited to, induced Pluripotent Stem Cells, CRISPR/Cas9 technology and organoids), has provided increasingly fast and precise platforms to facilitate the identification of the molecular basis of IEI.

In this study, 5 patients from unrelated families with biallelic *FCHO1* mutations and combined immunodeficiency were reported. Three of them died in childhood of overwhelming infections, one died 14.8 years after successful HSCT, most likely because of her poor conditions before transplant and the occurrence of a severe intestinal GVHD, and one patient is alive with full donor chimerism 3.5 years after allogeneic HSCT with cleared pre-transplantation infections. The severe clinical presentation, the lack of the thymic shadow displayed at chest radiography of two patients, the profound T cell lymphopenia found in all patients and the defects of B cells found in two patients suggested a combined defect of T and B cell origin. No apparent underlying gene defect was identified, and patients were diagnosed with SCID of unknown origin. Two patients were successfully treated with HSCT, but one of them died for pre- and post-transplantation complications, suggesting that the disease can be rescued with early HSCT. NGS studies performed on patients identified biallelic private *FCHO1* mutations as the most likely causative of the disease, which were subsequently verified and confirmed by means of Sanger sequencing.

Deleteriousness of the *FCHO1* variants was initially assessed by using of the scaled CADD score (26.3, 34, 28.9, 33 and 33, respectively), all above the conventional threshold of 15, indicating that the variants were within the top 1% of deleterious variants in the human genome. Moreover, the CADD scores were way above the MSC score (5.744, for *FCHO1*), which suggests that mutation in *FCHO1* can cause diseases with lower CADD scores, contrary to other genes that tend to gain variants with high CADD scores that are not disease-causing (and display higher MSCs). Moreover, in support to this notion, the *FCHO1* pLI (Loss of Function Intolerance Score) of 1 indicates that the *FCHO1* gene is highly intolerant to loss of function mutations.

The membrane-sculpting F-BAR domain-containing Fer/Cip4 homology domain-only proteins 1 and 2 (FCHO1/FCHO2) are part of the F-BAR protein superfamily and are involved in the maturation of clathrin-coated pit formation (13). Clathrin-mediated endocytosis (CME) is the major endocytic pathway by which eukaryotic cells internalize cell-surface cargo proteins and extracellular molecules, thereby enabling a broad range of biological processes, including cell signaling, nutrient and growth factor uptake, and cell fate and differentiation (3). Through the N terminal F-BAR domain, FCHO1 and FCHO2 bind to phosphatidylinositol 4,5-biphosphate on the inner side of the cell membrane, inducing and stabilizing membrane curvature. In addition, the C-terminal μ-homology domain mediates interaction with the epidermal growth factor receptor substrate 15 and cargo molecules (33). Moreover, the linker region of FCHO1 acts as an allosteric activator of the adaptor protein 2 complex, enabling recruitment of clathrin to the assembling coat (39, 40).

Western blotting and RT-PCR studies to assess the consequences on the FCHO1 protein confirmed the deleteriousness of the candidate variants, by showing that the frameshift mutations caused premature termination or complete absence of the FCHO1 protein, and that the splice site mutation produced an abnormal splicing with an in-frame, internally deleted FCHO1 protein. These abnormal proteins disrupt the evolutionary conserved domains of the protein, altering the physiological function of FCHO1 during CME.

Whether *FCHO1* and *FCHO2* are functionally redundant or have distinct roles is still unclear. *In silico* studies and quantitative real time PCR analysis of *FCHO1* and *FCHO2* indicated that *FCHO1* expression is restricted to the immune system and some areas of the nervous system, whereas *FCHO2* seemed to be more broadly expressed. These expression studies, underlying the

importance of *FCHO1* for the immune system, strengthened the role of *FCHO1* variants as cause of the patients' disease.

To address the hypothesis that T cell lymphopenia may reflect impaired thymopoiesis, high throughput sequencing of the T cell repertoire in P2 was performed, which showed no restriction, nor indicated presence of clonotypic expansions. Prior studies have demonstrated that clathrin-mediated endocytosis is important for mitosis (82). Upon stimulation *in vitro* with CD3/CD28, *FCHO1* deficient PBMCs were able to efficiently activate, but not proliferate, and high percentage of hypodiploid cells, a marker of apoptosis, and reduced percentages of cells in the S and G2/M phases of the cell cycle were observed. The preserved ability of *in vitro* activation, but impaired proliferation and survival upon TCR/CD3 engagement of *FCHO1* mutated T cell, strongly suggested that the increased activation-induced cell death, rather than impaired thymic output, are the major contributors to the T cell lymphopenia of patients.

Transferrin internalization relies mainly on clathrin-dependent endocytosis. A missense mutation in *TFRC*, which encodes the transferrin receptor (TfR), was previously identified as main cause for a combined immunodeficiency with defective T-cell proliferation (127) because of impaired transferrin internalization and intracellular iron delivery. In *FCHO1* deficient T cell, transferrin internalization was minimally detectable, which is consistent with previous observations that disruption of the *FCHO1* and *FCHO2* genes significantly affects the rate of TfR internalization but does not completely abrogate it (40). Along with the different degree of impairment of T-cell proliferation, these findings distinguish *FCHO1* deficiency from *TFRC* deficiency. On the contrary, TCR/CD3 internalization, which is reported to be clathrin-independent (25) was preserved in activated *FCHO1* deficient T-cells. These results have been shown to be in contrast with findings reported in a recent study on 10 patients with variable T and B cell lymphopenia carrying *FCHO1* biallelic mutations (188). Six distinct mutations of *FCHO1* were reported and the authors elegantly demonstrated that the variants impaired formation of CCP and CME occurrence. However, the authors identified an exclusive role of *FCHO1* for TCR internalization, which was showed to be impaired in CRISPR/Cas9 *FCHO1*-deficient Jurkat cells. They also concluded that *FCHO1* deficiency does not alter global CME, performing transferrin-internalization experiments on patients' fibroblast, which did not show any abnormalities as compared to healthy fibroblasts. The latter finding is easily explainable, considering that fibroblasts, along with many other non-immunological cells, seem to express *FCHO2* and not

FCHO1. *FCHO1*- deficient fibroblast are not expected to show any impairment of CME, that in fact, depends on *FCHO2.* The first observation should be addressed carefully. TCR/CD3 internalization experiments were performed on a CRISPR/Cas9 FCHO1-deficient Jurkat clone, an immortalized human T lymphocyte cell line. Causal validation between genotype and phenotype is always important when studying new genes, and alteration of expression or protein function must be experimentally demonstrated and confirmed through experiments on relevant cellular or animal phenotype. Cell lines are widely used during studies of cell biology; however they not always recapitulate the phenotype of the primary cell and comparison are not always possible.

To better understand the functions of *FCHO1* gene and further study the impact of its pathogenic mutations in mammalian organisms, two disease-modeling platforms were set up in this study and are currently being used for further investigations. The Artificial Thymic Organoid (ATO) technology allows in vitro studies of maturation of induced pluripotent stem cells (iPSCs) into naïve CD3+ TCRαβ T-cells. This platform will help in defining the molecular origin of the T-cells maturation defect, if present, of naïve T-cells differentiated from *FCHO1*-deficient iPSCs derived from patient 1's fibroblasts and patient 2's CD34+ hematopoietic stem cells. It will also allow the generation and collection of naïve *FCHO1* deficient T-cells, that can be used for further *in vitro*, and *in vivo* studies, including T cell activation, proliferation, and receptor internalization. One could speculate that, due to the importance of CME for IL-7 signaling (189), *FCHO1*-deficient thymocytes are not able to maturate into naïve T cell and therefore arrested during early stages of T cell development. Application of the CRISPR/Cas9 technology to *FCHO1*-deficient patient-derived iPSCs to generate a *FCHO1* k/i iPSCs line should be also considered to assess the rescue of the phenotype, if present.

No *Fcho1*-genetically modified mouse has ever been reported in literature. In this study, taking advantage of the CRISP/Cas9 technology, three *Fcho1* k-i mutant mice, mimicking the splice-site mutation found in patient 1, were generated. Despite the extremely severe clinical presentation of patient 1, preliminary analysis on the mutant mice on *Fcho1* expression, immune phenotyping, T cell and B cell in vitro activation and TCRαβ/CD3 receptor internalization suggested only a mild B-cell phenotype. This lack of an overt phenotype can likely be due to functional redundancy between murine *Fcho1* and *Fcho2*, or with other genes involved in clathrin-internalization in mice, or to the evolution of *FCHO1* with a novel function in the regulation of lymphocyte homeostasis. It should also be noted that the splicing defect observed in the *Fcho1* mutant mice only partially

resembled that found in human subjects. Generation of a complete *Fcho1* k/o mouse model would be important to assess any differences in *Fcho1* expression and function. In conclusion, this study uncovers a novel role for *FCHO1* in the human immune system. Further studies will need to be performed in order to fully investigate the immunopathogenesis of the *FCHO1* human disease, taking advantage of the technologies developed in this study. This study poses the initial groundwork to understanding the relevance of clathrin-mediated endocytosis in cellular immune responses, and opens the field to new mechanisms potentially involved in immune dysregulation and disease.

9. Collaborations and publications

9.1. Collaborations

The Patients and Families presented in this study were referred from the following centers. Family 1: The Pediatric Onco-Haematology and BMT Unit, Children's Hospital, ASST Spedali Civili of Brescia, Brescia, Italy; Family 2: The Division of Pediatric Immunology and Allergy, Meram Medical Faculty, Necmettin Erbakan University, Konya, Turkey; Family 3: The Department of Pediatrics and Adolescent Medicine and St Anna Children's Hospital and Children's Cancer Research Institute, Department of Pediatrics, Medical University of Vienna, Vienna, Austria; Family 4 and 5: The Division of Immunology, Boston Children's Hospital, Harvard Medical School, Boston, Massachussets, USA.

Whole Exome Sequencing studies were performed in collaboration with "A. Nocivelli" Institute for Molecular Medicine, Department of Molecular and Translational Medicine, University of Brescia, Brescia, Italy; The Laboratory of Clinical Immunology and Microbiology, National Institute of Allergy and Infectious Diseases, National Institutes of Health, Bethesda, MD, USA; The Division of Immunology, Boston Children's Hospital, Harvard Medical School, Boston, Massachussets, USA. Targeted PID gene panel analysis was performed in collaboration with The Ludwig Boltzmann Institute for Rare and Undiagnosed Diseases, Vienna, Austria.

Generation of *Fcho1* mouse model was made possible through a collaboration with Pamela L. Schwartzberg from the Laboratory of Immune System Biology, National Institute of Allergy and Infectious Diseases, National Instututes of Health, and Lisa Garrett from the Embryonic Stem Cell and Transgenic Mouse Core, National Human Genome Research Institute, National Institutes of Health.

In vitro T-cell differentiation of iPSCs through Artificial Organoid Technology was achieved in collaboration with Gay Crooks from the UCLA Broad Stem Cell Research Center, University of California and Anna Villa from the Pathogenesis and Treatment of Immune and Bone Diseases Unit, San Raffaele Theleton Institute for Gene Therapy.

9.2. Publications and presentations

Publications resulted from collaborations and collateral projects are listed below, the respective first page is attached in the Appendix.

1. **Calzoni E**, Platt CD, Keles S, Kuehn HS, Beaussant-Cohen S, Zhang Y, Pazmandi J, Lanzi G, Pala F, Tahiat A, Artac H, Heredia RJ, Dmytrus J, Reisli I, Uygun V, Uygun D, Bingol A, Basaran E, Djenouhat K, Benhalla N, Bendahmane C, Emiroglu M, Kirchhausen T, Pasham M, Jones J, Wallace JG, Zheng L, Boisson B, Porta F, Rosenzweig SD, Su H, Giliani S, Lenardo M, Geha RS, Boztug K, Chou J, Notarangelo LD. F-BAR domain only protein 1 (FCHO1) deficiency is a novel cause of combined immune deficiency in human subjects. J Allergy Clin Immunol. (2019) Jun; 143(6):2317-2321.e12.

2. Castagnoli R, Delmonte OM, **Calzoni E**, Notarangelo LD. Hematopoietic Stem Cell Transplantation in Primary Immunodeficiency Diseases: Current Status and Future Perspectives. Front Pediatr. (2019) Aug; 7:295.

3. Delmonte OM, Castagnoli R, **Calzoni E**, Notarangelo LD. Inborn Errors of Immunity with Immune Dysregulation: From Bench to Bedside. Front Pediatr. (2019) Aug; 7:353.

4. Verheijen J, Wong SY, Rowe JH, Raymond K, Stoddard J, Delmonte OM, Bosticardo M, Dobbs K, Niemela J, **Calzoni E**, Pai SY, Choi U, Yamazaki Y, Comeau AM, Janssen E, Henderson L, Hazen M, Berry G, Rosenzweig SD, Aldhekri HH, He M, Notarangelo LD, Morava E. Defining a new immune deficiency syndrome: MAN2B2-CDG. J Allergy Clin Immunol. (2020) Mar; 145(3):1008-1011.

5. Castiello MC, Bosticardo M, Sacchetti N, **Calzoni E**, Fontana E, Yamazaki Y, Draghici E, Corsino C, Bortolomai I, Sereni L, Yu HH, Uva P, Palchaudhuri R, Scadden DT, Villa A, Notarangelo LD. Efficacy and safety of anti-CD45-saporin as conditioning agent for RAG deficiency. J Allergy Clin Immunol. (2020) May; S0091-6749(20)30629-1.

6. Bosticardo M, Pala F, **Calzoni E**, Delmonte OM, Dobbs K, Gardner CL, Sacchetti N, Kawai T, Garabedian EK, Draper D, Bergerson JRE, DeRavin SS, Freeman AF, Güng.r T, Hartog N, Holland SM, Kohn DB, Malech HL, Markert ML, Weinacht KG, Villa A, Seet CS, Montel-Hagen A, Crooks GM, Notarangelo LD. Artificial thymic organoids represent a reliable tool to study T-cell differentiation in patients with severe T-cell lymphopenia. Blood Adv. (2020) Jun; 4(12):2611-2616.

7. **Calzoni E**, Castagnoli R, Giliani SC. Human inborn errors of immunity caused by defects of receptor and proteins of cellular membrane. Minerva Pediatr. 2020 Sep 22. Epub ahead of print. PMID: 32960006.

Poster presentations

1. Unraveling the cellular basis of Aicardi-Goutières Syndrome in the central nervous system with induced pluripotent stem cells", LCIM Research Retreat, National Institutes of Health (NIH), Bethesda, MD, USA, 15.03.2018.

2. Genotype-phenotype Correlation in Human RAG1 Deficiency", Poster session, Clinical Immunology Society Annual Meeting, Atlanta, GA, USA, 07.04.2019.

Oral presentations at Congresses

1. Conditioning with anti-CD45 immunotoxin in a mouse model of hypomorphic *Rag1* deficiency allows complete reconstitution of the immune system with lack of toxicity, Opening Plenary Session, Clinical Immunology Society (CIS), Toronto, Ontario, Canada, 26.04.2018.

2. An unexpected cause of SCID, NIAID Genomics and Immunology Brown Bag Lunch Series, National Institutes of Health (NIH), Bethesda, MD, USA, 11.09.2018.

3. F-BAR domain only protein 1 (*FCHO1*) deficiency is a novel cause of combined immune deficiency in humans, LCIM Research Conference, National Institutes of Health (NIH), Bethesda, MD, USA, 02.27.2019.

4. F-BAR domain only protein 1 (*FCHO1*) deficiency is a novel cause of combined immune deficiency in humans, HOT New defects in PID, CIS Annual Meeting, Atlanta, GA, USA, 07.04.2019.

5. When it looks like a duck, swims like duck but it is not a duck, 2019 CIS Summer School in Primary Immunodeficiency Diseases, Fort Lauderdale, FL, USA, 26.10.2019.

10. Bibliography

1. Roth TF, Porter KR. Yolk protein uptake in the oocyte of the mosquito aedes aegypti l. The Journal of Cell Biology. 1964;20.
2. Pearse BM. Clathrin: a unique protein associated with intracellular transfer of membrane by coated vesicles. Proceedings of the National Academy of Sciences of the United States of America. 1976;73.
3. Kaksonen M, Roux A. Mechanisms of clathrin-mediated endocytosis. Nature Reviews Molecular Cell Biology. 2018;19(5):313-26.
4. McMahon HT, Boucrot E. Molecular mechanism and physiological functions of clathrin-mediated endocytosis. Nature Reviews Molecular Cell Biology. 2011;12(8):517-33.
5. Ehrlich M, Boll W, Van Oijen A, Hariharan R, Chandran K, Nibert ML, et al. Endocytosis by random initiation and stabilization of clathrin-coated pits. Cell. 2004;118(5):591-605.
6. Nunez D, Antonescu C, Mettlen M, Liu A, Schmid SL, Loerke D, et al. Hotspots organize clathrin-mediated endocytosis by efficient recruitment and retention of nucleating resources. Traffic. 2011;12(12):1868-78.
7. Brach T, Godlee C, Moeller-Hansen I, Boeke D, Kaksonen M. The Initiation of Clathrin-Mediated Endocytosis Is Mechanistically Highly Flexible. Current Biology. 2014;24(5):548-54.
8. Antonescu CN, Aguet F, Danuser G, Schmid SL. Phosphatidylinositol-(4,5)-bisphosphate regulates clathrin-coated pit initiation, stabilization, and size. Molecular Biology of the Cell. 2011;22(14):2588-600.
9. Taylor MJ, Perrais D, Merrifield CJ. A high precision survey of the molecular dynamics of mammalian clathrin-mediated endocytosis. PLoS Biology. 2011;9(3):e1000604.
10. Blondeau F, Ritter B, Allaire PD, Wasiak S, Girard M, Hussain NK, et al. Tandem MS analysis of brain clathrin-coated vesicles reveals their critical involvement in synaptic vesicle recycling. Proceedings of the National Academy of Sciences of the United States of America. 2004;101(11):3833-8.
11. Robinson MS. Adaptable adaptors for coated vesicles. Trends in Cell Biology. 2004;14(4):167-74.
12. Motley A, Bright NA, Seaman MN, Robinson MS. Clathrin-mediated endocytosis in AP-2-depleted cells. Journal of Cell Biology. 2003;162(5):909-18.
13. Cocucci E, Aguet F, Boulant S, Kirchhausen T. The first five seconds in the life of a clathrin-coated pit. Cell. 2012;150(3):495-507.
14. Saffarian S, Cocucci E, Kirchhausen T. Distinct dynamics of endocytic clathrin-coated pits and coated plaques. PLoS Biology. 2009;7(9):e1000191.
15. Sweitzer AM, Hinshaw JE. Dynamin Undergoes a GTP-Dependent Conformational Change Causing Vesiculation. Cell. 1998;93.
16. Schlossman AM, Braell WA and Rothman JE. An Enzyme That Removes Clathrin Coats: Purification of an Uncoating ATPase. The Journal of Cell Biology. 1984;99.
17. Pelkmans L, Puentener D, Helenius A. Local Actin Polymerization and Dynamin Recruitment in SV40-Induced Internalization of Caveolae. Science. 2002;296.

18. Lamaze C, Dujeancourt A, Baba T, Lo CG, Benmerah A, Dautry-Varsat A. Interleukin 2 Receptors and Detergent-Resistant Membrane Domains Define a Clathrin-Independent Endocytic Pathway. Molecular Cell. 2001;7.
19. Sauvonnet N, Dujeancourt A, Dautry-Varsat A. Cortactin and dynamin are required for the clathrin-independent endocytosis of gammac cytokine receptor The Journal of Cell Biology. 2005;168(1):155-63.
20. Sundborger A, Soderblom C, Vorontsova O, Evergren E, Hinshaw JE, Shupliakov O. An endophilin-dynamin complex promotes budding of clathrin-coated vesicles during synaptic vesicle recycling. Journal of Cell Science. 2011;124(Pt 1):133-43.
21. Neumann S, Schmid SL. Dual role of BAR domain-containing proteins in regulating vesicle release catalyzed by the GTPase, dynamin-2. Journal of Biological Chemistry. 2013;288(35):25119-28.
22. Boucrot E, Ferreira APA, Almeida-Souza L, Debard S, Vallis Y, Howard G, et al. Endophilin marks and controls a clathrin-independent endocytic pathway. Nature. 2014;517(7535):460-5.
23. Renard HF, Simunovic M, Lemiere J, Boucrot E, Garcia-Castillo MD, Arumugam S, et al. Endophilin-A2 functions in membrane scission in clathrin-independent endocytosis. Nature. 2015;517(7535):493-6.
24. Glebov OO, Bright NA, Nichols BJ. Flotillin-1 defines a clathrin-independent endocytic pathway in mammalian cells. Nature Cell Biology. 2006;8(1):46-54.
25. Compeer EB, Kraus F, Ecker M, Redpath G, Amiezer M, Rother N, et al. A mobile endocytic network connects clathrin-independent receptor endocytosis to recycling and promotes T cell activation. Nature Communication. 2018;9(1):1597.
26. Sigismund S, Woelk T, Puri C, Maspero E, Tacchetti C, Transidico P, et al. Clathrin-independent endocytosis of ubiquitinated cargos. Proceedings of the National Academy of Sciences of the United States of America. 2005;102(8):2760-5.
27. Caldieri G, Barbieri E, Nappo G, Raimondi A, Bonora M, Conte A, Verhoef LGGC, Confalonieri S, Malabarba MG, Bianchi F, Cuomo A, Bonaldi T, Martini E, Mazza D, Pinton P, Tacchetti C, Polo S, Di Fiore PP, Sigismund S. Reticulon 3 dependent ER PM contact sites control EGFR nonclathrin endocytosis. Science. 2017;356.
28. Bonifacino JS, Glick BS. The Mechanisms of Vesicle Budding and Fusion. Cell. 2004;116.
29. Ferguson SM, De Camilli P. Dynamin, a membrane-remodelling GTPase. Nature Reviews Molecular Cell Biology. 2012;13(2):75-88.
30. Peter BJ, Kent HM, Mills IG, Vallis Y, Butler PJG, Evans PR, McMahon TH. BAR Domains as Sensors of Membrane Curvature: The Amphiphysin BAR Structure. Science. 2004;303:495 - 9.
31. Liu S, Xiong X, Zhao X, Yang X, Wang H. F-BAR family proteins, emerging regulators for cell membrane dynamic changes-from structure to human diseases. The Journal of Hematology & Oncology. 2015;8:47.
32. Frost A, Perera R, Roux A, Spasov K, Destaing O, Egelman EH, et al. Structural basis of membrane invagination by F-BAR domains. Cell. 2008;132(5):807-17.
33. Henne WM, Boucrot E, Meinecke M, Evergren E, Vallis Y, Mittal R, McMahon HT. FCHo Proteins Are Nucleators of Clathrin-Mediated Endocytosis. Science. 2010;328:1281 - 4.
34. http://www.ensembl.org/Homo_sapiens/Gene/Summary?db=core;g=ENSG00000130475;r=19:17747718-17788568 [

35. http://www.ensembl.org/Homo_sapiens/Gene/Summary?db=core;g=ENSG00000157107;r=5:72956041-73090522 [
36. http://www.ensembl.org/Mus_musculus/Gene/Summary?db=core;g=ENSMUSG00000070000;r=8:71708387-71725716. [
37. http://www.ensembl.org/Mus_musculus/Gene/Summary?db=core;g=ENSMUSG00000041685;r=13:98723403-98815449;t=ENSMUST00000040340. [
38. Umasankar PK, Sanker S, Thieman JR, Chakraborty S, Wendland B, Tsang M, et al. Distinct and separable activities of the endocytic clathrin-coat components Fcho1/2 and AP-2 in developmental patterning. Nature Cell Biology. 2012;14(5):488-501.
39. Hollopeter G, Lange JJ, Zhang Y, Vu TN, Gu M, Ailion M, et al. The membrane-associated proteins FCHo and SGIP are allosteric activators of the AP2 clathrin adaptor complex. Elife. 2014;3.
40. Umasankar PK, Ma L, Thieman JR, Jha A, Doray B, Watkins SC, et al. A clathrin coat assembly role for the muniscin protein central linker revealed by TALEN-mediated gene editing. Elife. 2014;3.
41. Huebers HA, Finch CA. The Physiology of Transferrin and Transferrin Receptors. Physiological Review. 1987;67.
42. Kawabata H. Transferrin and transferrin receptors update. Free Radical Biology and Medicine. 2019;133:46-54.
43. Hansen SH, Sandvig K, Van Deurs B. Internalization Efficiency of the Transferrin Receptor. Experimental cell research. 1992;1992.
44. A Soyano DC, M Layrisse. Effect of iron deficiency on the mitogen-induced proliferative response of rat lymphocytes. International Archives of Allergy and Immunology. 1982;69.
45. Kuvibidila S, Nauss KM, Baliga BS, Suskind RM. Impairment of blastogenic response of splenic lymphocytes from iron-deficient mice: in vivo repletion. The American Journal of Clinical Nutrition 1983;37.
46. Bayer AL, Baliga P, Woodward JE. Transferrin receptor in T cell activation and transplantation. Journal of Leukocyte Biology. 1998;64.
47. Neckers LM, Cossman J. Transferrin receptor induction in mitogen-stimulated human T lymphocytes is required for DNA synthesis and cell division and is regulated by interleukin 2. Proceedings of the National Academy of Sciences of the United States of America. 1983;80:3494 -8.
48. Cibrian D, Sanchez-Madrid F. CD69: from activation marker to metabolic gatekeeper. European Journal of Immunology. 2017;47(6):946-53.
49. Regis G, Bosticardo M, Conti L, De Angelis S, Boselli D, Tomaino B, et al. Iron regulates T-lymphocyte sensitivity to the IFN-gamma/STAT1 signaling pathway in vitro and in vivo. Blood. 2005;105(8):3214-21.
50. Brekelmans P, Van Soest P, Leenen PJ, Van Ewijk W. Inhibition of proliferation and differentiation during early T cell development by anti-transferrin receptor antibody. European Journal of Immunology. 1994;24.
51. Brekelmans P, Van Soest P, Voerman J, Platenburg PP, Leenen PJ, Van Ewuk W. Transferrin receptor as a marker of immature cycling tymocytes in the mouse. Cellular Immunology. 1994;159.
52. Wang Z YW, Zhu L, Li J, Yao Y, Chen F, Sun M, Zhang J, Shen N, Song Y and Chang K. Iron Drives T Helper Cell Pathogenicity by Promoting RNA-Binding Protein PCBP1-Mediated Proinflammatory Cytokine Production. Immunity. 2018;49.

53. Wieser S, Pines J. The biochemistry of mitosis. Cold Spring Harbor Perspectives in Biology. 2015;7(3):a015776.
54. Royle SJ, Bright NA, Lagnado L. Clathrin is required for the function of the mitotic spindle. Nature. 2005;434(7037):1148-52.
55. Royle SJ. The role of clathrin in mitotic spindle organisation. Journal of Cell Science. 2012;125(Pt 1):19-28.
56. G. Warren JD, A. Cockcroft. Recycling of transferrin receptors in A431 cells is inhibited during mitosis. The Embo Journal. 1984;3.
57. Sager PR, Brown PA, Berlin RD. Analysis of transferrin recycling in mitotic and interphase hela cells by quantitative fluorescence microscopy. Cell. 1984.
58. Pypaert M, Lucocq JM, Warren G. Coated pits in interphase and mitotic A431 cells. European Journal of Immunology. 1987;45.
59. Fielding AB, Royle SJ. Mitotic inhibition of clathrin-mediated endocytosis. Cellular and Molecular Life Sciences. 2013;70(18):3423-33.
60. Tacheva-Grigorova SK, Santos AJ, Boucrot E, Kirchhausen T. Clathrin-mediated endocytosis persists during unperturbed mitosis. Cell Rep. 2013;4(4):659-68.
61. Cendrowski J, Maminska A, Miaczynska M. Endocytic regulation of cytokine receptor signaling. Cytokine Growth Factor Review. 2016;32:63-73.
62. Blanco AM, Perez-Arago A, Fernandez-Lizarbe S, Guerri C. Ethanol mimics ligand-mediated activation and endocytosis of IL-1RI/TLR4 receptors via lipid rafts caveolae in astroglial cells. Journal of Neurochemistry. 2008;106.
63. Saha SS, Singh D, Raymond EL, Ganesan R, Caviness G, Grimaldi C, Woska Jr JR, Mennerich D, Brown SE, Mbow ML, Kao CC. Signal Transduction and Intracellular Trafficking by the Interleukin 36 Receptor. Journal of Biological Chemistry. 2015;290.
64. Walsh ST. Structural insights into the common gamma-chain family of cytokines and receptors from the interleukin-7 pathway. Immunological Review. 2012;250(1):303-16.
65. Sauvonnet N, Dujeancourt A, Dautry-Varsat A. Cortactin and dynamin are required for the clathrin-independent endocytosis of gammac cytokine receptor. Journal of Cell Biology. 2005;168.
66. Subtil A, Hemar A, Dautry-Varsat A. Rapid endocytosis of interleukin 2 receptors when clathrin coated pit endocytosis is inhibited. Journal of Cell Science. 1994;107.
67. Puel A, Ziegler SF, Buckley RH, Leonard WJ. Defective IL7R expression in T−B+NK+ severe combined immunodeficiency. Nature Genetics. 1998;20:394 - 7.
68. Faller EM, Ghazawi FM, Cavar M, MacPherson PA. IL-7 induces clathrin-mediated endocytosis of CD127 and subsequent degradation by the proteasome in primary human CD8 T cells. Immunology and Cell Biology. 2016;94(2):196-207.
69. Watanabe N, Kuriyama H, Sone H, Neda H, Yamauchi H, Maeda M, Niitsu Y. Continuous internalization of tumor necrosis factor receptors in a human myosarcoma cell line. Journal of Biological Chemistry. 1988;263.
70. D'Alessio A, Al-Lamki RS, Bradley JR, Pober JS. Caveolae participate in tumor necrosis factor receptor 1 signaling and internalization in a human endothelial cell line. The American Journal of Pathology. 2005;166.
71. Bradley JR, Johnson DR, Pober JS. Four different classes of inhibitors of receptor-mediated endocytosis decrease tumor necrosis factor-induced gene expression in human endothelial cells. Journal of Immunology. 1993;150.

72. Parlato S, Giammarioli AM, Logozzi M, Lozupone F, Matarrese P, Luciani F, Falchi M, Malorni W, Fais S. CD95 (APO-1/Fas) linkage to the actin cytoskeleton through ezrin in human T lymphocytes: a novel regulatory mechanism of the CD95 apoptotic pathway. Embo Journal. 2000;19.
73. Alcover A, Alarcon B and Di Bartolo V. Cell Biology of T Cell Receptor Expression and Regulation. Annual Review Immunology. 2018;36:103 - 25.
74. Schamel WW, Reth M. Monomeric and oligomeric complexes of the B cell antigen receptor. Immunity. 2000;13.
75. Reth M, Wienands J. Initiation and processing of signals from the B cell antigen receptor. Annual Review Immunology. 1997;15.
76. Depoil D, Fleire S, Treanor BL, Weber M, Harwood NE, Marchbank KL, Tybulewicz VLJ, Batista FD. CD19 is essential for B cell activation by promoting B cell receptor–antigen microcluster formation in response to membrane-bound ligand. Nature Immunology. 2007;9.
77. Puré E, Tardelli L. Tyrosine phosphorylation is required for ligand-induced internalization of the antigen receptor on B lymphocytes. Proceedings of the National Academy of Sciences of the United States of America. 1992;89.
78. Stoddart A, Jackson AP, Brodsky FM. Plasticity of B Cell Receptor Internalization upon Conditional Depletion of Clathrin. Molecular Biology of the Cell. 2005;16.
79. Pitcher C, Honing S, Fingerhut A, Bowers K, and, Marsh M. Cluster of Differentiation Antigen 4 (CD4) Endocytosis and Adaptor Complex Binding Require Activation of the CD4 Endocytosis Signal by Serine Phosphorylation. Molecular Biology of the Cell. 1998;10.
80. Greenberg ME, Bronson S, Lock M, Pavlakis GN, and Skowronski J. Co-localization of HIV-1 Nef with the AP-2 adaptor protein complex correlates with Nef-induced CD4 down-regulation. The Embo Journal. 1997;16.
81. Chang HR, Halimani M, Krause E, Rettig J and Pattu V. Endocytosis of cytotoxic granules in CD8 T lymphocytes is required for multiple killing of target cells. Journal of Immunology. 2015;194.
82. Boucrot E, Saffarian S, Zhang R, Kirchhausen T. Roles of AP-2 in Clathrin-Mediated Endocytosis. PLoS ONE. 2010;4.
83. Wood LA, Larocque G, Clarke NI, Sarkar S, Royle SJ. New tools for “hot-wiring” clathrin-mediated endocytosis with temporal and spatial precision. Journal of Cell Biology. 2016;216.
84. Kishimoti H, Sprent J. Several Different Cell Surface Molecules Control Negative Selection of Medullary Thymocytes. Journal of Experimental Medicine. 1999;190.
85. Vandenberghe P, Ceuppens JL. Immobilized anti-CD5 together with prolonged activation of protein kinase C induce interleukin 2-dependent T cell growth: evidence for signal transduction through CD5. European Journal of Immunology. 1991;21.
86. Sato S, Ono N, Steeber DA, Pisetsky DS and Tedder TF. CD19 regulates B lymphocyte signaling thresholds critical for the development of B-1 lineage cells and autoimmunity. Journal of Immunology. 1996;157.
87. Gary-Gouy HH, Bruhns P, Schmitt C, Dalloul A, Daeron M, Bismuth G. The Pseudo-immunoreceptor Tyrosine-based Activation Motif of CD5 Mediates Its Inhibitory Action on B-cell Receptor Signaling. the Journal of Biological Chemistry. 2000;275.
88. Lu X, Axtell RC, Collawn JF, Gibson A, Justement LB, Raman C. AP2 adaptor complex-dependent internalization of CD5: differential regulation in T and B cells. Journal of Immunology. 2002;168(11):5612-20.

89. Chuang E, Alegre ML, Duckett CS, Noel PJ, Vander Heiden MG, Thompson CB. Interaction of CTLA-4 with the clathrin-associated protein AP50 results in ligand-independent endocytosis that limits cell surface expression. Journal of Immunology. 1997;159.
90. Qureshi OS, Satdip K, Hou TZ, Jeffery LE, Poulter NS, Briggs Z, Kenefeck R, Willox AK, Royle SJ, Rappoport JZ, and Sansom DM. Constitutive Clathrin-mediated Endocytosis of CTLA-4 Persists during T Cell Activation. the Journal of Biological Chemistry. 2011;287.
91. Khailaie S, Rowshanravan B, Robert PA, Waters E, Halliday N, Badillo Herrera JD, Walker LSK,3 Sansom DM, and Meyer-Hermann M. Characterization of CTLA4 Trafficking and Implications for Its Function. Biophysical Journal. 2018;115.
92. Campbell KS, Hasegawa J. Natural killer cell biology: an update and future directions. Journal of Allergy and Clinical Immunology. 2013;132(3):536-44.
93. Lanier LL. Nk Cell Recognition. Annual Review of Immunology. 2005;23(1):225-74.
94. Purdy AK, Alvarez Arias DA, Oshinsky J, James AM, Serebriiskii I, Campbell KS. The ap-2 clathrin adaptor mediates endocytosis of an inhibitory killer cell Ig-like receptor in human NK cells. Journal of Immunology. 2014;193(9):4675-83.
95. Podack ER, Young JD, Cohn ZA. Isolation and biochemical and functional characterization of perforin 1 from cytolytic T-cell granules. Proceedings of the National Academy of Sciences of the United States of America. 1985;82.
96. Chowdhury D, Lieberman J. Death by a thousand cuts: granzyme pathways of programmed cell death. Annuual Review Immunology. 2008;26:389-420.
97. Keefe D, Shi L, Feske S, Massol R, Navarro F, Kirchhausen T, et al. Perforin triggers a plasma membrane-repair response that facilitates CTL induction of apoptosis. Immunity. 2005;23(3):249-62.
98. Mitsunari T, Nakatsu F, Shioda N, Love PE, Grinberg A, Bonifacino JS, et al. Clathrin adaptor AP-2 is essential for early embryonal development. Molecular Cellular Biology. 2005;25(21):9318-23.
99. Chen H, Ko G, Zatti A, Di Giacomo G, Liu L, Raiteri E, et al. Embryonic arrest at midgestation and disruption of Notch signaling produced by the absence of both epsin 1 and epsin 2 in mice. Proceedings of the National Academy of Sciences of the United States of America. 2009;106(33):13838-43.
100. Pozzi B, Amodio S, Lucano C, Sciullo A, Ronzoni S, Castelletti D, et al. The endocytic adaptor Eps15 controls marginal zone B cell numbers. PLoS One. 2012;7(11):e50818.
101. Milesi C, Alberici P, Pozzi B, Oldani A, Beznoussenko GV, Raimondi A, et al. Redundant and nonredundant organismal functions of EPS15 and EPS15L1. Life Science Alliance. 2019;2(1).
102. Klebig ML, Wall MD, Potter MD, Rowe EL, Carpenter DA, and Rinchik EM. Mutations in the clathrin-assembly gene Picalm are responsible for the hematopoietic and iron metabolism abnormalities in fit1 mice Proceedings of the National Academy of Sciences of the United States of America. 2004;100.
103. Hengst M, Naehrlich L, Mahavadi P, Grosse-Onnebrink J, Terheggen-Lagro S, Høsøien Skanke L, Schuch LA, Brasch F, Guenther A, Reu S, Ley-Zaporozhan J, Griese M. Hermansky-Pudlak syndrome type 2 manifests with fibrosing lung disease early in childhood. Orphanet Journal of Rare Diseases. 2018;13.
104. Olkkonen VM, Ikonen E. When intracellular logistics fails – genetic defects in membrane trafficking. Journal of Cell Science. 2006;119.

105. Notarangelo LD. Primary immunodeficiencies. Journal of Allergy Clinical Immunology. 2010;125(2 Suppl 2):S182-94.
106. Bousfiha A, Jeddane L, Picard C, Al-Herz W, Ailal F, Chatila T, et al. Human Inborn Errors of Immunity: 2019 Update of the IUIS Phenotypical Classification. J Clin Immunol. 2020;40(1):66-81.
107. Tangye SG, Al-Herz W, Bousfiha A, Chatila T, Cunningham-Rundles C, Etzioni A, et al. Human Inborn Errors of Immunity: 2019 Update on the Classification from the International Union of Immunological Societies Expert Committee. Journal of Clinical Immunology. 2020;40(1):24-64.
108. De Saint Basile G, Arveiler B, Oberle I, Malcolm S, Levinsky RJ, Lau YL, Hofker M, Debre M, Fischer A, Griscelli C. Close linkage of the locus for X chromosome-linked severe combined immunodeficiency to polymorphic DNA markers in Xqll-q13. Proceedings of the National Academy of Sciences of the United States of America. 1987;84:7576 - 9.
109. Puck JM, Nussbaum RL, Smead DL, Conley ME. X-linked Severe Combined Immunodeficiency: Localization within the Region Xql3.1-q21.1 by Linkage and Deletion Analysis. The American Journal of Human Genetics. 1989;44:724 - 30.
110. Noguchi M, Yi H, Rosenblatt HM, Filipovich AH, Adestein S, Modi WS, McBride OW, Leonard WJ. Interleukin-2 receptor g chain mutation results in X-linked severe combined immunodeficiency in humans. Cell. 1993;73:147 - 57.
111. Sharfe N, Shahar M, Roifman CM. An interleukin-2 receptor gamma chain mutation with normal thymus morphology. Journal of Clinical Investigation. 1997;100(12):3036-43.
112. Buckley RH, Schiff RI, Schiff SE, Markert ML, Williams LW, Harville TO, Roberts JL, Puck JM. Human severe combined immunodeficiency: Genetic, phenotypic, and functional diversity in one hundred eight infants. The Journal of Pediatrics. 1996;130(3):378 - 87.
113. Buckley RH, Schiff SE, Schiff RI, Markert ML, Williams LW, Roberts JL, Myers LA, Ward FE. Hematopoietic stem-cell transplantation for the treatment of severe combined immunodeficiency. The New England Journal of Medicine. 1999;340(7):508 - 16.
114. Cavazzana-Calvo M, Hacein-Bey S, de Saint Basile G, Gross F, Yvon E, Nusbaum P,. Gene therapy of human severe combined immunodeficiency (SCID)-X1 disease. Science. 2000;288.
115. Chaim M, Roifman JZ, David Chitayat, and Nigel Sharfe. A partial deficiency of interleukin-7R is sufficient to abrogate T-cell development and cause severe combined immunodeficiency. Blood. 2000;96:2803-6.
116. De Saint Basile G, Geissmann F, Flori E, Uring-Lambert B, Soudais C, Cavazzana-Calvo M, et al. Severe combined immunodeficiency caused by deficiency in either the delta or the epsilon subunit of CD3. Journal of Clinical Investigation. 2004;114(10):1512-7.
117. Harjit K, Dadi PD, Simon AJ, and Roifman CM. Effect of CD3d Deficiency on Maturation of a/b and g/d T-Cell Lineages in Severe Combined Immunodeficiency. The New England Journal of Medicine. 2003;349:1821-8.
118. Rieux-Laucat F, Hivroz C, Lim A, Mateo V, Pellier I, Selz F, Fischer A, and Le Deist F. Inherited and Somatic CD3ζ Mutations in a Patient with T-Cell Deficiency. The New England Journal of Medicine. 2006;354:1913 - 21.
119. Catherine M, Cale NJK, Novelli V, Veys P, Jones AM, Morgan G. Severe combined immunodeficiency with abnormalities in expression of the common leucocyte antigen, CD45. Archives of Disease in Childhood. 1997;76:163 - 4.

120. Roberts JL, Buckley RH, Luo B, Pei J, Lapidus A, Peri S, et al. CD45-deficient severe combined immunodeficiency caused by uniparental disomy. Proceedings of the National Academy of Sciences of the United States of America. 2012;109(26):10456-61.
121. Kotlarz D, Zietara N, Uzel G, Weidemann T, Braun CJ, Diestelhorst J, et al. Loss-of-function mutations in the IL-21 receptor gene cause a primary immunodeficiency syndrome. Journal of Experimental Medicine. 2013;210(3):433-43.
122. Recio MJ, Moreno-Pelayo MA, Kiliç SS, Guardo AC, Sanal O, Allende LM, et al. Differential Biological Role of CD3 Chains Revealed by Human Immunodeficiencies. The Journal of Immunology. 2007;178(4):2556-64.
123. Delmonte OM, Rowe JH, Dobbs AK, Palterer B, Castagnoli R, Notarangelo LD. Complete Absence of CD3γ Protein Expression Is Responsible for Combined Immunodeficiency with Autoimmunity Rather than SCID. Journal of Clinical Immunology. 2019;10.
124. Morgan NV, Goddard S, Cardno TS, McDonald D, Rahman F, Barge D, et al. Mutation in the TCRalpha subunit constant gene (TRAC) leads to a human immunodeficiency disorder characterized by a lack of TCRalphabeta+ T cells. Journal of Clinical Invest. 2011;121(2):695-702.
125. De la Calle-Martin O, Hernandez M, Ordi J, Casamitjana N, Arostegui JI, Caragol I. Familial CD8 deficiency due to a mutation in the CD8 alpha gene. Journal of Clinical Investigation. 2001;108(1):117-23.
126. Sawitsky B, Sawitsky A. Lymphocyte response to phytomitogens in iron deficiency. The American Journal of the Medical Sciences. 1976;272.
127. Jabara HH, Boyden SE, Chou J, Ramesh N, Massaad MJ, Benson H, et al. A missense mutation in TFRC, encoding transferrin receptor 1, causes combined immunodeficiency. Nature Genetics. 2016;48(1):74-8.
128. Conley ME, Dobbs AK, Farmer DM, Kilic S, Paris K, Grigoriadou S, et al. Primary B cell immunodeficiencies: comparisons and contrasts. Annual Review Immunology. 2009;27:199-227.
129. Granados E, Porpiglia AS, Hogan MB, Matamoros N, Krasovec S, Pignata C. Clinical and molecular analysis of patients with defects in micro heavy chain gene. Journal of Clinical Investigation. 2002;110(7):1029-35.
130. Minegishi Y, Wang YH, Cooper MD, Campana D, Conley ME. Mutations in the human lambda5/14.1 gene result in B cell deficiency and agammaglobulinemia. Journal of Experimental Medicine. 1998;187.
131. Minegishi Y, Rapalus L, Ersoy F, Campana D, Conley ME. Mutations in Igalpha (CD 79a) result in a complete block in B-cell development. Journal of Clinical Investigation. 1999;104.
132. Dobbs AK, Yang T, Farmer D, Kager L, Parolini O, Conley ME. Cutting edge: a hypomorphic mutation in Igbeta (CD79b) in a patient with immunodeficiency and a leaky defect in B cell development. Journal of Immunol. 2007;179(4):2055-9.
133. Van Zelm MC, Reisli I, Van der Burg M, Castaño D, Van Noesel CJM, Van Tol MJD, Woellner C, Grimbacher B, Patiño PJ, Van Dongen JJM, and Franco JL. An Antibody-Deficiency Syndrome Due to Mutations in the CD19 Gene. The New England Journal of Medicine. 2006;354:1901 - 11.
134. Van Zelm MC, Smet J, Adams B, Mascart F, Schandene L, Janssen F, et al. CD81 gene defect in humans disrupts CD19 complex formation and leads to antibody deficiency. Journal of Clinical Investigation. 2010;120(4):1265-74.

135. Kuijpers TW, Bende RJ, Baars PA, Grummels A, Derks IA, Dolman KM, et al. CD20 deficiency in humans results in impaired T cell-independent antibody responses. Journal of Clinical Investigation. 2010;120(1):214-22.
136. Thiel J, Kimmig L, Salzer U, Grudzien M, Lebrecht D, Hagena T. Genetic CD21 deficiency is associated with hypogammaglobulinemia. Journal of Allergy and Clinical Immunology. 2012;129(3):801-10.e6.
137. Grier JT, Forbes LR, Monaco-Shawver L, Oshinsky J, Atkinson TP, Moody C. Human immunodeficiency-causing mutation defines CD16 in spontaneous NK cell cytotoxicity. Journal of Clinical Investigation. 2012;122(10):3769-80.
138. Bruton OC. Agammaglobulinemia. Pediatrics. 1952;9.
139. http://ec.europa.eu/health-eu/health_problems/rare_diseases/index_en.htm.
140. Yu JE, Orange JS, Demirdag YY. New primary immunodeficiency diseases: context and future. Current Opinion in Pediatrics. 2018;30(6):806-20.
141. Bousfiha AA, Jeddane L, Ailal F, Benhsaien I, Mahlaoui N, Casanova JL, et al. Primary immunodeficiency diseases worldwide: more common than generally thought. Journal of Clinical Immunology. 2013;33(1):1-7.
142. Delmonte OM, Schuetz C, Notarangelo LD. RAG Deficiency: Two Genes, Many Diseases. Journal of Clinical Immunology. 2018;38.
143. Marodi L, Notarangelo LD. Immunological and genetic bases of new primary immunodeficiencies. Nature Reviews 2007;7.
144. Bucciol G, Moens L, Bosch B, Bossuyt X, Casanova J-L, Puel A, et al. Lessons learned from the study of human inborn errors of innate immunity. Journal of Allergy and Clinical Immunology. 2019;143(2):507-27.
145. Carneiro-Sampaio M, Coutinho A. Immunity to microbes: lessons from primary immunodeficiencies. Infection and Immunity. 2007;75(4):1545-55.
146. Casanova JL. Discovery of single-gene inborn errors of immunity by next generation sequencing. Current Opinion in Immunology. 2014;30.
147. Krumm N, Ko A, O'Roak BJ, Malig M, Coe1 BP, Quinlan AR, Nickerson DA and Eichler EE. Copy number variation detection and genotyping from exome sequence data. Genome Research. 2012;22.
148. Ng SB, Turner EH, Robertson PD, Flygare SD, Bigham AW, Lee C, Shaffer T, Wong M, Bhattacharjee A, Eichler EE, Bamshad M, Shendure J. Targeted capture and massively parallel sequencing of 12 human exomes. Nature. 2009;461.
149. Meyts I, Bosch B, Bolze A, Boisson B, Itan Y, Belkadi A, et al. Exome and genome sequencing for inborn errors of immunity. Journal of Allergy Clinical Immunology. 2016;138(4):957-69.
150. Casanova JLC, Conley ME, Seligman SJ, Abel L, Notarangelo LD. Guidelines for genetic studies in single patients: lessons from primary immunodeficiencies. Journal of Experimental Medicine. 2014;211.
151. Chevalier BS, Kortemme T, Chadsey MS, Baker D, Monnat RJ, Stoddard BL. Design, activity, and structure of a highly specific artificial endonuclease. Molecular Cell. 2002;10.
152. Bibikova M, Golic KG, Carroll D. Targeted chromosomal cleavage and mutagenesis in Drosophila using zinc-finger nucleases. Genetics. 2002;161.
153. Moscou MJ. A simple cipher governs DNA recognition by TAL effectors. Science. 2009;326.

154. Ishino Y, Makino K, Amemura M, Nakata A. Nucleotide sequence of the iap gene, responsible for alkaline phosphatase isozyme conversion in Escherichia coli, and identification of the gene product. Journal of Bacteriology. 1987;169.
155. Marraffini LA, EJS. CRISPR interference limits horizontal gene transfer in staphylococci by targeting DNA. Science. 2008;322.
156. Hsu PD, Lander ES, and Zhang F. Development and Applications of CRISPR-Cas9 for Genome Engineering. Cell. 2014;157.
157. https://eu.idtdna.com/pages/products/crispr-genome-editing/alt-r-crispr-cas9-system?utm_source=google&utm_medium=cpc&utm_campaign=ga_crispr_tracrrna&utm_content=ad_group_tracrrna&gclid=Cj0KCQiA2uH-BRCCARIsAEeef3mlRyJonjYLRvsS87QcrGtDsl2eVtj2yxiz1LlgZ2vLYpAfapVVlgQaAocVEALw_wcB. [
158. Robinton DA, Daley GQ. The promise of induced pluripotent stem cells in research and therapy. 2012; Nature.
159. Takahashi K, Yamanaka S. Induction of Pluripotent Stem Cells from Mouse Embryonic and Adult Fibroblast Cultures by Defined Factors. Cell. 2006;126.
160. Volpi S, Yamazaki Y, Brauer PM, Van Rooijen E, Hayashida A, Slavotinek A, Kuehn HS, Di Rocco M, Rivolta CC, Bortolomai I, Du L, Felgentreff K, Ott de Bruin L, Hayashida K, Freedman G, Marcovecchio GE, Capuder K, Rath P, Luche N, Hagedorn EJ, Buoncompagni A, Royer-Bertrand B, Giliani S, Poliani PL, Imberti L, Dobbs K, Poulain FE, Martini A, Manis J, Linhardt RJ, Rosenzweig SD, Lee H, Puck JM, Zúñiga-Pflücker JC, Zon L, Woo Park P, Superti-Furga A, Notarangelo LD. EXTL3 mutations cause skeletal dysplasia, immune deficiency, and developmental delay. Journal of Experimental Medicine. 2017;214.
161. Yamazaki Y, Franco LM, Giliani SC, Zhang K, Alazami AM, Dobbs AK, Masneri S, Joshi a, Otaizo-Carrasquero f, Myers TG, GanesanS, Bondioni MP, Lan Ho M, Marks C, Alajlan H, Mohammed RW, Zou F, Valencia CA, Filipovich AH, Facchetti F, Boisson B, Azzari C, Al-Saud BK, Al-Mousa H, Casanova JLC, Abraham RS, Notarangelo LD. PAX1 is essential for development and function of the human thymus. Science Immunology. 2020;5.
162. Rissone A, la Marca G, Bishop K, Giocaliere E, Jagadeesh J, Felgentreff K, Dobbs K, Al-Herz W, Jones M. Chandrasekharappa S, Kirby M, Wincovitch S, Lyn Simon K, Itan Y, DeVine A, Schambach A, Sood R, Notarangelo LD and Candotti F. Reticular dysgenesis–associated AK2 protects hematopoietic stem and progenitor cell development from oxidative stress. Journal of Experimental Medicine. 2015;212.
163. Laskowski TJ, Pourebrahim R, Ma C, Ni Z, Garate Z, Crane AM, Li S ,Liao W, Gonzalez-Garay M, Segovi JCa, Paschon DE, Rebar EJ, Holmes MC, Kaufman D, VandekerckhoveB, Davis BR. Gene Correction of iPSCs from a Wiskott-Aldrich Syndrome Patient Normalizes the Lymphoid Developmental and Functional Defects. Stem Cell Reports. 2016;7.
164. Raya A, Guenechea G, Vassena R, Navarro S, Barrero MJ, Consiglio A, Castellà M, Río P, Sleep E, González F, Tiscornia G, Garreta E, Aasen T, Veiga A, Verma IM, Surrallés J, Bueren JJ, Izpisúa Belmonte JC. Disease-corrected haematopoietic progenitors from Fanconi anaemia induced pluripotent stem cells. Nature. 2009;460.
165. Menon T, Scripture-Adams DD, Galic Z, Qualls SJ, Gilmore WB, Ke E, Singer O, Anderson LS, Bornzin AR, Alexander IE, Zack JA, Verma IM. Lymphoid regeneration from gene-corrected SCID-X1 subject-derived iPSCs. Cell Stem Cell. 2015;16.

166. Sweeney CL, Choi U, Merling RK, Liu A, Bodansky A, Burkett S, Kim JW, De Ravin SS, Malech HL. Targeted Repair of CYBB in X-CGD iPSCs Requires Retention of Intronic Sequences for Expression and Functional Correction. Molecular Therapy. 2017;25.
167. Senju S, Matsumura K, Matsunaga Y, Fukushima S, Ikeda T, Takamatsu K, Irie A, Nishimura Y. Generation of dendritic cells and macrophages from human induced pluripotent stem cells aiming at cell therapy. Gene Therapy. 2011;18.
168. Schmitt TM, Zuniga-Pfluecker JC.. Induction of T Cell Development from Hematopoietic Progenitor Cells by Delta-like-1 In Vitro. Immunity. 2002;17.
169. Ross N, La Motte-Mohs EH, Zúñiga-Pflücker JC. Induction of T-cell development from human cord blood hematopoietic stem cells by Delta-like 1 in vitro. Blood. 2005;105.
170. De Smedt M, Plum J. Human bone marrow CD34+ progenitor cells mature to T cells on OP9-DL1 stromal cell line without thymus microenvironment. Blood Cells, Molecules, and Diseases. 2004;33.
171. Poznansky MC, Foxall RB, Olszak IT, Piascik AH, Hartman KE, Meyer TH, Pykett MJ, Chabner KT, Kalams SA. Efficient generation of human T cells from a tissue-engineered thymic organoid. Nature Biotechnology. 2000;18.
172. Seet CS, He C, Bethune MT, Li S, Chick B, Gschweng EH, et al. Generation of mature T cells from human hematopoietic stem and progenitor cells in artificial thymic organoids. Nature Methods. 2017;14(5):521-30.
173. Montel-Hagen A, Seet CS, Li S, Chick B, Zhu Y, Chang P, et al. Organoid-Induced Differentiation of Conventional T Cells from Human Pluripotent Stem Cells. Cell Stem Cell. 2019;24(3):376-89 e8.
174. Bosticardo M, Pala F, Calzoni E, Delmonte OM, Dobbs K, Gardner CL, Sacchetti N, Kawai T, Garabedian EK, Draper D, Bergerson JRE, DeRavin SS, Freeman AF, Hartog N, Holland SM, Kohn DB, Malech HL, Markert ML, Weinacht KG, Villa A, S. Seet C, Montel-Hagen A, Crooks GM,15 and Notarangelo LD. Artificial thymic organoids represent a reliable tool to study T-cell differentiation in patients with severe T-cell lymphopenia. Blood Advances. 2020;4.
175. Erman B, Bilic I, Hirschmugl T, Salzer E, Boztug H, Sanal O, et al. Investigation of Genetic Defects in Severe Combined Immunodeficiency Patients from Turkey by Targeted Sequencing. Scandinavian Journal of Immunology. 2017;85(3):227-34.
176. https://www.benchling.com [
177. https://zlab.bio/guide-design-resources [
178. Doench JG, Fusi N, Sullender M, Hegde M, Vaimberg EW, Donovan KF, et al. Optimized sgRNA design to maximize activity and minimize off-target effects of CRISPR-Cas9. Nature Biotechnology. 2016;34(2):184-91.
179. Paila U, Chapman BA, Kirchner R, Quinlan AR. GEMINI: integrative exploration of genetic variation and genome annotations. PLoS Computational Biology. 2013;9(7):e1003153.
180. Maffucci P, Bigio B, Rapaport F, Cobat A, Borghesi A, Lopez M, et al. Blacklisting variants common in private cohorts but not in public databases optimizes human exome analysis. Proceedings of the National Academy of Sciences of the United States of America. 2019;116(3):950-9.
181. Rentzsch P WD, Cooper GM, Shendure J, Kircher M. . CADD: predicting the deleteriousness of variants throughout the human genome. Nucleic Acids Research. 2018;47.

182. Kitaura K ST, Matsutani T and Suzuki R. A new high-throughput sequencing method for determining diversity and similarity of T cell receptor (TCR) α and β repertoires and identifying potential new invariant TCR α chains. Immunology. 2016;17.
183. Castagnoli R, Delmonte OM, Calzoni E, Notarangelo LD. Hematopoietic Stem Cell Transplantation in Primary Immunodeficiency Diseases: Current Status and Future Perspectives. Frontiers in Pediatrics. 2019;7:295.
184. Aiuti A, Roncarolo M, Naldini L. Gene therapy for ADA-SCID, the first marketing approval of an ex vivo gene therapy in Europe: paving the road for the next generation of advanced therapy medicinal products. EMBO Molecular Medicine. 2017;9.
185. Candotti F. Gene therapy for Wiskott-Aldrich syndrome: here to stay. The Lancet Hematology. 2019;6.
186. Delmonte OM, Castagnoli R, Calzoni E, Notarangelo LD. Inborn Errors of Immunity With Immune Dysregulation: From Bench to Bedside. Frontiers in Pediatrics. 2019;7.
187. Delmonte OM, Notarangelo Ld. Targeted Therapy with Biologicals and Small Molecules in Primary Immunodeficiencies. Medical Principles and Practice. 2020;29.
188. Łyszkiewicz M, Ziętara N, Frey L, Pannicke U, Stern M, Liu Y, Fan Y, Puchałka J, Hollizeck S, Somekh I, Rohlfs M, Yilmaz T, Ünal E, Karakukcu M, Patiroğlu T, Kellerer C, Karasu E, Sykora KW, Simon A, Somech R, Roesler J, Hoenig M, Keppler OT, Schwarz K, Klein C. Human FCHO1 deficiency reveals role for clathrin- mediated endocytosis in development and function of T cells. Nature Communications. 2020;11.
189. Henriques JR, Nibbs FJ, Graham GJ and Barata JT. IL7 induces rapid clathrin mediated internalization and jak 3 dependent degradation of IL7RA in T cells. Blood. 2010;115:3269-77.

10. Acknowledgments e Ringraziamenti

Desidero ringraziare il Prof. Luigi Notarangelo e la Prof.ssa Silvia Giliani, relatori di questa tesi di dottorato, per le innumerevoli opportunità di crescita personale e professionale, e per il supporto, oltre che per la supervisione scientifica di altissimo livello, che mi hanno offerto in questi anni.

Ringrazio i molti collaboratori che hanno partecipato allo studio attraverso il rimando di pazienti, l'invio di materiale biologico, il supporto negli esperimenti e l'analisi e discussione costruttiva dei risultati e dei dati.

Ringrazio tutti i singoli componenti dei diversi team di ricerca che ho avuto il piacere di conoscere e chiamare colleghi in questi anni: l'LCIM team del Prof. Notarangelo al NIAID, NIH di Bethesda, l'unità Pathogenesis and Treatment of Immune and Bone Diseases Unit della dott.ssa Villa al San Raffaele Theleton Institute for Gene Therapy, Milano e il laboratorio della Prof.ssa Giliani nell'"A. Nocivelli" Institute for Molecular Medicine Spedali Civili and University of Brescia, Brescia. Non potrei mai esprimere propriamente a parole quanto ognuno di voi sia stato prezioso durante le diverse fasi del mio percorso di dottorato.

11. Appendix

for either $MVK^{V377I/+}$ or $MVK^{H20N/+}$). We have previously shown that protein prenylation is defective in PBMCs from this patient but not in either parent.[2] Stimulation with LPS and the NLRP3 activator nigericin elicited much greater IL-1β release in cells from the patient with MKD than from either parent, and this response was abolished by MCC950 (Fig 1, *J*).

Our observations clearly demonstrate that lack of prenylation in monocytic cells (using statin treatment, a pharmacologic model of MKD, or using authentic MKD cells from a patient) leads to enhanced formation of an NLRP3-dependent and pyrin-independent inflammasome upon LPS stimulation. Although loss of prenylation has been suggested to activate the pyrin inflammasome in mouse bone marrow–derived macrophages,[4,5] it is possible that defective prenylation promotes activity of distinct inflammasomes in different cell types. In monocytes, loss of protein prenylation caused by SIM treatment was alone insufficient for inducing NLRP3 inflammasome formation or caspase-1 activation (Fig 1, *B* and *C*) but substantially boosted LPS-induced inflammasome activity (speck formation, caspase-1 activation, IL-1β and IL-18 release, and pyroptosis) on stimulation with LPS (Fig 1, *B-D*, and see Fig E1, *C*). The underlying mechanism remains to be clarified but did not involve an enhancement of LPS-induced changes in mRNA levels (see Fig E2, *A*, in this article's Online Repository at www.jacionline.org) or changes in protein levels (see Fig E2, *B*) of pro–IL-1β, pro–IL-18, NLRP3, ASC, or pro–caspase-1. Enhanced inflammasome formation in prenylation-deficient THP-1 cells also occurred after stimulation with the TLR2 agonist Pam3CSK4 (Fig 1, *K*), which is consistent with the enhanced sensitivity of PBMCs from patients with MKD to both TLR2 and TLR4 agonists.[1]

These findings are of clinical relevance because they demonstrate that targeting the pyrin inflammasome in isolation might not be sufficient to resolve all the pathology associated with MKD. Rather, approaches to overcome the metabolic defect in the mevalonate pathway and restore normal protein prenylation could be more effective at preventing broader inflammasome activation.

We thank Professor Kirill Alexandrov and Dr Zakir Tnimov (University of Queensland) for providing reagents for the Rab prenylation assay and Dr Ryan Chai (Garvan Institute) and Dr Rebecca Coll (University of Queensland) for technical advice.

Oliver P. Skinner, BSc[a]
Julie Jurczyluk, BSc[a]
Paul J. Baker, PhD[b]
Seth L. Masters, PhD[b]
Alicia G. Rios Wilks, BSc[a]
Misaki S. Clearwater, BSc[a]
Avril A. B. Robertson, PhD, MChem, GCHEd[c]
Kate Schroder, PhD[d]
Sam Mehr, MBBS, BMedSci, FRCPA, FRACP[e]
Marcia A. Munoz, PhD[a]*
Michael J. Rogers, PhD[a]*

From [a]Bone Biology, Garvan Institute of Medical Research and St Vincent's Clinical School, UNSW Sydney, Sydney, Australia; [b]the Inflammation Division, Walter and Eliza Hall Institute of Medical Research, Melbourne, Australia; [c]the School of Chemistry and Molecular Biosciences and [d]the Institute for Molecular Bioscience, University of Queensland, Brisbane, Australia; and [e]the Department of Allergy/Immunology, Royal Children's Hospital, Melbourne, Australia. E-mail: m.rogers@garvan.org.au.

*These authors contributed equally to this work as senior authors.

Supported in part by NHMRC project grant APP1139644 (to M.J.R.), a grant from the Allergy and Immunology Foundation of Australasia (to M.A.M. and M.J.R.), Mrs Janice Gibson and the Ernest Heine Family Foundation, and the Marian & E.H. Flack Trust.

Disclosure of potential conflict of interest: A. A. B. Robertson and K. Schroder are co-inventors on patent applications for NLRP3 inhibitors, which have been licensed to Inflazome, a company headquartered in Dublin, Ireland. Inflazome is developing drugs that target the NLRP3 inflammasome to address unmet clinical needs in inflammatory disease. K. Schroder served on the Scientific Advisory Board of Inflazome in 2016-2017. The rest of the authors declare that they have no relevant conflicts of interest.

REFERENCES

1. Stoffels M, Jongekrijg J, Remijn T, Kok N, van der Meer JW, Simon A. TLR2/TLR4-dependent exaggerated cytokine production in hyperimmunoglobulinaemia D and periodic fever syndrome. Rheumatology (Oxford) 2015;54:363-8.
2. Munoz MA, Jurczyluk J, Mehr S, Chai RC, Arts RJW, Sheu A, et al. Defective protein prenylation is a diagnostic biomarker of mevalonate kinase deficiency. J Allergy Clin Immunol 2017;140:873-5.
3. Mandey SH, Kuijk LM, Frenkel J, Waterham HR. A role for geranylgeranylation in interleukin-1beta secretion. Arthritis Rheum 2006;54:3690-5.
4. Akula MK, Shi M, Jiang Z, Foster CE, Miao D, Li AS, et al. Control of the innate immune response by the mevalonate pathway. Nat Immunol 2016;17:922-9.
5. Park YH, Wood G, Kastner DL, Chae JJ. Pyrin inflammasome activation and RhoA signaling in the autoinflammatory diseases FMF and HIDS. Nat Immunol 2016;17:914-21.
6. Guo C, Chi Z, Jiang D, Xu T, Yu W, Wang Z, et al. Cholesterol homeostatic regulator SCAP-SREBP2 integrates NLRP3 inflammasome activation and cholesterol biosynthetic signaling in macrophages. Immunity 2018;49:842-56.e7.
7. Jurczyluk J, Munoz MA, Skinner OP, Chai RC, Ali N, Palendira U, et al. Mevalonate kinase deficiency leads to decreased prenylation of Rab GTPases. Immunol Cell Biol 2016;94:994-9.
8. Baker PJ, Boucher D, Bierschenk D, Tebartz C, Whitney PG, D'Silva DB, et al. NLRP3 inflammasome activation downstream of cytoplasmic LPS recognition by both caspase-4 and caspase-5. Eur J Immunol 2015;45:2918-26.
9. Coll RC, Robertson AA, Chae JJ, Higgins SC, Munoz-Planillo R, Inserra MC, et al. A small-molecule inhibitor of the NLRP3 inflammasome for the treatment of inflammatory diseases. Nat Med 2015;21:248-55.

Available online February 21, 2019.
http://dx.doi.org/10.1016/j.jaci.2019.02.013

F-BAR domain only protein 1 (FCHO1) deficiency is a novel cause of combined immune deficiency in human subjects

To the Editor:

Clathrin-mediated endocytosis (CME) is the major endocytic pathway by which eukaryotic cells internalize cell-surface cargo proteins and extracellular molecules, thereby enabling a broad range of biological processes, including cell signaling, nutrient and growth factor uptake, and cell fate and differentiation.[1] F-BAR domain only proteins 1 and 2 (FCHO1/FCHO2) are involved in the maturation of clathrin-coated pit formation.[2] Through the N-terminal F-BAR domain, they bind to phosphatidylinositol 4,5-biphosphate on the inner side of the cell membrane, inducing and stabilizing membrane curvature.[3] In addition, the FCHO1/FCHO2 C-terminal μ-homology domain mediates interaction with the epidermal growth factor receptor substrate 15 and cargo molecules.[3] Moreover, the linker region of FCHO1 acts as an allosteric activator of the adaptor protein 2 complex, enabling recruitment of clathrin to the assembling coat.[4,5]

Here we report 5 patients (P1-P5) from unrelated families of Italian (P1), Turkish (P2, P3, and P5) and Algerian (P4) origin (Fig 1, *A*) with biallelic *FCHO1* mutations and combined immunodeficiency, manifesting as recurrent and severe infections

frontiers in Pediatrics

REVIEW
published: 08 August 2019
doi: 10.3389/fped.2019.00295

Hematopoietic Stem Cell Transplantation in Primary Immunodeficiency Diseases: Current Status and Future Perspectives

Riccardo Castagnoli[1,2], *Ottavia Maria Delmonte*[1], *Enrica Calzoni*[1,3] *and Luigi Daniele Notarangelo*[1]*

[1] *Laboratory of Clinical Immunology and Microbiology, Division of Intramural Research, National Institute of Allergy and Infectious Diseases, National Institutes of Health, Bethesda, MD, United States,* [2] *Department of Pediatrics, Foundation IRCCS Policlinico San Matteo, University of Pavia, Pavia, Italy,* [3] *Department of Molecular and Translational Medicine, A. Nocivelli Institute for Molecular Medicine, University of Brescia, Brescia, Italy*

Primary immunodeficiencies (PID) are disorders that for the most part result from mutations in genes involved in immune host defense and immunoregulation. These conditions are characterized by various combinations of recurrent infections, autoimmunity, lymphoproliferation, inflammatory manifestations, atopy, and malignancy. Most PID are due to genetic defects that are intrinsic to hematopoietic cells. Therefore, replacement of mutant cells by healthy donor hematopoietic stem cells (HSC) represents a rational therapeutic approach. Full or partial ablation of the recipient's marrow with chemotherapy is often used to allow stable engraftment of donor-derived HSCs, and serotherapy may be added to the conditioning regimen to reduce the risks of graft rejection and graft versus host disease (GVHD). Initially, hematopoietic stem cell transplantation (HSCT) was attempted in patients with severe combined immunodeficiency (SCID) as the only available curative treatment. It was a challenging procedure, associated with elevated rates of morbidity and mortality. Overtime, outcome of HSCT for PID has significantly improved due to availability of high-resolution HLA typing, increased use of alternative donors and new stem cell sources, development of less toxic, reduced-intensity conditioning (RIC) regimens, and cellular engineering techniques for graft manipulation. Early identification of infants affected by SCID, prior to infectious complication, through newborn screening (NBS) programs and prompt genetic diagnosis with Next Generation Sequencing (NGS) techniques, have also ameliorated the outcome of HSCT. In addition, HSCT has been applied to treat a broader range of PID, including disorders of immune dysregulation. Yet, the broad spectrum of clinical and immunological phenotypes associated with PID makes it difficult to define a universal transplant regimen. As such, integration of knowledge between immunologists and transplant specialists is necessary for the development of innovative transplant protocols and to monitor their results during follow-up. Despite the improved outcome observed after HSCT, patients with severe forms of PID still face significant challenges of short and long-term transplant-related complications. To address this issue, novel HSCT strategies are

OPEN ACCESS

Edited by:
Kaan Boztug,
CeMM Research Center for Molecular Medicine (OAW), Austria

Reviewed by:
Daniele Zama,
Sant'Orsola-Malpighi Polyclinic, Italy
Aleš Janda,
Freiburg University Medical Center, Germany

****Correspondence:***
Luigi Daniele Notarangelo
luigi.notarangelo2@nih.gov

Specialty section:
This article was submitted to Pediatric Immunology, a section of the journal Frontiers in Pediatrics

Received: *03 May 2019*
Accepted: *03 July 2019*
Published: *08 August 2019*

Citation:
Castagnoli R, Delmonte OM, Calzoni E and Notarangelo LD (2019) Hematopoietic Stem Cell Transplantation in Primary Immunodeficiency Diseases: Current Status and Future Perspectives. Front. Pediatr. 7:295. doi: 10.3389/fped.2019.00295

frontiers in Pediatrics

REVIEW
published: 27 August 2019
doi: 10.3389/fped.2019.00353

Inborn Errors of Immunity With Immune Dysregulation: From Bench to Bedside

Ottavia Maria Delmonte[1], *Riccardo Castagnoli*[1,2], *Enrica Calzoni*[1,3] *and Luigi Daniele Notarangelo*[1]*

[1] *Laboratory of Clinical Immunology and Microbiology, Division of Intramural Research, National Institute of Allergy and Infectious Diseases, National Institutes of Health, Bethesda, MD, United States,* [2] *Foundation IRCCS Policlinico San Matteo, Department of Pediatrics, University of Pavia, Pavia, Italy,* [3] *Department of Molecular and Translational Medicine, A. Nocivelli Institute for Molecular Medicine, University of Brescia, Brescia, Italy*

Inborn errors of immunity are genetic disorders with broad clinical manifestations, ranging from increased susceptibility to infections to significant immune dysregulation, often leading to multiple autoimmune phenomena, lymphoproliferation, and malignancy. The treatment is challenging as it requires careful balancing of immunosuppression in subjects at increased risk of infections. Recently, the improved ability to define inborn errors of immunity pathophysiology at the molecular level has set the basis for the development of targeted therapeutic interventions. Such a "precision medicine" approach is mainly bases on the use of available small molecules and biologics to target a specific cell function. In this article, we summarize the clinical and laboratory features of various recently described inborn errors of immunity associated with immune dysregulation and hyperinflammation in which mechanism-based therapeutic approaches have been implemented.

Keywords: primary immunodeficiency diseases (PID), immunedysregulation, combined immunodeficiency, precision medicine, small molecules, monoclonals, gain of function (GOF)

OPEN ACCESS

Edited by:
Claudio Pignata,
University of Naples Federico II, Italy

Reviewed by:
Alessandro Aiuti,
Vita-Salute San Raffaele University, Italy
Eduardo Lopez-Granados,
University Hospital La Paz, Spain

***Correspondence:**
Luigi Daniele Notarangelo
luigi.notarangelo2@nih.gov

Specialty section:
This article was submitted to Pediatric Immunology, a section of the journal Frontiers in Pediatrics

Received: *08 May 2019*
Accepted: *08 August 2019*
Published: *27 August 2019*

Citation:
Delmonte OM, Castagnoli R, Calzoni E and Notarangelo LD (2019) Inborn Errors of Immunity With Immune Dysregulation: From Bench to Bedside. Front. Pediatr. 7:353. doi: 10.3389/fped.2019.00353

INTRODUCTION

With the increased availability of high-throughput DNA sequencing, the number of genes associated with inborn errors of immunity [historically named primary immune deficiency disorders (PIDs)] has exponentially increased over the last decade. The most recent PID classification from the International Union of Immunological Sciences includes more than 350 genes, and ∼50 of these have been discovered in the last 2 years (1). In addition to the identification of novel PID-associated genes, it has been recognized that distinct clinical phenotypes may be sustained by Gain of Function (GOF) or Loss of Function (LOF) mutations in the same gene. Finally, various degrees of activity of mutant proteins due to hypomorphic and hypermorphic mutations may also cause PID phenotypic variability (1, 2).

The clinical features of PIDs are broad, ranging from increased susceptibility to infections to significant immune dysregulation, often leading to multiple autoimmune phenomena, including cytopenias and solid organ autoimmunity, in addition to lymphoproliferation and malignancy. The treatment of immune disorders with coexisting immune deficiency and immune dysregulation is challenging, as it requires careful balancing of immunosuppression in subjects at increased risk of infections. In most recent years, the growing ability to define PID pathophysiology at the

Defining a new immune deficiency syndrome: MAN2B2-CDG

To the Editor:

Congenital disorders of glycosylation (CDGs) are a group of clinically heterogeneous disorders characterized by abnormal monosaccharide activation and protein and lipid glycosylation.[1] More than 147 CDG subtypes have currently been described to affect several glycosylation pathways, including *N*-glycosylation, *O*-glycosylation, glycosaminoglycan, dystroglycanopathy, and glycosylphosphatidylinositol (GPI)-anchor pathways.[1]

Several CDG subtypes involve enzymatic deficiencies in the *N*-linked glycosylation pathway. *N*-linked protein glycosylation is a highly conserved process occurring in the endoplasmic

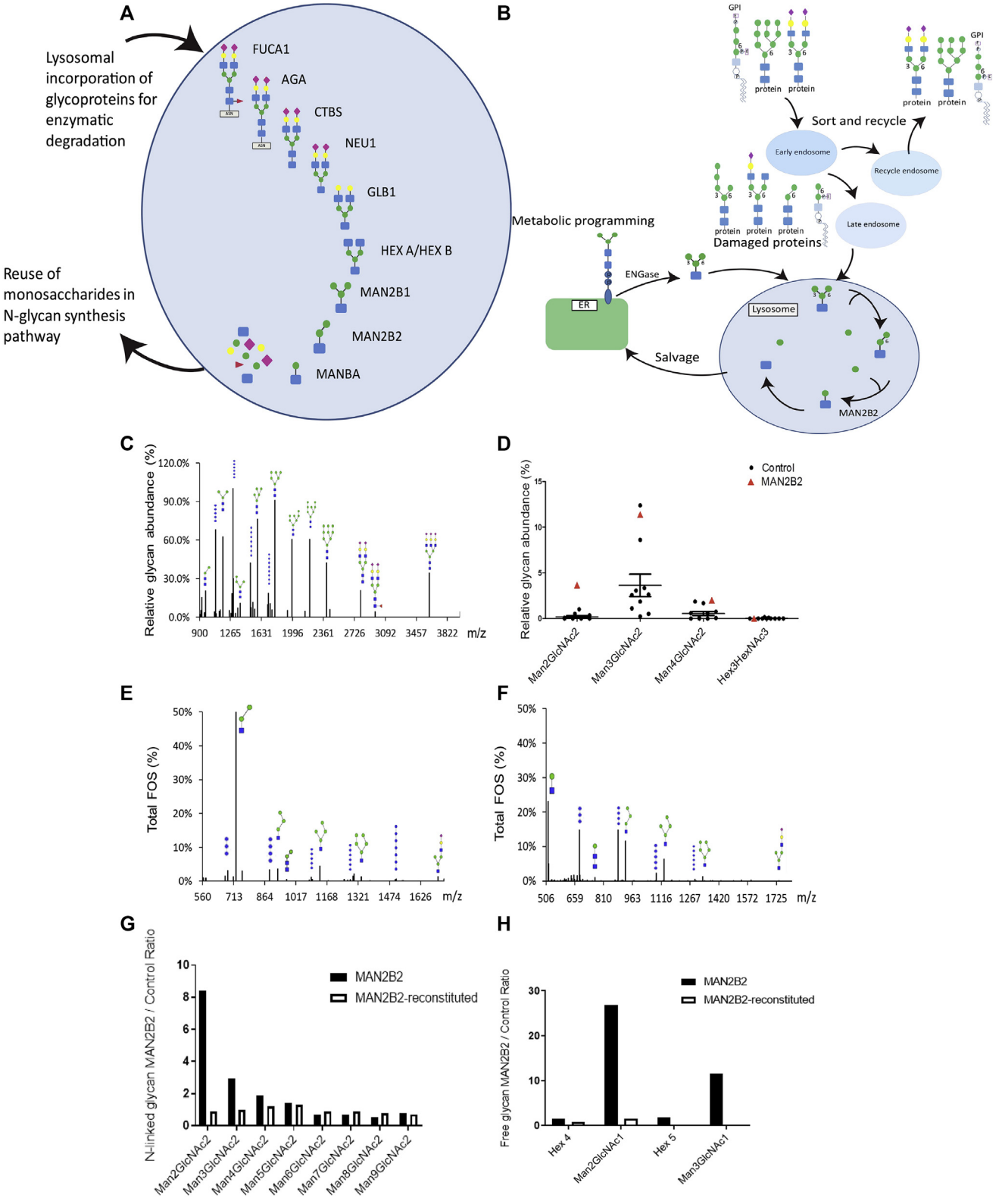

Efficacy and safety of anti-CD45–saporin as conditioning agent for RAG deficiency

Maria Carmina Castiello, PhD,[a,b]* Marita Bosticardo, PhD,[c]* Nicolò Sacchetti, PhD,[a] Enrica Calzoni, MD,[a,c] Elena Fontana, PhD,[b,d] Yasuhiro Yamazaki, MD, PhD,[c] Elena Draghici, BS,[a] Cristina Corsino,[c] Ileana Bortolomai, PhD,[a] Lucia Sereni, PhD,[a] Hsin-Hui Yu, MD, PhD,[c] Paolo Uva, PhD,[e] Rahul Palchaudhuri, PhD,[f,g,h] David T. Scadden, MD,[f,g] Anna Villa, MD,[a,b] and Luigi D. Notarangelo, MD[c] *Milan and Pula, Cagliari, Italy; Bethesda, Md; and Cambridge and Boston, Mass*

GRAPHICAL ABSTRACT

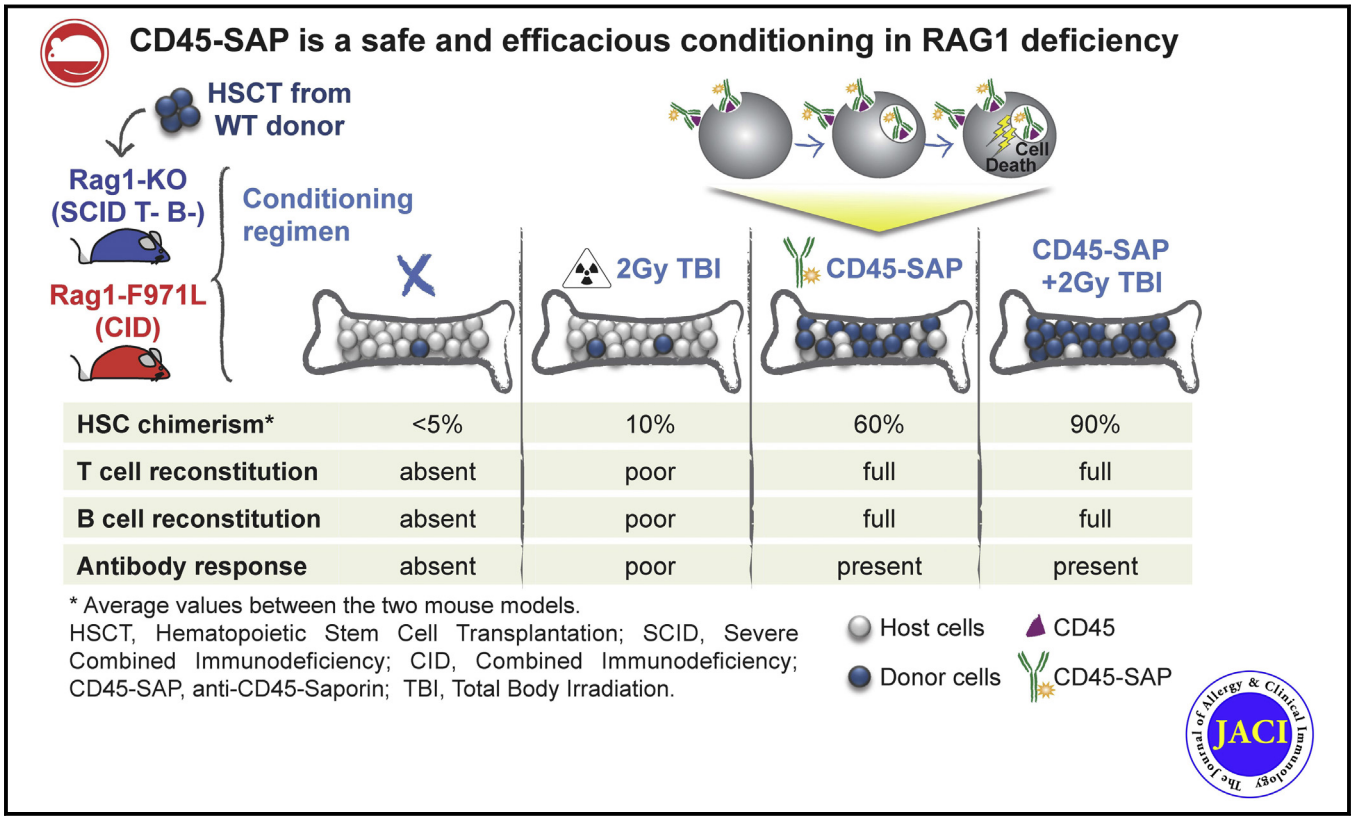

Background: Mutations in the recombinase-activating genes cause severe immunodeficiency, with a spectrum of phenotypes ranging from severe combined immunodeficiency to immune dysregulation. Hematopoietic stem cell transplantation is the only curative option, but a high risk of graft failure and poor immune reconstitution have been observed in the absence of myeloablation.

From [a]the San Raffaele Telethon Institute for Gene Therapy SR-Tiget, IRCCS San Raffaele Scientific Institute, Milan; [b]the Institute of Genetic and Biomedical Research Milan Unit, National Research Council, Milan; [c]the Laboratory of Clinical Immunology and Microbiology, Division of Intramural Research, National Institute of Allergy and Infectious Diseases, National Institutes of Health, Bethesda; [d]the Human Genome Lab, Humanitas Clinical and Research Center, Milan; [e]the CRS4, Science and Technology Park Polaris, Pula; [f]the Department of Stem Cell and Regenerative Biology, Harvard University, Harvard Stem Cell Institute, Cambridge; [g]the Center for Regenerative Medicine, Massachusetts General Hospital, Boston; and [h]Magenta Therapeutics, Cambridge.

*These authors are co-first authors.

Supported by a grant from the Division of Intramural Research, National Institute of Allergy and Infectious Diseases, National Institutes of Health (to L.D.N.); the National Institutes of Health Bench to Bedside grant RAG Deficiency: From Pathophysiology to Precise Gene Editing (to L.D.N. and A.V.); and grants Tiget E2 (to A.V.), Italian Ministry of Health PE-2016-02363691 (to E.F. and L.D.N.), EU2020 (SCIDNET) No. 666908 (to A.V.), and MIUR 2017-5XHBPN (to A.V.).

Disclosure of potential conflict of interest: The authors declare that they have no relevant conflicts of interest.

Received for publication January 28, 2020; revised April 8, 2020; accepted for publication April 10, 2020.

Corresponding author: Anna Villa, MD, SR-Tiget, Via Olgettina 58, Milan, 20127, Italy. E-mail: villa.anna@hsr.it. Or: Luigi D. Notarangelo, MD, Immune Deficiency Genetics Section, Laboratory of Clinical Immunology and Microbiology, National Institute of Allergy and Infectious Diseases, National Institutes of Health, Building 10, Room 5-3950, 10 Center Drive, Bethesda, MD 20892. E-mail: luigi.notarangelo2@nih.gov.

0091-6749

https://doi.org/10.1016/j.jaci.2020.04.033

REGULAR ARTICLE

blood advances

Artificial thymic organoids represent a reliable tool to study T-cell differentiation in patients with severe T-cell lymphopenia

Marita Bosticardo,[1] Francesca Pala,[1] Enrica Calzoni,[1,2] Ottavia M. Delmonte,[1] Kerry Dobbs,[1] Cameron L. Gardner,[1,3] Nicolo' Sacchetti,[1,4,5] Tomoki Kawai,[1] Elizabeth K. Garabedian,[6] Debbie Draper,[1] Jenna R. E. Bergerson,[1] Suk See DeRavin,[1] Alexandra F. Freeman,[1] Tayfun Güngör,[7] Nicholas Hartog,[8] Steven M. Holland,[1] Donald B. Kohn,[9] Harry L. Malech,[1] Mary Louise Markert,[10,11] Katja G. Weinacht,[12] Anna Villa,[4,13] Christopher S. Seet,[14] Amelie Montel-Hagen,[15] Gay M. Crooks,[15] and Luigi D. Notarangelo[1]

[1]Laboratory of Clinical Immunology and Microbiology, Division of Intramural Research, National Institute of Allergy and Infectious Diseases, National Institutes of Health (NIH), Bethesda, MD; [2]Department of Molecular and Translational Medicine, A. Nocivelli Institute for Molecular Medicine, University of Brescia, Brescia, Italy; [3]Department of Medicine, University of Oxford, Oxford, United Kingdom; [4]San Raffaele Telethon Institute for Gene Therapy, Division of Regenerative Medicine, Stem Cells and Gene Therapy, San Raffaele Scientific Institute, Milan, Italy; [5]Vita-Salute San Raffaele University, Milan, Italy; [6]Genetics and Molecular Biology Branch, National Human Genome Research Institute, NIH, Bethesda, MD; [7]Division of Stem Cell Transplantation, University Children's Hospital Zürich, Zürich, Switzerland; [8]Helen DeVos Children's Hospital Allergy and Immunology Department, Michigan State College of Human Medicine, Grand Rapids, MI; [9]Department of Microbiology, Immunology and Molecular Genetics, University of California, Los Angeles (UCLA), Los Angeles, CA; [10]Division of Pediatric Allergy, Immunology and Pulmonary Medicine, Department of Pediatrics, and [11]Department of Immunology, Duke University Medical Center, Durham, NC; [12]Division of Stem Cell Transplantation and Regenerative Medicine, Department of Pediatrics, Stanford School of Medicine, Stanford, CA; [13]Consiglio Nazionale delle Ricerche-Istituto di Ricerca Genetica e Biomedica, Milan Unit, Milan, Italy; and [14]Division of Hematology-Oncology, Department of Medicine, and [15]Department of Pathology and Laboratory Medicine, David Geffen School of Medicine, UCLA, Los Angeles, CA

Key Points

- The ATO system allows precise definition of developmental blocks in patients with gene defects that cause T-cell lymphopenia.
- The ATO system can help distinguish between hematopoietic autonomous and extra-hematopoietic defects that cause T-cell lymphopenia.

The study of early T-cell development in humans is challenging because of limited availability of thymic samples and the limitations of in vitro T-cell differentiation assays. We used an artificial thymic organoid (ATO) platform generated by aggregating a DLL4-expressing stromal cell line (MS5-hDLL4) with $CD34^+$ cells isolated from bone marrow or mobilized peripheral blood to study T-cell development from $CD34^+$ cells of patients carrying hematopoietic intrinsic or thymic defects that cause T-cell lymphopenia. We found that AK2 deficiency is associated with decreased cell viability and an early block in T-cell development. We observed a similar defect in a patient carrying a null *IL2RG* mutation. In contrast, $CD34^+$ cells from a patient carrying a missense *IL2RG* mutation reached full T-cell maturation, although cell numbers were significantly lower than in controls. $CD34^+$ cells from patients carrying *RAG* mutations were able to differentiate to $CD4^+CD8^+$ cells, but not to $CD3^+TCR\alpha\beta^+$ cells. Finally, normal T-cell differentiation was observed in a patient with complete DiGeorge syndrome, consistent with the extra-hematopoietic nature of the defect. The ATO system may help determine whether T-cell deficiency reflects hematopoietic or thymic intrinsic abnormalities and define the exact stage at which T-cell differentiation is blocked.

Introduction

Limited access to thymic samples and the relative inefficiency of in vitro T-cell development methods have hampered precise definition of the developmental blocks that characterize different forms of severe combined immune deficiency (SCID) in humans. A serum-free 3D artificial thymic organoid (ATO) system has recently been shown to support human T-cell differentiation efficiently and reproducibly in vitro from hematopoietic stem cells. It has advantages over previously published protocols for its technical simplicity, reliability, and efficient production of cells.[1] Here, we used the ATO system to

Submitted 24 February 2020; accepted 12 May 2020; published online 17 June 2020.
DOI 10.1182/bloodadvances.2020001730.
The full-text version of this article contains a data supplement.

Send data sharing requests to Luigi D. Notarangelo (luigi.notarangelo2@nih.gov).

Online version at http://www.minervamedica.it

Minerva Pediatrica 2020 October;72(5):393-407
DOI: 10.23736/S0026-4946.20.06000-4

REVIEW

NOVEL INSIGHTS INTO PEDIATRIC ALLERGY AND IMMUNOLOGY

Human inborn errors of immunity caused by defects of receptor and proteins of cellular membrane

Enrica CALZONI [1] *, Riccardo CASTAGNOLI [2, 3], Silvia C. GILIANI [1]

[1]Department of Molecular and Translational Medicine, A. Nocivelli Institute for Molecular Medicine, University of Brescia, Brescia, Italy; [2]Pediatric Clinic, IRCC2 San Matteo Polyclinic Foundation, Pavia, Italy; [3]Department of Clinical, Surgical, Diagnostic and Pediatric Sciences, University of Pavia, Pavia, Italy

*Corresponding author: Enrica Calzoni, Department of Molecular and Translational Medicine, A. Nocivelli Institute for Molecular Medicine, University of Brescia, Brescia, Italy. E-mail: enrica.calz@gmail.com

ABSTRACT

Inborn errors of immunity are diseases of the immune system resulting from mutations that alter the expression of encoded proteins or molecules. Total updated number of these disorders is currently 406, with 430 different identified gene defects involved. Studies of the underlying mechanisms have contributed in better understanding the pathophysiology of the diseases, but also the complexity of the biology of innate and adaptive immune system and its interaction with microbes. In this review we present and briefly discuss Inborn Errors of Immunity caused by defects in genes encoding for receptors and protein of cellular membrane, including cytokine receptors, T cell antigen receptor (TCR) complex, cellular surface receptors or receptors signaling causing predominantly antibody deficiencies, co-stimulatory receptors and others. These alterations impact many biological processes of immune-system cells, including development, proliferation, activation and down-regulation of the immunological response, and result in a variety of diseases that present with distinct clinical features or with overlapping signs and symptoms.

(*Cite this article as:* Calzoni E, Castagnoli R, Giliani SC. Human inborn errors of immunity caused by defects of receptor and proteins of cellular membrane. Minerva Pediatr 2020;72:393-407. DOI: 10.23736/S0026-4946.20.06000-4)

KEY WORDS: Primary immunodeficiency diseases; Receptors, cell surface; Severe combined immunodeficiency; Mutation.

Inborn errors of immunity are diseases of the immune system resulting from mutations that alter the expression of encoded proteins or molecules.[1] Since 2013, the International Union of Immunological Societies (IUIS) has been publishing updated classifications of Inborn Errors of Immunity (IEI) describing main clinical and laboratory features with the aim of supporting physicians at the bedside. The last update published in 2019[2] adds 65 new conditions to the previous update (year 2017),[3, 4] bringing the total number of distinct disorders up to 406, with 430 different identified gene defects, organized in ten tables according to their pathogenesis.[5] The advances in- and increased accessibility of-Next Generation Sequencing (NGS) techniques from their advent in 2010 have determined exponential progresses in the field of monogenic inborn errors of immunity, allowing discoveries of novel disease-causing genes as well as descriptions of new clinical phenotypes and manifestation of already known gene defects,[6, 7] and the increased planning of newborn screening programs.[8] Moreover, they have contributed in defining the actual prevalence and incidence of primary immunodeficiency diseases (PIDs), in both pediatric and adult population,[9] developing new diagnostic strategies and adding new insights to treatments.